

# University of St Andrews



Full metadata for this thesis is available in  
St Andrews Research Repository  
at:

<http://research-repository.st-andrews.ac.uk/>

This thesis is protected by original copyright



**Boron Heteroaromatic Compounds as  
Potential Building Blocks for  
Covalent Self-Assembly Processes**

**By  
Lyndsey Marie Greig**

**A Thesis Presented for the Degree of  
Doctor of Philosophy  
in the  
School of Chemistry  
University of St. Andrews**

**St. Andrews**



**February 2002**

Th E90

# Contents

<b>1</b>	<b>Introduction</b>	<b>1</b>
1.1	Self-Assembly Processes	1
1.1.1	Self-Assembly in Biological Systems	1
1.1.2	Chemical Systems – Non-Covalent Self-Assembly	5
1.1.3	Self-Assembly Using Covalent Bonds	14
1.1.4	Dynamic Combinatorial Libraries	19
1.1.5	Towards Micro- and Macroscopic Self-Assembling Systems	24
1.2	Boron-Containing Heterocycles	29
1.2.1	Boraza- and Boroxoaromatic Compounds	29
1.2.2	Synthesis of Boron Heteroaromatics	31
1.2.3	Aromaticity of Boron Heteroaromatics	34
1.2.4	The Potential of Boron Heteroaromatics in Self-Assembly	37
1.3	Aims and Objectives	43
<b>2</b>	<b>Properties of Boroxoaromatic Compounds</b>	<b>45</b>
2.1	Preamble	45
2.2	Synthesis of 10-Hydroxy-10,9-Boroxophenanthrene	45
2.3	Aromaticity and Electrophilic Reactivity	47
2.3.1	Aromaticity and the O-B bond	47
2.3.2	The Electrophilic Boron	54
2.3.3	The Calculated Structure of Bis-(boroxophenanthryl) ether	55
2.4	Solid State Structure	55
2.4.1	Solid State Structure of 10-Hydroxy-10,9-Boroxophenanthrene	55
2.4.2	Solid State Structure of Bis-(boroxophenanthryl) ether	57
2.5	Solid State Reactivity	58
2.5.1	Chemical Change	58
2.5.2	Structural Change	61
2.6	Solution Phase Reactivity	65
2.7	Aromaticity of Boron-Containing Heteroaromatic Compounds	68
2.8	Conclusions	72



<b>3</b>	<b>Bifunctional Boron-Heteroaromatic Systems</b>	<b>73</b>
3.1	Rigid Systems Designed to Form Linear Oligomers	73
3.1.1	Synthesis of 5,9-Dihydroxy-5,9-dibora-4,10-dioxapyrene	74
3.1.2	The Calculated Structure of 5,9-Dihydroxy-5,9-dibora-4,10-dioxapyrene	79
3.1.3	Solid State Reactivity of 5,9-Dihydroxy-5,9-dibora-4,10-dioxapyrene	79
3.1.4	Solution Phase Reactivity of 5,9-Dihydroxy-5,9-dibora-4,10-dioxapyrene	85
3.2	Rigid Systems Designed to Form Macrocycles	87
3.2.1	Synthesis of 3,6-Dihydroxy-3,6-dibora-4,5-diazadibenz[a,j]anthracene	89
3.2.2	Synthesis of 4,5-Dihydroxy-4,5-dibora-3,6-diazadibenz[a,j]anthracene	91
3.2.3	Synthesis of 3,6-Dihydroxy-3,6-dibora-4,5-dioxodibenz[a,j]anthracene	93
3.2.4	Synthesis of 4,5-Dihydroxy-4,5-dibora-3,6-dioxodibenz[a,j]anthracene	94
3.3	Flexible Bifunctional Boron-Heteroaromatic Systems	96
3.3.1	Synthesis of Bis-[2,2'(10-Hydroxy-10,9-boroxophenanthryl)]-ether	97
3.3.2	Synthesis of 3-[2-(10-Hydroxy-10,9-boroxophenanthren-3-yl)-ethyl]-(10-hydroxy-10,9-boroxo)-phenanthrene	100
3.3.3	Synthesis of 3-[2-(10-Hydroxy-10,9-boroxophenanthren-3-yl)-butyl]-(10-hydroxy-10,9-boroxo)-phenanthrene	101
3.4	Conclusions	103
<b>4</b>	<b>Further Investigations into the Reactivity of 10-Hydroxy-10,9-Boroxophenanthrene</b>	<b>104</b>
4.1	Preamble	104
4.1.1	<sup>11</sup> B NMR Spectroscopy of 10-Hydroxy-10,9-Boroxophenanthrene	104
4.1.2	MALDI-tof Mass Spectrometry of 10-Hydroxy-10,9-Boroxophenanthrene	106

4.2	Reaction of 10-Hydroxy-10,9-Boroxophenanthrene with Benzenedimethanols	106
4.3	Reaction of 10-Hydroxy-10,9-Boroxophenanthrene with Alkanediols	109
4.4	Reaction of 10-Hydroxy-10,9-Boroxophenanthrene with Aminoalcohols	113
4.5	Reactivity of Phenylboronic Acid with Nucleophiles	117
4.6	Solution Phase Reactivity of 5,9-Dihydroxy-5,9-Dibora-4,10-Dioxopyrene Revisited	121
4.7	Conclusions	122
<b>5</b>	<b>General Conclusions</b>	<b>123</b>
<b>6</b>	<b>Experimental Section</b>	<b>125</b>
6.1	General Section	125
6.2	NMR Spectroscopy	125
6.3	Mass Spectrometry	125
6.4	Thermal Studies	126
6.5	Infra-Red Spectroscopy	126
6.6	X-Ray Diffraction Studies	126
6.7	Computational Studies	127
6.8	Experimental Procedures	127
<b>7</b>	<b>References and Footnotes</b>	<b>163</b>

"You have two choices," Jamf cried, his last lecture of the year..."stay behind with carbon and hydrogen, take your lunch-bucket in to the works every morning with the faceless droves who can't wait to get in out of the sunlight – or move *beyond*...Silicon, boron, these can replace carbon, and can bond to nitrogen instead of hydrogen." A few snickers here, not unanticipated by the playful old pedagogue. "Move beyond life...here is no frailty, no mortality - here is Strength, and the Timeless." Then his well-known finale, as he wiped away the scrawled C-H on his chalkboard and wrote, in enormous letters, Si-N.

Thomas Pynchon, *Gravity's Rainbow*

We go on being children, all our born days, because again and again a new set of rules is set before us.

Milan Kundera (b. 1929)

## Acknowledgements

Thanks are due to many people, both at the University of Birmingham and the University of St. Andrews, for their support and guidance during my PhD: Dr Douglas Philp for his supervision, and all members of the Philp group, past and present, for their help and advice - particular thanks are due to Dr Paul Comina for his invaluable assistance during the first two years; Professor Kenneth Harris for supporting the research that utilised solid-state techniques; Dr Benson Kariuki and Scott Habershon, who solved the crystal structures described in Chapter 2; Dr Alex Slawin for solving the crystal structure described in Chapter 4, and for providing cheerful advice beyond the call of duty; Dr Neil Spencer and Melanja Smith for performing  $^{11}\text{B}$ , time-dependant and 2-dimensional NMR spectra; Peter Ashton, Nick May, Lianne Hill, Colin Millar and Caroline Horsburgh for EI and ES mass spectrometry; Dr Catherine Botting and Dr Robin Antrobus for persevering with the MALDI-tof spectrometry; Dr Joe Hriljac and Dr Philip Lightfoot for their assistance with variable temperature powder X-ray diffraction experiments; Sylvia Williamson for help with thermal analysis experiments; and the EPSRC for funding this project.

Last, but not least, heartfelt thanks are due to Mum, Dad and Elwyn, without whose unwavering support and encouragement this project would never have been completed, and to whom this thesis is dedicated.

## Abstract

Interest in the field of supramolecular chemistry has increased dramatically over the last two decades. In particular, the area of self-assembly has been the focus of much recent research effort. Noteworthy advances include the utilisation of reversible covalent bonds in self-assembly and the development of dynamic combinatorial libraries. This thesis describes an investigation into the potential utility of boron-containing heteroaromatic compounds as building blocks for covalent self-assembly. Our model compound, 10-hydroxy-10,9-boroxophenanthrene, was first synthesised in 1959, but at that time, only a very limited study of its reactivity properties was carried out. We undertake the clarification of the extent to which compounds of this type can be considered aromatic. It has been suggested that boroxoaromatics can simply be considered cyclic boronic acids, but we reveal evidence that this is not the case. We demonstrate that the carboxylic acid motif provides a good analogue for the boron-heteroatom functionality, sharing a similar polarisation pattern, and the ability to form cyclic hydrogen-bonded dimers. However, unlike carboxylic acids, hydroxyboroxophenanthrene also undergoes a solid state dehydration reaction to form an anhydride, implying the usefulness of this motif in the construction of self-assembled covalently-linked molecular solids. We describe the complete characterisation of this solid state process, and also an investigation of the solution phase reactivity of the building block. We establish that hydroxyboroxophenanthrene reacts extremely rapidly with nucleophiles, suggesting the possible utility of compounds of this type in a dynamic combinatorial library. However, recognising the restricted value of a compound with only one reactive centre, we also describe efforts towards the synthesis of several bis-functional boron heteroaromatic compounds.

## List of Abbreviations

In addition to the commonly-accepted abbreviations in use in Chemistry as defined by the Royal Society of Chemistry (J. Chem. Soc., Perkin Trans. 2, Instructions for Authors, 2001, Part 12), the following abbreviations are used in this thesis.

COSY	Correlated spectroscopy
DSC	Differential scanning calorimetry
GOESY	Gradient-enhanced nuclear Overhauser effect spectroscopy
HMBC	Heteronuclear multiple bond correlation
MALDI-tof	Matrix assisted laser desorption ionisation – time-of-flight
nOe	Nuclear Overhauser enhancement
TGA	Thermogravimetric analysis

# 1 Introduction

## 1.1 Self-Assembly Processes

The possibility of creating a functional device or superstructure by "engineering up" from a single molecule has become<sup>1</sup> an increasingly attractive prospect over the last 15 years. The activities associated with this kind of molecular engineering have become synonymous with the rapidly expanding area<sup>2</sup> of self-assembly. This expansion has been driven by a number of different potential user communities. Firstly, the drive for miniaturisation of integrated circuits, coupled with a growing awareness that the current "top-down" approach employed by the electronics industry may eventually reach<sup>3</sup> a physical limit, has necessitated the development of an alternative approach to device fabrication. Secondly, the realisation that chemical syntheses based on the stepwise, kinetic approaches used traditionally to construct large molecules, such as palytoxin<sup>4</sup> and vitamin B<sub>12</sub><sup>5</sup>, are incredibly demanding in terms of both time and resources has led chemists to appeal to the highly convergent, and therefore highly efficient, nature of self-assembly in order to achieve the rapid syntheses of large structures. Thirdly, the recognition that biological systems exploit highly complex self-assembly processes routinely in the construction of large, regular superstructures from small, simple subunits has led chemists to seek an understanding of the basic principles of biological self-assembling systems. Through this understanding, chemists may be able to emulate the natural systems, for example, in the development<sup>6</sup> of synthetic enzymes, efficient gene-therapy or drug delivery systems.

### 1.1.1 Self-Assembly in Biological Systems

Chemists have turned to biological systems in search of viable paradigms for the construction of large assemblies. Biological systems display a diverse array of functional nanoscale structures and devices in the size range 1 to 10000 nm. The processes of self-organisation and self-assembly of molecular components, which interact chemically and physically in certain well-defined ways, are used to construct these superstructures and arrays. The specificity and precision displayed by biological systems is derived from the highly-directed mutual recognition displayed by the constituent components of a structure. Clearly, the ultimate goal for the chemist seeking to match the achievements of biological systems in creating and maintaining

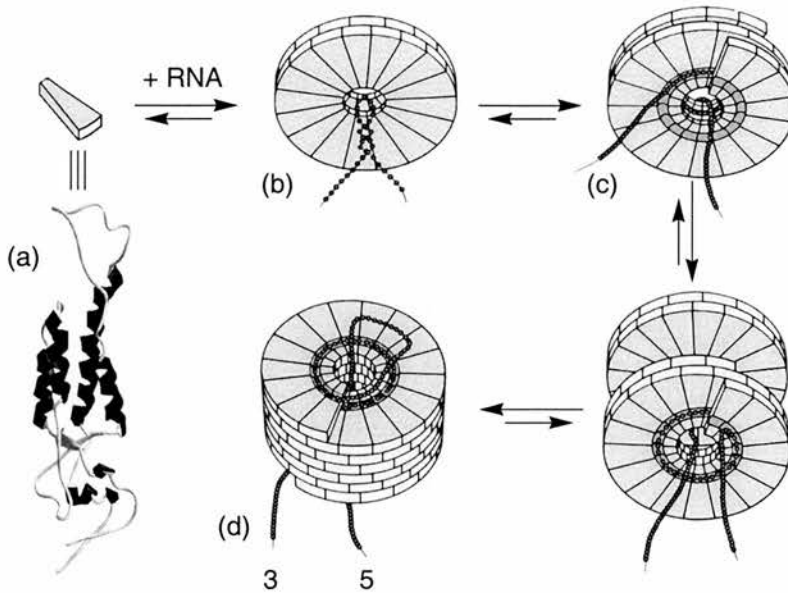
nanoscale structures is to control the assembly and function of synthetic structures from components with the same precision as that displayed by Nature. This objective can only be achieved by firstly understanding<sup>2</sup> the principles behind the self-organisation, self-assembly, and self-synthesis processes exhibited by biological systems. There are several important features common to all natural self-assembling systems which make them a desirable target for chemists to study. These features can be illustrated most easily by considering some examples.

Proteins are involved in almost all biological processes and are employed<sup>7</sup> in a wide range of different roles. They are synthesised as linear chains of amino acids in a defined order dictated by cellular DNA. Knowledge of their amino acid sequence is essential for an understanding of their mechanism of action, however, proteins do not function correctly until they are folded into a specific three-dimensional structure which is also determined by the primary amino acid sequence. This folding process<sup>8</sup> relies on the formation of a large number of non-covalent bonding interactions and is not yet fully understood. However, it is clear that the protein must fold rapidly and reliably into the correct structure from the huge number of possible structures, since the consequences<sup>9</sup> of incorrect folding can be catastrophic, *e.g.* amyloid diseases such as Alzheimers, and prion diseases. Further, all of the information necessary to ensure that the correct fold is reached must somehow be encoded in the non-covalent interactions implicit within the primary sequence. The folding pathway may have many different routes to the final folded structure and incorrect structures are undoubtedly formed as transient species. However, all the interactions involved in the folding process are formed reversibly, and only the stable native state will persist under normal conditions. Thus, the folding process could be regarded as the recognition-directed selection of a single tertiary structure from a large library of tertiary structures encoded by the primary sequence.

Viruses represent some of the best natural examples of self-assembly from which chemists can learn<sup>10</sup>, and the tobacco mosaic virus<sup>11</sup> (TMV) (**Figure 1**) is perhaps one of the simplest and best understood. TMV contains 2130 protein subunits (**Figure 1a**), all of which are identical, thus minimising the amount of genetic information required to encode the final helical structure assembled around a single strand of RNA. All of this information is contained within the constituent parts of the virus and no additional factors are required for the assembly. However, although all of the protein subunits are bound to each other in the same manner, thus creating the symmetrical helical structure, the assembly process is by no means as



straightforward as it might first appear.<sup>12</sup> A two-layer disc – a sub-assembly – is constructed first (**Figure 1b**), and this combines with a specific part of the TMV RNA located about 1000 base pairs from the 3' end. This priming, or nucleation, process (**Figure 1c**) is followed by helix propagation (**Figure 1d**) which gives rise to the intact viral particle.

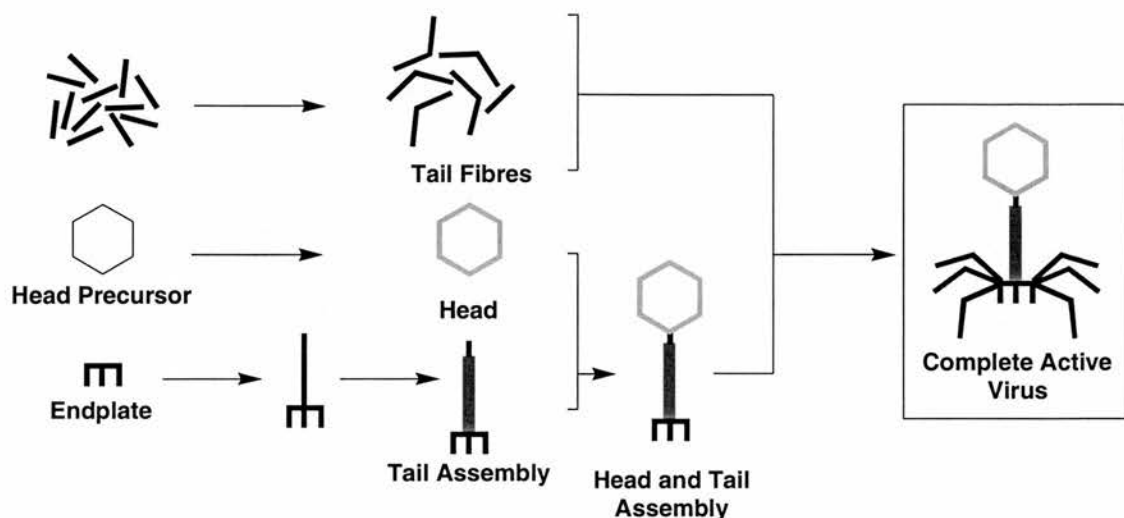


**Figure 1** The assembly of the Tobacco Mosaic Virus. Protein sub-units (a) associate with viral RNA to form a double disk structure (b). Conformational change results in the formation of a slipped double disk (c) and initiates viral assembly (d). Adapted from Ref. 13.

The self-assembly uses only reversible, non-covalent interactions, so the process is in dynamic equilibrium. The advantages of helix formation *via* this sub-assembly are clear. Firstly, the assembly is highly specific, as the nucleating region of the RNA must interact with up to 17 protein subunits, and foreign RNA is therefore recognised and rejected. Secondly, helix growth from the sub-assembly allows for the monitoring of protein subunits, so that the helix is efficiently and correctly assembled. Finally, the co-operative addition of 34 protein subunits more readily overcomes the entropic disadvantage of assembly.

The T4 bacteriophage virus<sup>13</sup> is much more complex than TMV in a structural sense, consisting of a head, a tail and six tail fibres. The assembly process<sup>14</sup> (**Figure 2**) is more involved, occurring in a precise sequence, however, it is also highly convergent and only a small set of different interactions and reactions are employed. This means that a relatively small amount of information is required to encode for the whole assembly. Indeed, only 53 out of a total of 135 genes contain information

directly related to the virus construction. The assembly occurs in a strict order meaning that only correct, complete virus particles are formed. T4 does not form using strict self-assembly alone, rather by a combination of self-assembly, scaffold-assisted assembly and enzyme-directed assembly.



**Figure 2** The assembly pathway for the construction of the T4 bacteriophage.

This paradigm suggests that strict self-assembly can be combined with conventional covalent chemistry to provide a sufficient level of sophistication to create complex structures readily.

These examples illustrate the basic principles of self-assembling systems that can be exploited by the synthetic chemist.

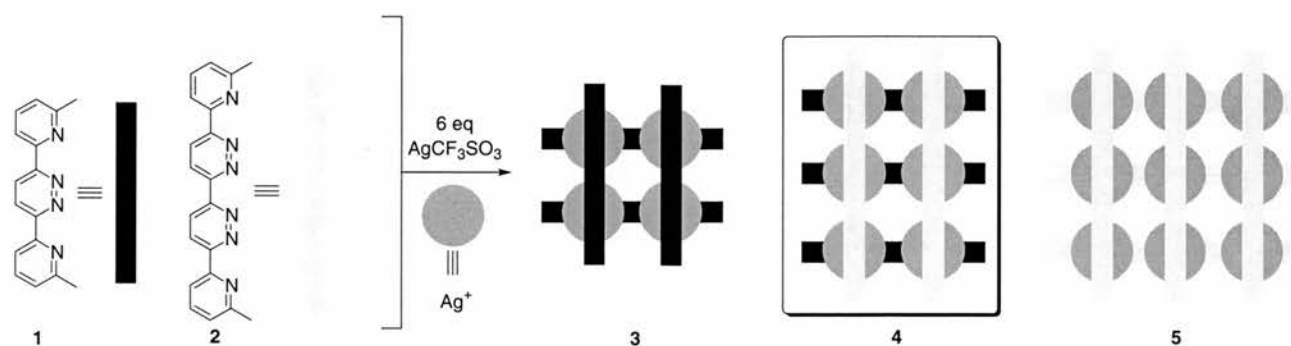
- Self-assembly processes are highly convergent, and therefore, potentially, extremely efficient.
- Simple, and often identical, subunits can be used to easily and accurately assemble large, functionally complex supermolecules.
- The amount of information required to describe a structure will be small if the number of different interactions required to construct it is small.
- Self-assembly processes generally use reversible interactions or reactions. Therefore, the assembly process is always at, or close to, dynamic equilibrium. In this situation, the synthetic pathway will be error-checking.

It is clear that biological systems construct and utilise nanoscale structures with a high degree of accuracy and efficiency. Thus, self-assembly has become the paradigm of choice for synthetic chemists wishing to construct nanoscale assemblies.

Understanding the interactions between non-covalently bonded molecules is clearly crucial to the successful design and synthesis of self-assembling wholly-synthetic structures. Thus, the science of supramolecular<sup>15</sup>, or host-guest<sup>16</sup> chemistry, has contributed significantly to the dramatic expansion of activity in the area of synthetic self-assembling systems in the last ten years. This introduction does not seek to provide comprehensive coverage of this literature, rather to discuss some important developments in the study of self-assembling systems that have been published in the last 5 years. For an overview of developments in this field prior to 1996, the reader is referred to several general review articles<sup>2</sup>.

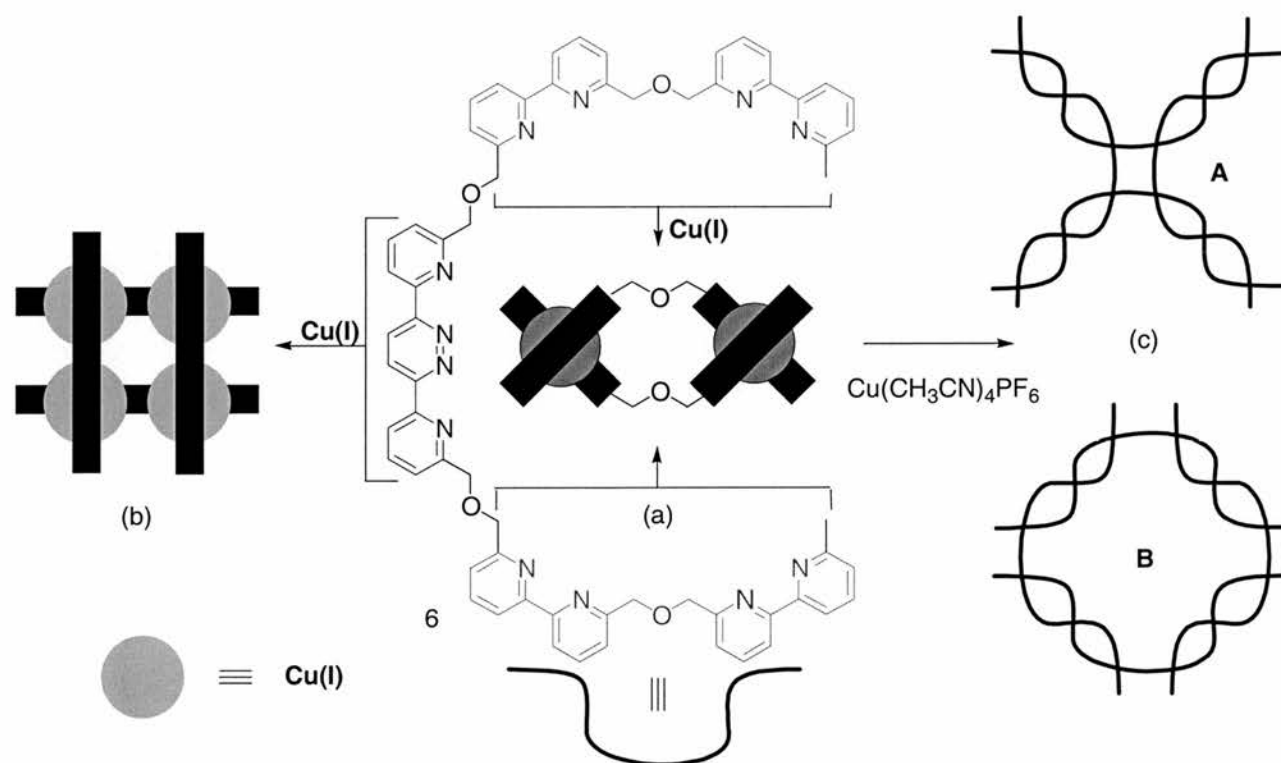
### 1.1.2 Chemical Systems – Non-Covalent Self-Assembly

Metal centres have been used extensively in self-assembly in the construction of a wide variety of structures including macrocycles,<sup>17</sup> linear<sup>18</sup> and circular<sup>19</sup> helicates, catenates,<sup>20</sup> grids<sup>21</sup>, cages<sup>22</sup>, ladders<sup>23</sup> and dendrimers<sup>24</sup>. Metal-ligand interactions are stronger than other non-covalent bonds and are highly directional. The use of metal ions in self-assembly could potentially lead to the generation of structures with interesting properties as a result of the redox or magnetic properties of the metal. These well-defined assemblies may be useful as models for the study of biological charge transport systems.<sup>25</sup> Furthermore, the preference of certain metals for specific coordination geometries provides the chemist with a basis for a more rational design approach to the synthesis<sup>2</sup> of particular architectures. Lehn and co-workers have recently constructed<sup>26</sup> rectangular grids (**Figure 3**) using a mixture of a bidentate **1** and a tridentate ligand **2** which complex Ag<sup>+</sup> ions. If the three possible grid structures, the 2x2 grid **3**, 2x3 grid **4** and the 3x3 grid **5**, form statistically, the expected ratio of **3:4:5** should be 36:46:16. However, the experimental ratio is 8:90:2. The overwhelming bias in preference of the heteroleptic grid **4** may possibly result from an active avoidance of the 3x3 grid **5** which requires the formation of the least favoured metal-ligand coordination interaction, *i.e.* the central Ag(pyridazine)<sub>4</sub> unit. It would therefore appear that both information provided by the ligand structure and the metal ion geometry are responsible for the formation of a single structure.



**Figure 3** The  $\text{Ag}^+$ -mediated self-assembly of a  $2 \times 3$  grid.

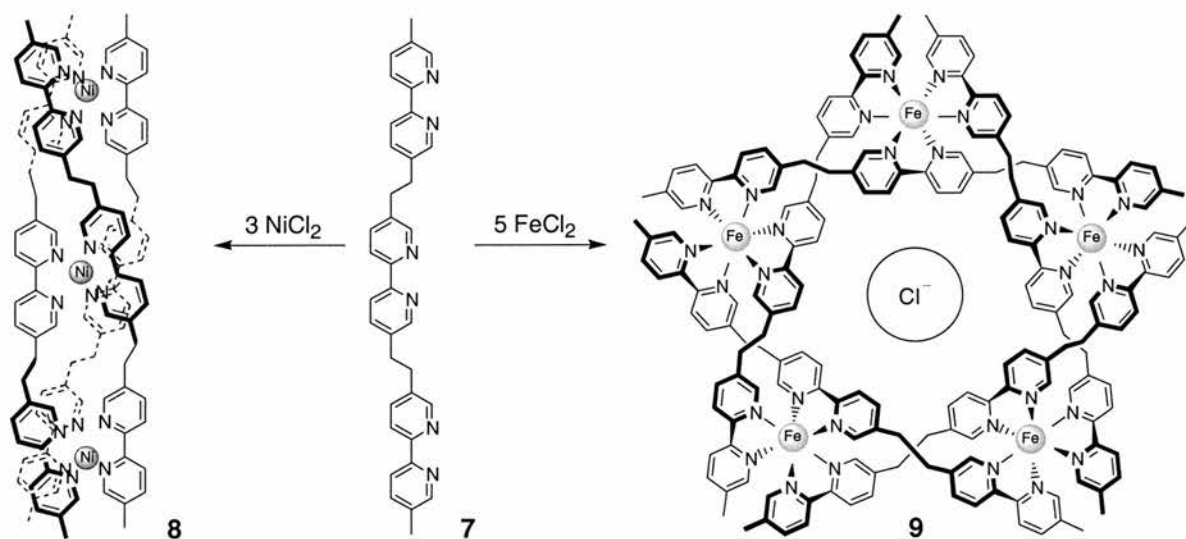
Lehn and co-workers have also investigated<sup>27</sup> the outcome of the integration of opposing programs, or subroutines – *i.e.* does the resulting architecture arise from the linear combination of the two subroutines, or from a more complex convolution of instructions, each subroutine clashing with the other? In order to answer this question, they designed the ligand **6** (**Figure 4**).



**Figure 4** The bipyridine ligands (a) encode a helical structure and the pyridylpyridazine ligand (b) encodes a grid structure. (c) Combination of these two subroutines can give either structure **A** (linear combination) or structure **B** (more complex convolution).

This ligand contains both a bis(bipyridine) ligand (**Figure 4a**) and a bis(pyridylpyridazine) ligand (**Figure 4b**). In isolation, the bis(bipyridine) ligand forms

a double helical structure (**Figure 4a**) with Cu(I) cations and the bis(pyridylpyridazine) ligand a square 2 x 2 grid (**Figure 4b**). Complete solution phase characterisation of the product of a copper (I) mediated self-assembly process involving four molecules of ligand **6** and twelve Cu(I) cations suggests the complex produced has either geometry **A** or **B** (**Figure 4c**). Structure **A** might be the expected product since it is the result of a linear combination of the two subroutines. Structure **B** would be the result of a more complicated combination of possible coordination geometries. Crystal structure solution demonstrated that the assembly process had, in fact, afforded structure **B**. Thus, for this case at least, the combination of the two different sub-routines produces a product which arises from a convoluted interaction between the two instruction sets and, hence, forms a novel structure. Self-assembly processes generally result in the formation of the thermodynamically most stable product. However, interesting recent work by Lehn and co-workers has shown<sup>28</sup> that the kinetic products may be formed as “intermediate” species on the pathway to the final assembly. The tris(bipyridine) ligand **7** (**Figure 5**) forms<sup>29</sup> a *linear triple* helicate **8** on the addition of Ni<sup>2+</sup> cations. However, the same ligand forms a *circular* helicate **9** when it complexes Fe<sup>2+</sup> cations, despite the fact that both these metals favour the same coordination geometry.

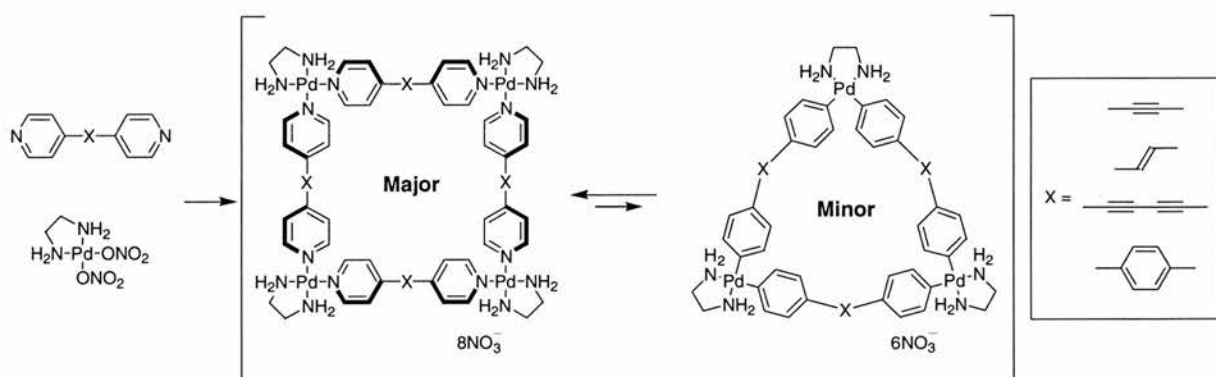


**Figure 5** Circular helicate **9** is the thermodynamic product of an assembly process which involves linear helicate **8** as an intermediate.

However, when the formation of the Fe(II) complex is monitored by NMR spectroscopy, the formation of the Fe(II) analogue of the linear triple helicate **8** can be detected. Indeed, this species, which is the kinetic product, formed fully in less

than one minute. This assembly process is reversible, and a partial disassembly allows the formation of the thermodynamic product – the circular helicate **9**. From these results, it appears that linear triple helicate **8** may represent a local minimum<sup>30</sup> on the energy hypersurface for the reaction when Fe(II) cations are used, although it is not immediately obvious why the circular helicate **9** should be the thermodynamic product in this case. A plausible explanation, however, is that it is stabilised by the electrostatic interaction with the bound counter anion (Cl<sup>-</sup>).

Many groups have studied<sup>31</sup> the self-assembly of macrocyclic receptors which employ metal cations to direct the assembly. Macrocyclisation under kinetic control is an unfavourable process, but the construction<sup>32</sup> of products of this kind is possible under thermodynamic control. These receptors may show new and interesting properties due to the inclusion of the metal ions in the structure. Fujita and co-workers have demonstrated (**Figure 6**) the assembly of square Pd- or Pt-linked complexes through use of appropriately protected Pd or Pt building blocks and ligands with a linear geometry. They note<sup>33</sup> that an equilibrium exists between a square and a triangular complex. Interestingly, Hong *et al.* found<sup>34</sup> it is possible to bias the equilibrium in favour of either complex by the addition of an appropriate guest. A large guest favours the square complex and a small guest the triangular complex.

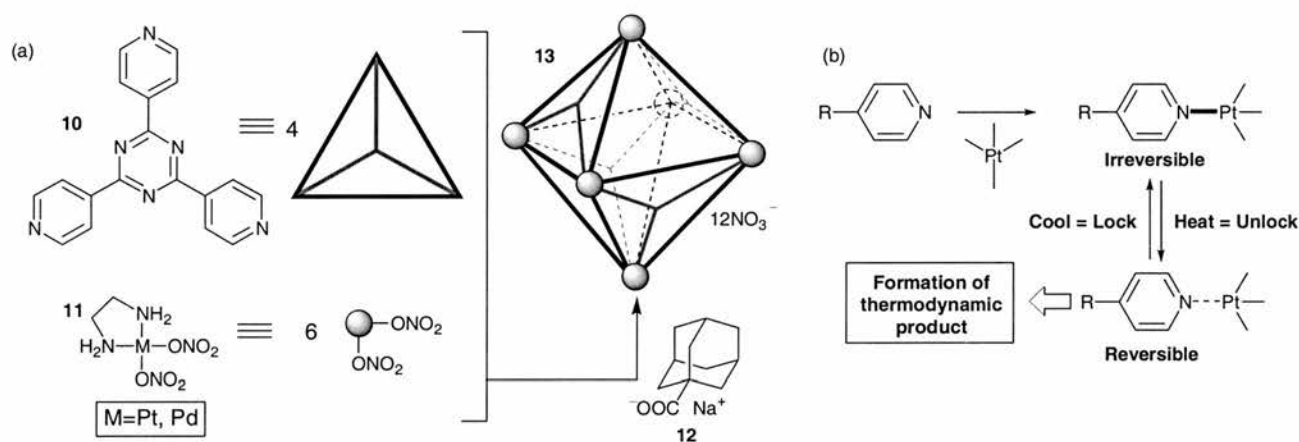


**Figure 6** The coordination geometry around the Pd centre encodes either a square (major product) or a triangular (minor product) complex.

Fujita and co-workers have also demonstrated<sup>35</sup> an interesting guest-templated self-assembly of a receptor molecule (**Figure 7a**). Ligand **10** and metal complex **11** react in the presence of the sodium salt of adamantane carboxylic acid **12**, a large guest, to form a molecular cage **13** containing ten separate molecular components –



four tridentate ligands and six metal centres. When the metal centre is Pd(II), the nanocage forms readily and reversibly. However, when Pt(II) is used, formation of the nanocage is hampered by the extremely slow exchange of the ligand sphere around the metal centre. Nonetheless, this slow exchange of the Pt(II)-pyridine coordinate bond can be used as a switchable lock (**Figure 7b**). Usually kinetically inert, the Pt-N bond becomes labile when heated to 100°C, and formation of the cage molecule can then be templated by sodium adamantancarboxylate. However, unlike many other templated receptors, once the heat source is removed the template could also be removed without destroying the receptor, since the inert Pt-pyridine bonds lock the cage molecule.

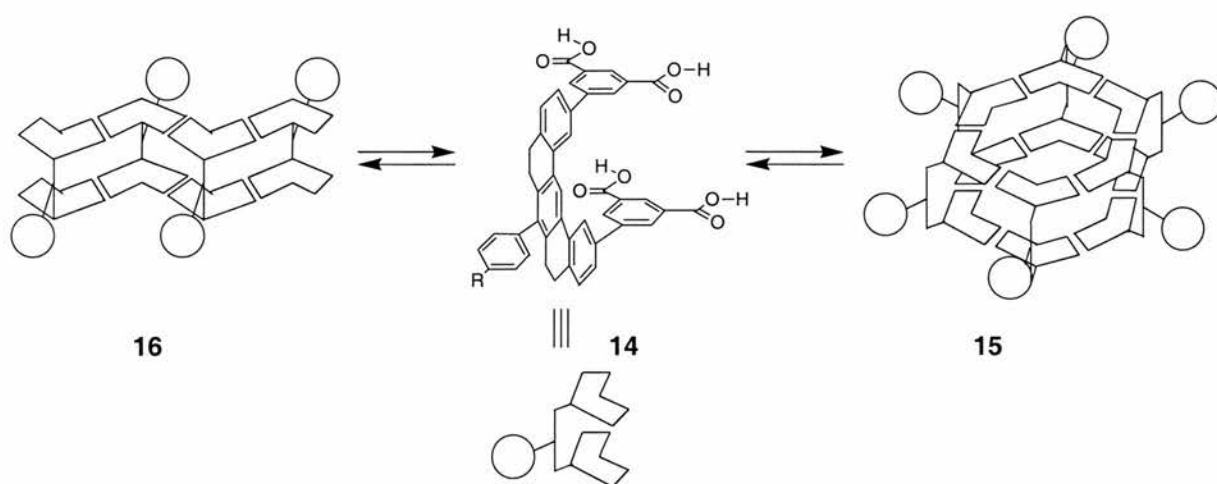


**Figure 7** (a) A combination of tridentate ligand **10** and a square planar metal centre **11** affords the octahedral cage **13**. (b) The formation of the thermodynamic product can be assured by using heating and cooling as a method to unlock and lock the Pt-N coordinate bond.

The nanocage constructed in this manner is extremely stable. The cage remains intact from pH 1 to pH 11 at room temperature and acid (HNO<sub>3</sub>), base (K<sub>2</sub>CO<sub>3</sub>) and even a good nucleophile (NEt<sub>3</sub>) can be added to a solution containing the cage with no ill effects to the cage structure. Fujita and co-workers have also used the same metal complex with different pyridine-based ligands to demonstrate<sup>36</sup> that the equilibration between a series of similar receptors can be biased by addition of appropriate templates that stabilise a particular receptor.

Hydrogen bonding interactions, with their strength, specificity and directionality, are also widely used in self-assembly of complex structures<sup>37</sup> from 'programmed' sub-units. In 1996, Zimmerman and co-workers described<sup>38</sup> the use of the hydrogen bonded carboxylic acid dimer motif in the self-assembly (**Figure 8**) of hexameric

dendritic structures. The self-assembly of dendrimers represents a way of synthetically generating species with molecular weights approaching those of proteins. Covalent synthesis under kinetic control rarely results in the generation of materials with nanoscale dimensions. The monomer unit **14** contains two isophthalic acid groups connected by a rigid aromatic spacer, on to which is also attached a poly(phenylether) dendritic wedge. On assembly, the monomer can form a cyclic hexamer **15** or a range of linear oligomers **16**, which are expected to be disfavoured enthalpically since they do not contain the maximum number of hydrogen bonds possible.



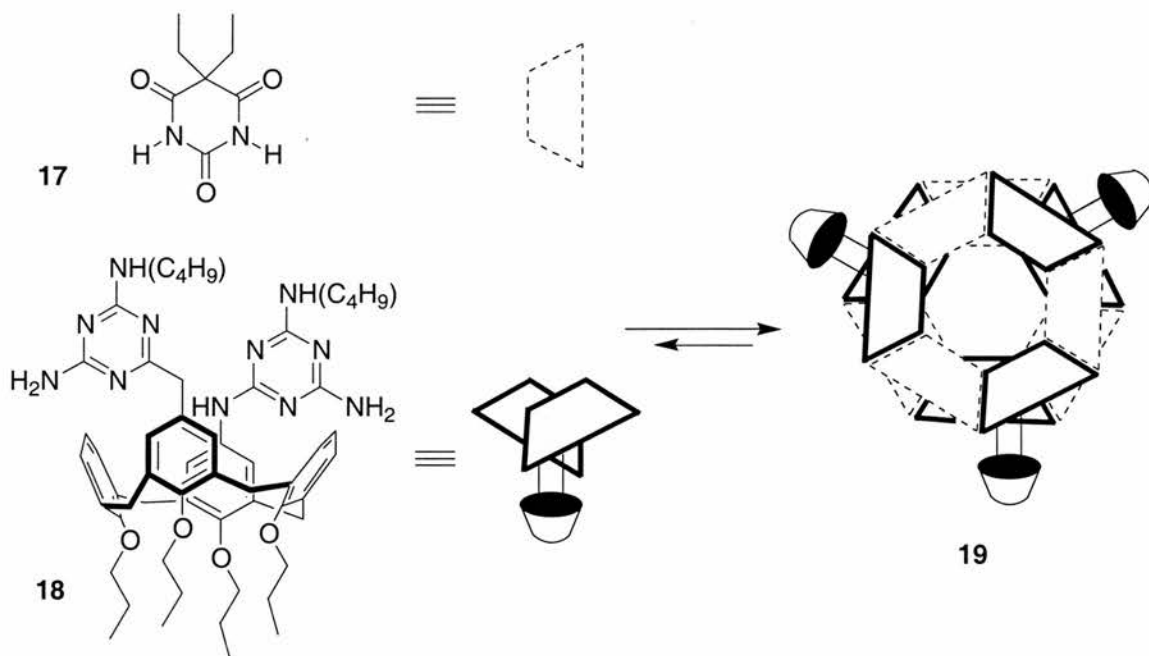
**Figure 8** Monomer **14** can self-assemble through the formation of hydrogen bonded carboxylic acid dimers into either a linear **16** or hexagonal **15** superstructure. The substituent R is an aromatic ether dendritic wedge and has been omitted for clarity.

$^1\text{H}$  NMR spectroscopy in apolar solvents shows broad signals due to aggregation, and size exclusion chromatography (SEC) suggests the formation of a discrete cyclic hexamer. In polar solvents, which disrupt the hydrogen bonding, NMR and SEC both give evidence for the existence of monomers. The stability of the hexamer appears to be generation dependent, *i.e.* smaller monomers (those with lower generation dendrimers attached) are more likely to exist as linear oligomers. The distance between adjacent dendrimer attachment points is smaller in the linear oligomers than in the cyclic hexamer and larger, rigid dendrimer substituents cannot be accommodated. This suggestion is backed up by the observation that a more flexible dendrimer substituent, although a similar size to the larger rigid dendrimers, does not form the cyclic hexamer in preference to linear oligomers. Molecular modelling suggests that several aromatic rings on adjacent dendrimer units are very close. It



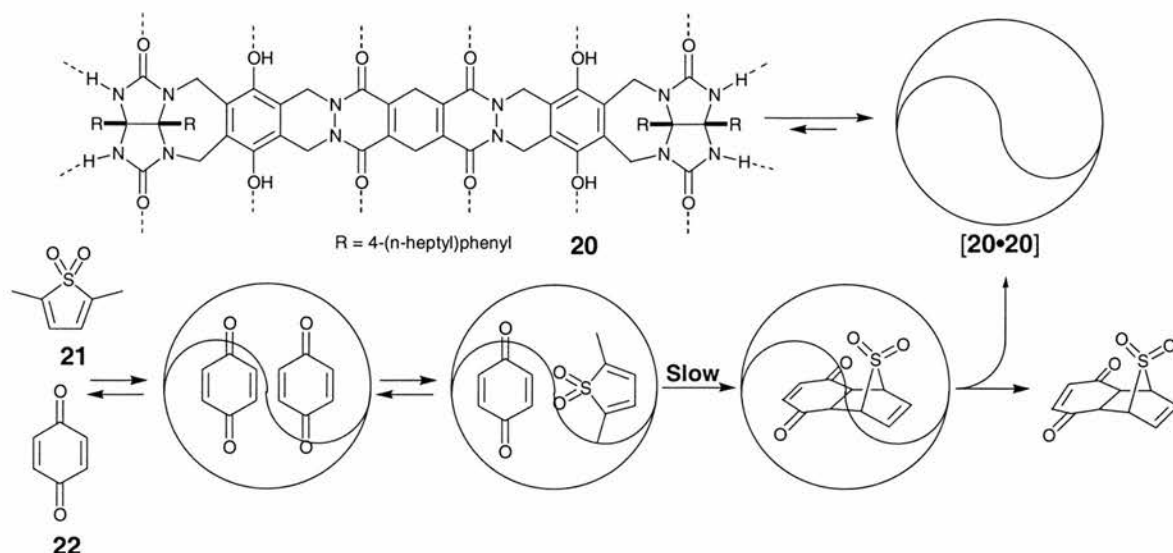
seems that there is a subtle and unpredictable balance between the influence of favourable van der Waals contacts and hydrogen bonds, and unfavourable steric repulsions. Later work by Zimmerman and co-workers<sup>39</sup> on the self-assembly of dendrimers, employed the complementary triple hydrogen bond motifs DDA and AAD. Self-assembly resulted in the formation of a highly stable, hexameric dendritic aggregate, demonstrating the unambiguous information content of this motif.

The network of complementary hydrogen bonds formed between melamine and cyanuric acid has been exploited by Reinhoudt and co-workers (**Figure 9**) to construct<sup>40</sup> self-assembling molecular boxes based on calix[4]arenes. In  $\text{CDCl}_3$  solution, diethylbarbiturate **17** assembles with the calix[4]arene **18** bearing two melamine residues. The formation of the classic<sup>41</sup> melamine•barbiturate rosette structure affords the molecular box **19**. This assembly possesses a double layer rosette structure with the two layers spaced apart by the calix[4]arene bowls. It is these calix[4]arenes which serve to preorganise the hydrogen bonding groups facilitating the formation of the final assembly. This methodology has been extended to allow<sup>42</sup> covalent capture of the assemblies and the construction<sup>43</sup> of rod-like hydrogen-bonded nanostructures.



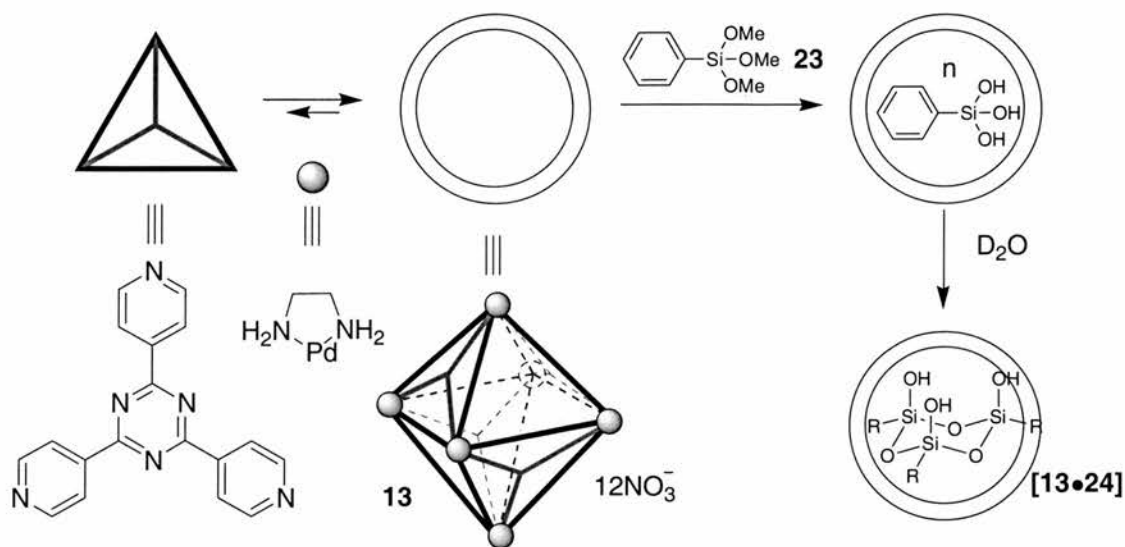
**Figure 9** Self-assembly of a double rosette superstructure through the interaction, mediated by hydrogen bonds, of barbiturate **17** with melamine derivative **18**.

Recently, reports concerning self-assembling capsules that can bind solvent or other guests inside a cavity have begun to appear. Rebek and co-workers have synthesised molecules that are capable of dimerisation through hydrogen bonding to form capsules.<sup>44</sup> The capsule formation may be templated by the incorporation of solvent molecules in the cavity.<sup>45</sup> Enclathration of a single large guest molecule (*e.g.* adamantane or ferrocene derivatives), however, is entropically favoured since it results in the release of several solvent molecules from the capsule.<sup>46</sup> The monomer **20** (**Figure 10**) is self-complementary and will form a hydrogen-bonded dimer [20•20], termed a softball, in solution. It was noted that the capsule readily encapsulates two molecules of benzene, and this raised the possibility of using the capsule as a chamber for a bimolecular reaction. Using these methods it is possible to construct systems which are capable of binding multiple guests and a reaction between the included guests may be accelerated within the capsule. Thus, Rebek and co-workers have used a self-assembled capsule to bind *p*-benzoquinone and cyclohexadiene and observed<sup>47</sup> significant rate enhancement, but not true catalysis, of the Diels-Alder reaction between them. In later work, it was envisaged<sup>48</sup> that the use of 2,5-dimethylthiophene-*S,S*-dioxide **21** as the diene would permit turnover through the aromatisation and loss of SO<sub>2</sub> from the cycloadduct formed between **21** and *p*-benzoquinone **22**. The softball does indeed catalyse the reaction between **21** and **22**, but for quite different reasons. The softball [20•20] shows relatively high affinity for quinone **22**, but no measurable affinity for the diene **21**. This observation led Rebek and co-workers to propose the catalytic cycle for the reaction shown in **Figure 10**. In the resting state, [20•20] contains two molecules of *p*-benzoquinone. Occasionally, one of the molecules of **22** is displaced by **21** to give the catalytically active complex. A moderately accelerated cycloaddition between **21** and **22** is followed by the ejection of the cycloadduct from the cavity of [20•20] and regeneration of the resting state complex. Analysis of kinetic data indicates that the reaction between **21** and **22** is accelerated by around an order of magnitude within the cavity of [21•22].



**Figure 10** Self-association of the cyclic bisurea derivative **20** through eight hydrogen bonds gives a structure which resembles a softball. (Points of interaction are indicated by the dashed lines.) The capsule is capable of catalysing the Diels-Alder reaction between **21** and **22**.

Fujita and co-workers have also reported<sup>49</sup> the use of a molecular capsule in the synthesis (**Figure 11**) of otherwise highly-labile cyclic trisilanol trimers and tetramers. Polycondensation of trialkoxysilanes, such as phenyltrimethoxysilane **23**, usually generates cyclic trimer **24** as a short-lived intermediate which transforms rapidly<sup>50</sup> into more thermodynamically stable oligomers. However, when the condensation reaction is carried out in the presence<sup>51</sup> of the self-assembled nanocage **13** (**Figure 11**) the pure hepta-hydrated complex [**13•24**] is readily isolated and found to be extremely stable. Furthermore, the reaction exhibits strong stereochemical control, with only the all-*cis* isomer being formed. This synthesis has been described<sup>52</sup> as “ship-in-a-bottle” synthesis, since the trialkoxysilanes can readily enter the capsule, but cannot exit from the capsule once reacted to form the larger trimer. Further work investigated the efficacy of the same self-assembled nanocage **13** as a phase transfer catalyst. **13** is highly soluble in water and also binds organic molecules well. It has been shown<sup>53</sup> that, with a Pd(II) co-catalyst, the nanocage catalyses the aerobic, aqueous oxidation of styrene to acetophenone, a reaction which does not occur in the absence of the cage.



**Figure 11** Stereoselective synthesis of the unstable trisilanol **24** occurs inside the cavity of the octahedral cage **13**.

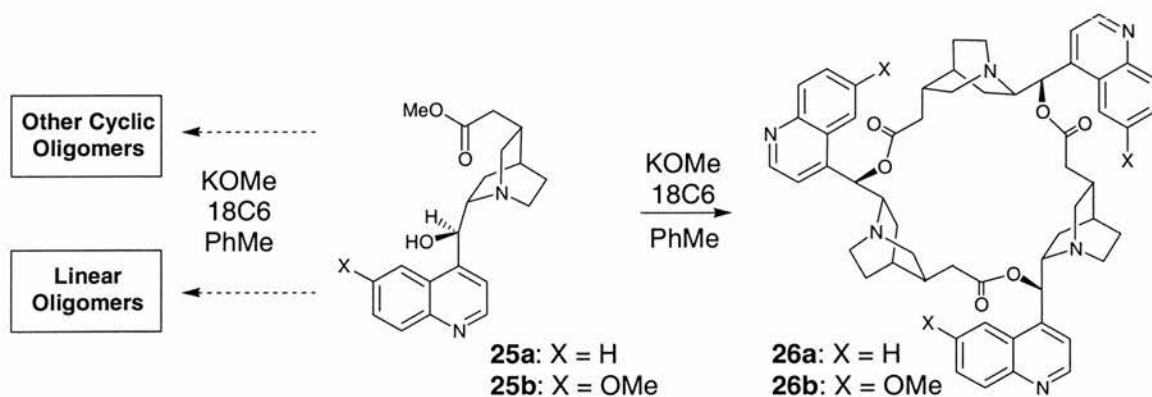
Several elegant examples of self-assembling capsules have also been reported<sup>54</sup> by Böhmer and co-workers. These capsules are based on calix[4]arene skeletons with urea groups on their upper rims. Self-recognition of the ureas then drives the formation of capsule dimers in non-polar solvents. Extensive NMR studies have probed the reversible dimerisation of these calix[4]arenes and the exchange of the small guests, such as benzene, included within the capsule cavities has been studied. A similar approach has led to the synthesis<sup>55</sup> of larger calixarene-based capsule by de Mendoza and co-workers.

### 1.1.3 Self-Assembly using Covalent Bonds

One major disadvantage of the use of non-covalent bonds in self-assembly is that non-covalent interactions are relatively weak. They are used to direct the formation of the structure, but also to stabilise the final product structure, and, hence, many interactions are needed to offset the unfavourable entropy arising from the association of several molecules. The prototypical example of this phenomenon is the formation<sup>56</sup> of the DNA double helix. This process proceeds by an essentially “all-or-nothing” mechanism and consists of two phases – nucleation and propagation. The nucleus is the shortest double strand for which the free energy of base pairing is negative. Formation of these first four base pairs is entropically disfavoured, but this unfavourable step is overcome by the negative free energy contribution of the many subsequent base-pairing interactions.

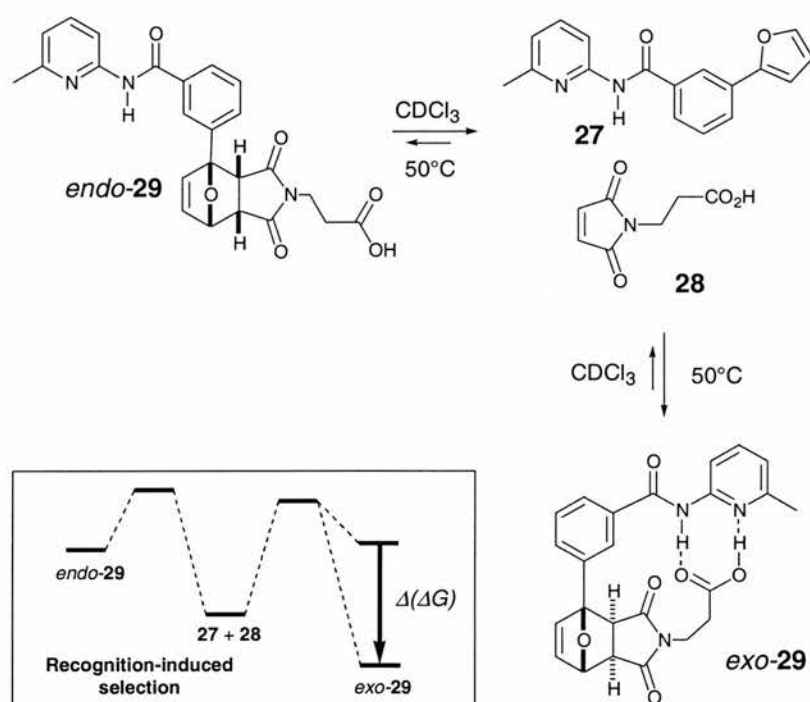
This problem can potentially be overcome by the use of covalent bonds to direct the assembly. Covalent interactions are significantly stronger than non-covalent bonds, so fewer stable bonds are required to offset the unfavourable entropy of self-assembly. In order to retain all the advantages of a non-covalent self-assembly process, however, we still require that the covalent bonds should form under thermodynamic control, *i.e.* their formation must be reversible. Covalent self-assembly has, so far, been relatively underexploited, possibly since examples of covalent bonds whose formation is reversible, which include imine, disulfide, alkene, carboxylate ester and borate ester linkages, are somewhat limited.

Sanders and co-workers have investigated<sup>57</sup> the use of transesterification as the source of reversible covalent chemistry in the synthesis of macrocycles from the methyl esters of quinine and cinchonidine alkaloids. Macrocyclisation under thermodynamic conditions was carried out in refluxing toluene, using a mixture of KOMe and 18-crown-6 as a transesterification catalyst, with azeotropic removal of methanol. Despite the fact that many cyclic and acyclic oligomers are possible, when monomers **25a** and **25b** (Figure 12) are subjected to these conditions, the transesterification process affords almost exclusively the cyclic trimers **26a** and **26b**. These results contradict theoretical predictions which suggest<sup>58</sup> a wide range of oligomers should be observed. It can be demonstrated that the reaction is indeed under thermodynamic control by re-subjecting a single pure cyclic oligomer to transesterification. Within minutes, the original distribution of products has been re-established.



**Figure 12** Monomers **25a** and **25b** are predisposed to form the cyclic trimers **26a** and **26b** respectively.

Cyclisations of synthetic linear oligomers were also carried out<sup>59</sup> under kinetic conditions, in order to prove that there was no kinetic barrier to the formation of cyclic oligomers other than the trimer. In this case, theory predicts the formation of a wide range of oligomers, with the smallest ring size as the predominant species. In practice, all oligomers up to the octamer are shown to be kinetically accessible, with the exception of the dimer, which is apparently too strained to exist. NMR spectroscopic studies show that the conformation of the cinchona alkaloid derived building block is altered on cyclisation, suggesting that the monomer is not *preorganised* to form the trimer, rather that it is *predisposed*. Constable first used<sup>60</sup> the term “predisposed”, in describing ligands that adopt<sup>61</sup> a helical conformation on complexation to a metal centre, but which are not necessarily helical in the free state. This term is distinguished from “preorganisation” which he uses to describe ligands<sup>62</sup> which are already in a helical conformation.

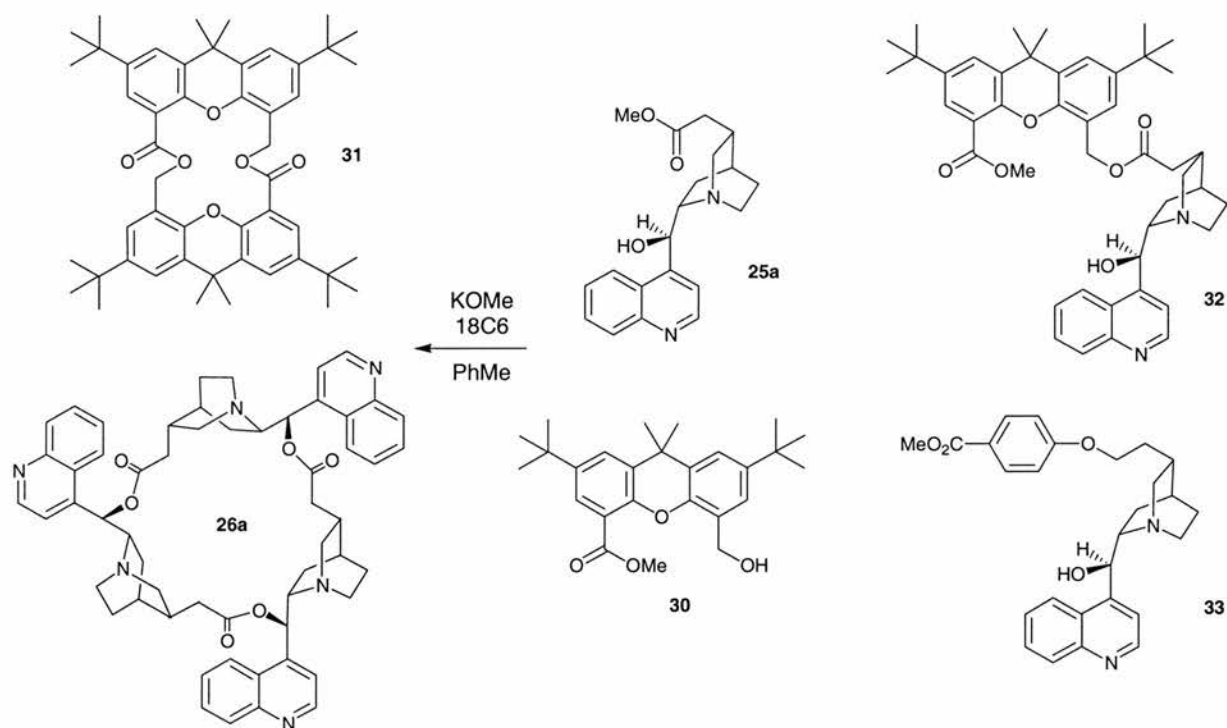


**Figure 13** The formation of two intramolecular hydrogen bonds in *exo-29* predisposes the system to form this cycloadduct exclusively. The presence of these intramolecular hydrogen bonds is confirmed by X-ray crystallography.

A simple example of predisposition can be found in a recognition-based approach<sup>63</sup> to the acceleration and facilitation of cycloaddition reactions. 2-Phenylfuran derivatives are extremely poor dienes since they possess a high level of conjugation that is destroyed during a Diels-Alder reaction. However, the location<sup>64</sup> of



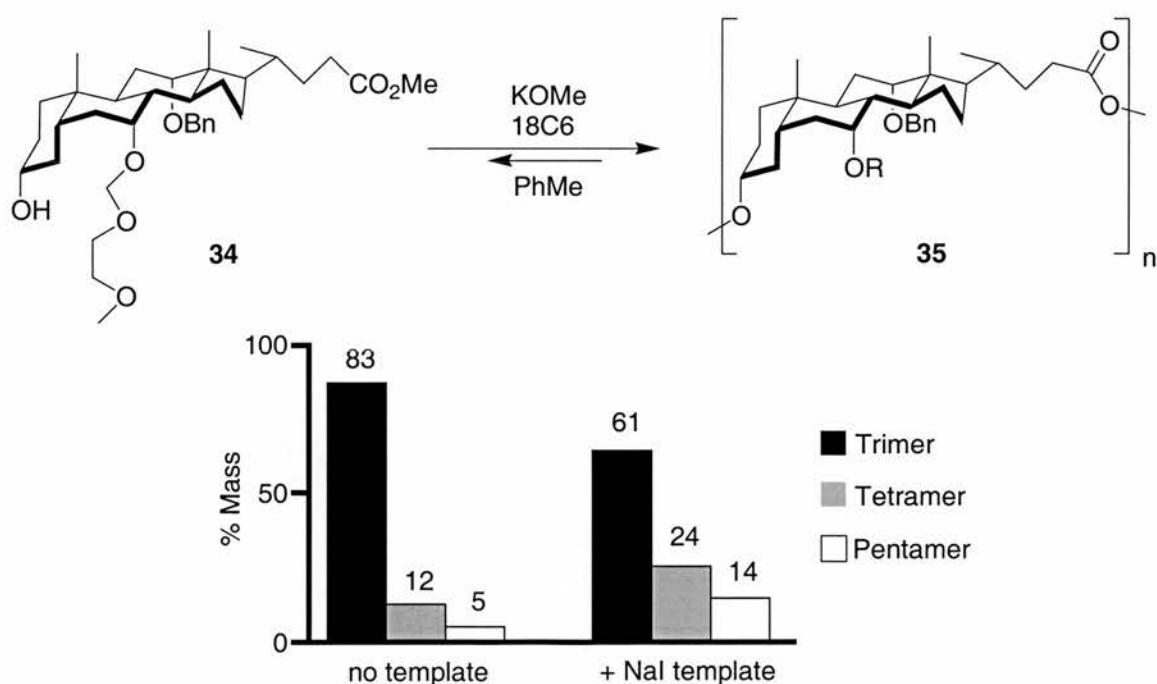
complementary recognition sites on the 2-phenylfuran derivative **27** and maleimide **28** (**Figure 13**) allows the formation of a **[27•28]** complex, rendering the reaction between **27** and **28** pseudointramolecular. Although the reaction within this complex is accelerated<sup>65</sup> with respect to the bimolecular process, a more important effect is selective stabilisation of the *exo*-**29** product ground state. The two intramolecular hydrogen bonds that are present in *exo*-**29**, but not in *endo*-**29** predispose the system to form only *exo*-**29**. The importance of the intramolecular hydrogen bonds ( $\Delta(\Delta G)$ , **Figure 13**) to the overall stability in this system can be readily demonstrated by the fact that the retro Diels-Alder reaction is rapid in  $d_6$ -DMSO, which disrupts the hydrogen bonds in *exo*-**29**. This system is an example of *predisposition*, which can best be described as a strong conformational or structural preference expressed by the product of a reaction and is therefore a thermodynamic effect, as opposed to preorganisation, which is a kinetic effect.



**Figure 14** Monomers **25a** and **30** self-sort under transesterification conditions affording the cyclic trimer **26a** and the cyclic dimer **31** respectively.

Sanders and co-workers have also synthesised<sup>66</sup> a xanthene monomer **30** (**Figure 14**) which is extremely rigid and is strongly preorganised to give only the cyclic dimer. When the xanthene monomer **30** and cinchonidine monomer **25a** are mixed and subjected to transesterification conditions, self-sorting is observed. That

is, predominantly the cinchonidine trimer **26a** and the xanthene dimer **31** are observed, although there is apparently no kinetic barrier to the formation of hetero-products, such as **32**. This process is essentially a covalent analogue of the self-sorting metal-based double and triple helices reported<sup>67</sup> by Lehn. The synthesis<sup>68</sup> of an extended monomer **33**, which differs from the original cinchonidine monomer **25a** only by the addition of a spacer group, is aimed at the creation of a thermodynamic combinatorial library, which will be discussed in more detail later. The extended monomer **33** is more flexible and this leads to a relaxation of predisposition on cyclisation. Similar experiments can be carried out<sup>69</sup> using cholate monomers **34**, which are more flexible than the cinchonidine monomers. In this case, the cyclisation is complete after 10 minutes and the distribution of cyclic oligocholates **35** is wider than for the cinchonidine monomer – still containing mainly trimer, but also tetramer and a small amount of dimer and pentamer. This distribution can be biased<sup>70</sup> by the addition of sodium ions, which cause a 100% increase in the amount of tetramer obtained. The equilibrium shift reflects the relative abilities of the oligomers to bind certain metal ions.



**Figure 15** Cholic acid derivative **34** forms a range of cyclic oligocholates **35** under thermodynamic control. The position of the equilibrium can be altered by the addition of a metal template.



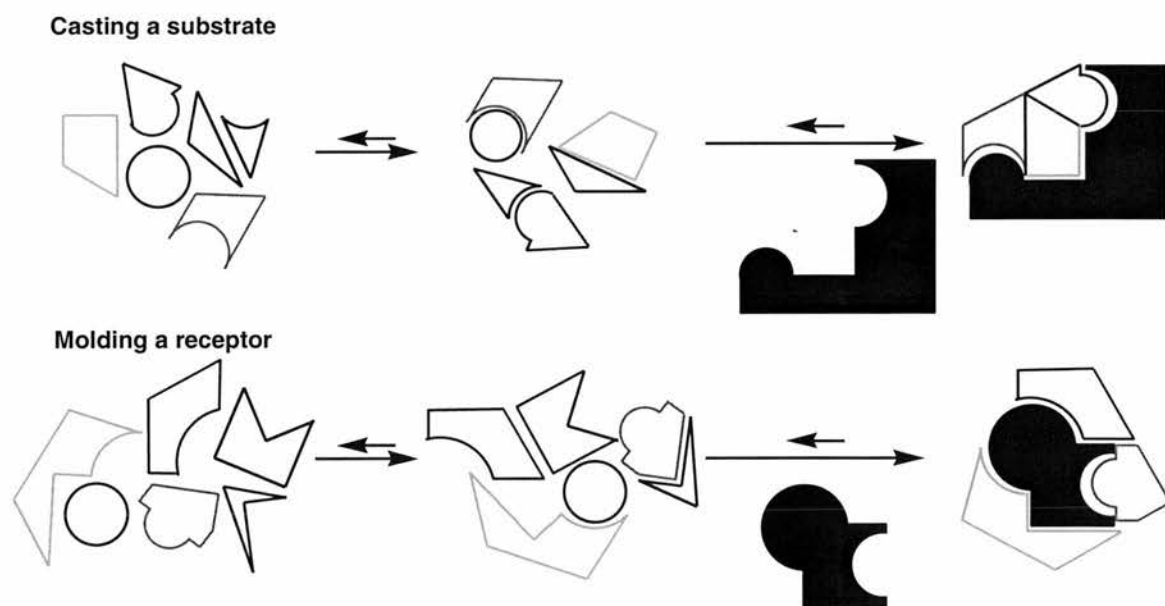
Ipaktschi and co-workers have developed<sup>71</sup> a method for the synthesis of large macrocycles based on the covalent self-assembly of quinodimethane derivatives. The monomer unit spontaneously self-assembles to form a spherical, cyclic tetramer. The macrocyclisation process is driven by the reversible formation of four weak carbon-carbon bonds. Any errors in the cyclisation process can be reversed and corrected. They also report the synthesis of further functionalised quinodimethane derivatives, which can be utilised in the preparation of a self-assembling dendrimer and a macrocycle with ferrocene units at the periphery of the molecule. The addition of such large substituents did not hinder the cyclisation process.

Protein structures are often stabilised through the reversible formation of a disulfide bridge and this thiol-disulfide interconversion involves forming strong, covalent S-S bonds at room temperature. Chang and co-workers have exploited<sup>72</sup> this principle to improve the thermodynamic stability of a tris(sulfide). The monomer thiol groups are preorganised in a conformation that resembles those adopted by the disulfides in the dimer, thus reducing the unfavourable entropy change on dimerisation.

#### 1.1.4 Dynamic Combinatorial Libraries

Combinatorial chemistry<sup>73</sup> is a rapidly growing field allowing the fast synthesis of a large number of potentially useful compounds, followed by separate screening for active compounds. The library is prepared using irreversible covalent chemistry, and a method for the screening of each component of the library must be developed. The generation<sup>74</sup> of dynamic combinatorial libraries (DCLs), utilising the formation of reversible covalent or non-covalent bonds, is a more recent development that represents a logical extension of the chemistry described in the previous section. Reaction of an initial component set potentially leads to the creation of a highly diverse array of products. However, since all these reactions are under thermodynamic control, the final product distribution will be influenced by the relative thermodynamic stability of each product. Whereas static combinatorial chemistry does not allow for any post-synthetic transformations, a dynamic combinatorial library can be biased by the addition of different receptors or templates.<sup>75</sup> Indeed, some components of the library may not exist in significant amounts in the absence of a suitable binding partner<sup>76</sup>, hence the description<sup>77</sup> of this process as a virtual combinatorial library. Once a receptor is bound to a particular library member, the equilibrium will tend to shift in favour of that component in order to maintain the

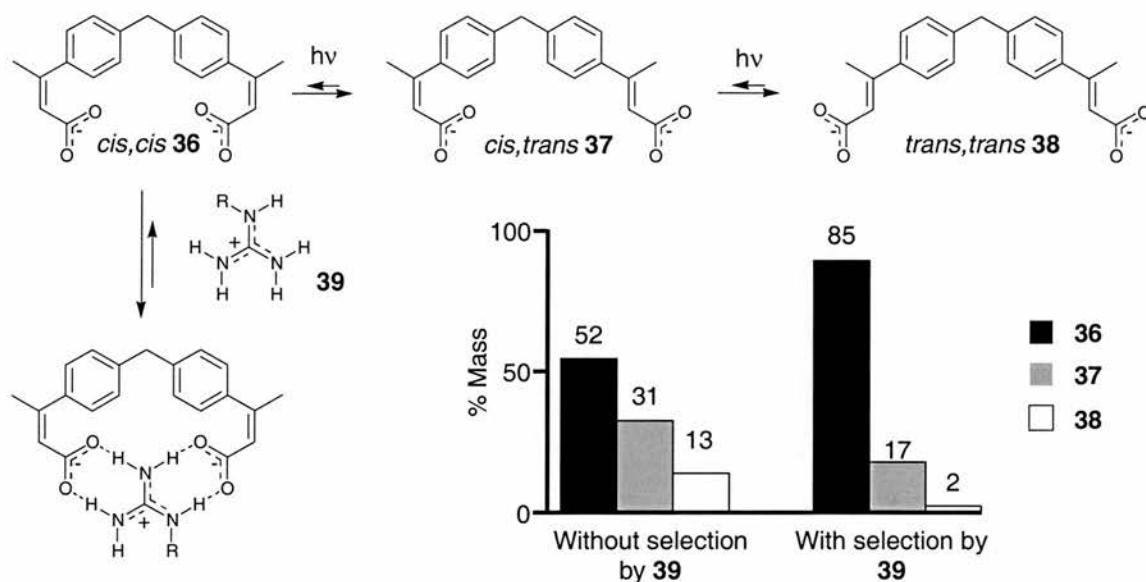
equilibrium. Thus, it is possible to select from the library the structure most suitable for the task for which it is required. Theoretically, it may even be possible to reduce the library to a single component, making isolation of the active species simple. Furthermore, the equilibrium population may be fixed by performing an irreversible covalent conversion. Dynamic combinatorial chemistry has also been described in the literature as molecular evolution, targeted equilibrium shifting, thermodynamic templating, receptor-driven ligand evolution and adaptive chemistry. The relevance of this approach to the efficient generation of receptors, substrates, catalysts and other substrate-specific reagents has already been demonstrated. The target driven assembly of and selection from a virtual combinatorial library may proceed along one of two courses – molding or casting (**Figure 16**). Both of these processes employ the reversible combination of a constituent set, generating a potentially large library, followed by the recognition led selection of a particular product. However, they differ in the nature of the template used. Molding describes the directed assembly of the best receptor for a target substrate – using the substrate as an exo-receptor. Casting utilises a target receptor to direct the assembly of the optimal substrate from the virtual substrate library – using the target as an endo-receptor.



**Figure 16** Applications of dynamic combinatorial libraries – molding a receptor and casting a substrate.

Eliseev and Nelen reported<sup>78</sup> one of the first examples of targeted equilibrium shifting in 1997. Their system (**Figure 17**), designed to select an anionic receptor for

arginine, was based on the photochemical interconversion of the three isomeric forms of an unsaturated dicarboxylate.

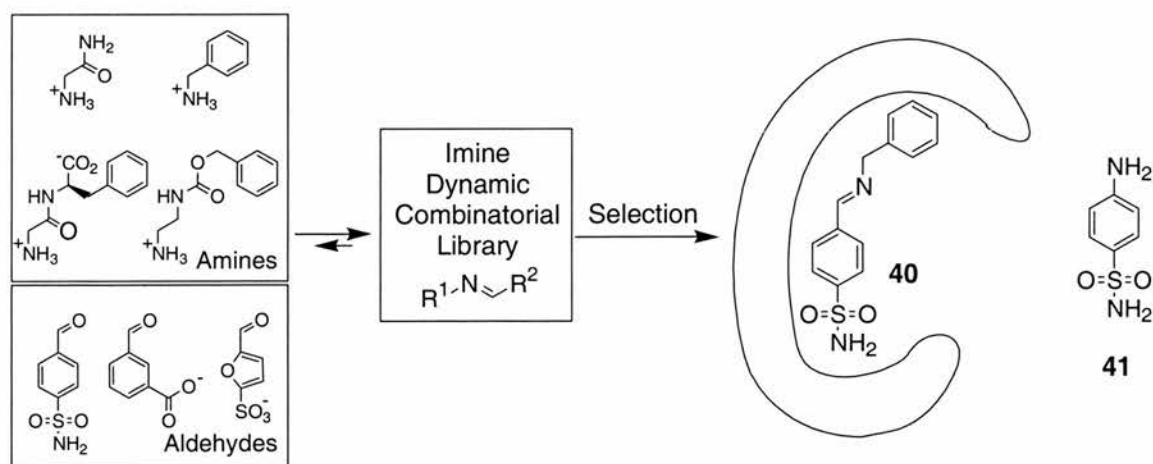


**Figure 17** Dynamic equilibrium shifting in action. Irradiation and complexation with a polymer-bound (R) guanidinium salt **39** shifts the equilibrium distribution of double bond stereochemistry strongly towards *cis-cis* **36**.

Binding constant determination in ethanol showed that, as expected, the *cis,cis* isomer **36** was ideal for binding methyl guanidinium hydrochloride, whereas the *cis,trans* **37** and *trans,trans* **38** isomers showed much weaker binding. Execution of the equilibration and binding experiment was effected using a two-chamber system. Ultra-violet irradiation of the receptor results in the formation of a distribution of isomers (**36:37:38** = 3:28:69) which is then passed through an affinity column consisting of the arginine substrate bound to a silica gel support. The *cis,cis* isomer **36** binds to the arginine **39** and is retained on the column. The remaining mixture, which is now depleted in **36**, is then passed back through the irradiation chamber, in order to regenerate the initial distribution of isomers. After 8 hours (30 mutation/selection cycles) the bound receptor is washed from the affinity column. The ratio of **36:37:38** is now 85:13:2. When the isomer is subjected to an 8 hour irradiation in the presence of the arginine column, but *without* the selection cycles, the ratio is found to be 52:31:17. This observation suggests that the concentration increase of the *cis,cis* isomer **36** observed during the 30 cycles is largely a result of the selection and amplification of that isomer by the immobilised arginine. Eliseev believes<sup>79</sup> that the physical separation of the equilibrium and binding sites will

eliminate any problems associated with possible side-reactions/binding events when the target compound is also present in the mixture. This example, as for many other early examples<sup>80</sup> of dynamic combinatorial chemistry, relied on prior identification of a suitable receptor for a specific target, followed by the generation of a very small set of components.

More recent illustrations of chemical evolution<sup>81</sup> show the practical potential with a larger reactant library. In 1997, Lehn and Huc reported<sup>82</sup> the application of dynamic combinatorial chemistry to the recognition-directed assembly of carbonic anhydrase II (CA) inhibitors (**Figure 18**). Formation of imines by the reversible reaction of aldehydes and amines was chosen as a suitable reaction for generating the library, since it is fast and takes place at physiological pH and temperature. Furthermore, reduction of the imines with  $\text{NaBH}_3\text{CN}$  allows easy product fixing, isolation and analysis. In the presence of CA, it is expected that the distribution of imines formed will mirror their strength of binding to the enzyme active site. Several aldehydes and amines with similar reactivity were reacted both in the presence and absence of CA. In the absence of CA, a mixture of 15 reduction products and 4 starting amines was isolated. In the presence of CA, the overall yield of amination is lower, but the imine proportions were biased in favour of those with the highest affinity for the CA active site. The enzyme induced some selectivity for one particular imine **40**, the structure of which is similar to that of known sulfonamide inhibitors, such as **41**.<sup>83</sup>

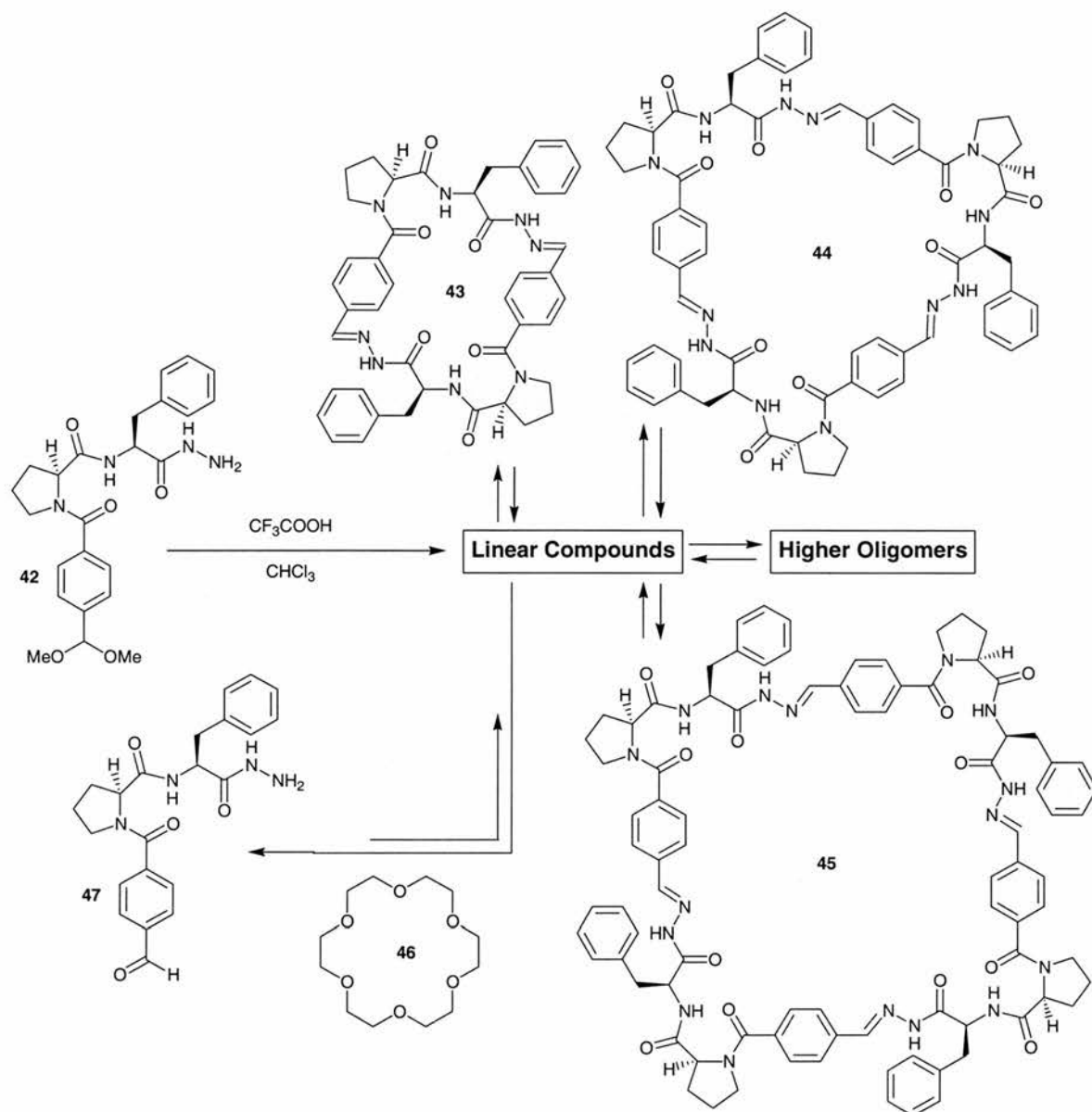


**Figure 18** Selecting an inhibitor for carbonic anhydrase from a dynamic combinatorial library of imines. The enzyme active site is represented by the C shape. The imine **40** selected is similar to known sulfonamide inhibitor **41**.

Work by Sanders and co-workers towards the development of a thermodynamic library for the generation of macrocyclic cinchona alkaloid condensation products has

already been discussed above. This system was not thought to be ideal, as the exchange reaction requires fairly harsh conditions (refluxing in toluene, with KOMe and 18-crown-6 as catalyst). Accordingly, they have developed libraries that operate under milder conditions, for example using trifluoroacetic acid as a catalyst for the generation<sup>84</sup> of a pseudo-peptide hydrazone DCL (**Figure 19**) from monomer **42**. Electrospray mass spectrometry confirms the presence of 10 cyclic oligomers, including **43**, **44** and **45**, which, they reason, must interconvert *via* 10 or more related linear oligomers, although these are not detectable using mass spectrometric or HPLC analyses. However, under acidic conditions, the hydrazide functionality of these linear species will be protonated and therefore susceptible to binding by a crown ether compound. Addition of 18-crown-6 **46** to the equilibrated mixture causes a considerable equilibrium shift, and analysis by HPLC shows a decrease in the concentration of large macrocycles and the appearance of a new species that was not previously detected. Although this cannot be isolated, it is identified as the aldehyde monomer **47**. This result – the amplification of an initially trace product to a major product – demonstrates the large amplification possible using a DCL. This pseudopeptide methodology has been extended<sup>85</sup> to the selection of a receptor for N-methyl alkylammonium cations. Another example,<sup>86</sup> involving the templating of the palladium-catalysed transesterification of three porphyrin dimers, has also been described.

Further examples of the use of targeted equilibrium shifting include those reported by the laboratories of Reinhoudt<sup>87</sup>, Albrecht<sup>88</sup> and Miller<sup>89</sup>. Although there are some areas where dynamic combinatorial chemistry may not prove useful<sup>90</sup> these experiments demonstrate that dynamic combinatorial chemistry is a versatile approach with many possible applications.



**Figure 19** The distribution of products formed by monomer **42** is influenced strongly by introduction of 18-crown-6 **46**.

### 1.1.5 Towards Micro- and Macroscopic Self-Assembling Systems

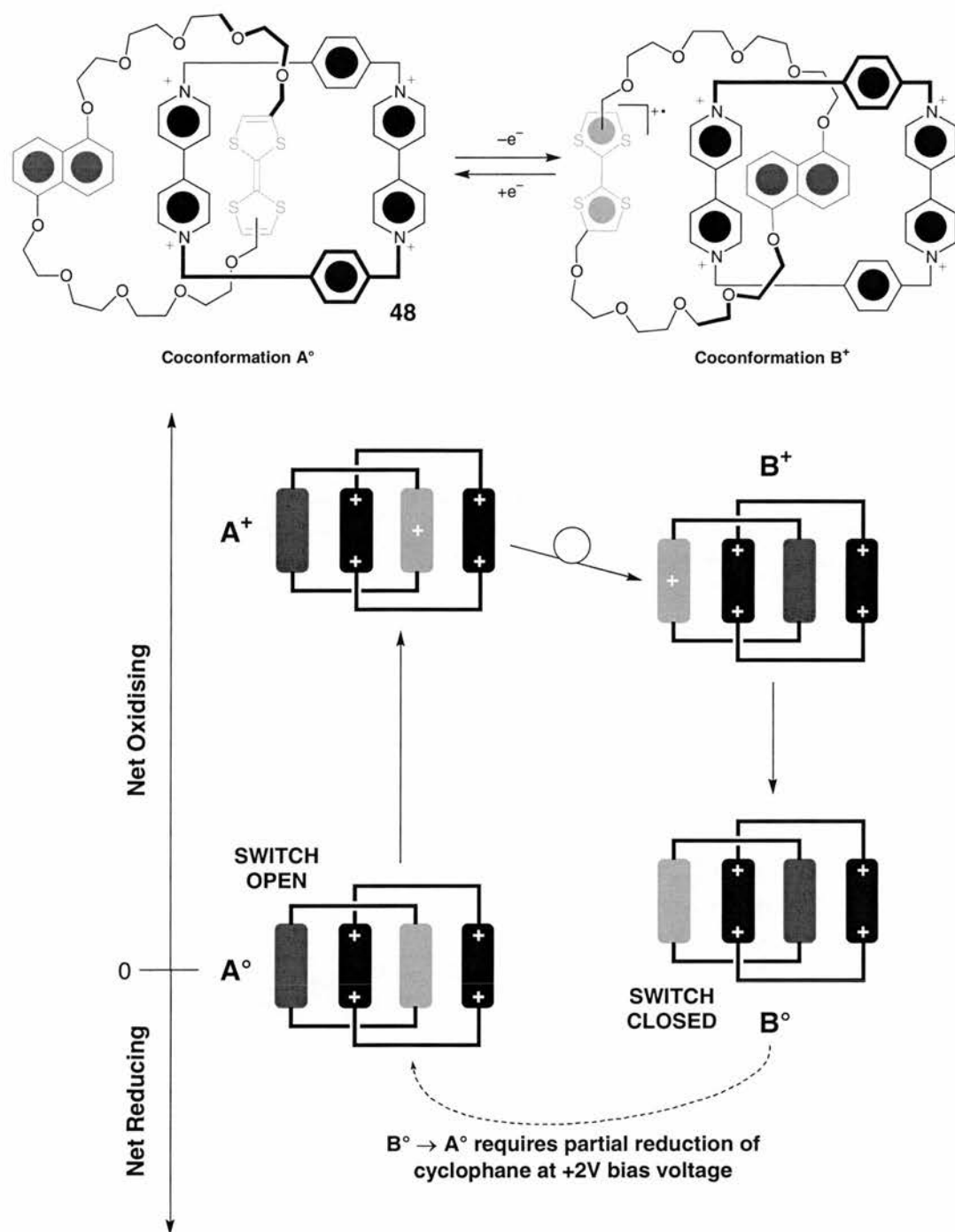
In the 1960's Moore first observed that the size of transistors decreases by a factor of 2 every 18 months. However, the size limits of current photolithographic techniques are rapidly being approached<sup>91</sup>, providing the impetus for the search for innovative methods of synthesising both nanoelectronic devices and materials with new magnetic, electronic or optical properties. There are two major approaches to this goal. The first is to use supramolecular chemistry to fabricate "micromachines"<sup>92</sup> which mimic their biological counterpart. Indeed, Nature has long been using the "bottom-up" approach to create complex devices such as bacterial flagella<sup>93</sup>, transmembrane ion channels<sup>94</sup> and cell proton pumps.<sup>66</sup> The second approach



concentrates on the construction of components which are direct analogues of existing electronic devices, but which are synthesised using a “bottom-up” approach. A further related tactic combines these approaches, using biological principles and/or interactions to direct the formation of “non-biological” assemblies.

Peptide- and protein-based tube structures are prevalent in nature. Cyclic peptide structures with alternating D- and L- amino acids form flat rings, which in turn stack to give hydrogen-bonded tubes.<sup>95</sup> Altering the amino acid side chains and the peptide ring size can vary the properties of the three-dimensional structures.<sup>96</sup> Addition of hydrophobic side chains allows the nanotubes to cross into a lipid layer, so that it can function in a transmembrane channel.<sup>97</sup> The final criterion is that the tubes must be positioned approximately perpendicular to the lipid membrane itself, in order that it should be traversable.<sup>98</sup>

Several routes have been investigated in the search for practical non-lithographic techniques for the construction<sup>99</sup> of electronic devices. The most successful route is that based on the use of interlocked molecules – rotaxanes and catenanes<sup>100</sup> – as molecular switches constructed by self-assembly processes. Several groups have successfully constructed interlocked molecular architectures that respond to external stimuli<sup>101</sup>, including those of Sauvage<sup>102</sup>, Leigh<sup>103</sup> and others<sup>104</sup>. However, the largest body of work in this area has emerged from the laboratories of Stoddart who has constructed a huge array of complex molecular and supramolecular structures based on recognition-mediated assembly processes. The reader is directed to the many reviews<sup>105</sup> of this body of work for further details. More recently, this group has turned their attention to the construction of bistable molecular devices that are deposited on electrodes and act as true electronic devices. The [2]catenane **48** has a resting state<sup>106</sup> (**A**<sup>o</sup>, **Figure 20**) in which the tetrathiafulvalene (TTF) ring system is encapsulated by the tetracationic cyclobis(paraquat-*p*-phenylene) ring.



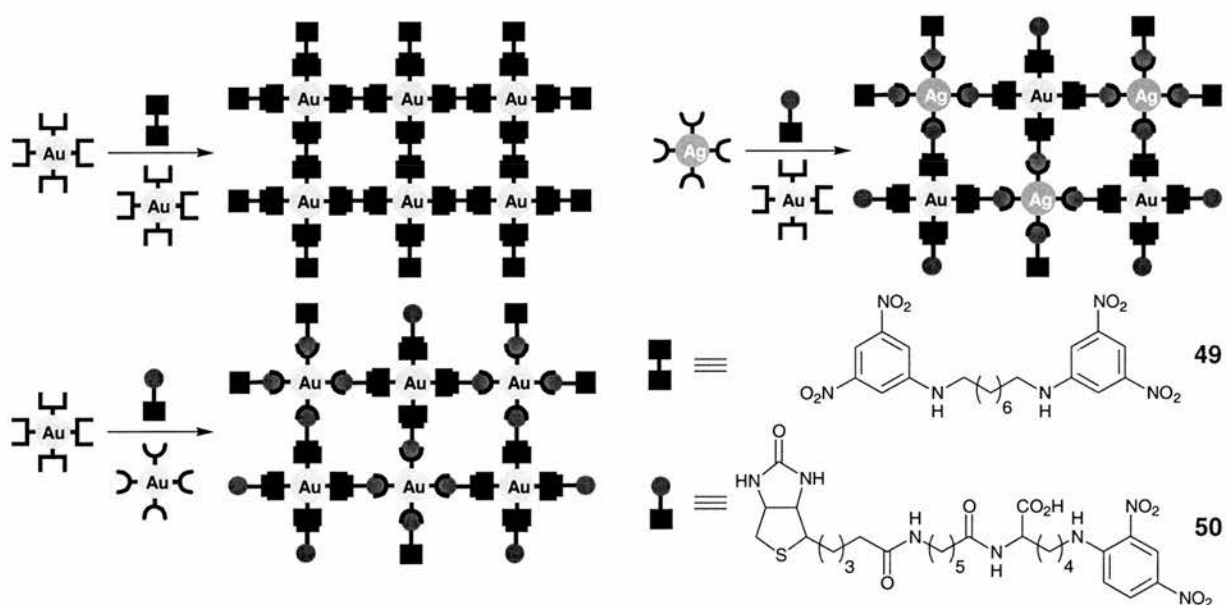
**Figure 20** An electronically reconfigurable electronic switch based on a [2]-catenane.

Oxidation of the TTF generates the corresponding radical cation and coulombic repulsion between the TTF<sup>•+</sup> ring and the tetracation causes circumrotation of the rings with respect to each other and the formation of structure **B<sup>+</sup>**. This voltage-driven bistable behaviour is exploited<sup>107</sup> as the basis of a solid state electronically reconfigurable switch. Using appropriate techniques, a device can be constructed based on this bistable behaviour. The active component of the device is a Langmuir-Blodgett film composed of the [2]catenane **48** and an anchor phospholipid.



Coconformer  $A^\circ$  represents the "switch-open" state of the device. Application of a  $-2V$  bias to the device results in the oxidation of the TTF unit (**Figure 20**) in [2]catenane and structure  $A^+$  is formed. The TTF unit then experiences a coulombic repulsion from the tetracation (**Figure 20**), resulting in circumrotation and formation of structure  $B^+$ . Reduction of the bias voltage to near zero results in reduction of the TTF unit to give structure  $B^\circ$ . This condition represents the "switch-closed" state of the device. The switch can only be opened, regenerating  $A^\circ$ , by application of bias of  $+2V$ . Analysis of the behaviour of the solid state device reveals that it operates through an almost identical mechanochemical mechanism to the solution phase.

Mann and co-workers have combined biotechnology and materials science to create<sup>108</sup> gold and silver nanoparticles coated with antibodies – specifically anti-dinitrophenyl (DNP) IgE or anti-biotin IgG (**Figure 21**). Both a homo-Janus (DNP-DNP) **49** and a hetero-Janus (DNP-biotin) antigen **50** were also synthesised. Mixing the appropriate antigen with a solution of the appropriately antibody coated nanoparticle results in the formation of a cross-linked microscopic structure with the idealised structures shown in **Figure 21**.

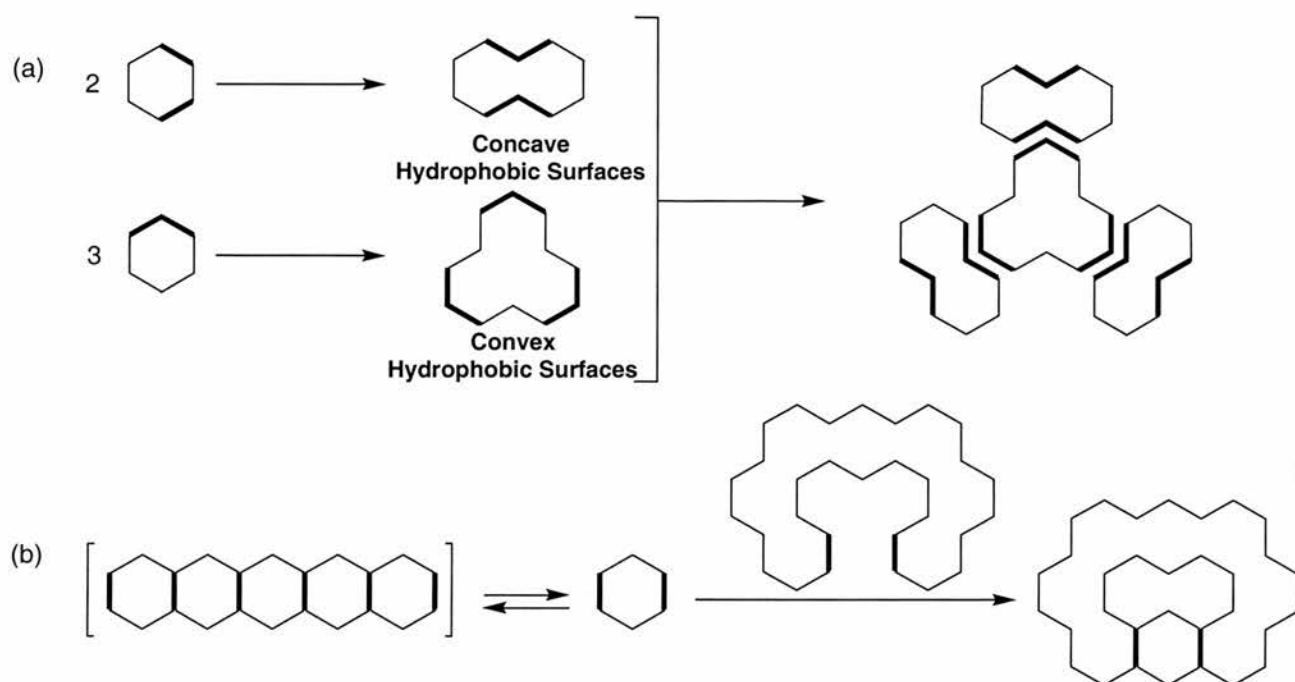


**Figure 21** Mixing antibody functionalised nanoparticles with appropriate antigens leads to the formation of networks. The networks are shown in an idealised form – in reality, the structures which form are highly disordered.

Adding the hetero-Janus antigen to a mixture of both the IgE and the IgG coated nanoparticles gives even higher order gold filaments. It is believed that the increased flexibility of the hetero- over the homo-antigen encourages directional

order. This work clearly benefits from the high specificity of the antibody-antigen recognition process. In certain cases, however, this high degree of specificity may not always be beneficial. In the synthesis of molecular tubes from protein sheets, Atkins and co-workers consider<sup>109</sup> that the specificity of biological macromolecules is a distinct disadvantage, and obtain more useful structures from proteins into which they have introduced a mutation.

Another example of the macroscopic expression of molecular recognition processes include those described<sup>110</sup> by Whitesides and co-workers. They have been investigating<sup>111</sup> the use of polydimethylsiloxane (PDMS) blocks as millimetre-scale extensions of the principles of molecular self-assembly. PDMS is hydrophobic, but one face and some of the sides of the plate may be rendered hydrophilic by oxidation with O<sub>2</sub> plasma. The plates are allowed to float at a water-perfluorodecalin interface and agitated at a specific frequency. When hydrophobic sides of two plates come within a critical distance, they move into contact to form<sup>112</sup> a “capillary bond”. A range of complex hierarchical arrays (**Figure 22**) can be formed in this way, simply by varying the relative position of the hydrophobic sides. The similarities between these macroscopic systems and molecular scale recognition and assembly are highlighted by an investigation<sup>113</sup> into the hierarchy of interactions connecting the plates. Permanent (“covalent”) interactions are made by physically gluing the plates together, strong non-covalent bonds are represented by the interaction between concave and convex hydrophobic surfaces, and weak non-covalent interactions are those made between two concave hydrophobic surfaces. The latter two types of interaction may give rise to a variety of assemblies, but the components can be designed to give specific arrays that maximise the favourable interactions. Furthermore, shape- and size-selective systems have been developed (**Figure 22b**).<sup>114</sup> However, there are some substantial differences between the interactions of polymer plates and the interactions of molecules. Firstly, collision frequencies are far lower for macroscopic than for molecular systems, and secondly, the relative energies of the polymer plates are likely to be similar, rather than being described by a Boltzmann distribution.

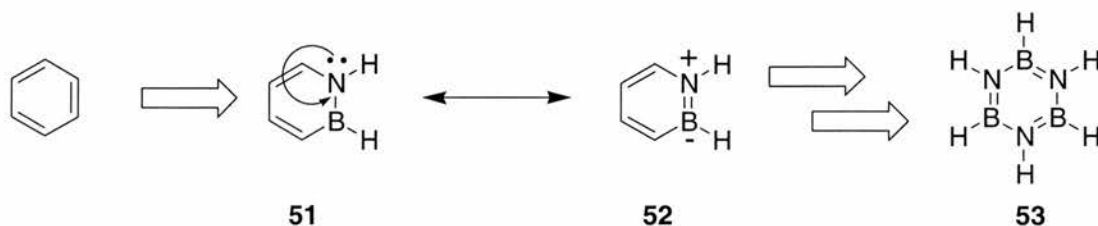


**Figure 22** (a) Hierarchical assembly using "capillary" bonds. (b) Receptor-like behaviour in a system using "capillary" bonds.

## 1.2 Boron-Containing Heterocycles

### 1.2.1 Boraza- and Boroxoaromatic Compounds

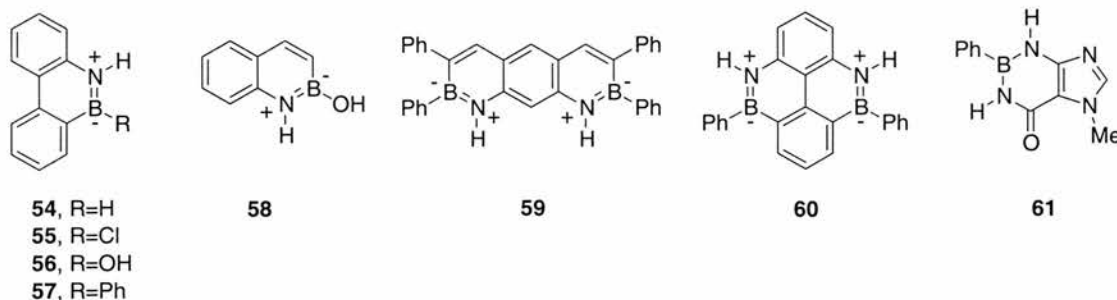
Borazaaromatics are arene derivatives in which a C=C unit has been substituted with the isoelectronic  $\text{B}=\text{N}^+$  unit.<sup>115</sup> Replacement of one C=C unit in benzene with a  $\text{B}=\text{N}^+$  unit gives rise to the structure **51** (**Figure 23**). Donation of the nitrogen lone pair electrons into the N-B bond (which can also be considered as the donation of an electron into the empty boron *p*-orbital) gives rise to the resonance structure **52**. Substitution of the other two C=C units in benzene results in the formation of borazine **53**, which is otherwise known as inorganic benzene. Prior to 1958, this compound was the only known example of this class.



**Figure 23** Borazaaromatics are arene compounds in which a C=C unit has been substituted by a B-N unit.

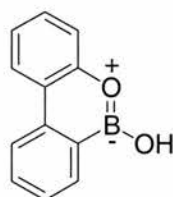
Dewar and co-workers described<sup>116</sup> the first synthesis of a borazaaromatic compound, 10,9-borazaphenanthrene **54** (**Figure 24**), and also its 10-chloro **55**, 10-hydroxy **56** and 10-phenyl **57** derivatives, *via* the reaction of commercially available 2-aminobiphenyl with boron trichloride. 10,9-borazaphenanthrene **54** is isoelectronic with phenanthrene, and Dewar also considered it to be isoconjugate with the parent arene. This assumption was based largely on two observations; firstly that the UV spectrum of **54** closely resembles that of phenanthrene, and secondly, that all the derivatives are extremely stable. They can be recovered unchanged from boiling alkali, suggesting that the B-N bond is rather stronger than in boric acid amides, and can also be nitrated and halogenated<sup>117</sup> without any observable fission of the B-N bond.

Throughout the 1960's, the group of Dewar synthesised a range of borazaaromatic compounds, including B-N analogues of naphthalene<sup>118</sup> **58**, anthracene<sup>119</sup> **59**, pyrene<sup>5</sup> **60** and purine **61**.<sup>120</sup> Several analogues in which the boron and nitrogen atoms are located at ring junction positions were also synthesised.<sup>121,122,123</sup> Although there was some interest<sup>124</sup> in the preparation of non-toxic boron-containing antimetabolites for use in cancer therapy, borazaaromatics were largely synthesised for their novelty as unusual aromatic compounds.



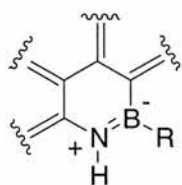
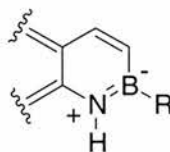
**Figure 24** Borazaaromatic analogues of some arene compounds.

Boroxoaromatics are arene derivatives in which a C=C unit has been replaced with the isoelectronic  $\text{B}=\text{O}^+$  unit. One of the simplest boroxoaromatic compounds, 10-hydroxy-10,9-boroxophenanthrene **62**, was first synthesised<sup>125</sup> by Dewar in 1959. The UV spectrum of this compound closely resembles those of the related 10,9-borazaphenanthrenes, rather than that of a substituted biphenyl such as 2-phenylphenol. This, along with the fact that 10-hydroxy-10,9-boroxophenanthrene is extremely stable in the presence of aqueous acid and alkali, was presented as evidence of its aromatic nature. However, it was also noted that, since oxygen is more electronegative than nitrogen, the contribution of the pseudoaromatic resonance structure should be less important than for the analogous borazaaromatic. This argument is considered in more detail below.

**62**

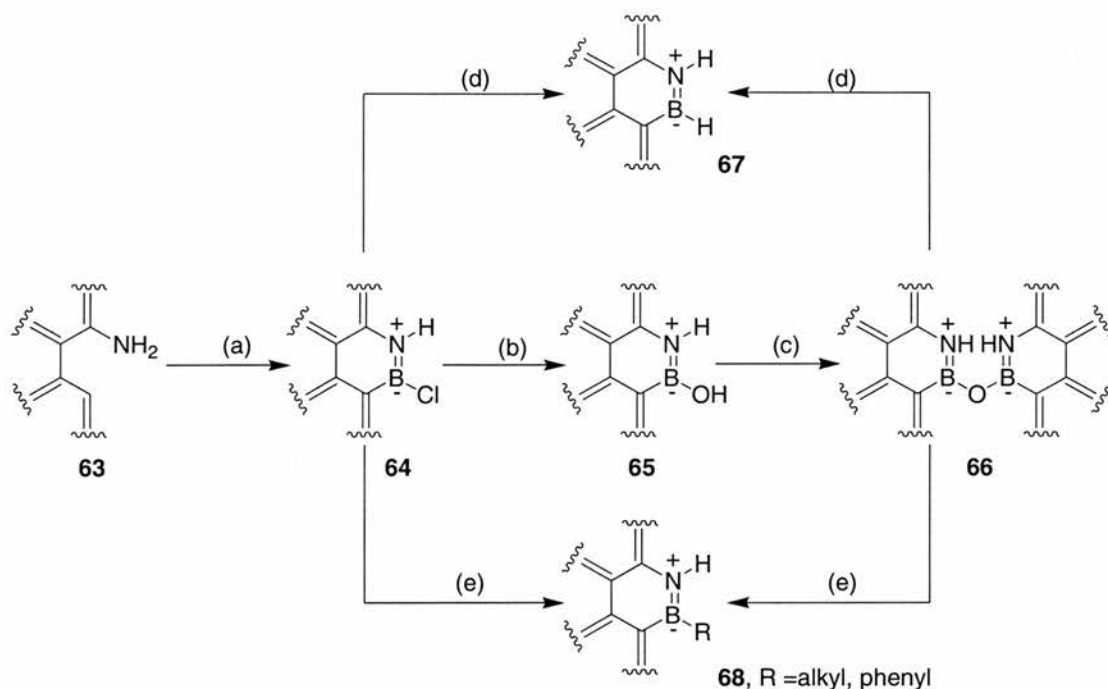
### 1.2.2 Synthesis of Boron Heteroaromatics

In general, borazaaromatics in which the heteroatoms do not occupy bridgehead positions are synthesised from aniline derivatives. These compounds can be divided into two further categories depending on the position of the boron atom; those in which the boron atom is attached to a carbon atom in an aromatic ring (type **A**), and those in which the boron atom is connected to a carbon atom that is  $\text{sp}^2$  hybridised, but not part of a fused ring system (type **B**).

Type **A**Type **B**

Group **A** includes phenanthrene and pyrene analogues (**54** and **60**), and group **B** includes naphthalene and anthracene analogues (**58** and **59**). Type **A** borazaaromatics are generally synthesised (**Scheme 1**) by reaction of a 2-phenyl

substituted aniline **63** with a boron halide, typically boron trichloride, followed by a Lewis acid (aluminium chloride) catalysed Friedel-Crafts type cyclisation. The resultant B-chloro compound<sup>2</sup> **64** is readily hydrolysed with water to afford the B-hydroxy derivative **65**, which can then be dehydrated to form the anhydride **66**. Alternatively, either the B-chloro compound **64** or the anhydride **66** can be reacted<sup>2</sup> with  $\text{LiAlH}_4$  to afford the parent B-hydride **67**, or with Grignard reagents<sup>126</sup> to give B-alkyl and B-phenyl derivatives **68**.

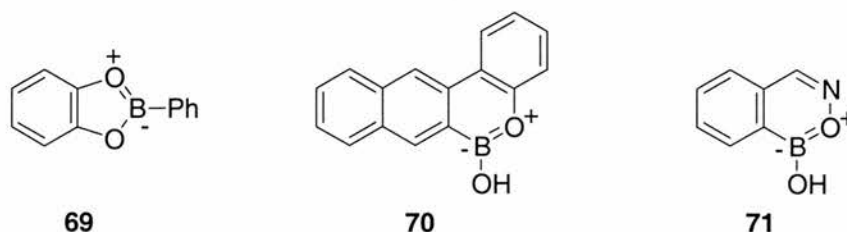


**Scheme 1** Typical reaction conditions for the formation of a type **A** borazaaromatic; (a) (i)  $\text{BCl}_3$ , xylene,  $\Delta$ , (ii)  $\text{AlCl}_3$ ,  $\Delta$ ; (b)  $\text{H}_2\text{O}$ ; (c)  $\Delta$ ; (d)  $\text{LiAlH}_4$ ; (e)  $\text{RMgBr}$ ,  $\text{R} = \text{alkyl, phenyl}$ .

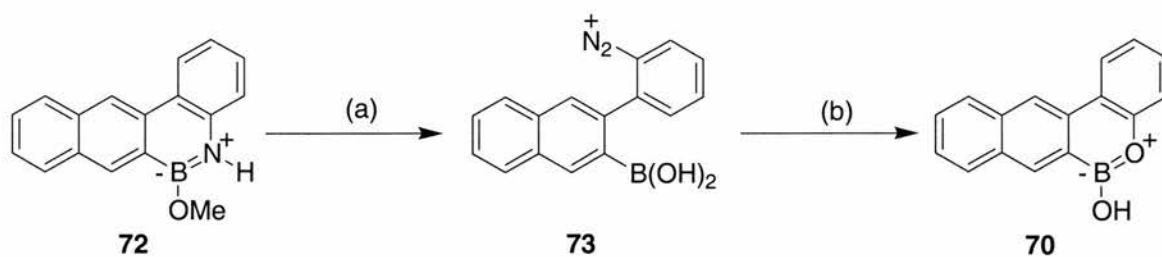
Type **B** borazaaromatics are typically synthesised by application of a similar procedure to 2-aminostyrene substrates, although no catalyst is required to effect the cyclisation. Again, these compounds can be hydrolysed to give the B-hydroxy derivative and dehydrated to afford the anhydride. The B-chloro compound and the anhydride can be reacted with  $\text{LiAlH}_4$  and Grignard reagents in an approach analogous to the type **A** borazaaromatics.

Dewar synthesised a far narrower range of boroxoaromatic than borazaaromatic compounds, including analogues of phenanthrene **62**, 2,3-benzofuran **69**, isoquinoline **70** and benzanthracene **71**.





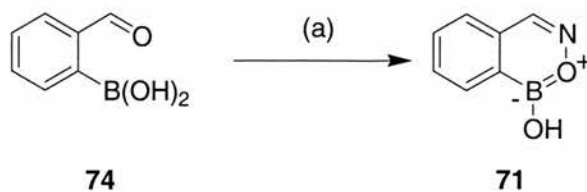
Their formation, however, employed a variety of different synthetic strategies. The first reported<sup>127</sup> synthesis of a boroxoaromatic compound was that of 2-phenylbenzo-1,3-dioxo-2-borole **69**. This was synthesised by reaction of catechol with phenylboron dichloride. The cyclisation occurred uncatylsed. 10,9-Boroxophenanthrene **62** was synthesised<sup>11</sup> using an analogous procedure to that for type **A** borazaaromatics, the reaction of 2-phenylphenol with boron trichloride, followed by the aluminium chloride catalysed cyclisation. The resulting B-chloro compound readily hydrolyses to give the B-hydroxy compound, or alternatively can be reacted with phenyl magnesium bromide to afford the B-phenyl derivative. Simply recrystallising the B-hydroxy compound from methanol generates the B-methoxy derivative. 6-Hydroxy-6,5-boroxo-benzanthracene **70** was synthesised<sup>128</sup> from 6-methoxy-6,5-borazabenzanthracene **72** *via* a diazotisation reaction (**Scheme 2**). The diazonium salt **73** of the borazaaromatic compound was poured onto boiling water and nitrogen was eliminated to form the boroxoaromatic. No further studies into the reactivity of that compound were carried out.



**Scheme 2** (a) (i) HCl, AcOH, (ii) NaNO<sub>2</sub>; (b) H<sub>2</sub>O, Δ.

The final example of a B-O heterocyclic compound reported<sup>129</sup> by Dewar is the isoquinoline analogue, 4-hydroxy-4,3-boroxoisoquinoline **71**. This was synthesised using a modification of the procedure previously described<sup>130</sup> by Snyder and co-workers, the reaction of 2-formylphenylboronic **74** acid with hydroxylamine hydrochloride (**Scheme 3**). Attempts to form the B-methyl derivative by reaction with methyl magnesium bromide failed.

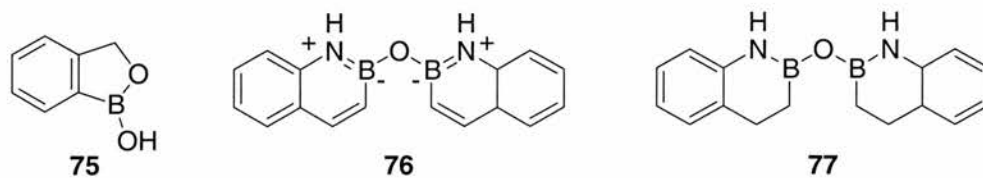




**Scheme 3** (a)  $\text{H}_2\text{NOH}\cdot\text{HCl}$

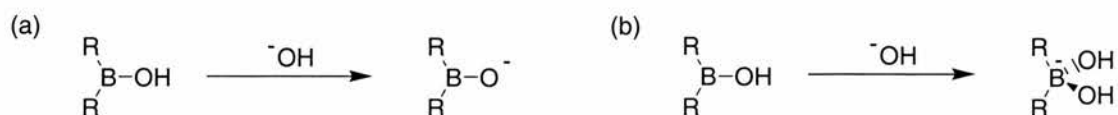
### 1.2.3 Aromaticity of Boron Heteroaromatics

The unusually high resistance to hydrolysis of many boraza- and boroxoaromatics synthesised by Dewar was the initial basis for the assertion that these compounds were aromatic. Additional evidence was provided by their UV spectra, which were often very similar to that of their hydrocarbon analogues. However, in 1960, Snyder reported<sup>131</sup> the synthesis of boronaphthalide **75**, *via* the cyclisation of 2-bromomethylphenylboronic acid. **75** was very stable to hydrolysis and could be nitrated. Since this compound is not aromatic, this suggested that heterocycles of this type might owe their stability simply to their cyclic nature. In reply to this Dewar presented<sup>132</sup> a comparison of the reactivities of bis(2,1-boraza-2-naphthyl)ether **76** and its 3,4-saturated analogue, bis(3,4-dihydro-2,1-boraza-2-naphthyl)ether **77**.



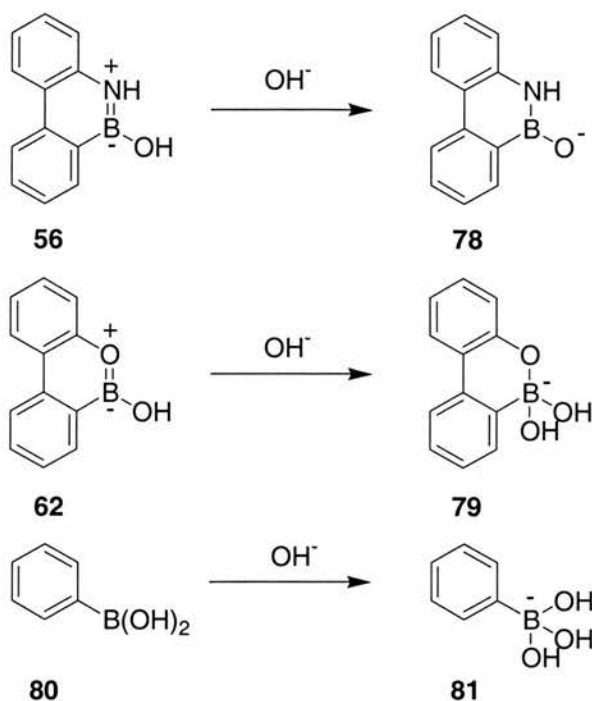
He hoped to demonstrate that the unusual properties of 2,1-borazanaphthalene **58** were indeed dependent on the 3,4-bond being unsaturated. It was discovered that, whereas the B-N bond in the unsaturated compound **76** was extremely resistant to hydrolysis, reduction of the 3,4-double bond caused a considerable decrease in the B-N stability, such that it could be cleaved by addition of water. Furthermore, it became possible to acetylate the amine functionality with acetic anhydride. Early electronic structure calculations suggested<sup>133</sup> that there is some  $\pi$ -electron density between the boron and nitrogen atoms. Dewar presented a study of the compounds' acidity as further verification of his argument. In the presence of hydroxide, a compound containing a  $\text{R}_2\text{B-OH}$  group may behave as a protic acid, or as a Lewis acid. The former case will result in the formation of  $\text{R}_2\text{B-O}^-$ , retaining the trigonal

configuration about the boron (**Figure 25a**). In the latter case, the boron atom coordinates to an additional hydroxide ion to give  $R_2B^-(OH)_2$ , and the boron atom is now tetrahedral (**Figure 25b**).



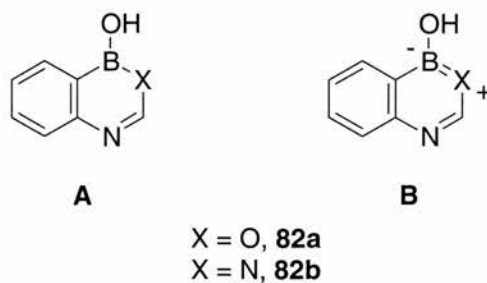
**Figure 25** (a) If  $R_2B(OH)$  behaves as a protic acid it forms a trigonal borate anion. (b) If  $R_2B(OH)$  behaves as a Lewis acid it forms a tetrahedral species.

Where the compound is stabilised by aromaticity, it will prefer to retain the planar, trigonal configuration, and will therefore behave as a protic acid. In forming the tetrahedral anion, the addition of hydroxyl results in the removal of the boron atom from conjugation and the loss of any aromatic stabilisation.  $^{11}B$  NMR spectroscopy<sup>134</sup> can be used<sup>135</sup> to probe the reaction of boraza- and boroxoaromatics in the presence of hydroxide, since any conversion from trigonal to tetrahedral boron will result in a large upfield shift due to the extra shielding afforded by the additional electrons. The formation of the trigonal anion, on the other hand, will cause a small downfield shift with significant broadening of the signal. Dewar *et al.* found (**Scheme 2**) that 10-hydroxy-10,9-borazaphenathrene **56** behaves as a protic acid, whereas 10-hydroxy-10,9-boroxophenanthrene **62** behaves<sup>136</sup> as a Lewis acid, as does phenyl boronic acid **80**. This was in agreement with Dewar's earlier assertion that boroxo-compounds should be less aromatic than their boron-nitrogen analogues. Several years later, however, another study<sup>137</sup> disputed these findings, asserting that 10,9-borazaphenathrenes did, in fact, behave as Lewis acids, and that  $^{11}B$  NMR evidence for their aromaticity was inconclusive.



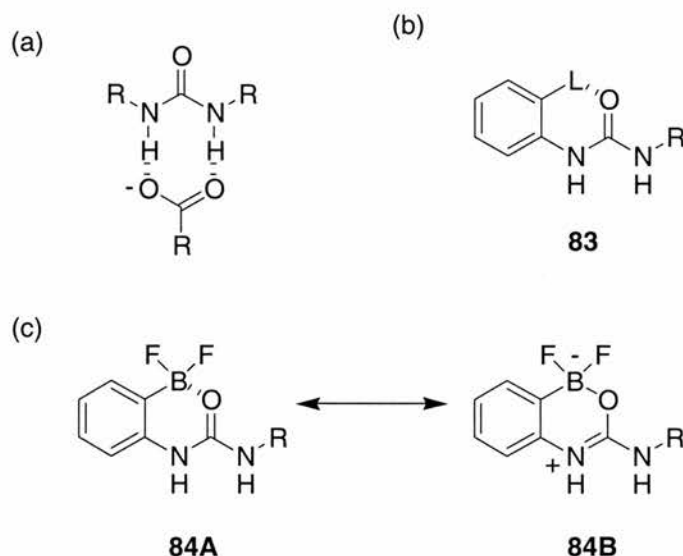
Scheme 4

In 1994, Groziak and co-workers published<sup>138</sup> an account of the structural properties and chemical reactivities of several boron-containing purine nucleoside analogues, including **82**. The similarity of the  $^{11}\text{B}$  NMR chemical shift in  $d_3\text{-MeCN}$  of **82a** (8.8 ppm), **82b** (11.9 ppm) and of related compounds such as phenylboronic acid (10.4 ppm) and 2-nitrophenylboronic acid (10.8 ppm), where boron is not part of an aromatic ring, convinced Groziak that there is only minimal donation of the heteroatom electrons into the boron empty  $p$ -orbital of **82**. Hence, he considers that the structure of **82** is best represented by the structure **A** (Figure 26), rather than the dipolar resonance structure **B**.

Figure 26 Two possible representations of **82**

Smith and co-workers have employed<sup>139</sup> similar molecules as neutral anion receptors, in which urea groups are commonly used as the recognition motif (Figure

**27a**). They noted that the ability of a urea to bind anions should be increased by the inclusion of an appropriately positioned Lewis acid group, and, accordingly, they designed the general urea derivative **83** (**Figure 27b**), where L is a Lewis acid.

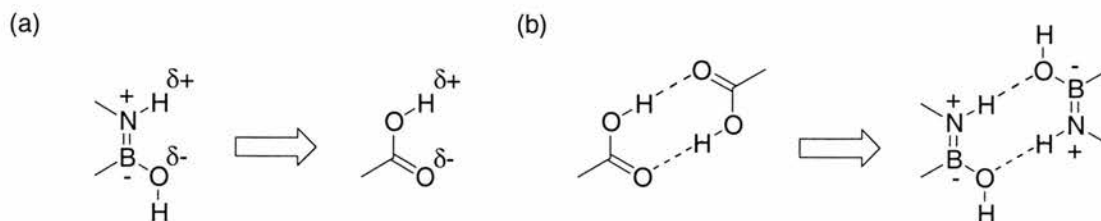


**Figure 27** (a) The urea recognition motif is often used to bind carboxylate anions. (b) The general urea derivative **83**, where L is a Lewis acid, is expected to show enhanced affinity for anions (c) **84** binds acetate 120 times more strongly than its non boron-containing analogue.

Cooperative polarisation of the urea *via* intramolecular coordination of the carbonyl oxygen with the Lewis acid results in an enhanced carboxylate-urea ion-dipole interaction, and an increased positive surface potential at the urea NH groups, strengthening any Coulombic interaction with the anion. Smith synthesised the organoboron compound **84**, which does indeed bind acetate 160 times more strongly than the non-boron containing control in  $d_6$ -DMSO solution. Based on Groziaks observations, they believe that **84B** is the major resonance contributor in this system.

#### 1.2.4 The Potential of Boron Heteroaromatics in Self-Assembly

Since the 1970's, the research effort in the area of borazaaromatics has reduced significantly. However, some facets of their reactivity were never fully investigated, and we have identified some important characteristics. Carboxylic acids provide us with a good structural analogue for hydroxyborazaaromatics. The polarisation patterns of their constituent atoms are very similar. Carboxylic acids are well known to form hydrogen-bonded cyclic dimers, and, indeed, this motif has been extensively used in synthetic self-assembling systems. Thus, by analogy, we might expect that hydroxyborazaaromatics will also form cyclic dimers.



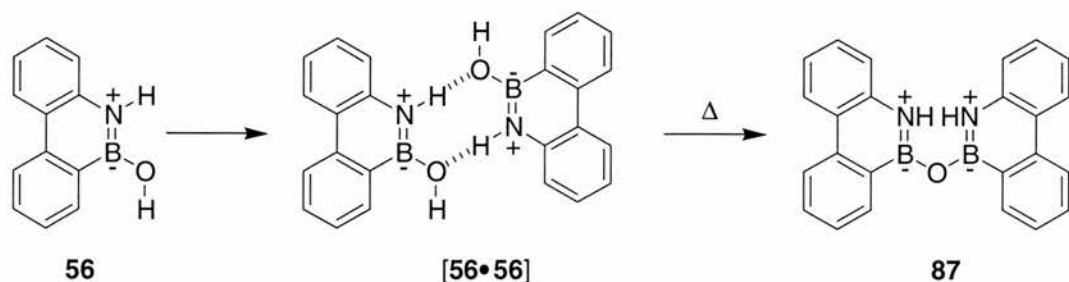
**Figure 28** (a) Hydroxyborazaaromatics show a similar polarisation pattern to that of carboxylic acids. (b) They may also show similar recognition properties.

It would appear, however, that the reactivity properties of carboxylic acids and borazaaromatics are quite different. Although carboxylic acids will undergo self-condensation and transesterification reactions, these are not generally facile processes. In contrast, Dewar often reported the ready formation of anhydrides **86** by hydroxyborazaaromatics **85**.



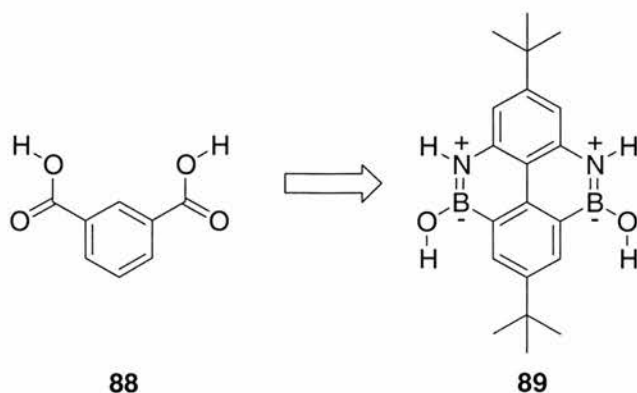
**Scheme 5** Dewar reported that borazaaromatics **85** readily undergo self-condensation reactions to form anhydrides **86**.

These observations suggested that hydroxyborazaaromatic compounds represented a useful building block for forming hydrogen-bonded self-assembled systems. Furthermore, due to their latent reactivity, they provide an opportunity for the formation of covalently-linked molecular solids which may retain some of the structural properties of the non-covalently self-assembled array. Our investigations began with a study<sup>140</sup> of the reactivity properties of 10-hydroxy-10,9-borazaphenanthrene **56**, which was synthesised using an adaptation of the method used by Dewar. The solid state structure, as solved from single crystal X-ray diffraction studies, shows, as predicted, the presence of cyclic hydrogen-bonded dimers [**56**•**56**] (**Figure 29**).



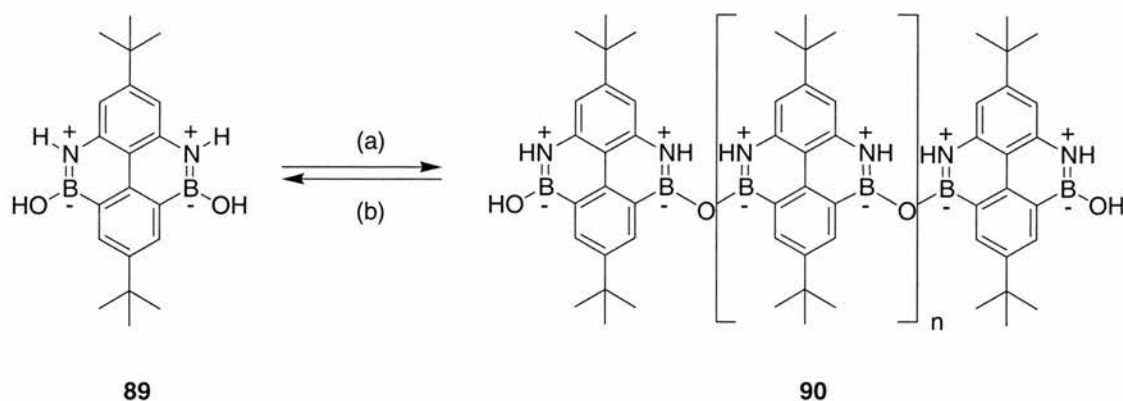
**Figure 29** **56** exists as hydrogen-bonded cyclic dimers **[56•56]** in the solid state. The anhydride **87** can be formed simply by heating **56** in the solid state.

As noted above, the related anhydride, bis(borazaphenanthryl)ether **87** can be formed simply by heating a solid state sample of **56** (**Figure 29**). This transformation can be followed by a variety of solid state techniques, including powder X-ray diffraction (PXRD), and thermogravimetric analysis (TGA). There also exists some additional solution phase reactivity in that the hydroxy-compound **56** is found to exist in equilibrium with anhydride **87** in solution. These observations imply the potential of borazaaromatics in the construction of molecular solids *via* the creation of a hydrogen-bonded array, followed by the formation of covalent B-O-B bonds. Obviously, however, 10-hydroxy-10,9-borazaphenanthrene **56**, possessing only one “reactive” (i.e. boron-nitrogen) functionality, can only form dimers. Clearly, in order to create a system that can form self-assembled polymeric anhydrides, it is necessary to design a bis-functional monomer. Two such systems can be envisaged; those which are predisposed to the formation of linear oligomers, and those which will tend to form macrocycles. 5,10-borazapyrene derivatives represent an example of a system possessing the ability to form linear molecules.<sup>141</sup> Bis(hydroxyboraza)pyrene **89** is a structural analogue of isophthalic acid **88**. During the synthesis of **89** t-butyl groups were added to the skeleton to increase the solubility and therefore aid the synthesis.



**Figure 30** Bis(hydroxyboraza)pyrene **89** is a structural analogue of isophthalic acid **88**.

$^1\text{H}$  NMR spectroscopy in  $\text{CDCl}_3$  shows an equilibrium mixture of the monomer **89** and the linear oligomers **90**, whereas, in  $d_6$ -acetone, the oligomers hydrolyse to **89** in a day. This observation verifies that **89** displays the same reversible solution phase reactivity as borazaphenanthrene **56**, and the formation of oligomers **90** is under thermodynamic control.



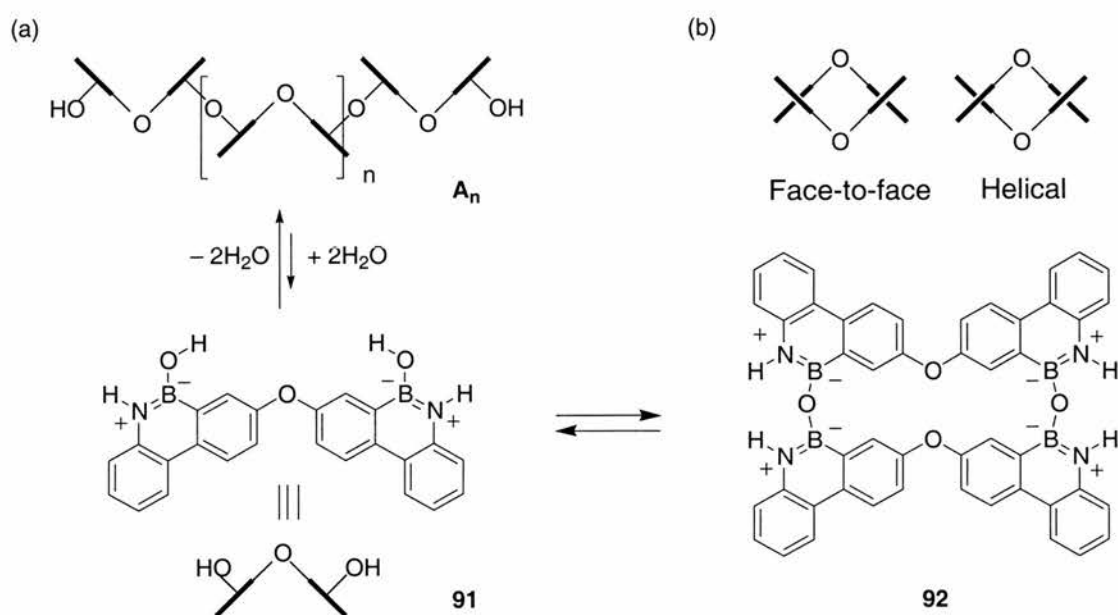
**Scheme 6** (a) 4Å molecular sieves, non-polar solvent, such as  $\text{CHCl}_3$ . (b)  $\text{H}_2\text{O}$ , polar solvent, such as acetone.

The formation of oligomers was examined in more detail using MALDI-TOF spectrometry. In  $\text{CHCl}_3$  solution, the molecular ion was the most prominent peak, but peaks corresponding to the oligomers **90** (up to  $n=5$ ) could also be seen. On the addition of molecular sieves, further dehydration occurred and higher mass peaks (up to  $n=7$ ) appeared. In contrast, in acetone solution, the spectrum showed a peak corresponding to **89** only, and the addition of molecular sieves had very little effect. From these observations we can deduce that in non-polar solvents, such as  $\text{CHCl}_3$ , the solution phase equilibrium between the oligo-anhydrides **90** and the hydroxy-compound **89** can be shifted in the direction of the anhydride **90** by the simple addition of molecular sieves. In polar solvents, however, the equilibrium naturally lies towards the hydroxy-compound **89**, and cannot be shifted easily by the addition of molecular sieves. Crystals of **89** could not be grown without the inclusion of acetone in the structure. The crystal structure showed a complex hydrogen-bonding network, which did not include the cyclic dimer motif noted in the structure of borazaphenanthrene **56**. However, the cyclic dimer is not necessarily expected, as the presence of the *tert*-butyl groups was bound to disrupt the packing arrangement. The solid state reactivity of **89** was investigated, once again using the techniques of PXRD and TGA. TGA demonstrated that, on heating, the mass of a sample of



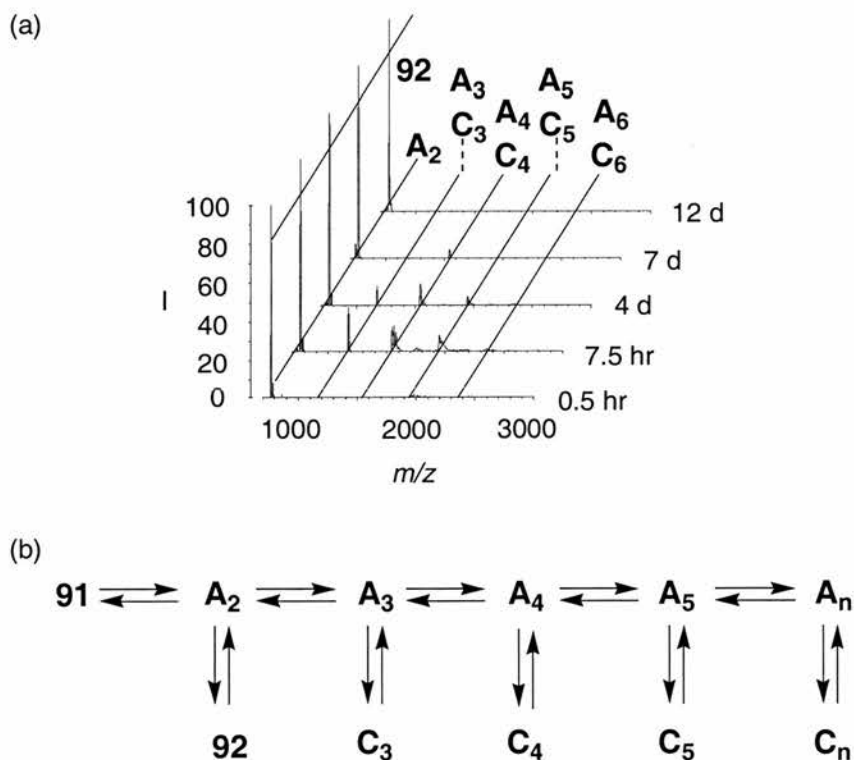
bis(hydroxyboraza)pyrene **89** decreased by around 13%, consistent with the loss of water and acetone from the sample and the formation of the anhydride **90**, as well as some sublimation. PXRD analysis confirmed the existence of a phase change on heating, showing that, on heating, the reflections characteristic of the hydroxy-compound **89** diminished and were not replaced by a new set of reflections, indicating that the oligo-anhydride structure is amorphous. Analysis of the resulting samples by MALDI-TOF spectrometry proved that they were indeed the higher oligomers expected. These experiments demonstrate the extension of the useful reactivity exhibited by borazaphenathrenes to bis-functional compounds.

Compound **89** is based on a rigid pyrene skeleton. Our next target was the more flexible bis(10-hydroxy-10,9-boraza-2-phenathryl)ether **91** (**Scheme 7**), which can be prepared in five steps from diphenyl ether. Although the individual phenanthrene units are rigid, rotation about the ether linkage is possible. On dehydration, the formation of several different products can be envisaged. The monomer may form linear oligomers (**A<sub>n</sub>**, **Scheme 7a**), or cyclic oligomers, the simplest of which is the cyclic dimer (**92**, **Scheme 7b**). In fact, it is the cyclic dimer **92** that is observed when a sample of monomer is dissolved in acetone, and 4 Å molecular sieves added. This process is readily reversed by the addition of water.



**Scheme 7** On dehydration, bis(borazaaromatic) **91** may form (a) linear oligomers **A<sub>n</sub>**, or (b) cyclic oligomers, such as dimer **92**. **92** may exist in a face-to-face or a helical conformation.

In order to study the self-assembly process in more detail, the formation of the dimeric macrocycle **92** was monitored<sup>142</sup> by MALDI-TOF spectrometry (**Figure 31a**). Initially, the only two species present in solution are the acyclic (**A**<sub>2</sub>) and cyclic dimer **92**. After seven hours, the evolution of higher weight molecular species is observed, in addition to the two dimers. The concentration of these higher oligomers is significantly diminished after 4 days, and after 12 days, the only species present in solution is the cyclic dimer. This behaviour can be rationalised in terms of the equilibrium shown (**Figure 31b**). The first species that forms must always be the acyclic dimer. We would expect that the cyclisation to form the dimeric macrocycle **92** would be favoured<sup>143</sup> as it is intramolecular. However, if the effective molarity<sup>144</sup> for this process is low, the chain extension pathways forming higher oligomers will be able to compete with the cyclisation. At this point, higher weight molecular species are observed. However, all the reactions involved in the assembly process are reversible, and eventually, all the material in the reaction manifold is recycled back through the acyclic dimer to afford the cyclic dimer, which must be the thermodynamic product of the process.



**Figure 31**

(a) The evolution of the MALDI-TOF spectrum of a sample of **91** dissolved in acetone over 4 Å molecular sieves as a function of time. All spectra are scaled such that the peak arising from **92** is the base peak in all spectra. It should be noted, however, that at 0.5 hr, the sample contains mainly monomer **91**. (b) Proposed kinetic scheme for the equilibration of oligomers of **91**.

Once the system has reached equilibrium, therefore, the only species remaining in solution is the cyclic dimer **92**. The crystal structure of **92** has been solved and shows that it exists in the two enantiomeric forms of the helical dimer (**Scheme 7b**). Thus, the utility of bis(borazaaromatic) compounds as building blocks for covalent self-assembly processes has been demonstrated. However, it is possible to highlight several problems associated with the use of these compounds. The ease with which they react with themselves to form anhydrides means that, as well as being challenging to isolate and purify, they have a limited ability to form more complex structures. Although they do react with other nucleophiles, they do not do so rapidly, and the bis(borazaphenanthryl)ether-based system above takes 12 days to reach equilibrium.

### 1.3 Aims and Objectives

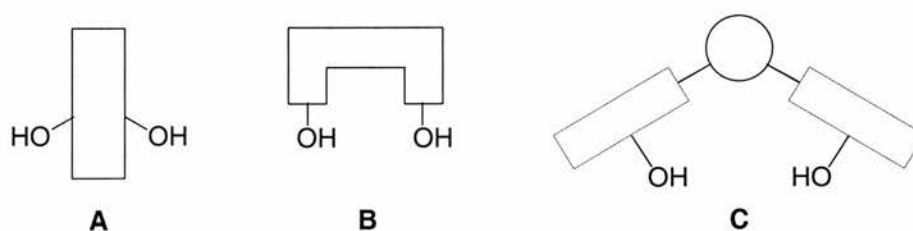
The following chapters describe the logical extension of the concepts outlined in this chapter. Our particular objectives are:

- To investigate and fully understand the structural and chemical properties of 10-hydroxy-10,9-boroxophenanthrene **62**, and to make a comparison of these properties with those of the analogous borazaaromatic **56**. This will be achieved using a number of different techniques.
  - To perform structure calculations in order to assess the extent to which boroxoaromatic compounds can be considered aromatic.
  - To probe the solid state reactivity of **62** using thermal analytical methods, such as thermogravimetric analysis (TGA) and differential scanning calorimetry (DSC), and also X-ray diffraction techniques.
  - To analyse the solution phase reactivity of **62** with itself, and with other nucleophiles, using solution phase  $^1\text{H}$  and  $^{11}\text{B}$  NMR spectroscopy.
- To extend our understanding of the properties of the model compound **62** to the development of bifunctional boroxoaromatic systems, which we anticipate will be more useful in constructing complex assemblies. In particular, we are

interested in investigating rigid building blocks (**A, Figure 32**), predicted to form linear oligomers, and also those with more convergent reactive centres (**B, Figure 32**), which may form macrocycles. We are also interested in the synthesis of monomers in which rigid units are joined by a flexible spacer unit (**C, Figure 32**).

-To develop a reliable synthesis of bifunctional boroxoaromatic compounds.

-To characterise the solid state reactivity of these building blocks using TGA, DSC and XRD, and their solution phase reactivity using  $^1\text{H}$  and  $^{11}\text{B}$  NMR spectroscopy.



**Figure 32** Cartoon representation of three possible bis-functional boron heteroaromatic building blocks.

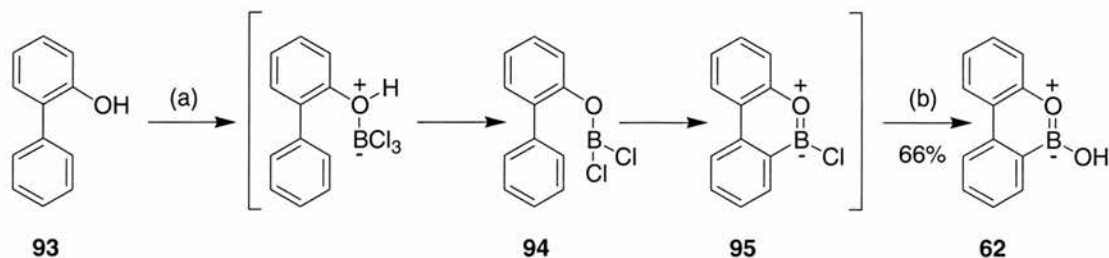
## 2 Properties of Boroxoaromatic Compounds

### 2.1 Preamble

The systems described in **Section 1.2** demonstrate the utility of borazaaromatic compounds in covalent self-assembly process, but their spontaneous formation of anhydrides, and particularly their low reactivity towards other nucleophiles, limits the complexity of structures that can be assembled using these building blocks. We therefore identified the corresponding oxygen-containing boroxoaromatics as suitable compounds for investigation in our quest to extend the use of boron-containing heteroaromatics in covalent self-assembly processes. This chapter will describe in depth the properties, both in the solution and solid state, of one of the simplest boroxoaromatics, 10-hydroxy-10,9-boroxophenanthrene. Also explained are the reactivity features of this compound that make it a potentially useful building block for self-assembly processes.

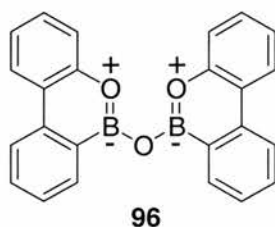
### 2.2 Synthesis of 10-Hydroxy-10,9-boroxophenanthrene

The synthesis of 10-hydroxy-10,9-boroxophenanthrene **62** was achieved using an adaptation of the method described<sup>125</sup> by Dewar in 1959 (**Scheme 8**). A solution of 2-phenylphenol **93** in dry diethyl ether was treated with boron trichloride in hexane at low temperature forming the corresponding oxoborondichloride **94** *in situ* as a white precipitate. This was not isolated and caution was required to ensure the complete exclusion of moisture from the system, as the adduct is extremely unstable in the presence of water, and will readily hydrolyse to re-form starting material. It was discovered that cyclisation did not take place in diethyl ether and we believe this may have been due to the insolubility of the adduct in that solvent. Accordingly, all solvents were removed from the reaction mixture under a reduced pressure - with care necessary to maintain the product under a dry atmosphere - prior to the addition of dry hexane, in which the adduct was noticeably more soluble. Lewis acid catalysed cyclisation of the adduct was effected by the addition of 0.15 equivalents of AlCl<sub>3</sub> and refluxing the reaction mixture for 3 hours. The B-chloro compound **95** is readily converted to the corresponding B-hydroxy compound on hydrolysis with water, affording 10-hydroxy-10,9-boroxophenanthrene **62** as a colourless powder in 66% yield.

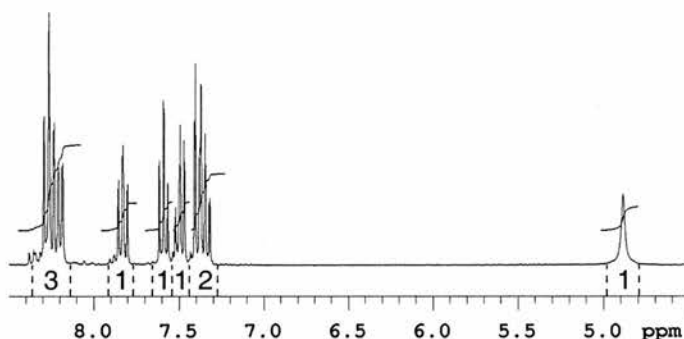


**Scheme 8** Synthesis of 10-hydroxy-10,9-boroxophenanthrene **62**. (a) (i)  $\text{BCl}_3$ ,  $\text{Et}_2\text{O}$ ,  $-78\text{ }^\circ\text{C} \rightarrow \text{r.t.}$ , (ii)  $\text{AlCl}_3$ , hexane,  $\Delta$ . (b)  $\text{H}_2\text{O}$ .

In 1960, Dewar also reported<sup>145</sup> that the anhydride, bis(boroxophenanthryl) ether **96**, could be formed in the solid state by heating **62**, but the synthesis of this compound was never proven unambiguously.



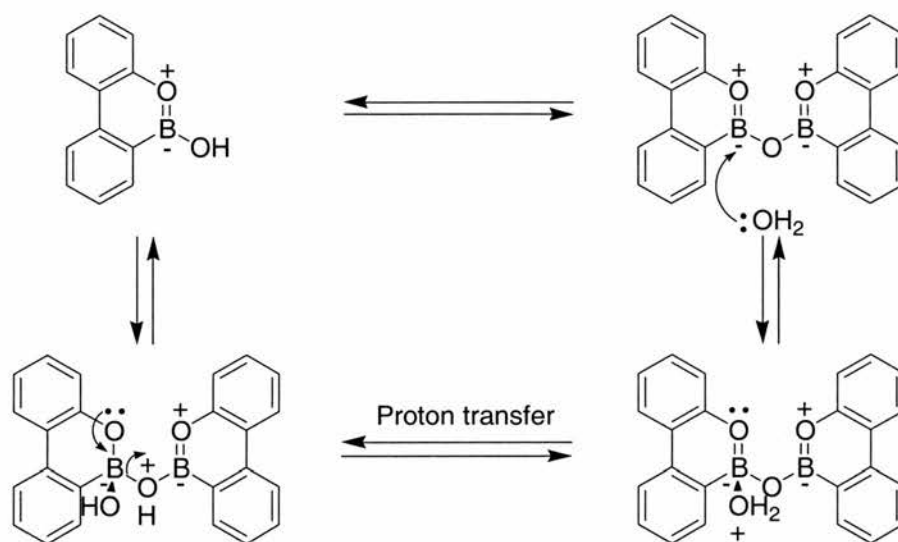
Solution phase  $^1\text{H}$  NMR spectra of **62**, recorded at 300 MHz in both  $(\text{CD}_3)_2\text{CO}$  and in  $\text{CDCl}_3$  (**Figure 33**), indicate the presence of **62** only, and offer no evidence of the formation of the anhydride **96**.



**Figure 33** Partial  $^1\text{H}$  300 MHz NMR spectrum of **62** in  $\text{CDCl}_3$ , recorded at 293 K. Integration values are shown below each resonance.

This observation is in stark contrast to the behaviour<sup>140</sup> in solution of the closely related borazaaromatic 10-hydroxy-10,9-borazaphenanthrene **56**. Solution phase  $^1\text{H}$  NMR spectra of **56** show both the B-hydroxy compound and the corresponding anhydride **87** are present in equilibrium. It appears that

hydroxyboroxophenanthrene **62** certainly does not thus dehydrate to form anhydride **96** in solution. A sample of the **96** can be prepared by heating a sample of **62** in the solid state for 2 hours *in vacuo*, and an EI mass spectrum of a sample prepared in this manner shows a strong signal at  $m/z$  374, the mass of the expected anhydride product. However, when this material is dissolved in  $\text{CDCl}_3$ , the 300 MHz  $^1\text{H}$  NMR spectrum of the solution reveals the presence of **62** only. It is therefore evident that rehydration of **96** occurs almost immediately in solution and it is impossible to record a  $^1\text{H}$  NMR spectrum of the anhydride **96** in  $\text{CDCl}_3$  solution, *i.e.* **96** is clearly very unstable to hydrolysis.



**Scheme 9** The proposed mechanism of formation of **96** from **62**, involves nucleophilic attack at boron, and elimination of water.

The proposed mechanism of anhydride formation is shown in **Scheme 9**. This mechanism involves nucleophilic attack at boron, and it should be recalled that, as in the case of the borazaaromatic compounds, despite the conventional notation of boron with a formal negative charge, it does, in fact, represent a maximum on the electrostatic potential surface. This will be discussed in more detail in **Section 2.3.2**.

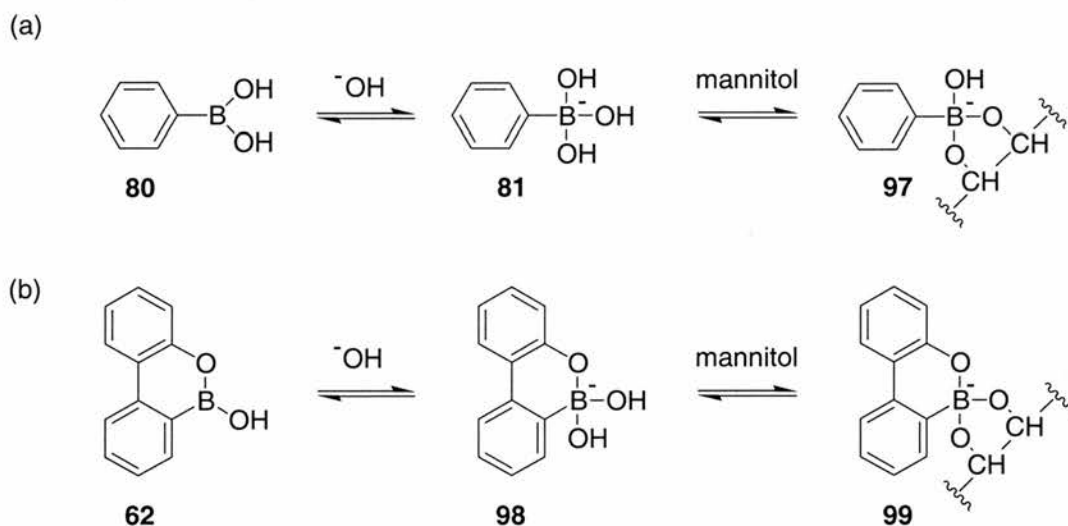
## 2.3 Aromaticity and Electrophilic Reactivity

### 2.3.1 Aromaticity and the O-B bond

As explained earlier, boroxoaromatics are conventionally represented as aromatic. However, they might also be considered as cyclic boronic esters and there is some debate in the literature as to whether compounds of this type owe their



stability to their cyclic structure, or to the aromaticity of their boron-containing heterocycles. There is experimental evidence to suggest that they exhibit both aromatic and borate ester properties. For example, the ultraviolet spectrum of 10-hydroxy-10,9-boroxophenanthrene **62** suggests<sup>145</sup> that it is aromatic, indicating it is likely to behave as a protic acid, rather than as a Lewis acid, as discussed in **Section 1.2.3**. However, the  $pK_a$  value of **62** has been estimated<sup>132</sup> to be 9.1, making it one of the strongest boronic acids known and significantly more acidic than several boron-nitrogen heterocycles studied (typical  $pK_a = 12.0$ ). It is known<sup>146</sup> that the phenyl boronate anion **81** is tetrahedral because the addition of polyols, particularly mannitol, to a solution of phenyl boronic acid **80** increases its acidity, due to the potential for formation of complex **97**, as shown in **Figure 34a**. A solution of **62** in 1:1 aqueous ethanol can be half-neutralised by the addition of aqueous sodium hydroxide. Dewar discovered that this solution, on addition of mannitol, responded similarly to solutions of phenyl boronic acid, with an increase in the acidity, and it was therefore assumed that the conjugate anion of **62** also forms cyclic esters **99** with mannitol. (**Figure 34b**).

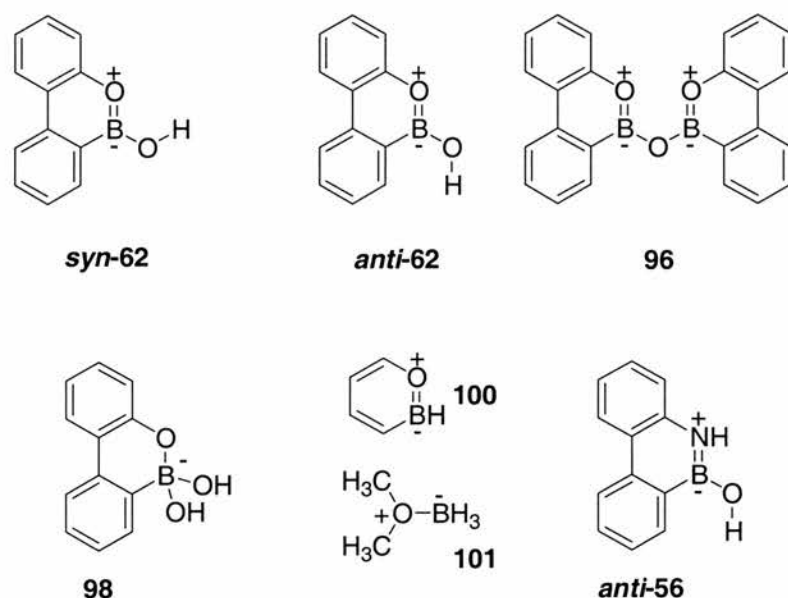


**Figure 34** (a) In the presence of hydroxide, **80** acts as a Lewis acid, forming the tetrahedral anion **81**, and forming complexes **97** with mannitol. (b) In the presence of hydroxide, **62** also reacts with mannitol to form cyclic boronic esters **99**, implying the formation of the anion **98**.

From this observation, it was deduced that the anion of **62** must be tetrahedral (**98**, **Figure 34**) (i.e. **62** was acting as a Lewis acid), and this behaviour implies that **62** is less aromatic than previously believed. Dewar's proposed explanation for this observation was that the strain present in the boron-oxygen system (as indicated by

unpublished models!) is relieved when the boron atom adopts a tetrahedral configuration.

In order to gain some insight into the molecular and electronic structure of boroxophenanthrenes, and to confirm or refute the existence of strain in **62**, we carried out a series of *ab initio* electronic structure calculations at the HF/6-31G(d,p) level of theory. Selected bond lengths and Löwdin<sup>147</sup> bond orders of 10-hydroxy-10,9-boroxophenanthrene **62** and the corresponding anhydride **96** are shown in **Table 1**. Also examined are the geometry optimised structures of the tetrahedral hydroxide adduct **98** and the putative parent compound boroxobenzene **100**. For comparison, calculations were also carried out on the boron-nitrogen analogue, 10-hydroxy-10,9-borazaphenanthrene **56**, as well as on benzene, ethene, phenanthrene and on the dimethyl ether-borane complex **101** (**Figure 35**).

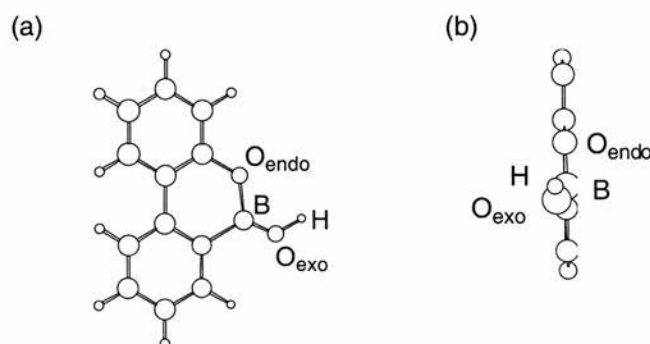


**Figure 35** *Ab initio* calculations were carried out on several different boron heteroaromatic compounds.

The lowest energy structure of **62** (**Figure 36**) is planar with the O-H bond vector in a *syn* orientation with respect to the endocyclic O-B bond. At this level of theory, *syn*-**62** is around  $14.5 \text{ kJmol}^{-1}$  more stable than *anti*-**62**, in which the O-H bond vector is *anti* with respect to the O-B bond.

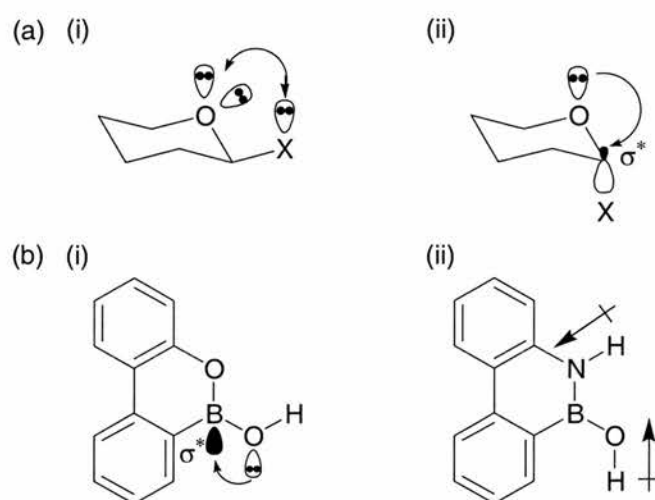
**Table 1** Calculated (HF/6-31G(d,p)) bond lengths and bond orders for selected compounds.

Compound	Bond	Length / Å	Bond Order
<b><i>syn</i>-62</b>	Endocyclic O-B	1.37	1.32
	Exocyclic O-B	1.35	1.45
	C-Endocyclic O	1.35	1.17
	C-B	1.55	1.04
<b><i>anti</i>-62</b>	Endocyclic O-B	1.36	1.33
	Exocyclic O-B	1.35	1.44
	C-Endocyclic O	1.35	1.18
	C-B	1.56	1.03
<b>96</b>	Endocyclic O-B	1.36	1.34
	Exocyclic O-B	1.36	1.34
	C-Endocyclic O	1.35	1.17
	C-B	1.55	1.04
<b>98</b>	Endocyclic O-B	1.52	0.90
	Exocyclic O-B	1.46	1.14
	C-Endocyclic O	1.31	1.36
	C-B	1.62	0.90
<b>100</b>	O-B	1.38	1.34
	C-O	1.33	1.29
	C-B	1.53	1.19
	B-H	1.19	0.96
<b><i>anti</i>-56</b>	N-B	1.41	1.31
	B-O	1.36	1.40
	C-N	1.38	1.20
	C-B	1.55	1.03
<b>101</b>	O-B	1.72	0.57
	C-O	1.41	1.04
<b>Benzene</b>	C-C	1.39	1.49
<b>Phenanthrene</b>	C-C (9,10)	1.34	1.78
<b>Ethene</b>	C-C	1.32	2.12

**Figure 36**

(a) The lowest energy calculated (HF/6-31G(d,p)) structure of **62** is planar with the O<sub>exo</sub>-H bond *syn* with respect to the O-B bond vector. (b) The side view of the calculated structure demonstrates that it is planar. Aromatic protons have been omitted for clarity.

Data for the *anti* conformation is provided in **Table 1** for comparison. This preference for the *syn* conformation is in sharp contrast<sup>141</sup> to the analogous borazaaromatic *anti*-**56**, in which the O-H bond vector prefers the *anti* orientation with respect to the endocyclic N-B bond. One possible reason for this difference is to be found in a consideration of the electronic properties of the two compounds (**Figure 37**). The *syn* conformation adopted by **62** is actually the expected conformation as it allows for the donation of the exocyclic oxygen lone pair electrons into the  $\sigma^*$  antibonding orbital of the B-O bond. This is a variation of the anomeric effect (**Figure 37a**), which dictates that electronegative substituents (X) at the anomeric centre of a sugar will adopt an axial position, avoiding repulsion of the O and X lone pair electrons, and allowing donation of electrons from the oxygen atom into the low energy antibonding orbital of the C-X bond.

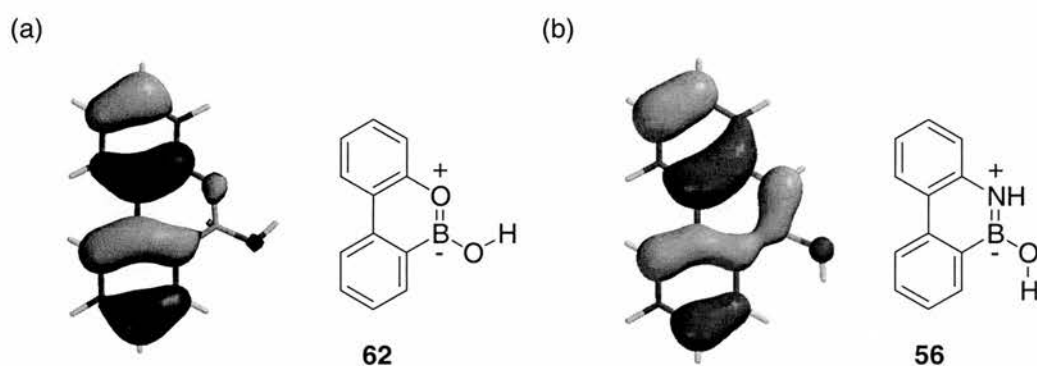


**Figure 37** (a) In sugars, the anomeric effect dictates that electronegative substituents X will adopt an axial conformation in order to (i) avoid repulsion between lone pairs, and (ii) allow charge donation into the  $\sigma^*$  orbital. (b) (i) *syn*-**62** allows for the donation of electrons into the  $\sigma^*$  orbital of the B-O bond, whereas **56** (ii) adopts the *anti* conformation to avoid an unfavourable dipole alignment.

Conversely, **56** adopts the *anti* conformation, which does not allow for the donation of the oxygen lone pair electrons, as the lone pairs are no longer in the same plane as the antibonding orbital. According to the anomeric effect, this conformation is not favoured. However, in the case of **56**, there is another consideration to be taken into account. In the *syn* conformation the dipoles of the N-H and the O-H bond are aligned. In the *anti* conformation, this is no longer the case (**Figure 37b**), and it must be assumed that any extra stabilisation resulting from the

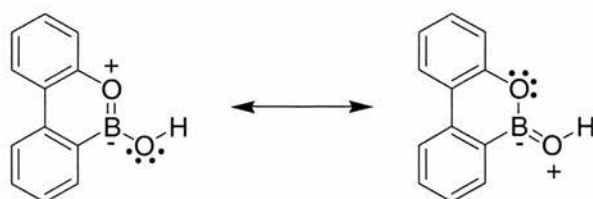
adoption of a *syn* conformation and the consequences of the anomeric effect are more than offset by the unfavourable dipole alignment. This consideration is not relevant for **62**.

The calculated structure of **62** shows it to be planar, and this confirms that both the endocyclic oxygen and boron atoms are  $sp^2$  hybridised. The endocyclic O-B bond order (1.32) suggests that this bond has significant  $\pi$  character. The existence of  $\pi$ -type bonding is also illustrated by the calculated HOMO of **62** (**Figure 38a**), which shows the O-B  $\pi$ -orbital overlap. The calculated HOMO of **56**, however, which is shown for comparison (**Figure 38b**), clearly shows a greater degree of overlap.



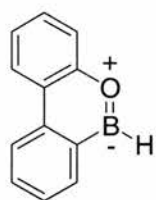
**Figure 38** The calculated (HF/6-31G(d,p)) HOMO of **62** (a), and HOMO of **56** (b).

Interestingly, the bond order of the exocyclic O-B bond in **62** (1.45 Å) suggests that this also has considerable  $\pi$ -character. For a partial bond to exist between the B atom and the exocyclic O atom, the hybridisation of the oxygen atom must be  $sp^2$ , and the calculated C-B-O and B-O-H angles (126.6° and 115.5° respectively) indeed demonstrate that the hybridisation of the oxygen atom is closer to  $sp^2$  than  $sp^3$ . A consideration of the extended  $\pi$  system across the O-B-O atoms suggests the existence of a second resonance form of **62** (**Figure 39**). Incidentally, the calculated bond angles (O-B-O = 118°, C<sub>B</sub>-B-O = 123°, where C<sub>B</sub> is the Carbon atom to which Boron is attached, **Figure 39**) provide little support for Dewar's assertion that this molecule is particularly strained.



**Figure 39** Two resonance forms of **62**.

In the absence of any delocalisation, a formal O=B double bond would have a bond order of about 2. This is epitomised by the C=C bond order in ethene of 2.12 (**Table 1**). Where the double bond is delocalised over an extended  $\pi$ -system, as in benzene, the bond order is reduced to 1.5. However, the 9,10 C-C bond in phenanthrene is found to have a bond order of 1.78. This illustrates the well-known fact that this bond is not strongly delocalised, being present in four of the five resonance structures that can be drawn for phenanthrene. The length of the endocyclic O-B bond, at 1.37 Å, lies between those of benzene (1.39 Å) and phenanthrene (1.34 Å). Both the endocyclic and exocyclic O-B bond lengths (1.37 and 1.35 Å respectively) are significantly shorter than the O-B single bond in the dimethyl ether-borane complex **101** (1.72 Å). The calculated endocyclic bond order (1.32) does not provide any indication of its delocalisation over the aromatic framework. The bond may be comparatively strong and significantly delocalised, or it may be weaker, but isolated. The existence of the second resonance structure will further decrease the 9,10-bond order, and it is therefore expected that the O-B bond order in 9,10-boroxophenanthrene **102** (the direct O-B analogue of phenanthrene) will be higher than in **62**.

**102****Figure 40** 9,10-Boroxophenanthrene is the B-O analogue of phenanthrene

The calculated bond orders and bond lengths can also be compared with those of the analogous borazaaromatic **56**. As oxygen is more electronegative than nitrogen, Dewar stated that the dipolar resonance structure will be less significant for **62** than for **56**. At a first consideration, it might therefore be expected that the N-B bond will be stronger than the O-B bond. In actual fact this is not the case, and the O-B bond in **62** is shorter and has a higher bond order than the N-B bond in **56**. This is easily explained by considering the increased B→O  $\sigma$ -framework donation that results from the higher electronegativity of the oxygen atom. (Pauling electronegativities<sup>148</sup> of oxygen and nitrogen are 3.5 and 3.0 respectively). This shortens the O-B bond, which in turn improves the overlap in the  $\pi$ -system.

### 2.3.2 The Electrophilic Boron

The calculated natural atomic occupancy (NAO) of the boron  $p_z$  orbital (0.39) (**Table 2**) of **62** further supports the existence of O→B electron donation in the  $\pi$ -framework, but this is less than half the value (1.1) calculated for a carbon atom in the extended  $\pi$ -system of benzene.

**Table 2** Calculated (HF/6-31G(d,p)) Natural Atomic Occupancy of  $p_z$  orbitals of selected atoms in **62**. Data are also provided for benzene and **56** for comparison.

Compound	Atom	N.A.O ( $p_z$ )
<i>syn</i> - <b>62</b>	Exocyclic O	1.82
	B	0.39
	Endocyclic O	1.68
<i>anti</i> - <b>56</b>	O	1.59
	B	0.48
	N	1.52
<b>Benzene</b>	C	1.10

As the boron  $p_z$  orbital is only partially occupied, it is expected that the boron atom will be relatively electrophilic. As expected, the occupancy of the boron  $p_z$  orbital of **56** is greater than for **62**, suggesting that **62** will indeed be more susceptible to nucleophilic attack. The calculated electrostatic potential surface (ESP) of **62** provides additional evidence of the electrophilicity of boron (**Table 3**). The ESP surfaces on the oxygen and carbon atoms are all minima, with similar energies to the carbon atoms of benzene ( $-84 \text{ kJmol}^{-1}$ ). In contrast, the ESP surface on boron is a maximum ( $+98 \text{ kJmol}^{-1}$ ). This demonstrates that, although the O→B charge transfer in the  $\pi$ -system is considerable, it must be outweighed by the B→O charge transfer in the  $\sigma$ -framework.

**Table 3** Calculated (HF/6-31G(d,p)) maximum and minimum values for the electrostatic potential surface on selected atoms of **62** and benzene.

Compound	Atom	ESP <sub>max/min</sub> /kJmol <sup>-1</sup>
<i>syn</i> - <b>62</b>	Endocyclic O	-28
	B	+98
	O aromatic ring <sup>a</sup>	-32
	B aromatic ring <sup>b</sup>	-52
<b>Benzene</b>	C	-84

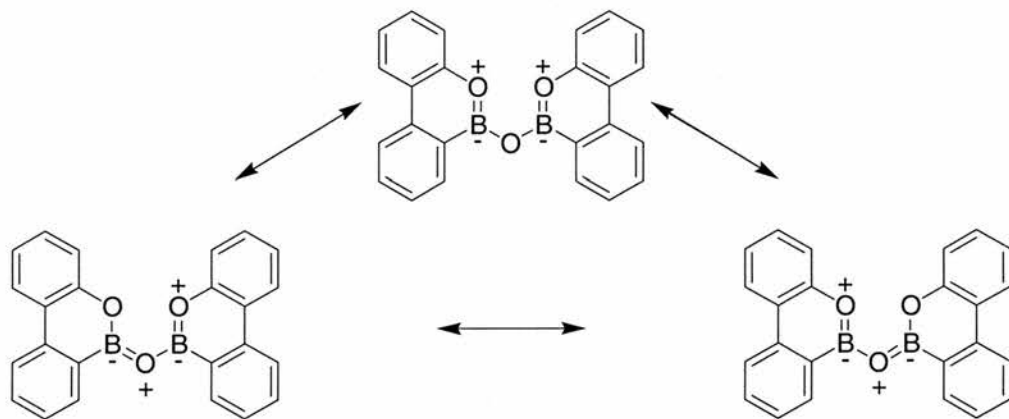
<sup>a</sup> The C atom to which the endocyclic O is attached. <sup>b</sup> The C atom to which boron is attached.



The electropositive surface on boron, together with the partially occupied  $p_z$  orbital, explains why this boron atom is susceptible to nucleophilic attack.

### 2.3.3 The Calculated Structure of Bis-(boroxophenanthryl)ether

Electronic structure calculations at the HF/6-31G(d,p) level of theory were also performed on the anhydride **96**. In contrast to the borazaaromatic anhydride **87**, the structure was calculated to be planar, with a B-O-B bond angle of  $133^\circ$ . This is relatively high for an  $sp^2$  hybridised atom, although not as open as the B-O-B angle in **87**, which has a value of  $143^\circ$ . It seems likely, given the planarity of the molecule, that alternative resonance structures exist, causing the hybridisation of the oxygen atom to tend towards  $sp$ . This would account for the openness of the B-O-B angle. Indeed, all the B-O bonds do have some  $\pi$ -character (**Table 1**), and the endo- and exocyclic B-O bonds are all of equal length ( $1.36 \text{ \AA}$ ), suggesting the presence of resonance structures (**Figure 41**).



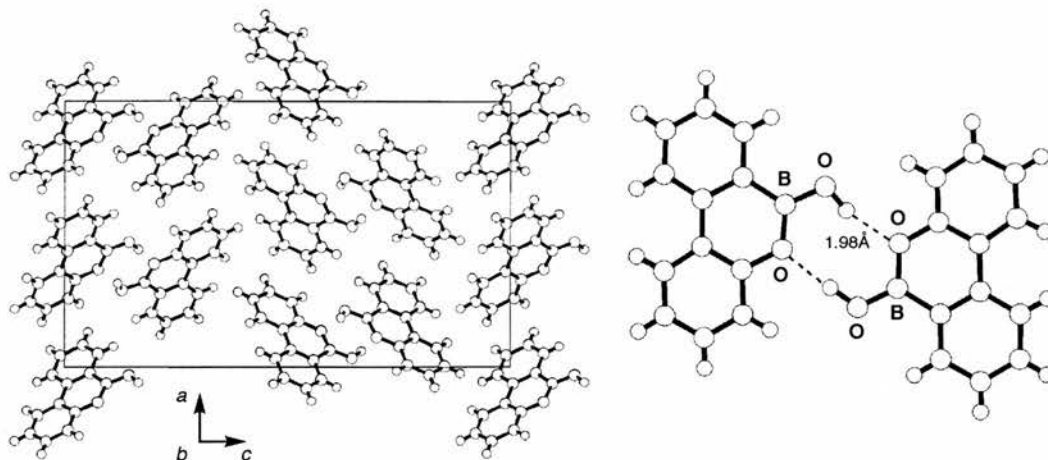
**Figure 41** Three possible resonance structures for **96**.

## 2.4 Solid State Structure

### 2.4.1 Solid State Structure of 10-Hydroxy-10,9-boroxophenanthrene

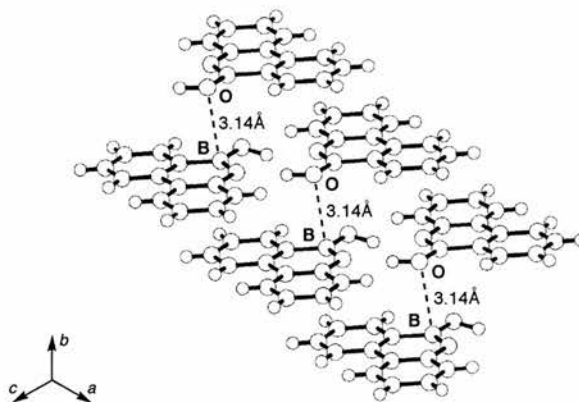
Single crystals of 10-hydroxy-10,9-boroxophenanthrene **62** suitable for X-ray diffraction were grown by vapour diffusion of hexane into a solution of **62** in diethyl ether. The solid state structure<sup>149</sup> of **62** (**Figure 42**), determined by single crystal X-ray diffraction, reveals that **62** forms  $R_2^2(8)^{150}$  hydrogen-bonded homodimers [**62**•**62**] in the solid state in an analogous manner to the carboxylic acid  $R_2^2(8)$  motif and also

to the  $R_2^2(8)$  motif observed in the crystal structure of hydroxyborazaphenanthrene **56**.



**Figure 42** (a) Projection of the solid state structure of **62** along the crystallographic  $b$  axis. The projection of the unit cell is represented by the solid lines. (b) Ball and stick representation of the  $[62\cdot62]$  homodimer within the solid state structure of **62**. Dashed lines represent hydrogen bonds.

All eight of the molecules in the unit cell are involved in cyclic hydrogen bonded dimers. This is unlike the solid state structure of **56**, which has two peripherally hydrogen-bonded molecules associated with each homodimer. Clearly, **62** has no free protons to interact in this manner. The two molecules within each  $[62\cdot62]$  homodimer participate in two  $O-H\cdots O$  hydrogen bonds. These two bonds have the same length (1.98 Å), but their  $O-H\cdots O$  angles differ significantly ( $157^\circ$  vs.  $176^\circ$ ).

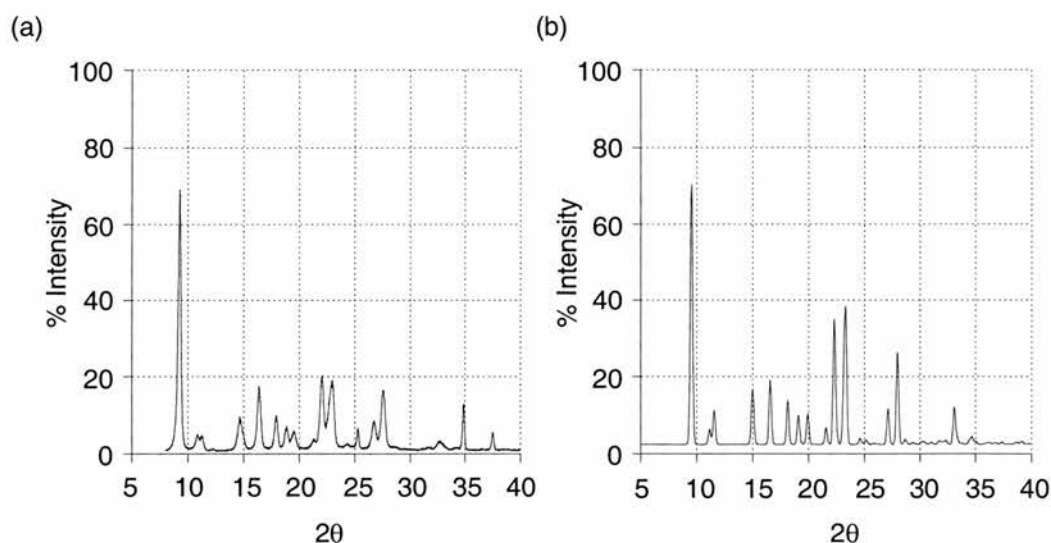


**Figure 43** The solid state structure of **62** shows stacks of hydrogen-bonded dimers, which propagate along the crystallographic  $b$  axis. One oxygen atom *per* dimer displays a short contact with a boron atom in the layer below.

The oxygen atom associated with the less linear hydrogen bond displays a relatively short contact (3.14 Å) to a boron atom in the layer below (**Figure 43**). Stacks of the [62•62] homodimers propagate along the crystallographic *b* axis. Whilst the solid state structure of **56** shows several different phases, only one phase was observed in the crystal structure of **62**.

#### 2.4.2 Solid State Structure of Bis-(boroxophenanthryl) ether

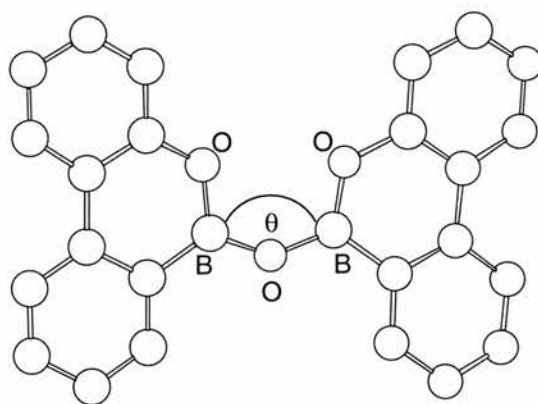
The solid state structure of the anhydride **96** has been determined<sup>151</sup> previously by Sheldrick and co-workers using single crystals prepared by sublimation. Unfortunately, we were unable to repeat this preparation and, as a result of its instability to hydrolysis, single crystals of the **96** could not be grown by vapour diffusion methods. Recognising that the crystal structure of a reaction product generated directly *via* a solid state reaction is not always the same as the crystal structure of the same material in crystals grown by crystal growth techniques, we investigated the structure of a sample of **96** formed by solid state dehydration of **62**.



**Figure 44** (a) The powder X-ray diffraction pattern recorded for **96** is very similar to the (b) powder X-ray diffraction pattern generated using CrystalDiffract (Version 3.06, CrystalMaker Software, Oxford, UK, 2001) for the previously determined<sup>151</sup> structure of **96**.

These solid state processes are described in more detail in **Section 2.5**. The solid state structure<sup>152</sup> of **96** was determined by an analysis of the powder X-ray diffraction pattern and appears to be consistent with the previously reported structure. The powder X-ray diffraction data recorded for **96** (**Figure 44a**) are almost identical to those generated by CrystalDiffract software (CrystalDiffract, Version 3.06, CrystalMaker Software, Oxford, UK, 2001) (**Figure 44b**) for the structure described

by Sheldrick. Any differences in the patterns are explained by the presence of disorder in the Sheldrick structure. We are unable to state with any certainty whether the structure we have determined is ordered or disordered, since both models fit the data equally well. The crystal structure (**Figure 45**) shows that **96** is planar, with a B-O-B bond angle of  $139^\circ$ .

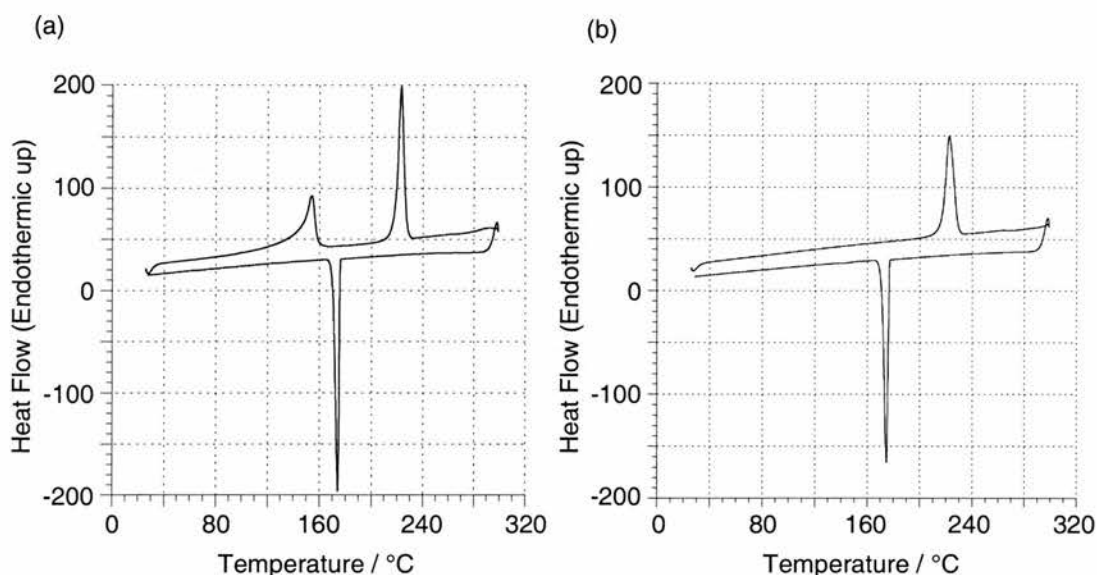


**Figure 45** The solid state structure of **96**, determined from powder X-ray diffraction data, shows the molecule to be planar, with  $\theta = 139^\circ$ . Aromatic protons have been omitted for clarity.

## 2.5 Solid State Reactivity

### 2.5.1 Chemical Change

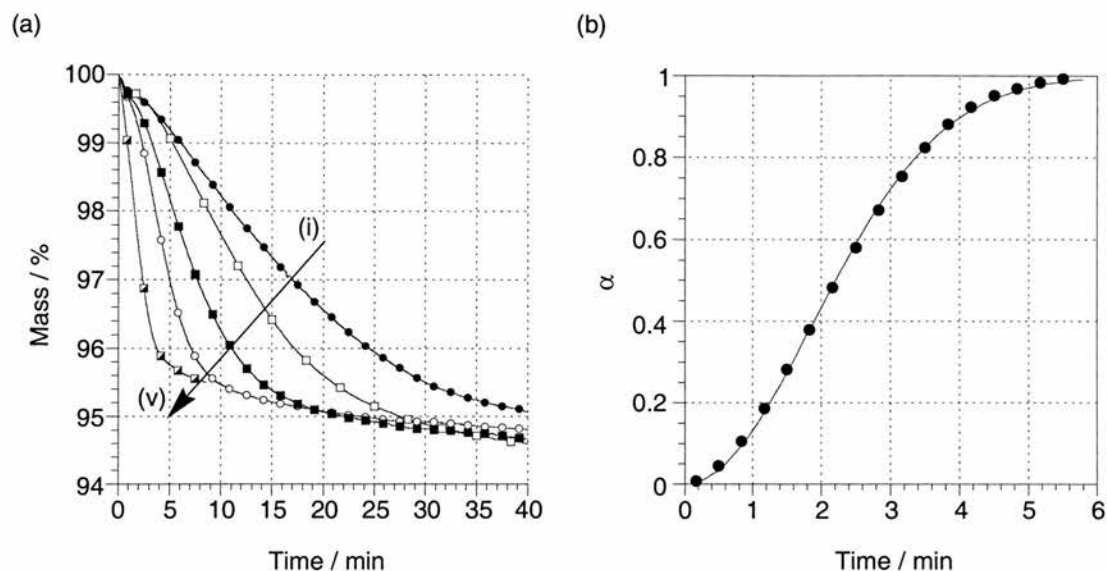
When heated, the observed melting points of both 10-hydroxy-10,9-boroxophenanthrene **62** and bis(boroxophenanthryl)ether **96** are  $214\text{--}216^\circ\text{C}$ . In order to determine the nature of the phase change between **62** and the **96**, thermal analysis was carried out using differential scanning calorimetry (DSC). A known mass of **62** (typically 5 mg) was heated from room temperature to  $300^\circ\text{C}$  at a rate of  $100^\circ\text{C}$  per minute and the rate of heat flux measured throughout the experiment (**Figure 46a**). Two endotherms are observed, one at  $130\text{--}160^\circ\text{C}$ , and the second at around  $215\text{--}225^\circ\text{C}$ . On cooling, also at a rate of  $100^\circ\text{C}$  per minute, an exotherm is noted at  $165^\circ\text{C}$ . Once the sample had cooled to ambient temperature it was reheated to  $300^\circ\text{C}$  at a rate of  $20^\circ\text{C}$  per minute (**Figure 46b**). The endotherm at  $215\text{--}225^\circ\text{C}$  is still present, but the endotherm evident in the previous experiment at  $130$  to  $160^\circ\text{C}$  is no longer observed.



**Figure 46** (a) DSC plot recorded on heating a sample of **62** from room temperature to 300°C, at 100 °Cmin<sup>-1</sup>. The onset of the solid state transformation is clearly visible at ~145°C. (b) DSC plot recorded on reheating the same sample at 20 °Cmin<sup>-1</sup>. The exotherm at 145°C is now absent.

From these results we deduce that the first endotherm is due to the chemical change from **62** to the anhydride **96**, and that the second endotherm occurs when **96** melts. In contrast to the situation in solution, **96** is quite stable in the solid state, and therefore, the chemical change is not observed during the second experiment. Heating a sample of **62** will therefore not give a melting point for **62**. Rather, the sample will dehydrate to form **96**, which will subsequently melt at its melting point of 215°C.

During the reaction that forms the anhydride **96** from the B-hydroxy compound **62**, one molecule of water is lost for every two molecules of **62**. This loss of water should correspond to a 4.6% mass loss from the sample, which can be determined using thermogravimetric analysis (TGA). In a typical experiment, a known mass of **62** (typically 10 mg) was heated to a given temperature and then held under isothermal conditions until the measured mass reached 95.4% of its original value. Further isothermal heating results in a continued but significantly reduced mass loss, believed to be due to a process such as sublimation. Indeed, sublimation had been observed previously when gently heating a sample of **62** under high vacuum. This type of TGA experiment was then repeated at several different temperatures in order to investigate the effect of temperature on the reaction rate (**Figure 47a**).



**Figure 47** (a) TGA data for the solid state transformation of **62** to **96**. Isothermal heating experiments were carried out at (i) 70°C, (ii) 75°C, (iii) 80°C, (iv) 90°C and (v) 100°C. (b) TGA data obtained at 100°C plotted as extent of reaction ( $\alpha$ ) vs. time. The solid line represents the best fit of the Avrami-Erofeev equation to the data.

It was noted that the rate of dehydration decreased with temperature, as expected. At temperatures below 70°C the reaction rate decreased dramatically. EI mass spectra of the materials formed during these experiments show, in all cases, strong signals at  $m/z$  374, indicative of the expected anhydride product **96**. Plotting the fractional extent of reaction  $\alpha$  vs. time  $t$  for each temperature illustrates the variation of the reaction rate as the temperature of isothermal heating is varied from 55°C to 100°C. The end of the reaction (*i.e.*  $\alpha=1$ ) was defined as the point at which a total mass loss of 4.6 % was reached. The data obtained at each temperature was then fitted using the Avrami-Erofeev equation<sup>153</sup> (equation 1), which is commonly used to describe solid state reactions. A typical fit of the experimental data to the Avrami-Erofeev equation is shown in **Figure 47b**.

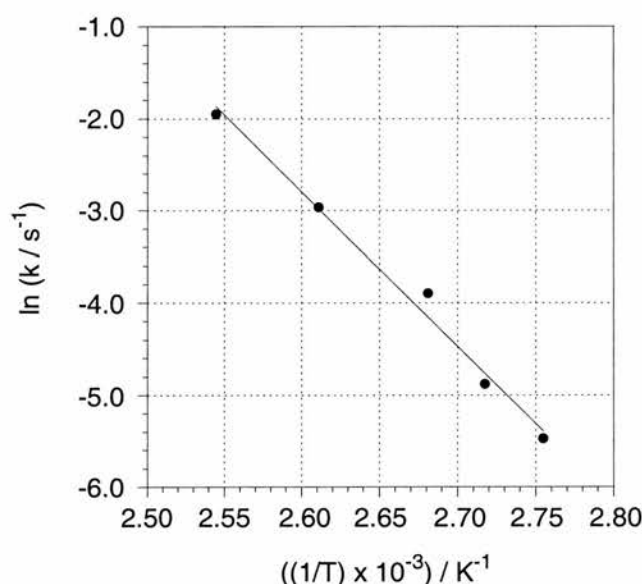
$$\alpha(t) = 1 - \exp(-kt^n) \quad \text{Equation 1}$$

where  $\alpha(t)$  = fractional extent of reaction  
 $k$  = rate constant  
 $n$  = integer

Empirically, it has been found that the value of  $n$  usually lies between 2 and 4. The value of  $n$  is described as being comprised of two components,  $\beta$  and  $\lambda$ . The



component  $\beta$  represents the number of steps involved in formation of crystal nuclei and usually takes the value 0 (corresponding to instantaneous nucleation) or 1 (single step nucleation). The component  $\lambda$  represents the number of dimensions in which growth of the nuclei occurs and may take a value of 1, 2 or 3. In this case, the best fit of the experimental data was obtained where  $n = 2$ . The data recorded at temperatures above 70°C can all be fitted to the Avrami-Erofeev equation using the same value of  $n$  within experimental error. The values of the rate constant  $k$  extracted at different temperatures were then analysed using a variant<sup>154</sup> of the Arrhenius equation. A plot of  $\ln k$  vs.  $1/T$  (**Figure 48**) has a gradient of  $E_a/R$ , where  $E_a$  is the activation energy for the mass loss from the solid. Applying a linear fit to the data presented in **Figure 48** affords a value of  $\sim 140 \text{ kJmol}^{-1}$  for the activation energy of the observed process, which is in the area we would expect for a reaction of this kind.



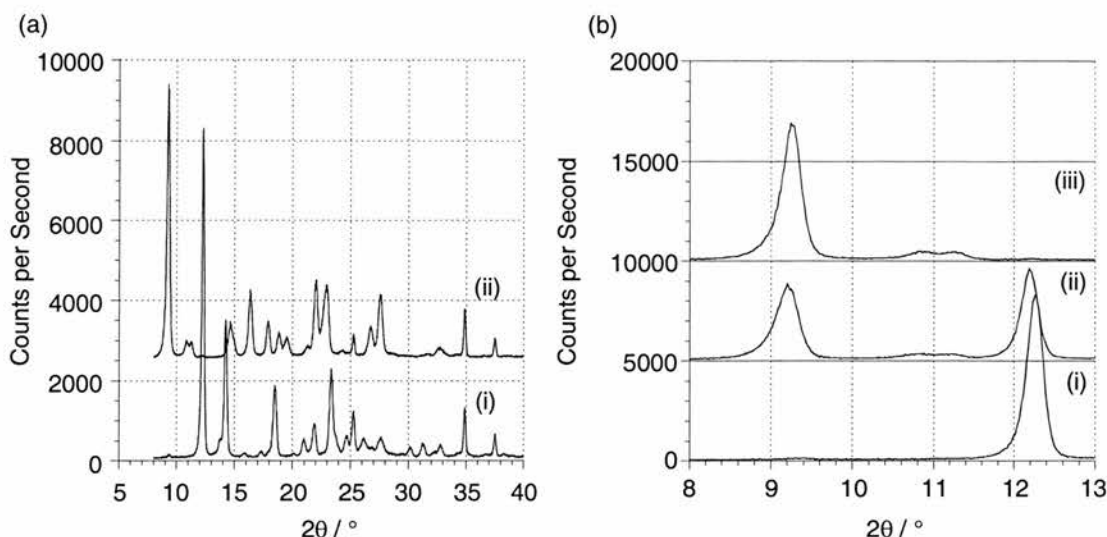
**Figure 48** Arrhenius plot ( $\ln k$  vs.  $1/T$ ) for the mass loss due to the solid state transformation of **62** to **96** at temperatures higher than 70°C. The data are fitted by a straight line, the gradient of which is  $E_a/R$ , where  $E_a$  is the free energy of activation for the process. ( $E_a = 140 \text{ kJmol}^{-1}$ )

### 2.5.2 Structural Change

TGA measures the rate of chemical change within a sample. In order to determine the rate of structural change, the rate of dehydration of 10-hydroxy-10,9-boroxophenanthrene **62** was studied using variable temperature powder X-ray diffraction. An initial diffraction pattern of **62** was recorded at room temperature and the sample heated rapidly to the desired temperature. Further diffraction data were subsequently recorded at regular time intervals at this temperature and this

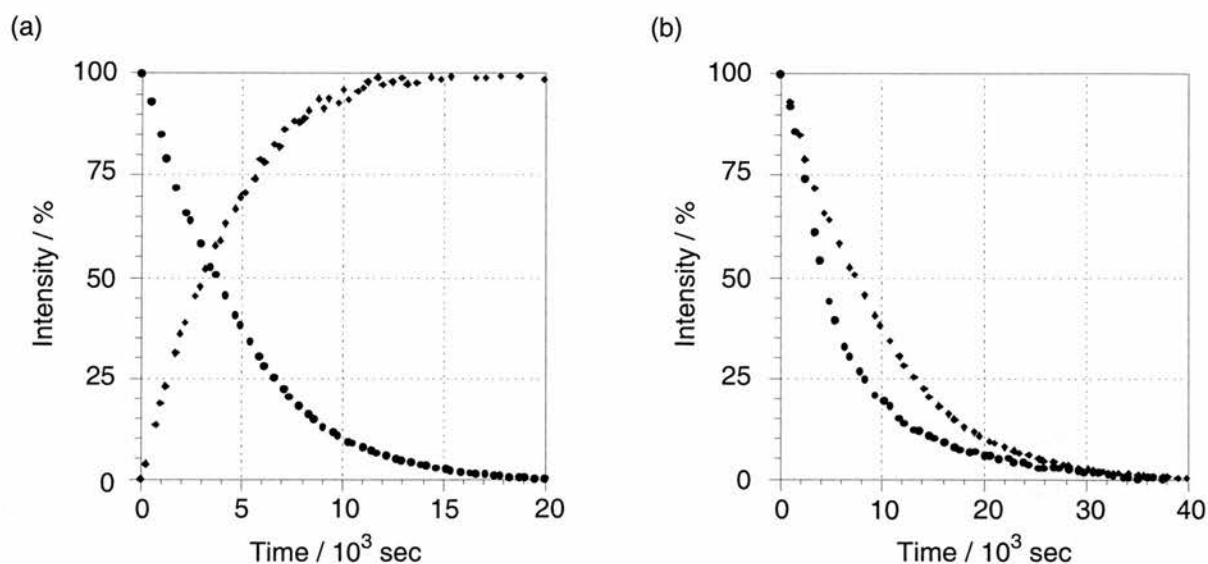


procedure was repeated at several different temperatures. In each case, the loss of the reflections characteristic of the reactant phase corresponded exactly with the growth of a new set of reflections, characteristic of the product phase (**Figure 49a**).



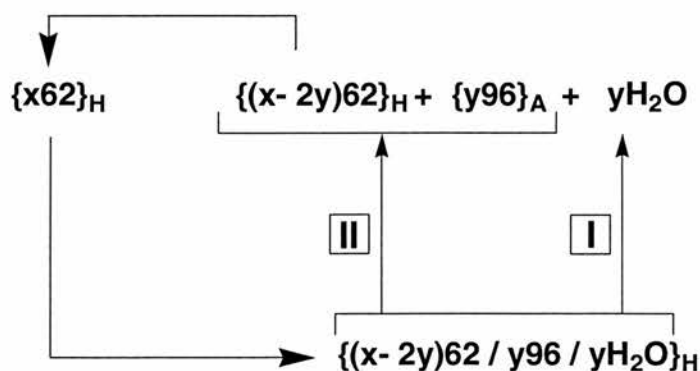
**Figure 49** (a) Powder X-ray diffraction patterns recorded (i) at the start of the experiment, and (ii) after heating at 100°C for 120 mins illustrate the structural change that occurs. (b) The solid state reaction can be followed using the well resolved reflections in the range  $8^\circ < 2\theta < 13^\circ$ . The reflections in this region are shown (i) at the start of the experiment, (ii) during the experiment, and (iii) after heating at 100°C for 120 minutes.

The PXRD pattern recorded using a sample of the material recovered from the TGA heating experiments described above is identical to the diffraction pattern obtained at the end of the high temperature PXRD experiments. This data therefore allows us to equate the chemical change observed by TGA with the structural change determined by PXRD. The structural change observed by PXRD was reproducible and occurred within 1 hour at 100°C. Hereafter, the crystalline phases characteristic of **62** and **96** are signified by  $\{ \}_H$  and  $\{ \}_A$  respectively, and the actual chemical identities of the molecules present within the crystalline phases are represented as **62** and **96**. The rate of the solid state transformation may be followed by observing the loss of reflections characteristic of reactant phase  $\{62\}_H$ , and the concurrent growth of reflections characteristic of the product phase  $\{96\}_A$  (**Figure 50a**). **Figure 49b** shows the diffraction pattern in the range  $8^\circ < 2\theta < 13^\circ$  recorded before, during and after heating.



**Figure 50** (a) The growth of the reflection at 9° (◆) coincides exactly with the disappearance of the reflection at 12° (●). (b) The solid state transformation occurs faster at 95 °C (●) than at 85 °C (◆).

As the peaks in this region are particularly well resolved, they were used to follow the course of the reaction. A graph showing peak intensity vs. time (**Figure 50b**) demonstrates that the product phase  $\{96\}_A$  is formed more rapidly at higher temperatures, as expected. Although the reaction occurs within 2 hours at temperatures of 80°C and above, at lower temperatures there is a significant decrease in the reaction rate and below 60 °C some amount of the reactant phase  $\{62\}_H$  is still present even after 18 hours. The kinetic data obtained from PXRD experiments can also be fitted to the Avrami-Erofeev equation. In this case, the best fit to the experimental data is obtained with a value of  $n = 1$ , in contrast to the TGA data, which were best fitted using  $n = 2$ .



**Figure 51** A schematic representation of the solid state transformation from **62** to **96**. The products shown refer to the situation at  $a = 2y/x$ , with  $2y < x$ . The notation  $\{ \}_H$  and  $\{ \}_A$  denote the crystal structures of **62** and **96** respectively. Process I is measured by TGA, and process II by PXRD.

This difference can be explained by recalling that the two different techniques (TGA and PXRD) actually observe different aspects of the solid state transformation (processes I and II respectively) (**Figure 51**).

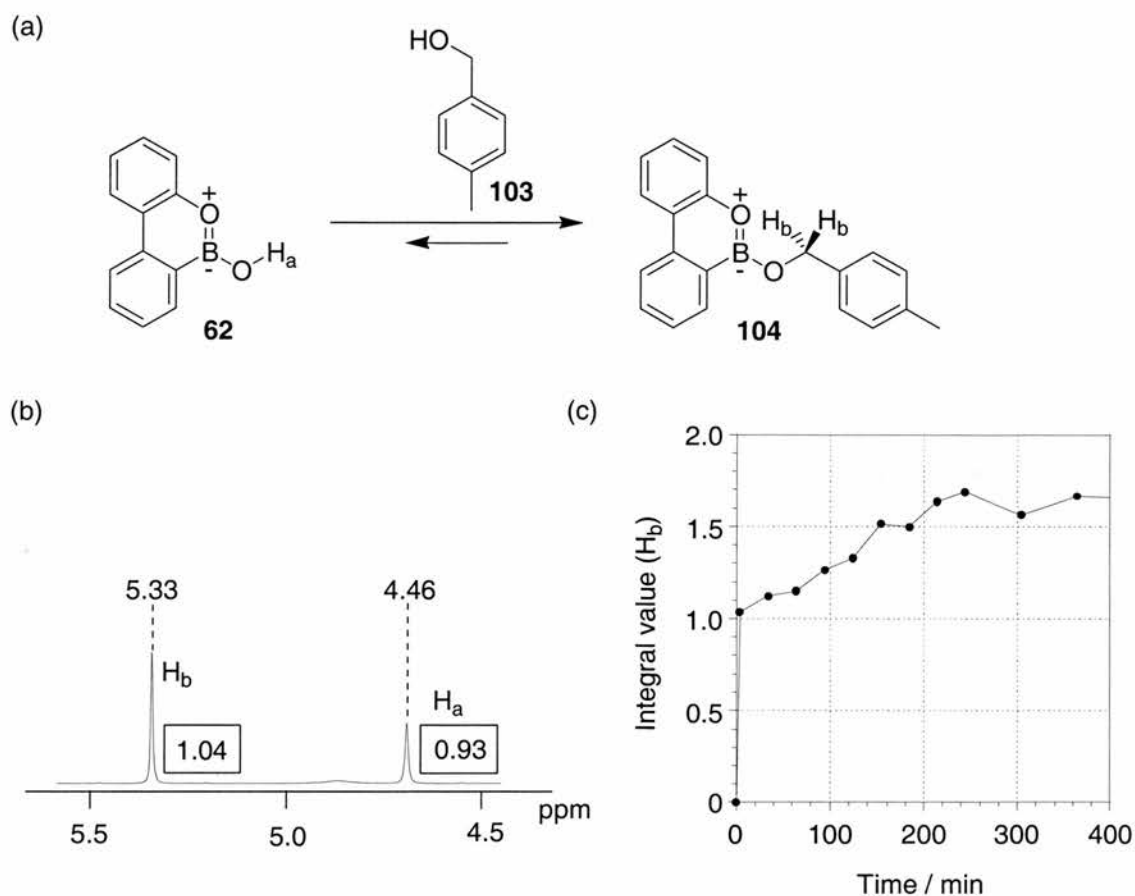
In particular, they monitor the change in two different aspects of the system as a function of time. The kinetic and mechanistic aspects of these processes are not necessarily related to each other, and, furthermore, neither technique directly probes the chemical transformation of **62** to **96**. Specifically, the isothermal TGA experiment monitors the rate of mass loss from the sample (Process I), which arises as a result of liberation of water from the solid sample to the vapour phase. This process is not necessarily equal to the rate of production of water within the solid crystalline phase, and therefore may not truly reflect the rate of chemical reaction. (The rate of mass loss will be equal to the rate of chemical reaction only when the rate of liberation of water molecules from the solid to the vapour phase is significantly faster than the rate of production of water). In contrast, the isothermal PXRD experiments monitor the changing identity of the crystalline phase. Only crystalline material can be observed using PXRD, and furthermore, in order to observe sharp reflections, the crystalline particles must be of a sufficient size. Once more, the rate of growth of crystalline particles of the anhydride  $\{\mathbf{96}\}_A$  large enough to give a PXRD pattern characteristic of the product phase is not necessarily the same as the rate of chemical transformation of **62** to **96**. Indeed, at low values of the extent of reaction  $\alpha$  molecules of anhydride can be incorporated within the crystalline phase of hydroxyboroxophenanthrene  $\{\mathbf{62}\}_H$ , forming a solid solution  $\{\mathbf{62},\mathbf{96}\}_H$ . At this stage PXRD techniques will not detect the presence of anhydride, as the crystalline phase of **62** is still the only one present. Only once the amount of **96** within the crystalline phase of **62** exceeds its solid state solubility, will phase segregation occur, and eventually crystalline particles of the product phase  $\{\mathbf{96}\}_A$  of sufficient size will form (Process II). At this point the PXRD pattern will show evidence of the anhydride phase. As noted above the kinetic and mechanistic aspects of these two processes I and II are not necessarily related to each other, although they are both related to the overall rate of chemical transformation. The PXRD data provide no evidence of any intermediate crystalline phases other than **62** and **96**, and, in fact, since the rate of loss of  $\{\ }_H$  is directly comparable to the rate of production of  $\{\ }_A$ , the data strongly suggest that no intermediate phases at all, crystalline or amorphous, are formed. It can also be noted that the liberation of water from the solid sample, as detected by TGA, occurs much faster at a specified temperature than the generation of the product crystalline phase.

However, these results do not provide any information about the solubility of anhydride **96** within { }<sub>H</sub>, or about the extent of reaction  $\alpha$  at which phase segregation occurs.

Thus far, the solid state behaviour of 10-hydroxy-10,9-boroxophenanthrene **62** has been shown to be largely identical to that of the analogous borazaaromatic **56**. 10-Hydroxy-10,9-borazaphenanthrene **56** also dehydrates on heating to form a single anhydride phase **87**, although a total of 5 different phases of **56** exist in the solid state.

## 2.6 Solution Phase Reactivity

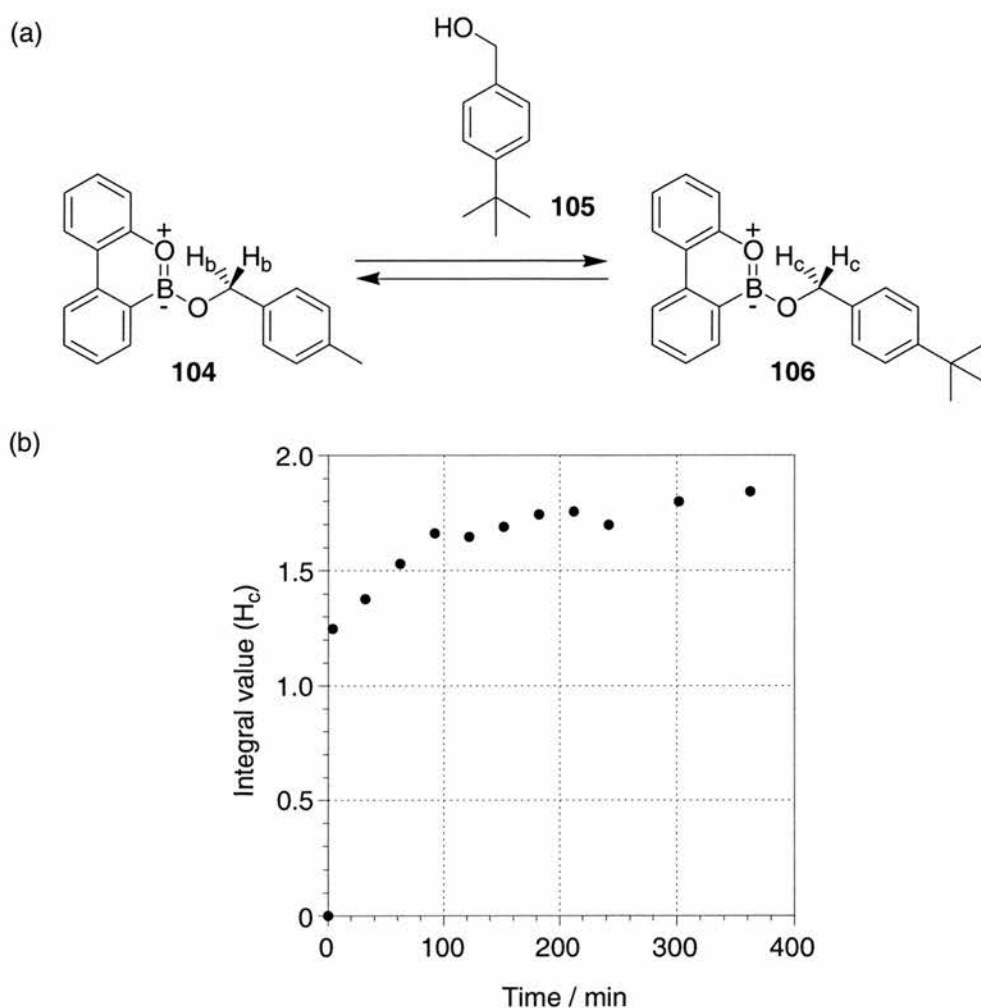
The solution phase reactivity of **62** is markedly different than the solution phase reactivity of **56**. It has already been stated above that **56** exists in equilibrium in solution with the anhydride **87**, and both species are visible in the solution phase NMR spectrum. In contrast, the NMR spectrum of 10-hydroxy-10,9-boroxophenanthrene **62** shows no evidence of the anhydride. **62** does not react with itself in solution. It has been established that 10-hydroxy-10,9-borazaphenanthrene **56** reacts slowly with other alcohols, such as benzyl alcohol, to form the corresponding alkoxy-esters. In order to compare the solution phase reactivities of **62** and **56**, we attempted to follow the reaction between **62** and 4-methylbenzyl alcohol **103** (**Figure 52a**) using <sup>1</sup>H NMR spectroscopy. Equimolar amounts of the two compounds were dissolved in CDCl<sub>3</sub>, and stirred over 4 Å molecular sieves. 300 MHz <sup>1</sup>H NMR spectra of this solution were then recorded at regular intervals. The resonances arising from protons H<sub>a</sub> and H<sub>b</sub> (**Figure 52b**) are well resolved and the progress of the reaction was followed by monitoring the change in integration value of these two signals (**Figure 52c**).



**Figure 52** (a) The reaction between **62** and **103** is extremely fast and can be followed by monitoring resonances due to  $H_a$  and  $H_b$ . (b) Partial  $^1H$  300 MHz NMR spectrum of a 1:1 mixture of **62** and **103** in  $CDCl_3$  after 3 minutes. Integral values are shown in boxes. (c) A plot of the integral value of  $H_b$  vs. time demonstrates the rapidity with which equilibrium is reached. An integral value of 2.0 represents complete conversion to **104**.

After approximately 3 minutes, the reaction had reached almost 55% completion, but then showed a significant decrease in rate. This observation indicates that nucleophilic attack of benzyl alcohol at boron is an inherently fast reaction, but suggests that the water formed during the reaction quickly overwhelms the molecular sieves and acts to slow the formation of the ester. In order to eliminate this problem, we then set up a “transesterification” equilibrium between 10-(4-methylbenzyloxy)-10,9-boroxophenanthrene **104** and a second nucleophile, 4-*tert*-butylbenzyl alcohol **105** (**Figure 53a**). In this case, no water is formed during the reaction and we would therefore expect to observe the reaction without any decrease in rate due to hydrolysis of the ester. **105** was chosen as, in terms of nucleophilicity, it is similar to **103**. Hence, we anticipated that the reaction rate observed would simply be a manifestation of the electrophilicity of the boron atom, rather than any other factors such as the nucleophilicity of the alcohol. The methyl- and *tert*-butyl-substituted benzyl alcohols also have convenient resonances in their  $^1H$  NMR

spectra, which aid the interpretation of the equilibrium process by  $^1\text{H}$  NMR spectroscopy.



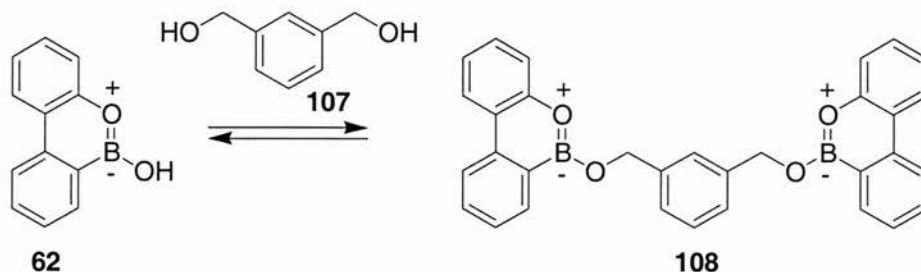
**Figure 53** (a) The reaction between **104** and **105** reaches equilibrium very quickly, as shown by (b) the growth of the NMR signal due to  $H_c$ . An integral value of 2.0 represents complete conversion to **106**.

A sample of 10-(4-methylbenzyloxy)-10,9-boroxophenanthrene **104** was prepared by stirring a solution of **62** and 4-methylbenzyl alcohol **103** over 4 Å molecular sieves in  $\text{CDCl}_3$  under  $\text{N}_2$  for 2 days. Once  $^1\text{H}$  NMR spectroscopy indicated that the condensation reaction had gone to completion, the molecular sieves were removed and an equimolar amount of 4-*tert*-butylbenzyl alcohol **105** was added. Variable temperature  $^1\text{H}$  NMR spectroscopic analysis of the reaction indicated that it had attained spectroscopic equilibrium within 3 minutes, even at  $-40^\circ\text{C}$ .

In a further experiment, a 1:1 solution of **62** and 1,3-benzenedimethanol **107** in  $\text{CHCl}_3$  was analysed by MALDI-TOF spectrometry. Somewhat surprisingly, the major peak observed was that at  $m/z$  494, representing the 2:1 adduct **108** (Figure 54). A small



peak due to the 1:1 adduct at  $m/z$  316 was also seen. This result will be discussed in more detail in **Chapter 4**.



**Figure 54** MALDI-TOF spectrometry shows that reaction of **62** with **107** leads to the formation of the 2:1 adduct **108**.

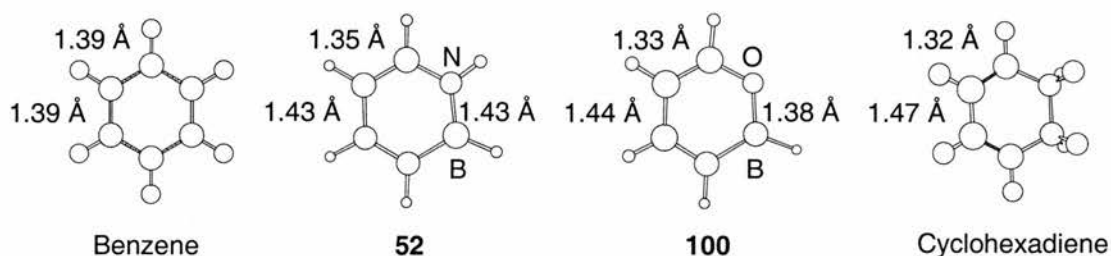
These experiments demonstrate conclusively that the solution phase chemistry of 10-hydroxy-10,9-boroxophenanthrene **62** is markedly different to that of the corresponding borazaaromatic **56**. The rapidity with which these systems reach equilibrium indicates their potential use in, for example, dynamic combinatorial libraries, which will be discussed further in **Chapter 3**.

## 2.7 Aromaticity of Boron-Containing Heteroaromatic Compounds

As discussed in **Section 2.3.1**, the calculated bond order and bond length of the B-O bond in **62** do not provide us with any indication of the degree of aromaticity present in the system. We cannot deduce any information about the delocalisation of the B-O bond from these values. In order to evaluate the extent to which systems of this kind can be considered aromatic, the equilibrium geometries of borazabenzene **52** and boroxobenzene **100**, and their hydrogenated derivatives (those compounds resulting from the successive hydrogenation of the  $sp^2$ - $sp^2$  bonds) were calculated at the HF6/31G(d,p) level of theory. Selected bond lengths in these structures are compared in **Table 4** with those calculated for benzene and its hydro-derivatives. The difference in C1-C2 bond length between benzene and cyclohexadiene (0.07 Å) is indicative of the extent of delocalisation in benzene. By analogy, the delocalisation of the B-N and B-O bonds is implied by the difference between the boron-heteroatom bond lengths in **52** or **100** respectively, and that in the appropriate mono-hydrogenated derivative. In **52** this difference is small (0.03 Å), but suggests a significant level of aromaticity. In **100**, the difference (0.02 Å) is even smaller. The C3-C4, C4-C5 and C5-C6 bond lengths in both **52** and **100** change in a manner



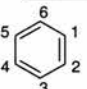
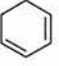
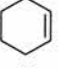

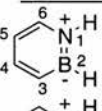
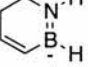
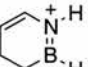
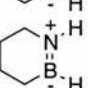
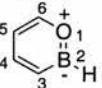
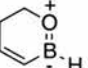
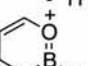
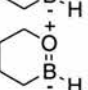
consistent with the changes observed in benzene. However, whereas the C-C bond lengths in benzene are all equal (1.39 Å), the bond lengths in the two boron heteroaromatics are not. The bond lengths of borazabenzene **52** (Figure 55) are almost exactly intermediate between those of a fully delocalised system (e.g. benzene) and a non-delocalised system (e.g. cyclohexadiene). In contrast, boroxobenzene **100** has bond lengths that are rather closer to those in cyclohexadiene, further suggesting the absence of any substantial delocalisation, and supporting evidence that suggests that boroxoaromatics are less aromatic than borazaaromatics.



**Figure 55** Selected bond lengths in the calculated (HF/6-31G(d,p)) equilibrium geometries of benzene, borazabenzene **52**, boroxobenzene **100** and cyclohexadiene.

The extent of delocalisation in the  $\pi$ -system of **52**, **100**, and in benzene itself is also demonstrated by the calculated average resonance energy (Figure 56). The resonance energy of benzene is the difference in the enthalpy change for the hydrogenation of one of the unsaturated C-C bonds in benzene, compared with the same value for the hydrogenation of a further unsaturated C-C bond in the non-conjugated derivatives, cyclohexadiene or cyclohexene. The resonance energy of benzene is around  $155 \text{ kJmol}^{-1}$ , as shown in Figure 56. Similar calculations performed on borazabenzene **52** reveal the resonance energy of **52** ( $90 \text{ kJmol}^{-1}$ ) to be close to half that of benzene, reinforcing the theory that **52** is in fact aromatic, although the degree of delocalisation is significantly less than for the hydrocarbon arene analogues. **100** also possesses some level of aromaticity, but the value calculated for the resonance energy is just over half that for **52**. **100** is therefore appreciably less resonance stabilised than benzene.

**Table 4** Selected bond lengths in the calculated (HF/6-31G(d,p)) equilibrium geometries of benzene, **52** and **100**, and their hydrogenated derivatives.

	$d_{C1-C2}$	$d_{C3-C4}$	$d_{C4-C5}$	$d_{C5-C6}$
	1.39	1.39	1.39	1.39
	1.32	1.32	1.51	1.53
	1.32	1.53	1.53	1.53
	1.53	1.53	1.53	1.53
	$d_{B-N}$	$d_{C3-C4}$	$d_{C4-C5}$	$d_{C5-C6}$
 <b>52</b>	1.43	1.35	1.43	1.35
	1.40	1.33	1.51	1.53
	1.40	1.54	1.51	1.32
	1.39	1.54	1.53	1.53
	$d_{B-O}$	$d_{C3-C4}$	$d_{C4-C5}$	$d_{C5-C6}$
 <b>100</b>	1.38	1.35	1.44	1.33
	1.35	1.33	1.51	1.52
	1.36	1.54	1.51	1.32
	1.34	1.54	1.53	1.52

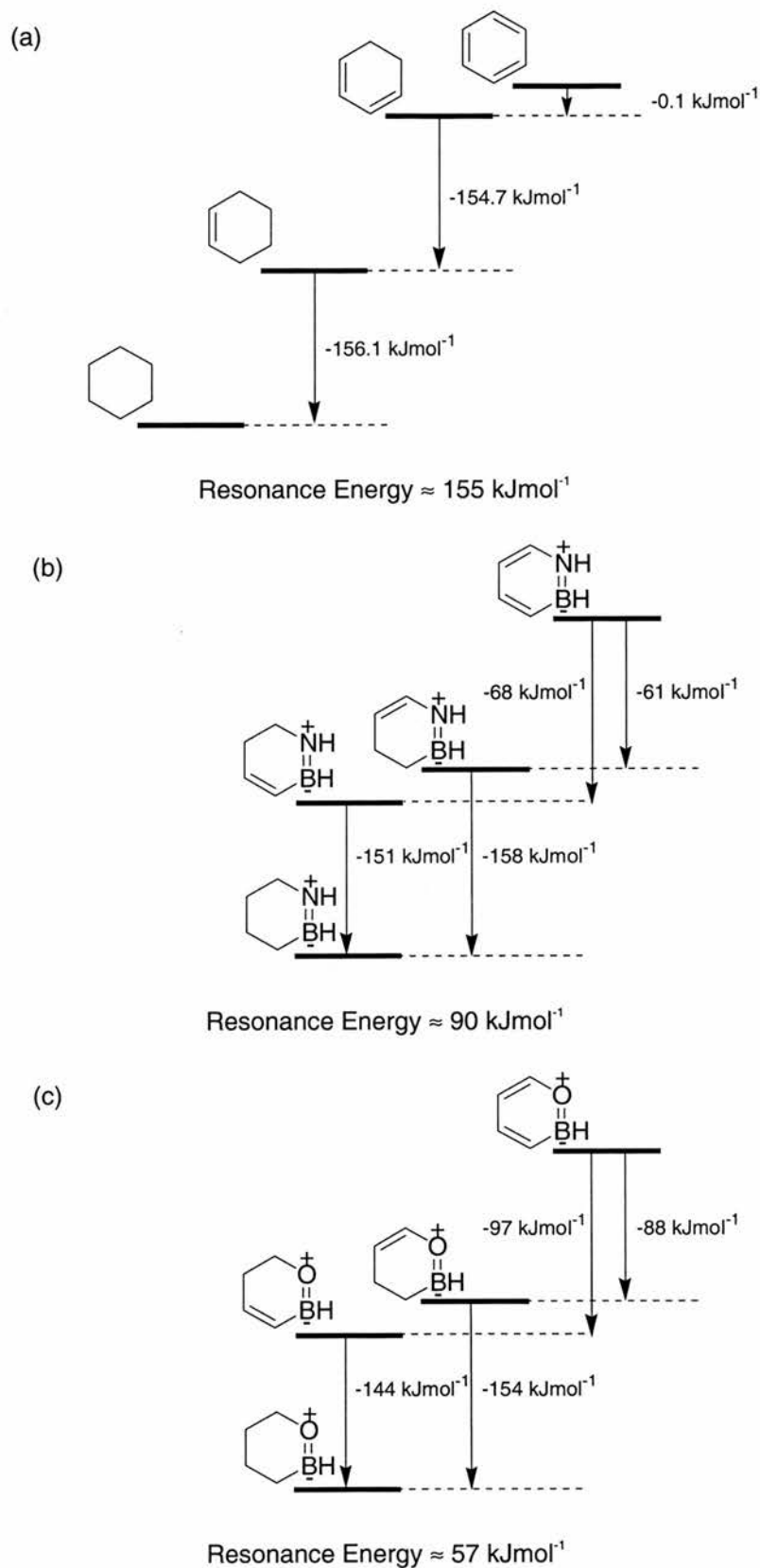


Figure 56

Calculated (HF/6-31G(d,p)) enthalpies of hydrogenation of benzene and its hydro-derivatives, compared with **52** and **100**, and their hydro derivatives. The resonance energy is the average difference between the enthalpy of hydrogenation for the conjugated system and the enthalpy of hydrogenation for the non-conjugated hydro-derivative.

## 2.8 Conclusions

The crystal structure of hydroxyboroxophenanthrene **62** illustrates the similarity between the recognition properties of boroxoaromatics and carboxylic acids, as both are capable of forming hydrogen-bonded dimers in the solid state. The reactivity of **62** in the solution phase, however, is manifestly different than the reactivity of either carboxylic acids, or the corresponding borazaaromatic **56**. **62** does not react with itself in solution, whereas self-condensation of **56** in solution is a facile process. Equally, borazaaromatics and carboxylic acids do not readily undergo reactions with other nucleophiles. Hydroxyboroxophenanthrene **62**, on the other hand, reacts extremely rapidly with nucleophiles and these reactions are under thermodynamic control.

The solid state reactivity of **62** is also different to that of carboxylic acids. The self-condensation reaction to form the anhydride **96** occurs at relatively low temperature, and **96** is stable in the solid state. This dehydration reaction to form the homoanhydride occurs slower at lower temperatures and can be followed easily using techniques such as TGA and PXRD.

The reaction of **62** with itself and with other nucleophiles involves nucleophilic attack at boron. The electrophilicity of the boron atom is attributed to the presence of a partially filled  $p_z$ -orbital on boron, combined with the incidence of strong B $\rightarrow$ O  $\sigma$  donation. The calculated electrostatic potential surface is a maximum at boron, providing further evidence of its electrophilicity.

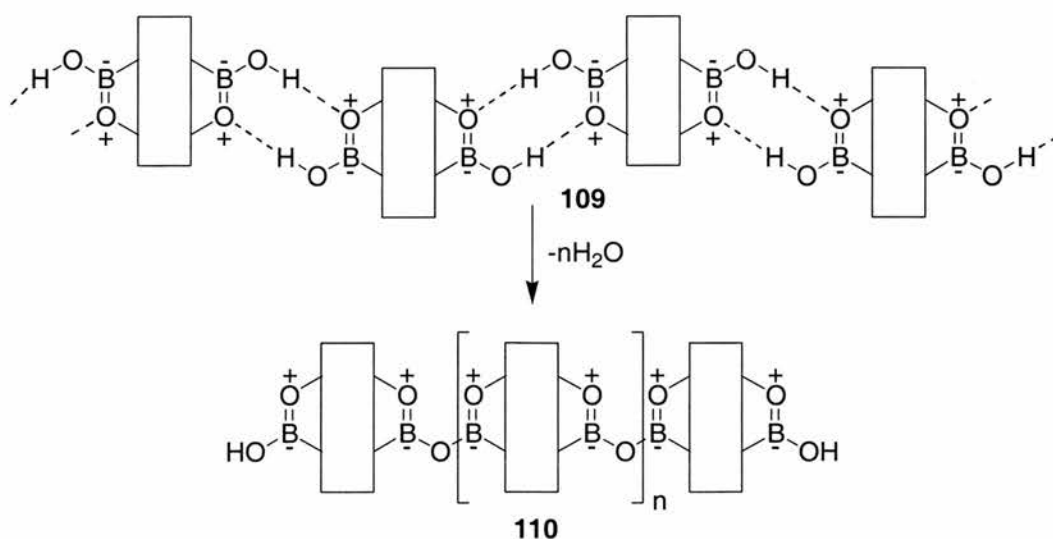
Electronic structure calculations confirm that both the endocyclic and exocyclic B-O bonds have significant  $\pi$ -character suggesting the system is delocalised. This extended delocalisation results in an unusually large B-O-B bond in the anhydride crystal structure. The degree to which these systems can be deemed aromatic, however, is not clear from these calculations, however a study of the resonance energies, and bond lengths of the parent compound boroxobenzene **100**, compared with the boron-nitrogen analogue **52**, suggests that both are aromatic, as judged by the presence of significant resonance energy, although the boron-oxygen compound is considerably less so than the boron-nitrogen compound.

### 3 Bifunctional Boron-Containing Heteroaromatic Systems

Despite the interesting differences in reactivity between boroxo- and borazaaromatics, the complexity of systems that can be formed by monofunctional building blocks, such as 10-hydroxy-10,9-boroxo-phenanthrene **62**, is limited. As has already been described in **Section 1.2.4**, alternative systems can be envisaged, which have the potential to form self-assembled polymeric anhydrides, through the incorporation of two B-OH functionalities. This chapter discusses the attempted synthesis of several different bifunctional boron heteroaromatic compounds, their expected reactivities and possible applications.

#### 3.1 Rigid Systems Designed to Form Linear Oligomers

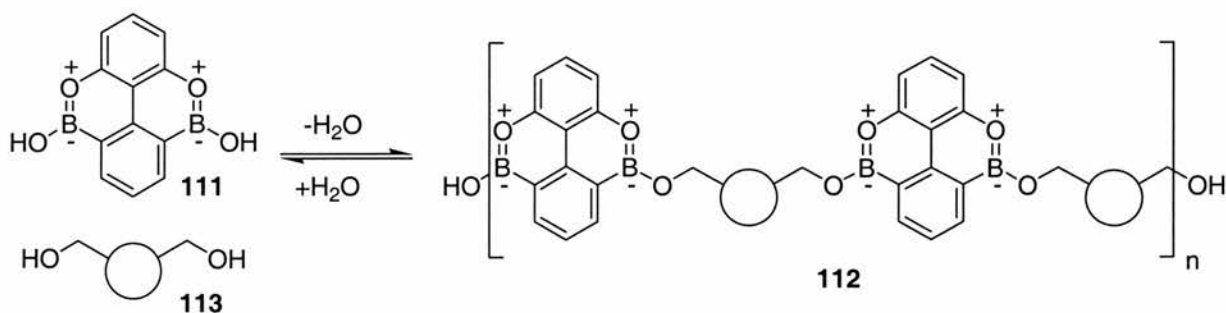
Perhaps one of the most obvious designs for a bis-boroxoaromatic is that illustrated in **Figure 57**, whereby a rigid aromatic skeleton separates two boron-oxygen functionalities. Theoretically, this system would be expected to form an extended hydrogen-bonded array **109** in the solid state, bringing the reactive B-hydroxy centres into close proximity. Heating the compound in the solid state may then initiate the self-condensation reaction to form the poly-anhydride **110**, which may preserve some of the structural organisation exhibited by the hydrogen-bonded hydroxy-compound.



**Figure 57** A bis-boroxoaromatic compound which is capable of forming hydrogen-bonded linear oligomers **109** in the solid state, may dehydrate on heating to afford the polymeric anhydride **110**.

Examples of thermally-initiated bond-forming reactions in the solid state are scarce,<sup>155</sup> and in particular, the use of molecular recognition to facilitate and direct a reaction has not been widely researched.<sup>156</sup>

The borazaaromatic **89** described in **Section 1.2.4** is an analogue of this kind of system. Based on a rigid pyrene skeleton, this compound forms linear oligomers both in solution and in the solid state. In solution, the reaction is reversible, and is therefore under thermodynamic control. As such, the length of the oligomers is governed by several factors, including the solvent, the amount of water present in solution, and the stability of the various oligomers. It is logical to assume that the boroxoaromatic compound **111** will also form an extended hydrogen-bonded array in the solid state. However, considering the reactivity of our model compound **62** we must suppose that the pyrene based boroxoaromatic compound, although it may dehydrate when heated in the solid state, is unlikely to do so in the solution phase. In contrast, if **111** (**Figure 58**) reacts rapidly with nucleophiles, in a similar fashion to that observed for **62**, it might be possible to monitor the formation of linear hetero-oligomers **112** in solution (**Figure 58**). The reaction between **111** and a nucleophile **113** in solution would be under thermodynamic control. It is also possible that these oligomers may cyclise to form macrocycles.



**Figure 58** Bis-boroxoaromatic **111** may react with diol **113** in solution to form linear oligomers **112**.

### 3.1.1 Synthesis of 5,9-Dihydroxy-5,9-dibora-4,10-dioxopyrene

It was proposed that the synthesis of **111** would be readily accessible *via* the precursor diol **114** (**Figure 59**), which would in turn be constructed by applying standard cross-coupling methodology<sup>157</sup> to a protected 2,6-dihydroxyhalogenobenzene **115**.

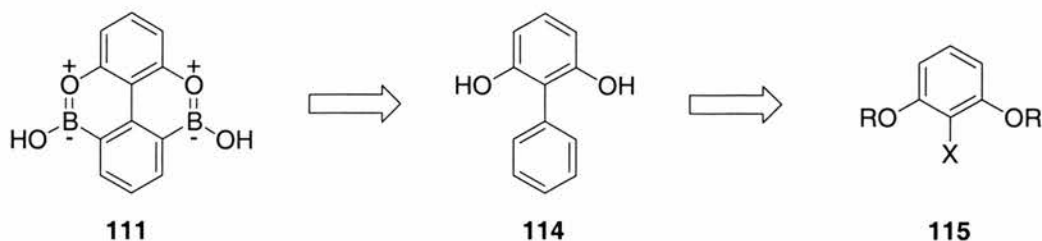
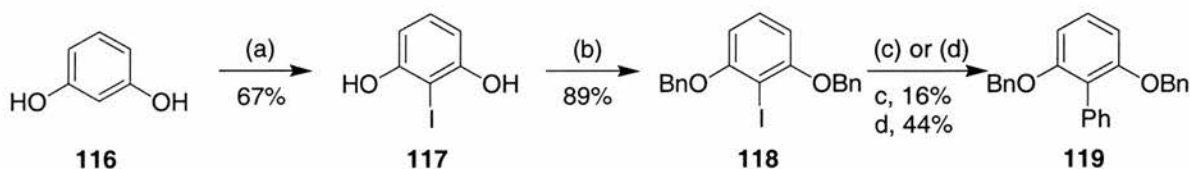


Figure 59

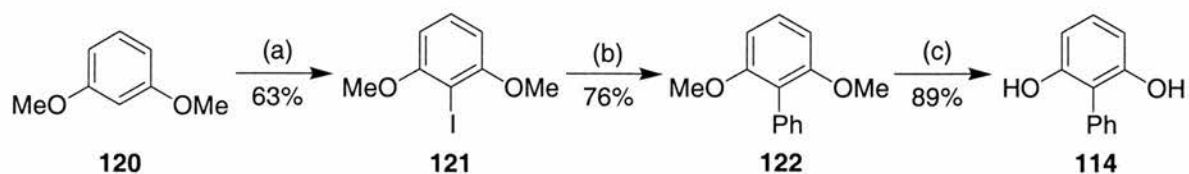
Initially, the synthesis of **114** was attempted using the methodology described in **Scheme 10**. Addition of sodium hydrogen carbonate to an equimolar mixture of resorcinol **116** (1,3-dihydroxybenzene) and iodine in water resulted<sup>158</sup> in the precipitation of 2,4,6-triiodoresorcinol, which was isolated by filtration. However, work up of the filtrate afforded 2-iodoresorcinol **117**, with a small contaminant (believed<sup>158</sup> to be 4,6-diiodoresorcinol), which was readily removed by recrystallisation. Bumagin and co-workers have reported<sup>159</sup> that it is possible to couple organomagnesium reagents with aryl halides containing hydroxyl functionalities, using an excess of Grignard reagent to “protect” these groups. This procedure was not described for 1,3-diols, however, and attempts at the direct cross-coupling of the unprotected diol **117**, using both Kharasch<sup>160</sup> and Suzuki<sup>161</sup> coupling methodologies, were unsatisfactory, with low yields of the desired compound **114** proving difficult to isolate.



**Scheme 10** (a)  $I_2$ ,  $NaHCO_3$ ,  $H_2O$ ; (b)  $BnBr$ ,  $K_2CO_3$ , 18-C-6, acetone; (c)  $PhB(OH)_2$ ,  $Pd(PPh_3)_4$ ,  $Na_2CO_3$ , DME, EtOH,  $H_2O$ , 18hr; (d)  $PhMgBr$ ,  $Ni(dppe)Cl_2$ ,  $Et_2O$ , 18hr.

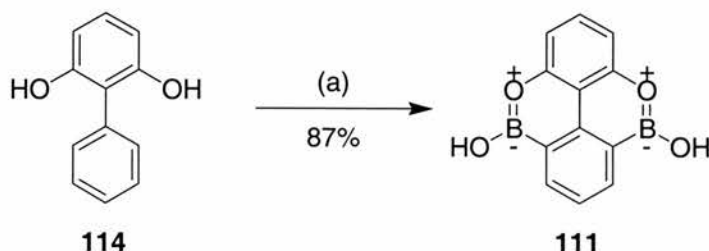
It was obviously necessary to protect the hydroxyl functionalities, and this was readily achieved in near quantitative yield using benzyl bromide. Cross-coupling of **118** using either Kharasch<sup>160</sup> or Suzuki<sup>161</sup> methodology gave the desired benzyl-protected 2,6-dihydroxybiphenyl **119**. However, since this route added an extra step to the synthesis, it was improved by using resorcinol dimethyl ether (1,3-dimethoxybenzene) **120**, rather than resorcinol itself, as the starting point (**Scheme 11**).





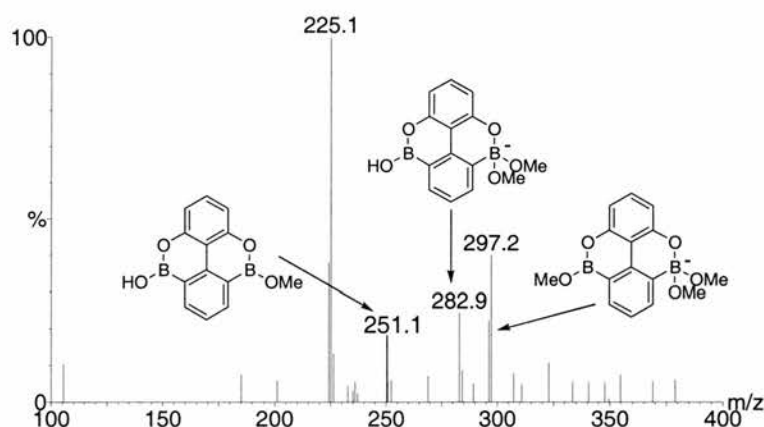
**Scheme 11** (a) (i) *t*-BuLi, THF, 0°C, (ii) I<sub>2</sub>, THF; (b) PhMgBr, Ni(PPh<sub>3</sub>)<sub>4</sub>Cl<sub>2</sub>, Et<sub>2</sub>O, Δ; (c) BBr<sub>3</sub>, CH<sub>2</sub>Cl<sub>2</sub>.

Treatment<sup>162</sup> of 1,3-dimethoxybenzene **120** with *t*-BuLi led to selective deprotonation of the 2-position, and reaction with iodine gave 2,6-dimethoxyiodobenzene **121** in moderate yield. The yield of the subsequent Ni-catalysed Kharasch coupling with phenyl magnesium bromide was found to vary greatly with the identity of the catalyst. With [Ni(dppe)Cl<sub>2</sub>], the desired 2,6-dimethoxybiphenyl **122** was obtained only in low yield (18%), with the homocoupling product, biphenyl, accounting for the majority of the recovered material. The yield was significantly improved (78%) on changing the catalyst to Ni(PPh<sub>3</sub>)<sub>2</sub>Cl<sub>2</sub>, and furthermore, this method used only 2 mol% catalyst, rather than the 10 mol% required previously. The coupling was also attempted using Stille<sup>163</sup> and Suzuki<sup>161</sup> methodology, but neither resulted in an improved yield. Deprotection of **122** using boron tribromide gave the diol **114** in good yield. The cyclisation of **114** to afford the target 5,9-dibora-4,10-dioxapyrene **111** proved problematic and was attempted using three different approaches. Under the same conditions applied to the synthesis of boroxophenanthrene **62**, *i.e.* reaction of **111** with BCl<sub>3</sub>, and subsequent cyclisation with AlCl<sub>3</sub>, only starting material was recovered. Reaction of **111** with BCl<sub>3</sub> results in the evolution of HCl, and it is possible that the adduct is not stable under these increasingly acidic conditions. With this in mind, we used BHCl<sub>2</sub>•Me<sub>2</sub>S as the boron source, hoping that this would solve this problem, however, once again, only starting material was recovered from the mixture. It is possible to follow the reaction of **111** with BHCl<sub>2</sub> by measuring the volume of H<sub>2</sub> gas produced during the process. In all cases this was found to be consistent with the expected volume, indicating that the oxoborondichloride adduct is indeed formed. Calculations (**Chapter 2**) have shown that the boron-oxygen bond is somewhat weaker than the boron-nitrogen bond. It may be that the oxoborondichloride adduct is simply too fragile to withstand the reaction conditions, and the O-B bond is hydrolysed before the cyclisation has taken place.



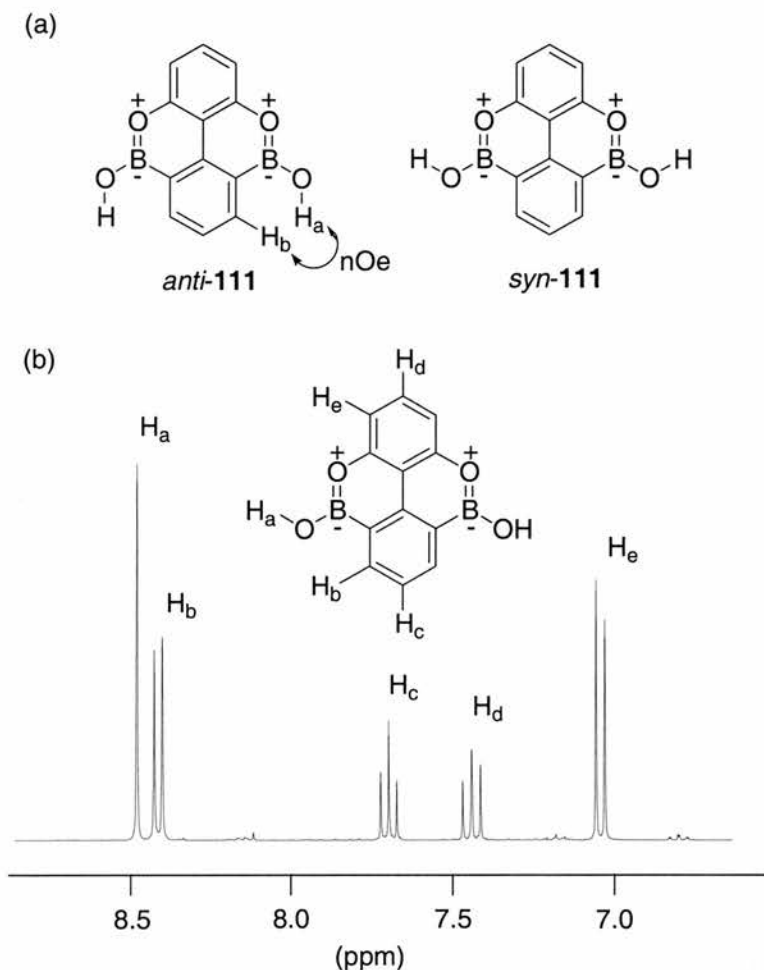
**Scheme 12** (a) (i)  $\text{BHCl}_2$ , PhMe, (ii)  $\text{AlCl}_3$ , PhMe,  $\Delta$ .

A third method (**Scheme 12**) employed uncomplexed  $\text{BHCl}_2$ , generated *in situ* by the reaction of  $\text{BHCl}_2 \cdot \text{Me}_2\text{S}$  with  $\text{BCl}_3$ . This resulted in the successful formation, in good yield, of **111**, which was identified initially by electrospray mass spectrometry (ESMS) in methanol, as a mixture of the methyl esters (**Figure 60**).



**Figure 60** The negative electrospray mass spectrum of crude **111**, (MeOH, Flow rate:  $50 \mu\text{Lmin}^{-1}$ , Cone voltage: 40 V) shows several methoxy esters of **111**.

These are readily converted to the bis-hydroxy form of **111** on dissolution in wet acetone. Attempts to assign the NMR resonances due to the aromatic protons were hampered by the lack of any observable nOe effect between protons  $\text{H}_a$  and  $\text{H}_b$ , (**Figure 61a**). This possibly provides some evidence that the hydroxyl group adopts a *syn* conformation with respect to the boron-oxygen bond, rather than an *anti* conformation (in which an nOe effect would be observed). This is consistent with the preference for the *syn*-conformation expressed by **62** (**Section 2.3.1**).



**Figure 61** (a) The absence of any observable nOe may suggest that **111** adopts a *syn*, rather than an *anti* conformation. (b) Partial 300 MHz  $^1\text{H}$  NMR spectrum of **111**, recorded at 293K in  $d_6$ -acetone. The resonance due to  $\text{H}_a$  is assigned on the basis of its disappearance on addition of  $\text{D}_2\text{O}$ . The remaining four resonances can be tentatively assigned by COSY analysis.

However, the singlet resonance at  $\delta$  8.45 undoubtedly arises from the exchangeable hydroxyl proton, since this signal disappears when a drop of  $\text{D}_2\text{O}$  is added to the sample. It seems likely – by comparison with the resonances observed in the  $^1\text{H}$  NMR spectra of the precursors to **111** – that the doublet observed just upfield of this at  $\delta$  8.39 is due to  $\text{H}_b$ . The other resonances are then readily assigned (**Figure 61b**) by COSY experiments.  $^1\text{H}$  NMR analysis in  $d_6$ -acetone shows the bis-hydroxy monomer **111** only, as expected. It is useful to recall here that the boron-nitrogen pyrene analogue **89**, which does undergo self-condensation in chloroform, does not react with itself in acetone. Unfortunately, the compound is not soluble in  $\text{CDCl}_3$ , so it cannot be stated with any certainty that **111** does not react with itself in non-polar solvents. However, even after rigorous drying of the acetone solution over Drierite<sup>®</sup> (anhydrous  $\text{CaSO}_4$ ) for 2 weeks, there is no evidence of any higher oligomers.

### 3.1.2 The Calculated Structure of 5,9-Dihydroxy-5,9-dibora-4,10-dioxopyrene

In order to compare the structural and electronic properties of **111** with the mono-functional compound **62** we carried out *ab initio* calculations at the HF/6-31G(d,p) level of theory. Selected bond lengths and Löwdin<sup>147</sup> bond orders of **111** and, for ease of comparison, **62** are shown in **Table 5**, and are almost completely identical. The calculated structure is planar, and both O-H bond vectors are *syn* with respect to the endocyclic B-O bond. At this level of theory, *syn,syn-111* is around 30 kJmol<sup>-1</sup> more stable than *anti,anti-111*.

**Table 5** Selected bond lengths and Löwdin<sup>147</sup> bond orders in the calculated (HF/6-31G(d,p)) structures of **111** and **62**.

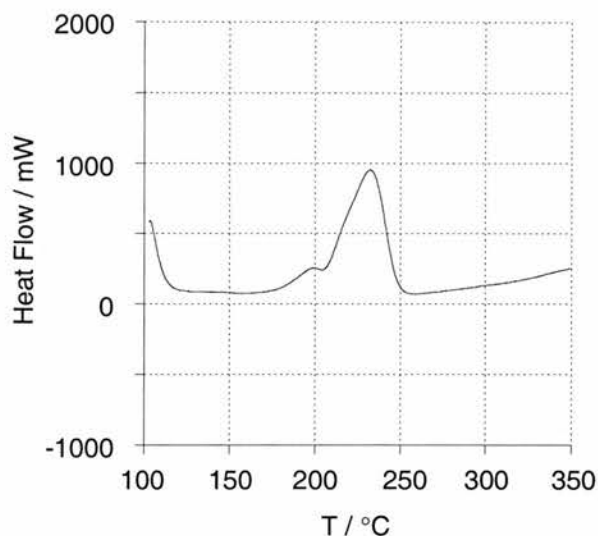
Compound	Bond	Length / Å	Bond Order
<i>syn-62</i>	Endocyclic O-B	1.37	1.32
	Exocyclic O-B	1.35	1.45
	C-Endocyclic O	1.35	1.17
	C-B	1.55	1.04
<i>syn,syn-111</i>	Endocyclic O-B	1.37	1.30
	Exocyclic O-B	1.35	1.45
	C-Endocyclic O	1.35	1.18
	C-B	1.55	1.04

As in **62**, the hybridisation of the exocyclic oxygen is confirmed to be closer to  $sp^2$  than  $sp^3$  by the C-B-O<sub>exo</sub> and O<sub>endo</sub>-B-O<sub>exo</sub> bond angles (123° and 118° respectively), and the calculated bond orders predict considerable  $\pi$ -character for both the endocyclic and exocyclic O-B bonds.

### 3.1.3 Solid State Reactivity of 5,9-Dihydroxy-5,9-dibora-4,10-dioxopyrene

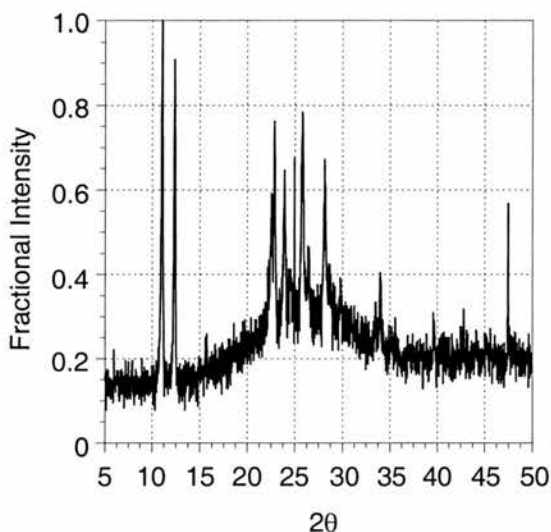
Samples of **111** do not melt below 400 °C, which is suggestive of polymerisation occurring in the solid state.<sup>164</sup> The solid state reactivity of **111** was investigated using differential scanning calorimetry (**Figure 62**). When heated to 350 °C at a rate of 50 °Cmin<sup>-1</sup>, an endotherm is observed with an onset temperature of 217 °C. The sample is subsequently cooled at the same rate, with no exotherm observed. This endotherm is obviously not due to the melting of the sample, and must therefore suggest a phase change. The DSC plot also appears to show a second small endotherm with an onset temperature of around 175 °C. The reason for

this peak has so far not been identified, but it may be due to a reorganisation in the solid state structure.



**Figure 62** DSC trace recorded on heating a sample of **111** from 100 °C to 350 °C, at 50 °Cmin<sup>-1</sup>. The onset of the solid state dehydration of the sample is clearly visible at 217 °C.

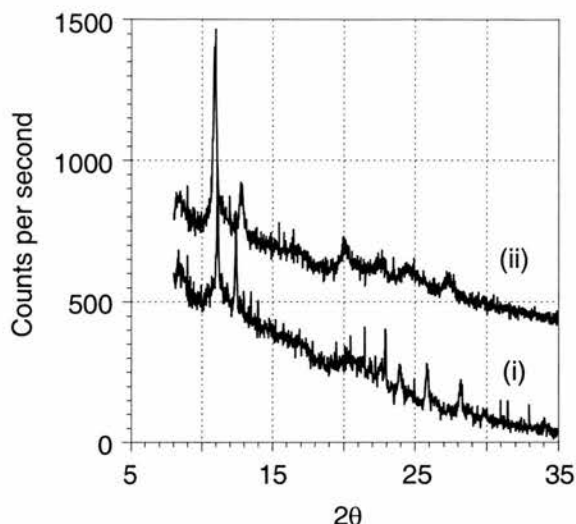
The powder X-ray diffraction pattern of **111** at room temperature is shown in **Figure 63**.



**Figure 63** Powder X-ray diffraction pattern of a sample of **111**, recorded at room temperature.

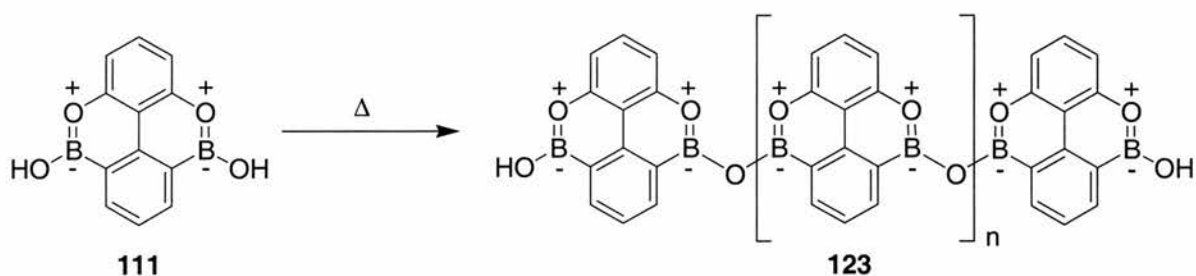
The change in the solid state structure of **111** that occurs on heating was confirmed by variable temperature X-ray diffraction experiments. When heated to 300 °C, the reflections gradually become less intense. However, even after 3 hours, the sample does not appear to be completely amorphous (**Figure 64**), as would be expected if a complete conversion to oligo-anhydride **123** had taken place. This provides possible

affirmation that there may be an intermediate crystalline phase or that the polymer formed retains some long-range order.



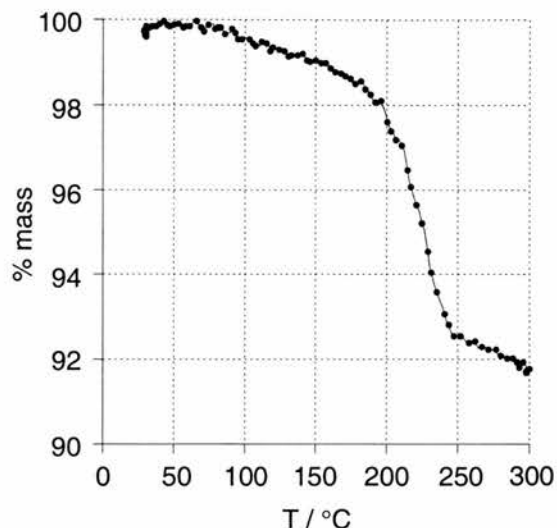
**Figure 64** Powder X-ray diffraction patterns recorded (i) at 30 °C, of a sample of **111**, and (ii) after heating a sample of **111** at 300 °C for 180 minutes, illustrate the structural change that occurs.

The solid state reactivity of **111** was confirmed using thermogravimetric analysis (TGA) to measure the loss of water from the sample. The formation of oligo-anhydrides **123** by loss of water from **111** (**Scheme 13**) corresponds to a 7.6% mass loss



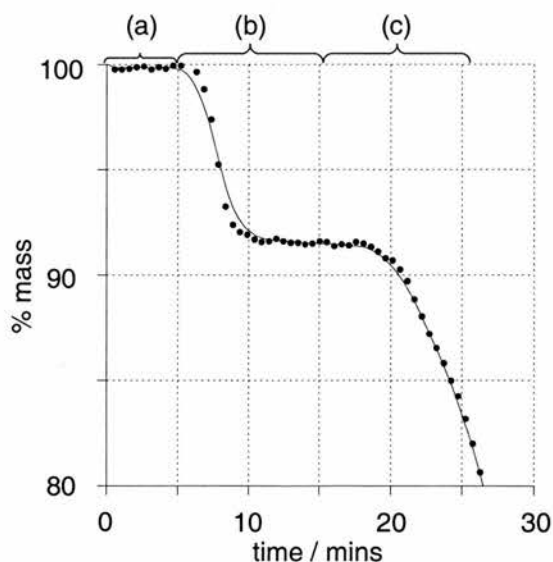
**Scheme 13** **111** forms oligomers **123** on heating in the solid state.

Initially, a small sample (typically 3 mg) of **111** was heated from 30 °C to 300 °C at a rate of 50 °Cmin<sup>-1</sup>. At this rate, a slight loss of mass from the sample is visibly evident at temperatures of around 75 °C, and above (**Figure 65**). At about 200 °C, the rate of mass loss is noticeably increased, until a total % mass loss of around 8% has occurred. After this point, a further slower mass loss is recorded, possibly due to sublimation or decomposition of the sample.



**Figure 65** On heating a sample of **111** from 30 °C to 300 °C, a continued mass loss is observed at temperatures greater than 75 °C. The results shown were recorded over a period of around 10 minutes. The line represents the actual data recorded, and 1 in every 30 data points are marked.

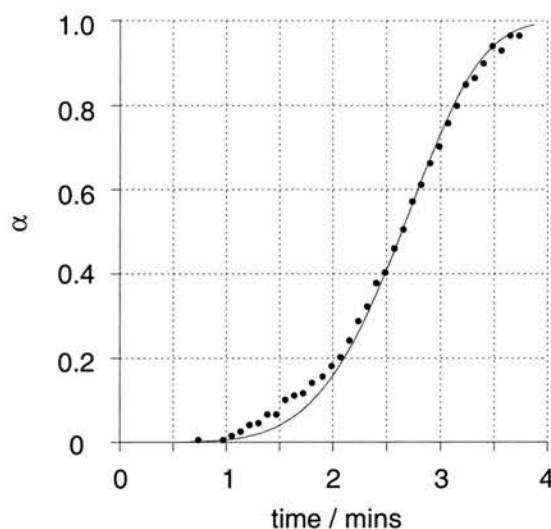
In order to study the mass loss more accurately, a sample of **111** was heated swiftly ( $100\text{ °Cmin}^{-1}$ ) to 200 °C, in order to minimise any mass loss prior to the subsequent isothermal stage (**Figure 66**). The sample was then held at 200 °C for 10 minutes and a mass loss of around 8% was observed which is consistent with the formation of the oligo-anhydride **123**. Continued heating from 200 °C to 700 °C, leads only to a further mass loss, due to sample decomposition.



**Figure 66** During thermogravimetric analysis, a sample of **111** was (a) held at 30 °C for 5 minutes, before heating to 200 °C at a rate of  $100\text{ °Cmin}^{-1}$ . (b) The sample was held isothermal at 200 °C for 10 minutes, showing a mass loss of around 8%, before (c) continued heating to 700 °C at a rate of  $50\text{ °Cmin}^{-1}$ . The sample shows a continued mass loss during this time. 1 in every 30 recorded data points are marked. The line represents a smooth curve through the experimental data.

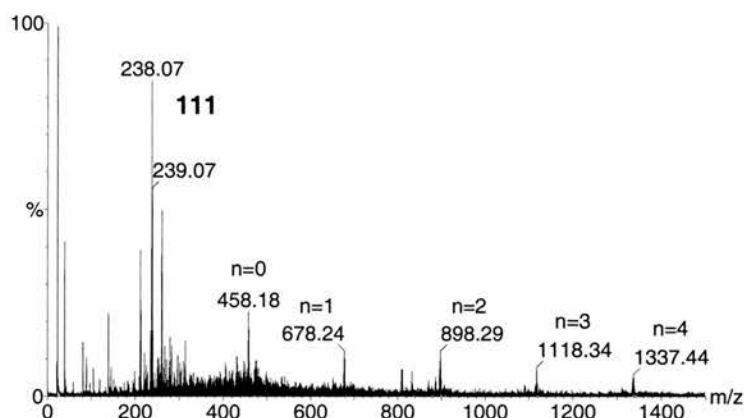


A plot of the fractional extent of reaction  $\alpha$  vs. time  $t$ , is shown in **Figure 67**. Attempts to fit the TGA data using the Avrami-Erofeev equation (**Equation 1, Section 2.5.2**) show that the best fit of the experimental data is obtained with  $n=4$ . However, since the fit obtained with  $n=5$  is almost as good, no real conclusions can be drawn without conducting further experiments at different temperatures.



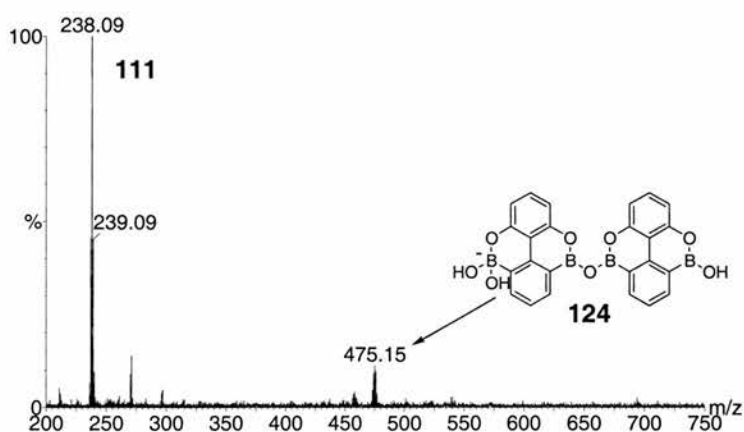
**Figure 67** TGA data obtained by heating a sample of **111** at 200 °C, plotted as extent of reaction  $\alpha$  vs. time. The solid line represents the best fit of the Avrami-Erofeev equation (with  $n=4$ ) to the experimental data.

In order to confirm the formation of the oligo-anhydride **123** the sample was analysed by MALDI-TOF spectrometry. It was necessary to dissolve the sample in acetone prior to application to the MALDI sample plate. In order to minimise hydrolysis of any higher oligomers, the acetone was pre-dried over 4Å molecular sieves, however  $^1\text{H}$  NMR analysis indicated that a significant proportion of water remained. Despite this, MALDI-TOF analysis of the sample resulting from the isothermal heating confirms the formation of oligomers up to the hexamer (**Figure 68**,  $n=4$ ). Although the most intense peak is that due to the monomer **111**, it should be noted that MALDI spectrometry does not provide any quantitative measurement of the proportions of oligomers present.



**Figure 68** MALDI-TOF mass spectrum of a sample of **111** recorded after heating at 200 °C for 10 minutes. The spectrum shows oligomers **123** up to the hexamer ( $n=4$ )

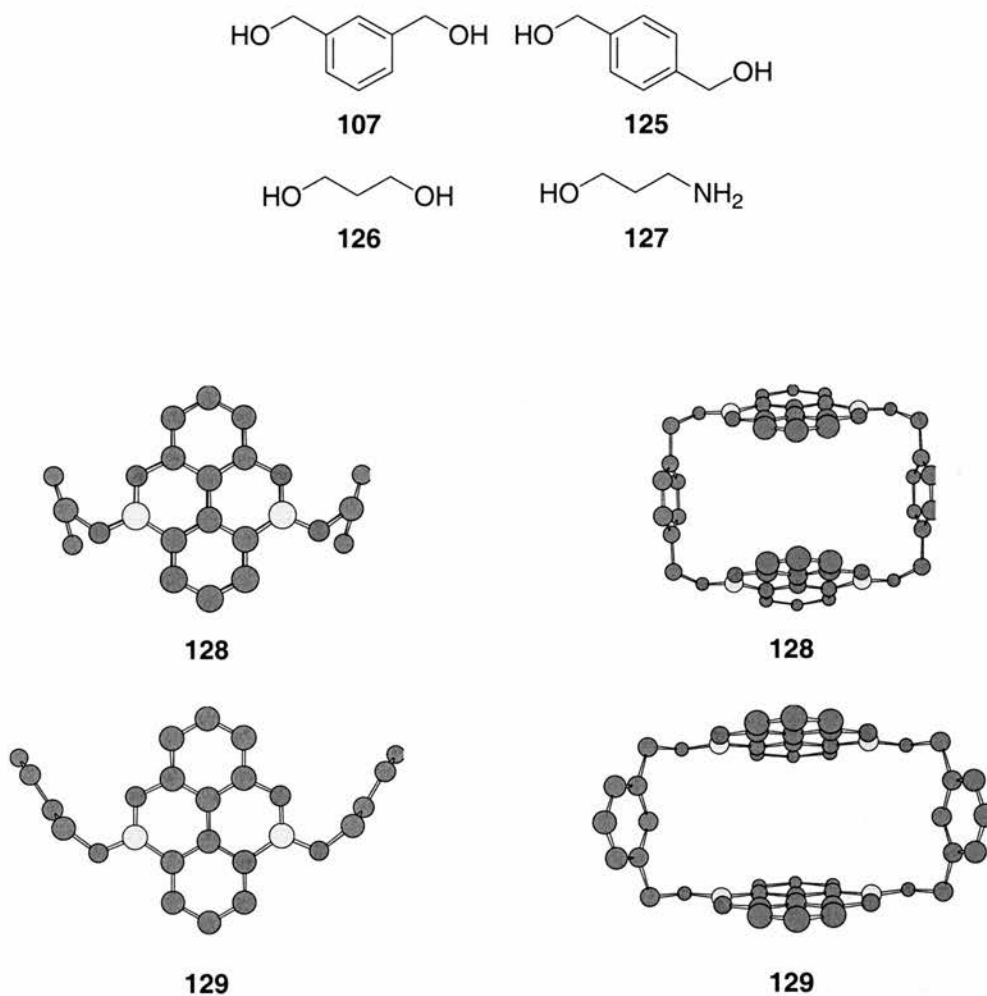
The MALDI-TOF mass spectrum of a sample of **111** dissolved in acetone (**Figure 69**), recorded prior to heating under the conditions described above, shows the monomer at  $m/z$  238, and, unexpectedly, also shows a small peak at  $m/z$  475, which may be due to structure **124**. Since there is no evidence for this compound in the  $^1\text{H}$  300 MHz NMR spectrum of **111**, it is difficult to be sure whether this material is present in the sample, or the consequence of reactions occurring on the MALDI sample plate. We can at least be certain that any higher oligomers observed in **Figure 68** are genuine, and not the result of dehydration occurring during the recording of the spectrum.



**Figure 69** MALDI-TOF mass spectrum of **111**.

### 3.1.4 Solution Phase Reactivity of 5,9-Dihydroxy-5,9-dibora-4,10-dioxopyrene

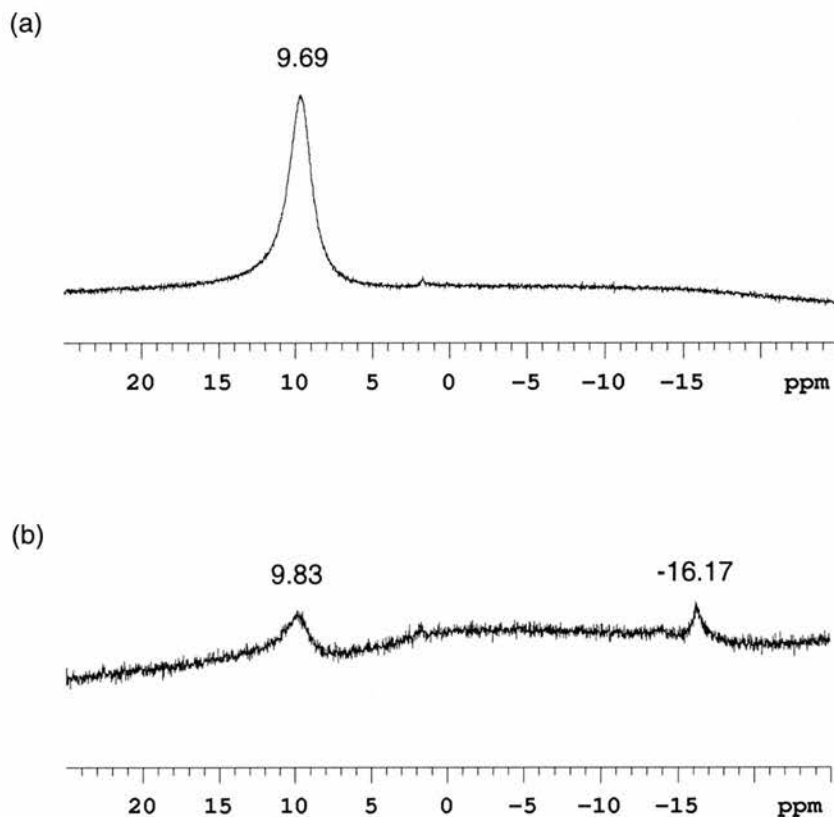
Following the discovery of the unusual solution phase reactivity of **62** with nucleophiles (which will be discussed in more detail in **Chapter 4**), we were interested in investigating the possible solution phase formation of oligomers by **111**. Potentially, reaction with bis-nucleophiles, such as benzenedimethanols **107** and **125**, could result in the formation of linear hetero-oligomers, of the type illustrated in **Figure 58**. However, semi-empirical calculations suggested that macrocycles were also accessible, as shown in **Figure 70**. In order to test these possibilities, 1;1 solutions of **111** with a series of nucleophiles, **107** and **125-127**, were made up, and examined by  $^{11}\text{B}$  NMR spectroscopy and MALDI-TOF mass spectrometry, in an attempt to identify any reaction.



**Figure 70** AM1 structure calculations suggest that there is no barrier to the formation of macrocycles **128** and **129** by reaction of **111** with **125** and **107** respectively.

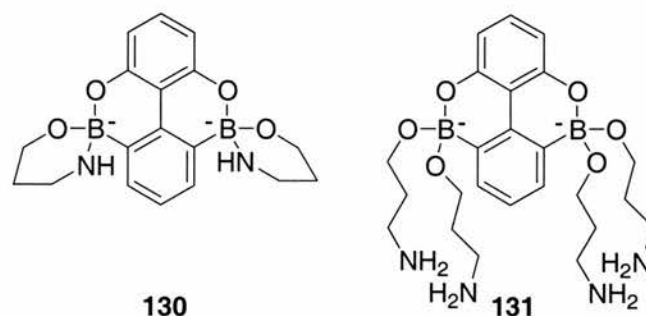
Due to the extreme insolubility of **111** in solvents such as chloroform and acetonitrile, these experiments were performed in acetone. As water is particularly soluble in

acetone, it was necessary to dry the solvent thoroughly over anhydrous  $\text{CaSO}_4$  prior to use. However, it proved impossible to completely dry the acetone, and this created significant problems. MALDI-TOF spectrometry was inconclusive, showing neither nucleophiles or **111**, or any of the products we had predicted.  $^1\text{H}$  NMR spectra, recorded in  $d_6$ -acetone showed resonances characteristic of the unreacted starting materials only. Only the  $^{11}\text{B}$  NMR spectrum of a 1:1 mixture of **111** and 1-amino-3-propanol **127** exhibited any change at all (**Figure 71**).



**Figure 71** (a) The  $^{11}\text{B}$  160 MHz NMR spectrum of **111** recorded at 293 K in  $d_6$ -acetone, using  $\text{B}(\text{OMe})_3$  in the same solvent as an external reference ( $\delta=0.0$ ), shows only one resonance, at 9.7 ppm. (b) The  $^{11}\text{B}$  spectrum of a 1:1 solution of **111** and **127** in  $d_6$ -acetone, shows two signals, one at around 9.8 ppm, and the other much further upfield, at -16 ppm.

Whilst the  $^{11}\text{B}$  NMR spectrum of **111** only shows a single resonance at 9.7 ppm, the addition of **127** results in the appearance of a second signal much further upfield at -16.2 ppm. We recall (**Section 1.2.3**) that an upfield shift of an  $^{11}\text{B}$  resonance is suggestive of a conversion from a trigonal to a tetrahedral environment. It therefore seems likely that the second resonance arises from the formation of a structure such as **130** or **131**, shown in **Figure 72**.

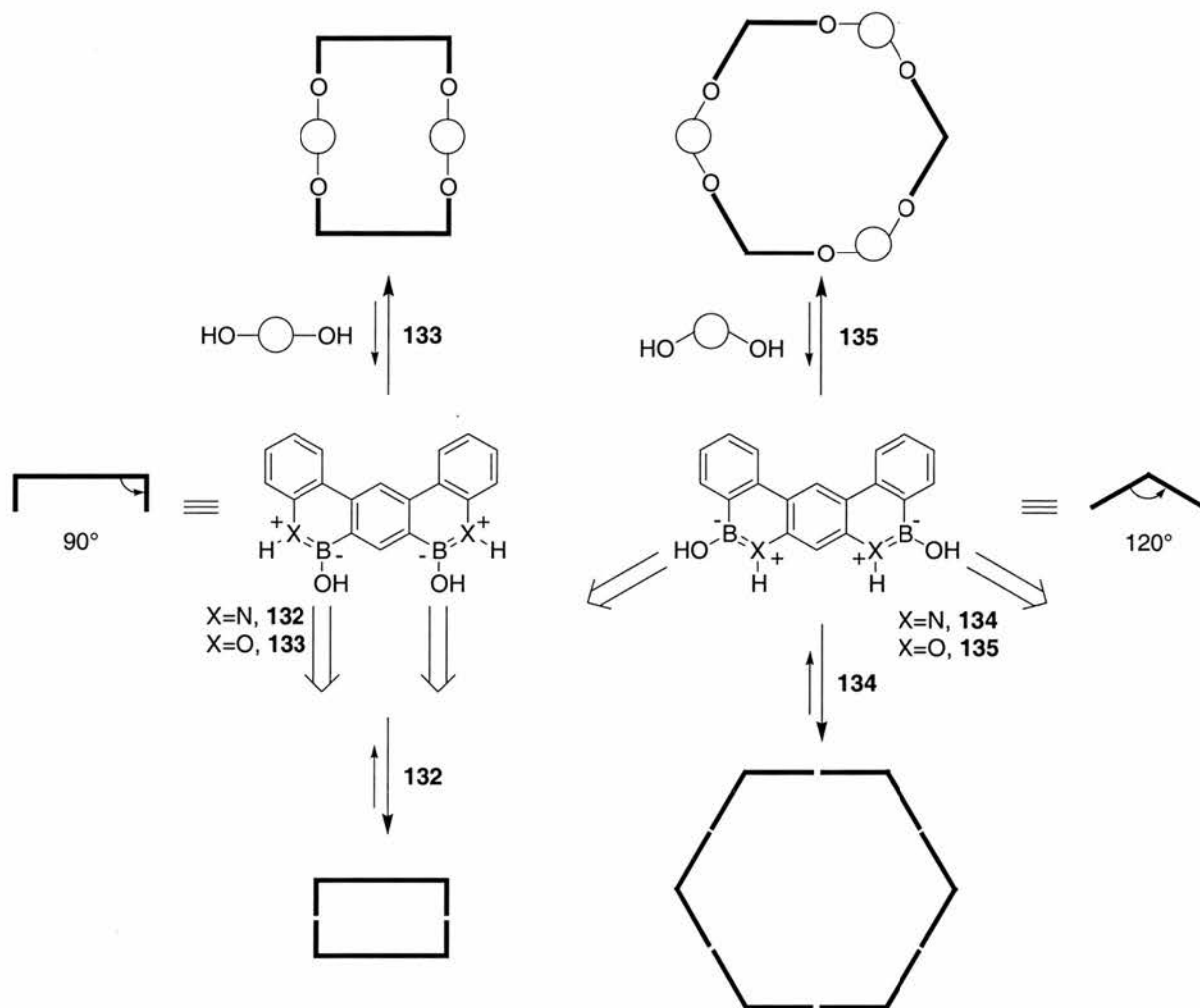


**Figure 72** Possible adducts arising from the reaction of **111** and **127**.

There is, however, no evidence for either of these species in the MALDI-TOF spectrum. A rationale for this result, and a discussion of the implications will be found in **Chapter 4**. It seems that the insolubility of **111** in non-polar solvents seriously limits its potential utility in constructing unusual or complex assemblies in solution.

### 3.2 Rigid Systems Designed to form Macrocycles

In the solid state, the pyrene-based system described above is expected to form linear oligomers, and not macrocycles. Although there is free rotation around the anhydride B-O-B bonds, the two B-O functionalities are on opposite faces of the molecule, and hence, only very large oligomers could possibly undergo macrocyclisation. On the other hand, bis-boron heteroaromatic compounds with more convergent B-OH functionalities may form macrocycles readily. For this reason, the monomers **132** - **135** were designed, based on a dibenz[*a,j*]anthracene skeleton.

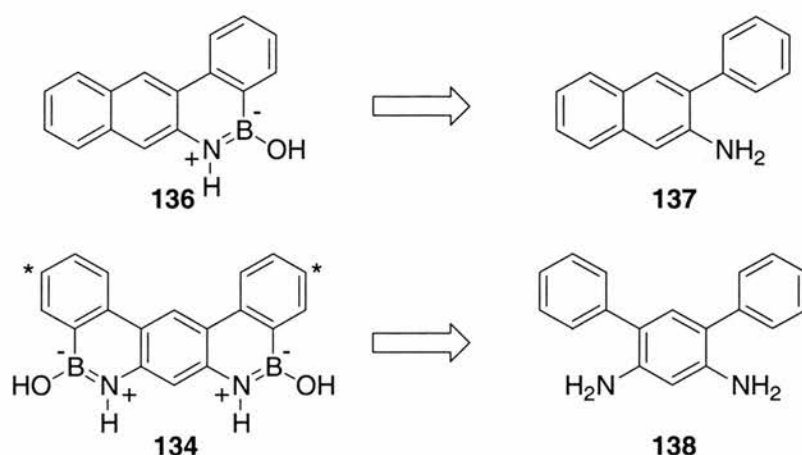


**Figure 73** Boron-heteroaromatics **132** and **134** are designed to form a homo-dimer and a homo-hexamer, respectively, whilst **133** and **135** may react with nucleophiles to form similar hetero-oligomers.

These monomers can form extended chains, but are also able to form different cyclised structures. The schematic representation in **Figure 73** illustrates how **132**, having “internal angles” of 90°, may form a rectangular dimer, whereas the related **134** has 120° “internal angles” and is predicted to associate to form a hexamer. These cyclised products should be thermodynamically more stable than the acyclic oligomers, and are therefore be the expected outcome if the assembly process is under thermodynamic control, as is expected for the borazaaromatic compounds in the solution phase. The analogous boroxoaromatic compounds **133** and **135**, on the other hand, may not react with themselves in solution, but may still form macrocyclic structures with other nucleophiles.

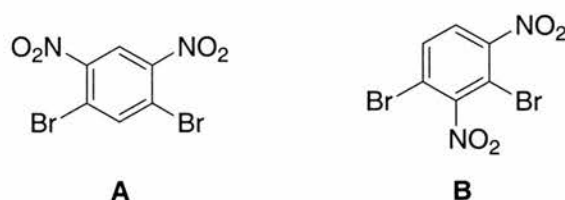
### 3.2.1 Synthesis of 3,6-Dihydroxy-3,6-dibora-4,5-diazadibenz[*a,j*]anthracene **134**

In 1963, Dewar reported<sup>128</sup> the synthesis of a boron-containing analogue of benz[*a*]anthracene **136** by treating a solution of the amine **137** in xylene with  $\text{BCl}_3$ , and cyclisation with catalytic  $\text{AlCl}_3$ . We hoped to extend this strategy to the synthesis of the related bis-borazaaromatic **134** from the amine **138**.



**Figure 74** Synthesis of **134** relied on the successful cyclisation of **138**. It was planned to include solubilising *t*-butyl groups on positions 3 and 11 (\*) on the aromatic skeleton.

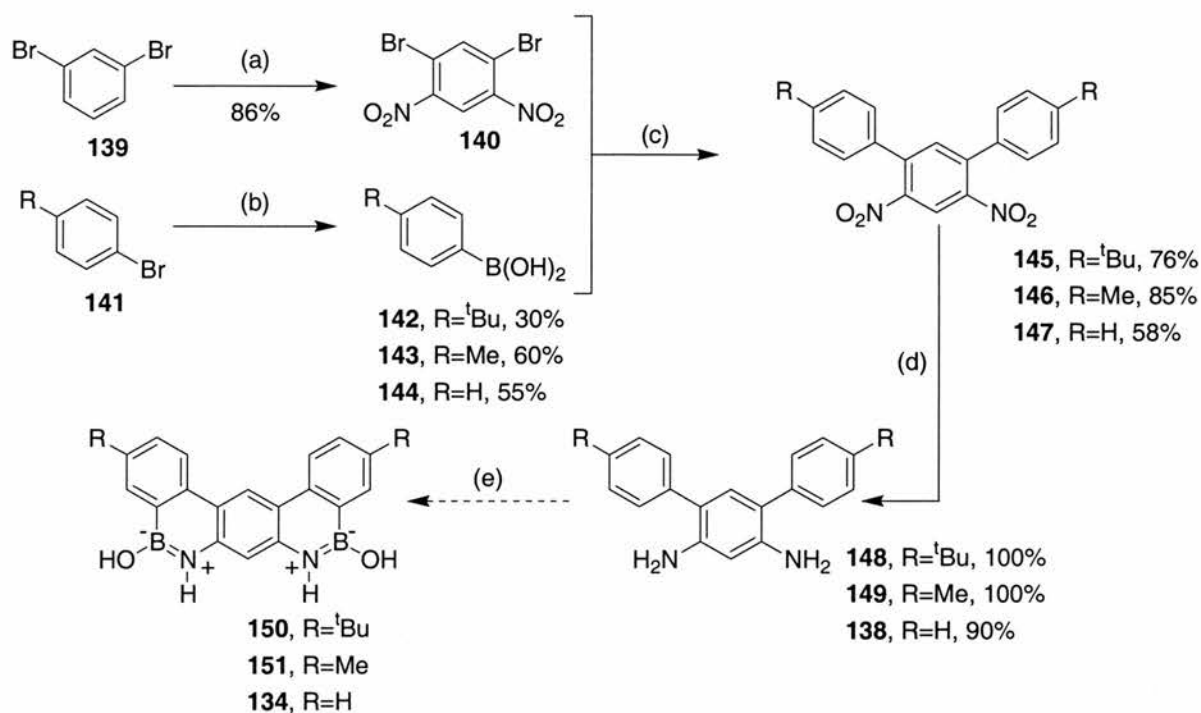
Initially, we also planned to include *tert*-butyl groups in positions 3 and 11 (\* in **Figure 74**) on the aromatic skeleton, thus increasing the solubility of the amine and other synthetic intermediates. The parent diamine was successfully synthesised using the series of reactions outlined in **Scheme 14**. Good yields were obtained for the nitration<sup>165</sup> of 1,3-dibromobenzene **139**, although the presence of two regioisomers was indicated by  $^1\text{H}$  NMR spectroscopy. The two singlet proton signals expected for 1,3-dibromo-4,6-dinitrobenzene (isomer **A**, **Figure 75**) were observed, along with a third peak. A heteronuclear ( $^1\text{H}$ - $^{13}\text{C}$ ) correlation NMR experiment (HMQC) revealed this signal to be due to two protons with identical chemical shifts. 1,3-dibromo-2,4-dinitrobenzene (isomer **B**) was identified as the most likely structure for the second regioisomer, and  $^1\text{H}$  NMR spectroscopic data indicates the ratio of **A**:**B** to be approximately 7:1.



**Figure 75** Nitration of 1,3-dibromobenzene **139** resulted in the formation of two isomers **A** and **B**.



The two isomers were inseparable by column chromatography, and attempts at purification by sublimation only resulted in decomposition. The subsequent Suzuki coupling reaction was carried out using the isomeric mixture, as it was expected that separation would prove easier at the next stage.



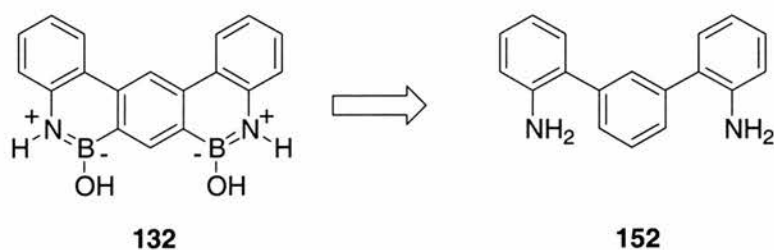
**Scheme 14** (a)  $\text{HNO}_3$ ,  $\text{H}_2\text{SO}_4$ ,  $\Delta$ ; (b) (i) Mg,  $\text{Et}_2\text{O}$ , (ii)  $\text{B}(\text{OMe})_3$ ,  $\text{Et}_2\text{O}$ ,  $-78\text{ }^\circ\text{C} \rightarrow \text{r.t.}$ ; (c)  $\text{Pd}(\text{PPh}_3)_4$ ,  $\text{Na}_2\text{CO}_3$ , DME, EtOH,  $\text{H}_2\text{O}$ ,  $\Delta$ ; (d)  $\text{H}_2$ , Pd/C, EtOAc; (e) (i)  $\text{BHCl}_2 \cdot \text{DMS}$ , xylene,  $\Delta$ , (ii)  $\text{AlCl}_3$ ,  $\Delta$ .

All three boronic acids **142** through **144** were easily prepared using standard literature procedures<sup>166</sup>, and the coupling reactions proceeded in good yield. The catalytic hydrogenation of the di-nitro compounds **145** through **147** gave the corresponding diamines **138**, **148** and **149** in near quantitative yields, but the amines were found to be light and air sensitive. Since TLC analysis appeared to indicate that the reductions proceeded cleanly, further purification was not undertaken, so as to minimise decomposition. On treatment of **138** with  $\text{BHCl}_2 \cdot \text{Me}_2\text{S}$ , some reaction did occur, and analysis of the recovered crude product using MALDI-TOF spectrometry revealed a small signal due to the desired product molecular ion at  $m/z$  423. However, the isolation of the clean product **134** was never achieved by recrystallisation or column chromatography, and furthermore,  $^1\text{H}$  NMR spectra suggested that the large majority of recovered material was the products of diamine decomposition. We have noted<sup>167</sup> that the stability of hydroxy-borazaaromatics

appears to be related to the stability of the parent amine, an observation which may account for the difficulties described here.

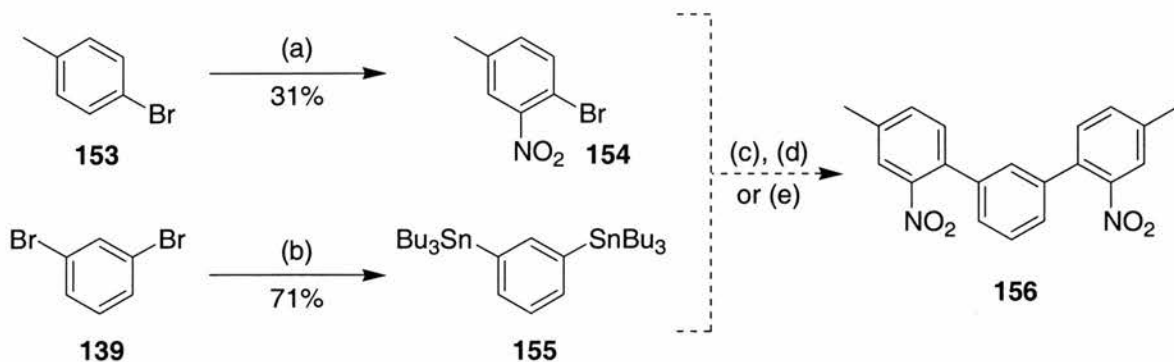
### 3.2.2 Synthesis of 4,5-Dihydroxy-4,5-dibora-3,6-diazadibenz[*a,j*]anthracene **132**

It was envisaged that the synthesis of **132** could be achieved more readily than that of **134**, since the immediate precursor, the diamine **152**, will not possess the inherent instability of the 1,3-diamine **138**.



**Figure 76** Bis-borazaaromatic **132** can be prepared from diamine **152**.

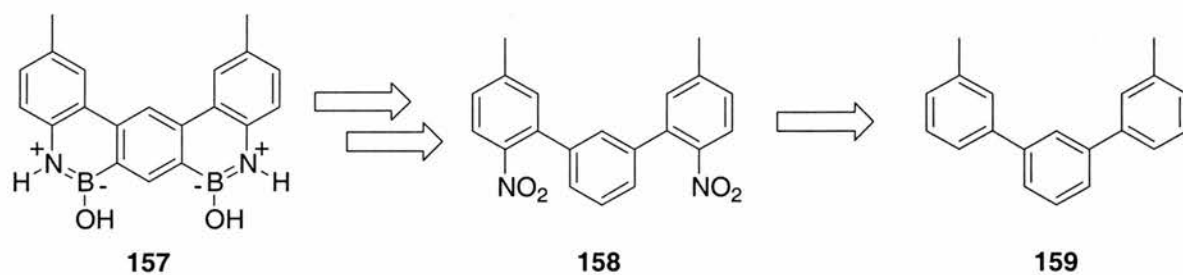
Initially, we intended to synthesise the required dinitro-terphenyl **156** through reaction of 1,3-dibromobenzene **139** with the appropriately nitrated boronic acid. However all attempts at nitration of the boronic acids were unsuccessful, so a new synthetic route was proposed (**Scheme 15**).



**Scheme 15** (a)  $\text{HNO}_3$ ,  $\text{H}_2\text{SO}_4$ ,  $0^\circ\text{C}$ ; (b) (i)  $t\text{-BuLi}$ ,  $\text{Et}_2\text{O}$ ,  $-78^\circ\text{C}$ , (ii)  $\text{Bu}_3\text{SnCl}$ ,  $-78^\circ\text{C}$ , (iii)  $\text{H}^+$ ; (c)  $\text{Pd}(\text{PPh}_3)_4$ ,  $\text{PhMe}$ ,  $90^\circ\text{C}$ ; (d)  $\text{Pd}(\text{PPh}_3)_2\text{Cl}_2$ ,  $\text{DMF}$ ,  $110^\circ\text{C}$ ; (e)  $\text{Pd}(\text{PPh}_3)_2\text{Cl}_2$ ,  $\text{LiCl}$ ,  $\text{DMF}$ ,  $110^\circ\text{C}$ .

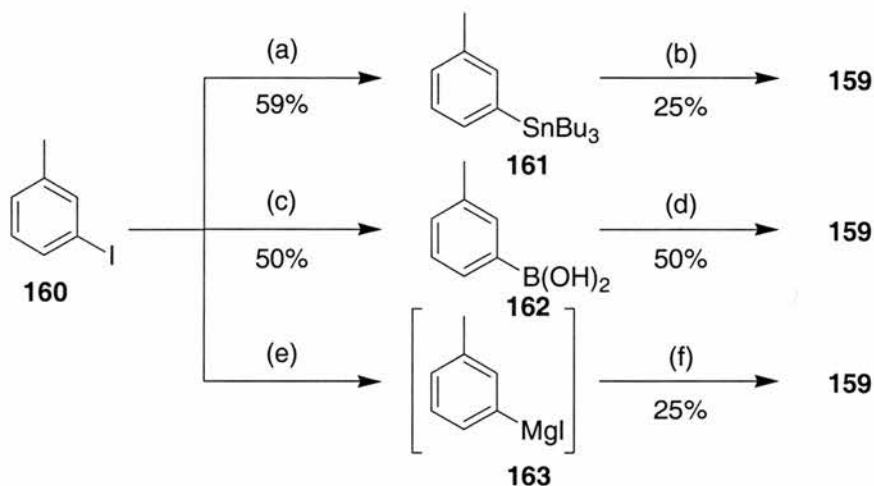
This procedure involved the reversal of the functionalities of the components of the coupling reaction. The nitration of 4-bromotoluene **153** resulted in a mixture of two isomers, 2-nitro-3-bromotoluene **154** and 2-nitro-4-bromotoluene, which were

separable and readily identified using gradient nuclear Overhauser effect spectroscopy (GOESY). As all attempts to synthesise a bis-boronic acid from 1,3-dibromobenzene **139** were unsuccessful, we identified 1,3-bis-(tributylstannyl) benzene **155** as an alternative coupling partner. The synthesis of **155** by standard literature methods<sup>168</sup> was readily accomplished, but none of the desired terphenyl product **156** was produced in the three attempted Stille coupling reactions. Since the inclusion of the nitro-group at this stage appeared to be causing problems, another alternative methodology was proposed, using the position of the methyl groups in 1,3-bis-(3-methylphenyl)benzene **159** to direct the subsequent nitration.



**Figure 77** Borazaaromatic **157** can be prepared from triphenyl **159**.

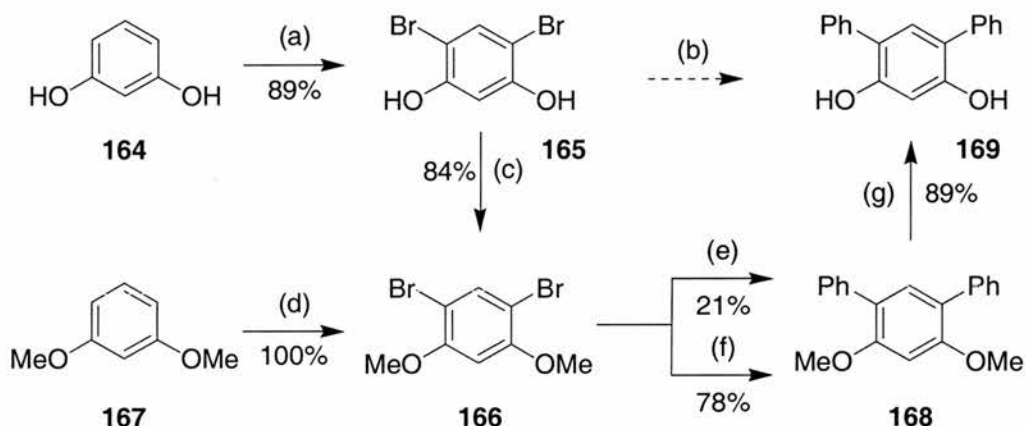
The synthesis of **159** was attempted *via* Suzuki, Stille and Kharasch coupling reactions, to identify the optimal route. **Scheme 16** shows a comparison of the three different methodologies. Both 3-methylphenyl tributyl stannane **161** and 3-methylphenyl boronic acid **162** were prepared in good yield using standard literature procedures. The Grignard reagent **163** was not isolated, but cannulated directly into a solution containing 1,3-dibromobenzene **139** and nickel catalyst. The Suzuki and Kharasch methodologies, with a disappointing yield of 25% over the two steps, gave the best result, but the subsequent selective nitration was never achieved successfully.



**Scheme 16** (a) (i) *t*-BuLi, Et<sub>2</sub>O, -78 °C, (ii) Bu<sub>3</sub>SnCl, -78 °C→r.t.; (b) 1,3-dibromobenzene, Pd(PPh<sub>3</sub>)<sub>4</sub>, PhMe; (c) (i) Mg, Et<sub>2</sub>O, (ii) B(OMe)<sub>3</sub>, -78 °C; (d) 1,3-dibromobenzene, Pd(PPh<sub>3</sub>)<sub>4</sub>, Na<sub>2</sub>CO<sub>3</sub>, DME, EtOH, H<sub>2</sub>O; (e) Mg, Et<sub>2</sub>O; (f) 1,3-dibromobenzene, Ni(dppe)Cl<sub>2</sub>, Et<sub>2</sub>O.

### 3.2.3 Synthesis of 3,6-Dihydroxy-3,6-dibora-4,5-dioxodibenz[*a,j*]anthracene 135

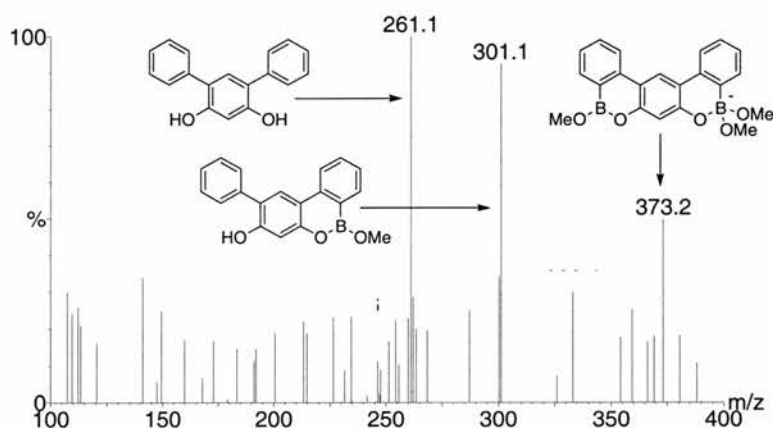
The synthesis of 3,6-dihydroxy-3,6-dibora-4,5-dioxodibenz[*a,j*]anthracene **135** was attempted using the series of reactions outlined in **Scheme 17**.



**Scheme 17** (a) Br<sub>2</sub>, CHCl<sub>3</sub>; (b) 6 eq. PhMgBr, Pd(PPh<sub>3</sub>)<sub>2</sub>Cl<sub>2</sub>, THF; (c) CH<sub>3</sub>I, K<sub>2</sub>CO<sub>3</sub>, MeCN; (d) Br<sub>2</sub>, CH<sub>2</sub>Cl<sub>2</sub>; (e) 5 eq. PhMgBr, Ni(PPh<sub>3</sub>)<sub>2</sub>Cl<sub>2</sub>, Et<sub>2</sub>O; (f) PhB(OH)<sub>2</sub>, Pd(PPh<sub>3</sub>)<sub>4</sub>, Na<sub>2</sub>CO<sub>3</sub>, DME, EtOH, H<sub>2</sub>O; (g) BBr<sub>3</sub>, CH<sub>2</sub>Cl<sub>2</sub>, -78 °C→r.t.

Bromination of resorcinol **164** was carried out according to standard literature procedures<sup>169</sup> and, once more, attempts were made to couple **165** using an excess of Grignard reagent to protect the hydroxyl groups. Again, this proved unsuccessful, with several unidentifiable products being isolated from the column. We therefore chose instead to use the dimethoxy compound **166** as a coupling partner, which can

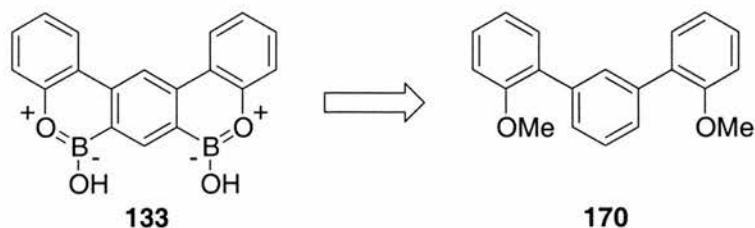
be generated either by the protection of the previously synthesised dibromoresorcinol **165**, or preferably, through the bromination of 1,3-dimethoxybenzene **167**. Suzuki cross-coupling to phenyl boronic acid afforded the dimethoxyterphenyl **168**, which was readily deprotected to give the 1,3-diol **169**. The cyclisation of **169** was unsuccessful using  $\text{BCl}_3$  as the boron source, but was eventually achieved by the addition of  $\text{BHCl}_2$  to a solution of **169** in toluene. ES mass spectrometry of the crude reaction product (**Figure 78**) confirms the presence of a mixture the methyl esters of starting material **169**, the required bis-boroxoaromatic **135** and the mono-cyclised product. It was believed these would readily be hydrolysed. It proved difficult to separate **135** from the mono-cyclised compound, and the yield was disappointingly low, at around 5%, and, hence, full characterisation of **135** could not be obtained.



**Figure 78** Negative electrospray mass spectrum (MeOH, Flow rate:50  $\mu\text{L}$ , Cone voltage:40 V) of the crude recovered material from reaction of **169** with  $\text{BHCl}_2$ , shows a mixture of methyl esters of **169**, desired product **135** and the mono-cyclised product.

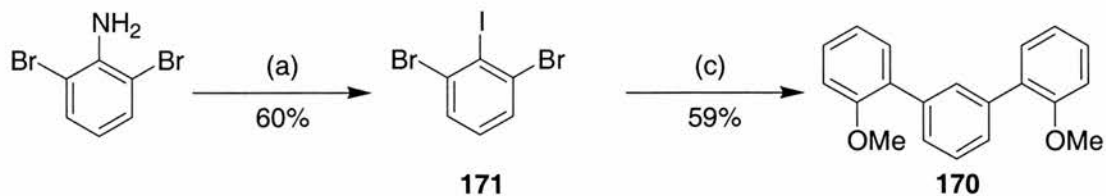
### 3.2.4 Synthesis of 4,5-Dihydroxy-4,5-dibora-3,6-dioxodibenz[*a,j*]anthracene **133**

The proposed synthesis of **133** proceeded *via* the dimethoxy-terphenyl **170** (**Figure 79**).



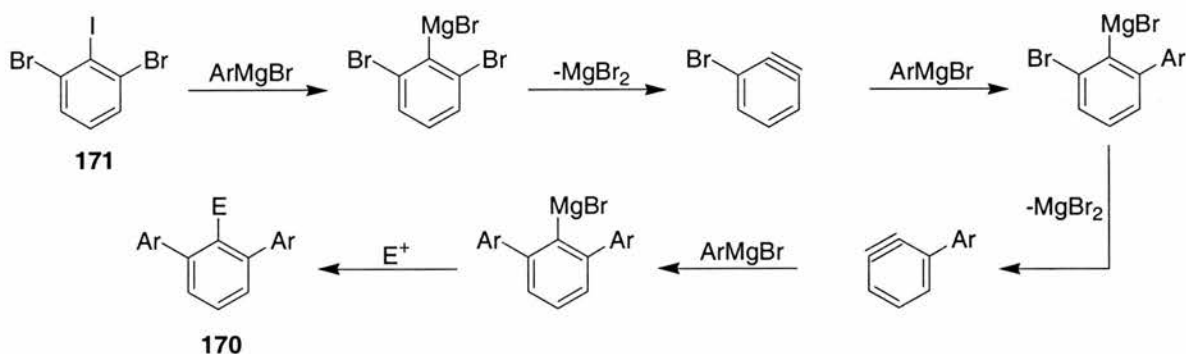
**Figure 79** Bis-boroxoaromatic **133** can be prepared from **170**.

The synthesis of **170** was achieved using the methodology described in **Scheme 18**. Diazaotisation<sup>170</sup> of 1,3-dibromoaniline, followed by nucleophilic substitution with iodide, affords 2,6-dibromiodobenzene **171**, and the synthesis of **170** was achieved *via* coupling<sup>171</sup> of **171** with 2-methoxyphenylmagnesium bromide.



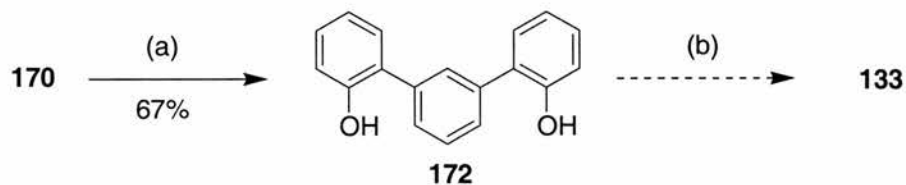
**Scheme 18** (a) (i)  $\text{NaNO}_2$ ,  $\text{HCl}$ , (ii)  $\text{KI}$ ,  $\text{H}_2\text{O}$ ; (c) 2-methoxyphenyl magnesium bromide,  $\text{THF}$ .

The cross-coupling reaction occurs *via* a diaryne mechanism, with a selective metal-halogen exchange followed by two successive elimination-addition steps (**Scheme 19**) and quenching of the organometallic species, in this case *via* acidic work up.



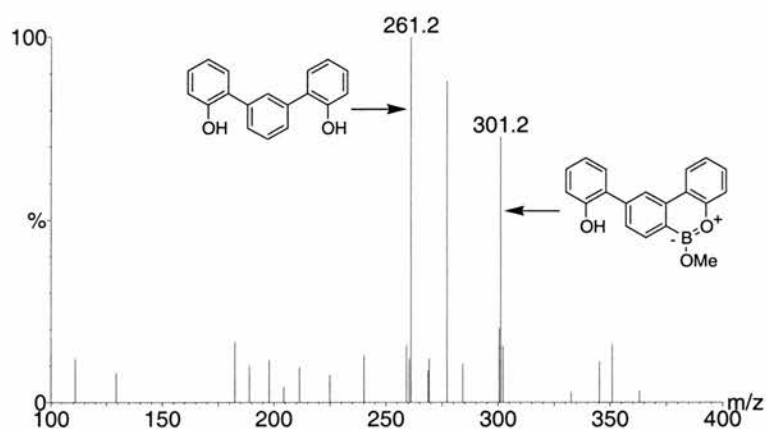
**Scheme 19** *m*-Terphenyl **170** is synthesised *via* a diaryne mechanism.

The terphenyl **170** is easily deprotected using boron tribromide (**Scheme 20**), but all attempts to effect the cyclisation failed.



**Scheme 20** (a)  $\text{BBr}_3$ ,  $\text{CH}_2\text{Cl}_2$ ,  $-78^\circ\text{C} \rightarrow \text{r.t.}$ , (b) (i)  $\text{BCl}_2$ ,  $\text{PhMe}$ ,  $\text{r.t.}$ , (ii)  $\text{AlCl}_3$ ,  $\Delta$ .

It may be that the double cyclisation on to the same aromatic ring is disfavoured, and, in this case, we might expect to isolate some of the mono-cyclised product. The ES mass spectrum (**Figure 80**) of the crude isolated reaction product does indeed show peaks at  $m/z$  261 (indicative of starting material **172**) and 301 (indicative of the mono-cyclised product). It seems possible that if the mono-cyclised product can be isolated, and resubjected to the cyclisation conditions, **133** could be formed.

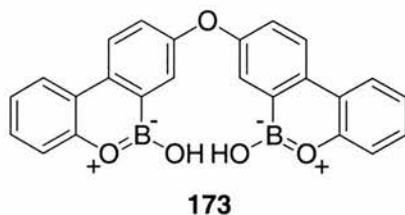


**Figure 80** Negative electrospray mass spectrum (MeOH, flow rate:50  $\mu$ L, cone voltage:40 V) of crude recovered product from reaction of **172** with  $\text{BHCl}_2$ , showing a mixture of starting material **172** and mono-cyclised product.

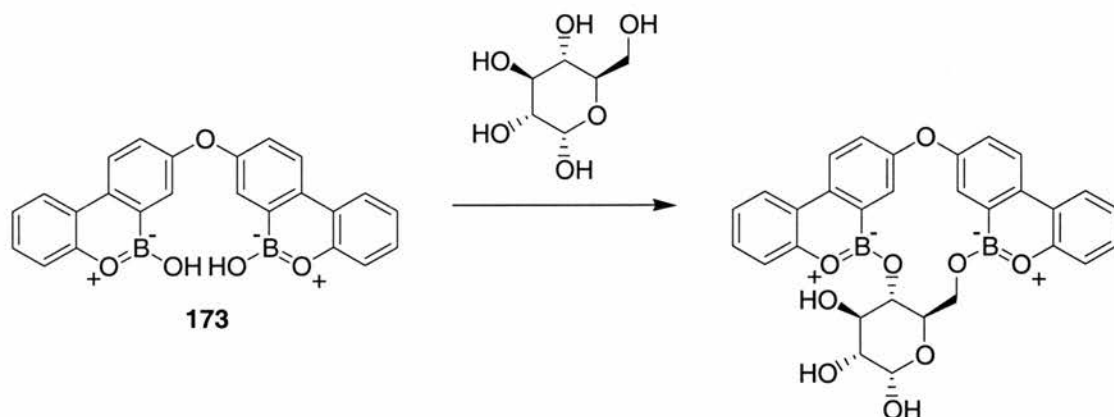
### 3.3 Flexible Bifunctional Boron-Containing Heteroaromatics

The systems described in **Sections 3.1** and **3.2** are all rigid molecules. Although clearly more complex than the monofunctional boroxoaromatic examined in **Chapter 2**, they are still somewhat limited in the range of oligomers they can form. In some sense, they can be described as “preorganised”, which, we recall, implies the adoption of a favoured conformation in the ground state, and the retention of that conformation when incorporated into larger structures. We were interested in designing systems with a higher degree of flexibility, which would potentially have access to a greater area of conformational space. Accordingly, we devised the monomer **173**, which is the direct oxygen analogue of the earlier described bis-2,2'-(10-hydroxy-10,9-boroxophenanthryl) ether **91**. It should be recalled that **91** shows a thermodynamic preference for the cyclic dimer, although many other oligomers, both cyclic and acyclic, are accessible to it, and, are in fact observed in the MALDI-TOF spectrum. However, it should also be remembered that this system took around 12 days to reach equilibrium.





The reactivity of the boron-oxygen analogue could potentially be very interesting for two main reasons. Firstly, it is of interest to investigate whether the solution phase reactivity of **173** is comparable to that of the boron-nitrogen analogue **91**, or to our model boroxoaromatic compound, **62**. If the latter were true, then clearly, we would not expect to observe the solution phase formation of any of the same cyclic or linear oligomers which are detected in a solution of the borazaaromatic compound. If **173** behaves in an analogous manner to **62**, then an investigation of the reaction of **173** with nucleophiles may prove to be of interest. We might expect that **173** will react with diols, and we may observe some selectivity based on the shape and size of the diol.



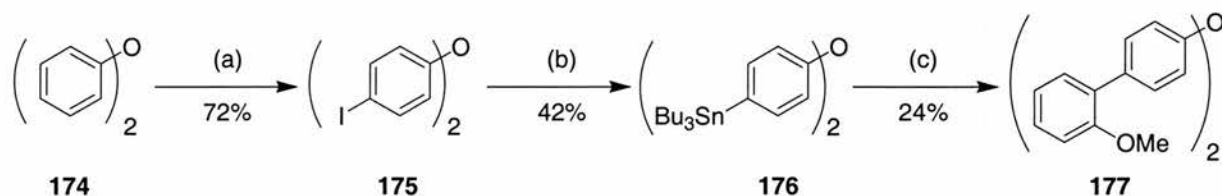
**Scheme 21** Certain sugars may be selectively bound by **173**, due to their size and shape compatibility.

Furthermore, the speed with which our model boroxoaromatic system **62** reacts with nucleophiles indicates that **173** may be able to select the best bound diol from a mixture of nucleophiles extremely quickly.

### 3.3.1 Synthesis of Bis-[2,2'(10-Hydroxy-10,9-boroxophenanthryl)]-ether **173**

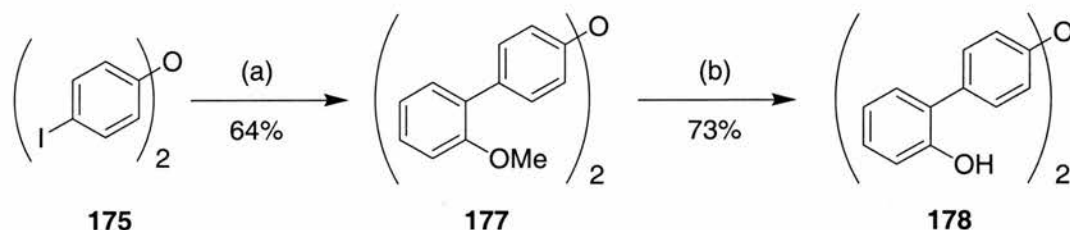
The synthesis of the required precursor diol can be achieved with little difficulty in 3 or 4 steps from commercially-available diphenyl ether **174** (**Scheme 22**). Iodination<sup>172</sup> of diphenyl ether was effected in good yield using a mixture of iodine, periodic acid and sulfuric acid in aqueous acetic acid. The proposed next step was the coupling of

2-bromoanisole to **175**, and we foresaw that this could be achieved in a number of ways. The first attempted method was Stille coupling, which required the conversion of one of the reactive partners into a stannane. Stannylation of **175** was achieved *via* reaction with *tert*-butyllithium, followed by quenching with tributyl tin chloride. All of the stannane appeared to be consumed in the subsequent coupling reaction, however, after distillation of excess tributyl tin chloride, and removal of other tin residues by column chromatography, **177** was isolated in disappointingly low yield.



**Scheme 22** (a)  $I_2$ ,  $HIO_4$ ,  $H_2SO_4$ ,  $AcOH$ ,  $H_2O$ ; (b) (i) *t*-BuLi, hexane,  $-78^\circ C$ , (ii)  $Bu_3SnCl$ ,  $-78^\circ C \rightarrow r.t.$ ; (c) 2-bromoanisole,  $Pd(PPh_3)_4$ , PhMe.

A potentially more attractive pathway was the Kharasch coupling, which does still require the conversion of one of the reactive partners into an organometallic reagent, but it is not necessary to isolate the Grignard, so this is a more direct route. We chose to synthesise the Grignard from 2-bromoanisole, and effect a nickel-catalysed coupling reaction to the iodinated phenyl ether **175** (**Scheme 23**). This was achieved in reasonable yield.

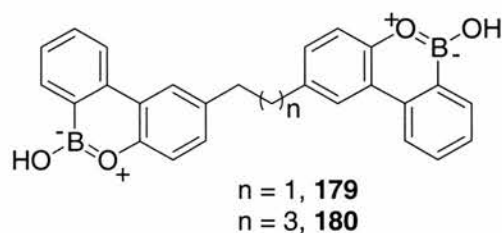


**Scheme 23** (a) 2-methoxyphenylmagnesium bromide,  $Ni(PPh_3)_2Cl_2$ ,  $Et_2O$ ,  $\Delta$ ; (b)  $BBr_3$ ,  $CH_2Cl_2$ ,  $-78^\circ C \rightarrow r.t.$

The formation of the bis-hydroxy compound **178** was readily accomplished using a standard boron tribromide deprotection. The cyclisation proved more problematic, however, and was attempted using three slightly different methods, as described in **Section 3.1.1**. Reaction with boron trichloride was unsuccessful, and the boron halide source was changed to dichloroborane-dimethyl sulfide complex. As before, measurement of the gas evolved during the reaction implied the successful formation

of the boron-dichloride adduct, but the cyclisation itself was not accomplished. Finally, the cyclisation was attempted using dichloroborane generated by the reaction of dichloroborane-dimethylsulfide complex with boron trichloride, but, again, only starting material was isolated from the reaction.

Due to the many variables involved in the cyclisation reactions (e.g. solvent, temperature) there are several possible reasons for the failure of the cyclisation, and it is not certain that, given the correct conditions, the cyclisation would not occur. However, it is also worth noting that the reaction involves cyclisation onto a non-activated position of the aromatic ring (*meta* to oxygen), and this, combined with the relative instability of the oxoborondichloride adduct, may be one reason for the failure of the reaction. In order to remove that problem, we proposed the synthesis of the compounds **179** and **180**, in which the ether linkage is replaced with an alkyl spacer.



We chose the  $C_2$  ( $n=1$ , **179**) and  $C_4$  ( $n=3$ , **180**) spacers initially, because these appeared to have the simpler synthesis. Obviously, these compounds are more flexible than the ether linked compound, which should allow access to a wider range of oligomers, particularly on addition of nucleophiles. Reaction with nucleophiles in solution would be under thermodynamic control and we believe that compounds of this type will offer an approach to the formation of a dynamic combinatorial library. **62** demonstrates extremely rapid equilibration with nucleophiles (**Section 2.6**) in solution. We hope that these compounds will demonstrate similar reactivity, and on addition of a number of different nucleophiles, will rapidly select and amplify the thermodynamically most stable adduct. These compounds could potentially sample a high number of library components in a very short space of time.

### 3.3.2 Synthesis of 3-[2-(10-Hydroxy-10,9-boroxophenanthren-3-yl)-ethyl]-(10-hydroxy-10,9-boroxo)-phenanthrene **179**

The synthesis of the bis(boroxoaromatic) **179** relied upon the synthesis of the precursor diol **181**. It was envisaged that this could be prepared by the application of standard Wittig methodology to *p*-methoxybenzaldehyde **184**.

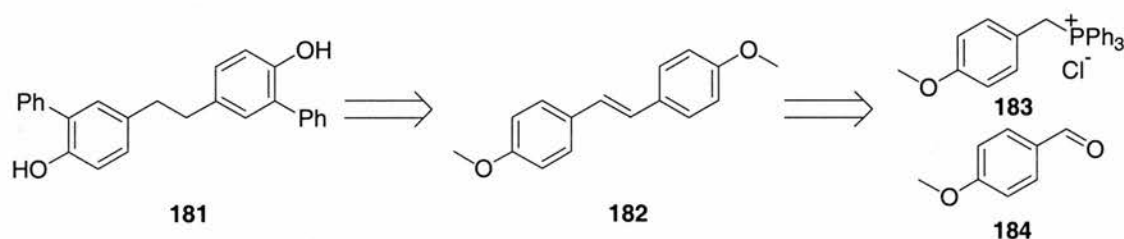
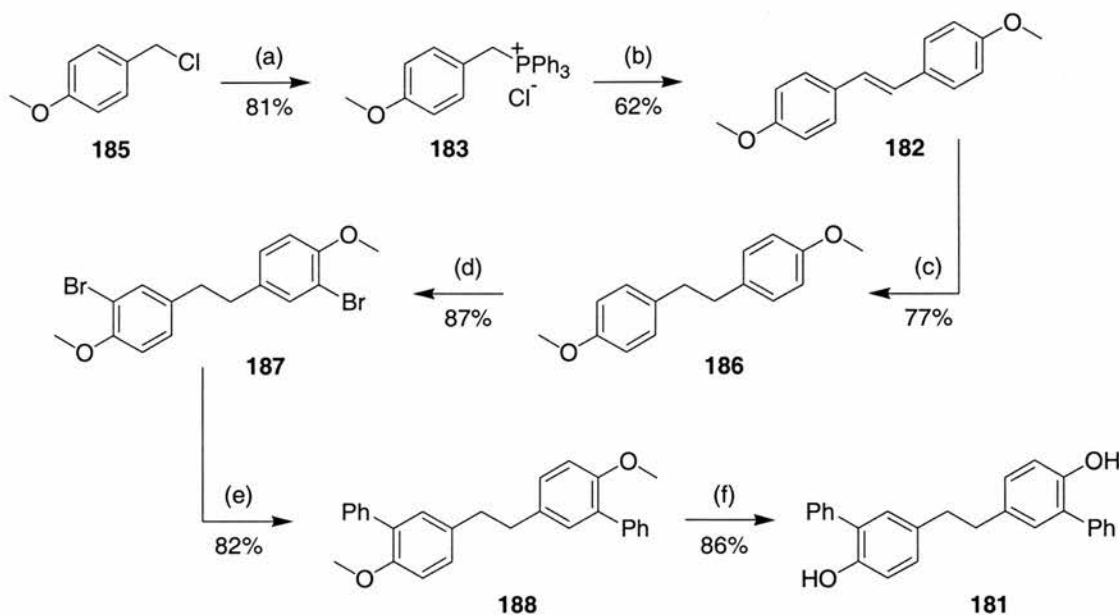


Figure 81

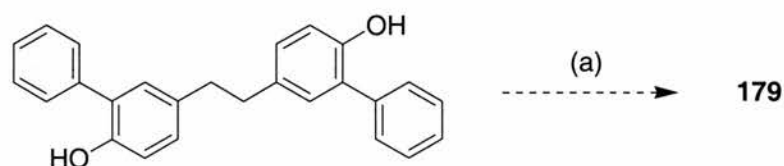
The formation of **181** was achieved using the synthetic pathway outlined in **Scheme 24**. *p*-Methoxybenzylchloride **185** was reacted with  $\text{PPh}_3$ , and the resulting phosphonium salt **183** was used in a Wittig condensation reaction<sup>173</sup> with *p*-methoxybenzaldehyde **184** to give the methoxystilbene derivative **182**.



**Scheme 24** (a)  $\text{PPh}_3$ ,  $\text{PhMe}$ ,  $\Delta$ ; (b) *t*-BuOK, 4-methoxybenzaldehyde, EtOH; (c)  $\text{H}_2$ , Pd/C, EtOAc; (d)  $\text{Br}_2$ ,  $\text{CHCl}_3$ ; (e)  $\text{PhB(OH)}_2$ ,  $\text{Pd(PPh}_3)_4$ ,  $\text{Na}_2\text{CO}_3$ , DME, EtOH,  $\text{H}_2\text{O}$ ; (f)  $\text{BBr}_3$ ,  $\text{CH}_2\text{Cl}_2$ .

The alkene was reduced by catalytic hydrogenation and selective bromination *ortho* to the methoxy groups achieved in good yield, although it was necessary to exclude

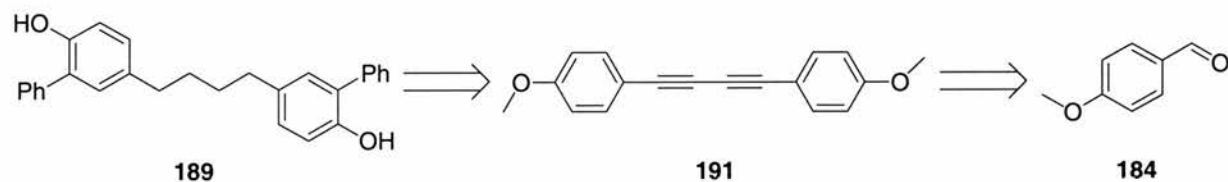
light from this reaction to prevent halogenation of the alkyl spacer. Suzuki coupling of **187** with phenylboronic acid, followed by boron tribromide deprotection afforded the diol **181** in 24% yield over 6 steps. As previous cyclisation efforts had intimated that reaction with dichloroborane was the most reliable method, this was the first means attempted (**Scheme 25**). Unfortunately, none of the desired product was recovered from the reaction mixture.



**Scheme 25** (a) (i)  $\text{BHCl}_2$ , PhMe, r.t., (ii)  $\text{AlCl}_3$ ,  $\Delta$ , 18 hrs.

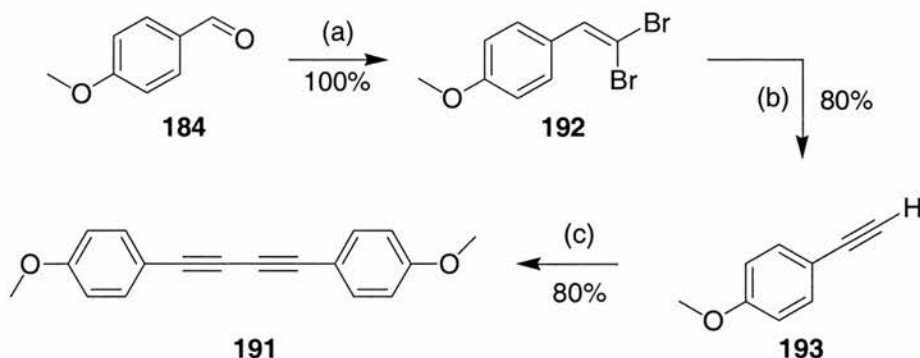
### 3.3.3 Synthesis of 3-[2-(10-Hydroxy-10,9-boroxophenanthren-3-yl)-butyl]-(10-hydroxy-10,9-boroxo)-phenanthrene **180**

The proposed synthesis of bis(boroxoaromatic) **180** also relied on the use of *p*-methoxybenzaldehyde **184** as a starting material, with the synthesis this time proceeding *via* the bis-alkyne **191**.



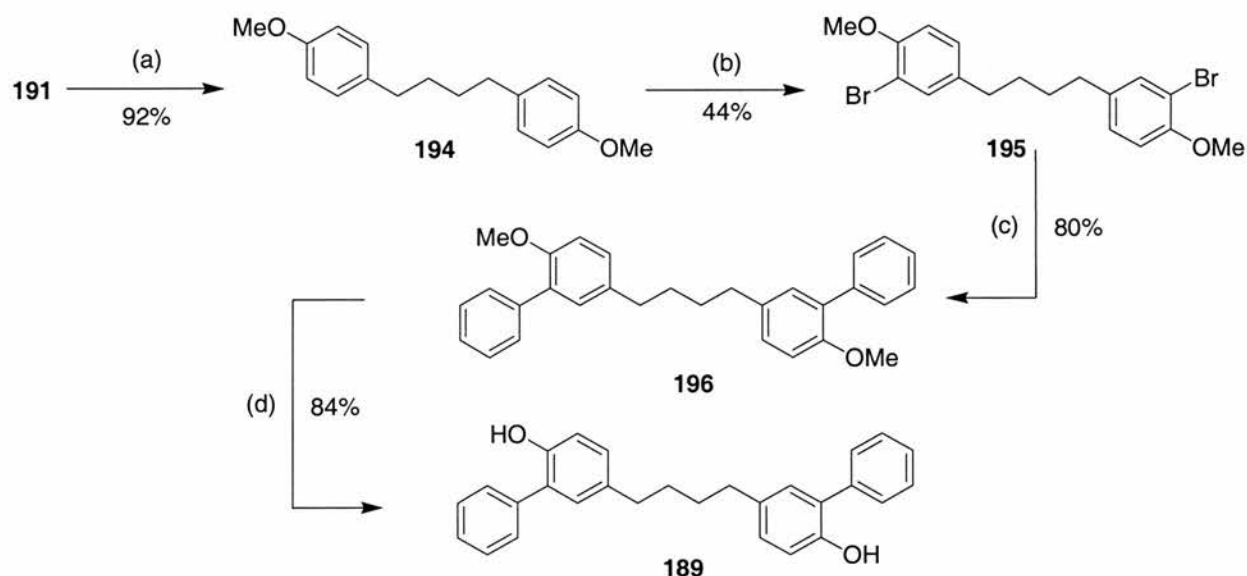
**Figure 82** Precursor diol **189** can be synthesised from **184** *via* bis-alkyne **191**

The synthesis of the bis-alkyne **191** was achieved using the methodology outlined in **Scheme 26**. Corey-Fuchs homologation<sup>174</sup> (i.e. reaction with a mixture of triphenylphosphine, zinc powder and carbon tetrabromide, followed by reaction with butyllithium) of *p*-anisaldehyde **184** afforded the terminal alkyne **193** in an 80% yield over the two steps. The homo-coupling of **193** was achieved by passing air through a solution of **193** and catalysed by copper (II) acetate.



**Scheme 26** (a)  $\text{PPh}_3$ ,  $\text{CBr}_4$ ,  $\text{Zn}$ ,  $\text{CH}_2\text{Cl}_2$ ,  $0\text{ }^\circ\text{C}\rightarrow\text{r.t.}$ ; (b)  $n\text{-BuLi}$ , THF,  $-78\text{ }^\circ\text{C}\rightarrow\text{r.t.}$ ; (c)  $\text{Cu}(\text{OAc})_2$ , pyridine, air.

The bis-alkyne **191** was readily reduced by a palladium on carbon catalysed hydrogenation (**Scheme 27**). Again, the alkyl spacer was extremely susceptible to bromination on reaction of **194** with bromine, but this problem was avoided by performing the reaction in the absence of light, although the yield was disappointing. Suzuki coupling with phenylboronic acid was successful, and deprotection of **196** afforded diol **189**.



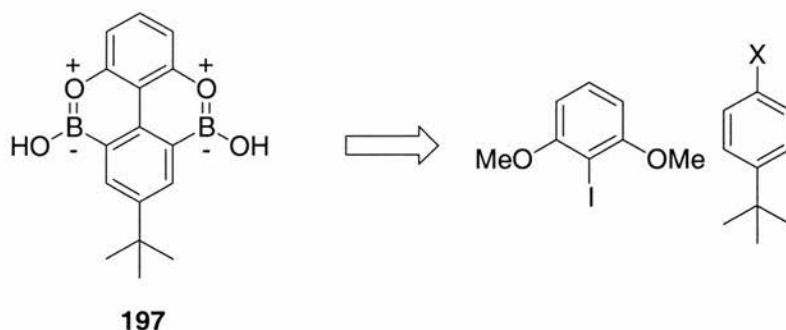
**Scheme 27** (a)  $\text{H}_2$ ,  $\text{Pd/C}$ ,  $\text{EtOAc}$ ; (b)  $\text{Br}_2$ ,  $\text{CHCl}_3$ ,  $-40\text{ }^\circ\text{C}\rightarrow\text{r.t.}$ ; (c)  $\text{PhB}(\text{OH})_2$ ,  $\text{Pd}(\text{PPh}_3)_4$ ,  $\text{Na}_2\text{CO}_3$ , DME,  $\text{EtOH}$ ,  $\text{H}_2\text{O}$ ; (d)  $\text{BBr}_3$ ,  $\text{CH}_2\text{Cl}_2$ ,  $-78\text{ }^\circ\text{C}\rightarrow\text{r.t.}$

The cyclisation of **189** was attempted using dichloroborane, generated *in situ* by reaction of  $\text{BCl}_3$  with  $\text{BHCl}_2\cdot\text{DMS}$ , however this was not successful.

Although neither **179** or **180** was successfully isolated using our first-choice conditions, we are hopeful that the syntheses will eventually be achieved, since both building blocks are based on phenanthrene units.

### 3.4 Conclusions

We have demonstrated the successful extension of the synthesis of boroxoaromatic compounds to the formation of a bifunctional boron-containing heteroaromatic compound, based on a rigid pyrene skeleton. In the solid state, **111** can undergo a dehydration reaction to form oligomeric anhydrides, with up to six repeat units. Due to its poor solubility in non-polar solvents, little can be deduced about the solution phase reactivity of **111**, although it seems likely that it will behave in a similar manner to **62**. The inclusion of solubilising groups (e.g. *tert*-butyl groups) on the aromatic skeleton may help to solve this problem. For example, the compound **197** (**Figure 83**) should be simple to synthesise using the same methodology described for **111**, *via* coupling of 1,3-dimethoxyiodobenzene with a *p*-halogenated *tert*-butylbenzene.



**Figure 83** Bis-boroxoaromatic **197** could be synthesised *via* the cross-coupling of 1,3-dimethoxyiodobenzene, and a 4-*tert*-butylhalogenobenzene.

Attempts to synthesise and isolate bifunctional boroxoaromatics **132** through **135** based around dibenzanthracene skeletons, which, by virtue of the convergent direction of their hydroxyl functionalities, may be more likely to form macrocyclic than linear oligomers, have so far proved unsuccessful. However, the reliable syntheses of the precursor diols have been achieved, and the eventual isolation of the desired compounds seems possible.

The synthesis of several flexible boroxoaromatic compounds has also been attempted, but has unfortunately been unsuccessful so far. The precursor diols have been isolated in all cases, however, and efforts to effect the cyclisation will be continued.



## 4 Further Investigations into the Reactivity of 10-Hydroxy-10,9-Boroxophenanthrene

### 4.1 Preamble

The reaction of hydroxyboroxophenanthrene **62** with three nucleophiles, namely 4-methylbenzyl alcohol **103**, 4-*tert*-butylbenzyl alcohol **105**, and 1,3-benzenedimethanol **107** has already been discussed briefly in **Chapter 2**. We recall that the related hydroxyborazaphenanthrene reacts only very slowly with nucleophiles other than itself, and that its tendency to dehydrate, even in solution, limits the utility of this family of compounds in more complex systems. Calculations (**Section 2.3.1**) show that the replacement of the nitrogen atom in hydroxyborazaphenanthrene with the more electronegative oxygen atom results in a significant increase in the electrophilicity of boron, which explains the increased reactivity of **62** towards nucleophiles.

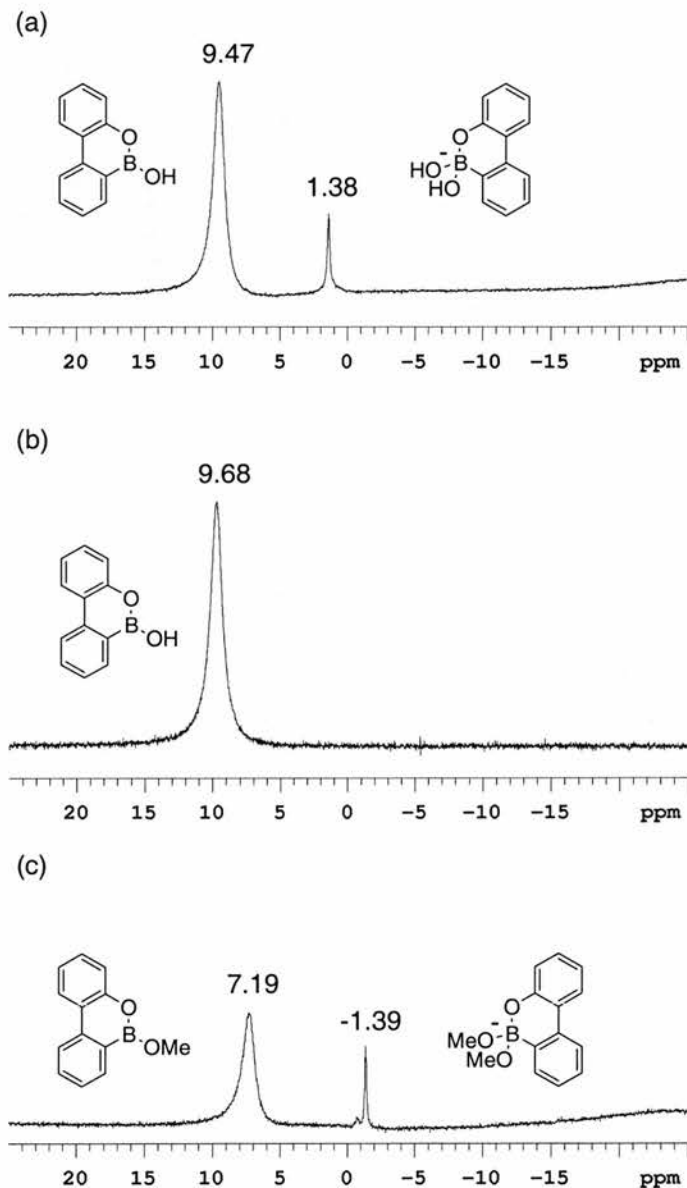
We wished to carry out a more comprehensive study of the reaction of **62** with nucleophiles, in order to determine the generality of the interaction, and to better understand the reactivity of **62**. We believed that  $^{11}\text{B}$  NMR spectroscopy would enable us to monitor any change in the environment of the boron atom, whilst MALDI-TOF spectrometry would aid the identification of the reaction product.

#### 4.1.1 $^{11}\text{B}$ NMR Spectroscopy of 10-Hydroxy-10,9-Boroxophenanthrene

Boron is a quadrupolar nucleus, and can therefore give comparatively broad NMR signals. However, the heavier of the two naturally occurring isotopes,  $^{11}\text{B}$ , is about 80% abundant, and is relatively receptive in an NMR sense.  $^{11}\text{B}$  NMR spectroscopy can provide useful information about the coordination environment of the boron atom.<sup>175</sup> The  $^{11}\text{B}$  NMR spectrum of **62** was recorded in several different solvents. We recall (**Section 1.2.3**) that an  $^{11}\text{B}$  signal in the range 9-10 ppm is indicative of boron in a trigonal ( $sp^2$  hybridised) environment, whereas a signal further upfield results from boron in a tetrahedral ( $sp^3$  hybridised) environment.

In  $d_3$ -MeCN solution the  $^{11}\text{B}$  NMR spectrum (**Figure 84a**) of **62** shows two separate resonances, one noticeably weaker than, and upfield from, the other. It seems likely that the more intense peak ( $\delta$  9.47) is due to the trigonal boron, whereas the weaker signal ( $\delta$  1.38) results from the tetrahedral boron formed by coordination of an extra water molecule. Tellingly, in  $\text{CDCl}_3$  (**Figure 84b**), in which water is less

soluble, only one peak ( $\delta$  9.68) – that due to the trigonal boron – is visible. In  $d_4$ -MeOH (**Figure 84c**), two resonances, one due to the trigonal methyl ester of **62** ( $\delta$  7.19), and the second presumed to be due to the tetrahedral bis-methoxy adduct ( $\delta$  -1.39), are visible.

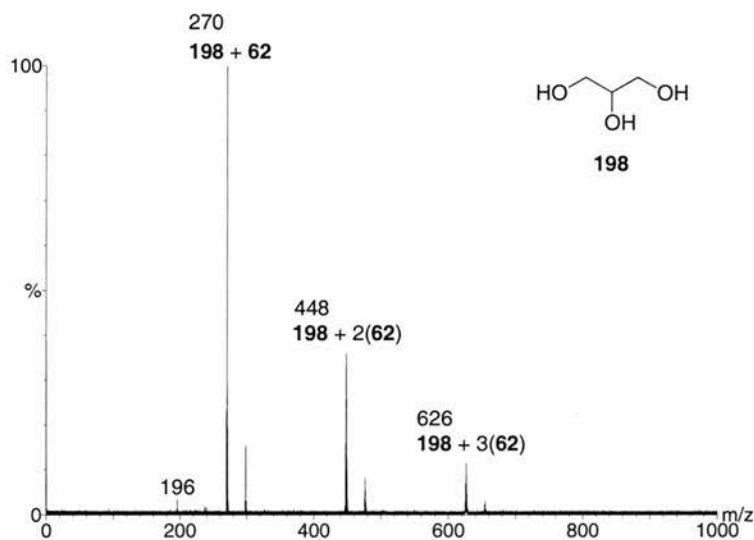


**Figure 84** (a) The  $^{11}\text{B}$  160.4 MHz NMR spectrum of **62** recorded at 293 K in  $d_3$ -MeCN, shows two signals, due to trigonal and tetrahedral boron. (b) In  $\text{CDCl}_3$ , the  $^{11}\text{B}$  spectrum shows one signal only. (c) The  $^{11}\text{B}$  spectrum of **62** in  $\text{CD}_3\text{OD}$  shows two signals. Chemical shifts are given relative to external  $\text{B}(\text{OMe})_3$  ( $\delta=0.0$  ppm) in the same solvent

It has already been established that **62** can react with nucleophiles, such as water and methanol, to adopt a tetrahedral conformation about the boron atom.

### 4.1.2 MALDI-TOF Mass Spectrometry of 10-Hydroxy-10,9-boroxophenanthrene

MALDI-TOF mass spectra were recorded using a cobalt matrix, which was made up simply by sonicating a suspension of cobalt (II, III) oxide powder in methanol. Initially, glycerol **198** was also added to the mixture to help give a uniform dispersion of cobalt oxide. However, MALDI-TOF mass spectra run using this matrix (**Figure 85**) gave unexpected peaks at  $m/z$  270, 448 and 626, with only a small peak due to the predicted molecular ion at  $m/z$  196.



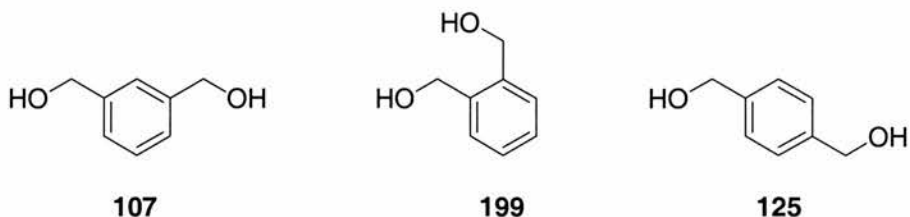
**Figure 85** The MALDI-TOF mass spectrum of a sample of **62** run using a cobalt matrix containing glycerol **198**.

These peaks are due to the nucleophilic reaction of **62** with **198**, accounting for the association of one, two and three molecules of **62** to **198** respectively. Accordingly, all subsequent MALDI-TOF mass spectra were run using a cobalt oxide matrix to which glycerol had not been added.

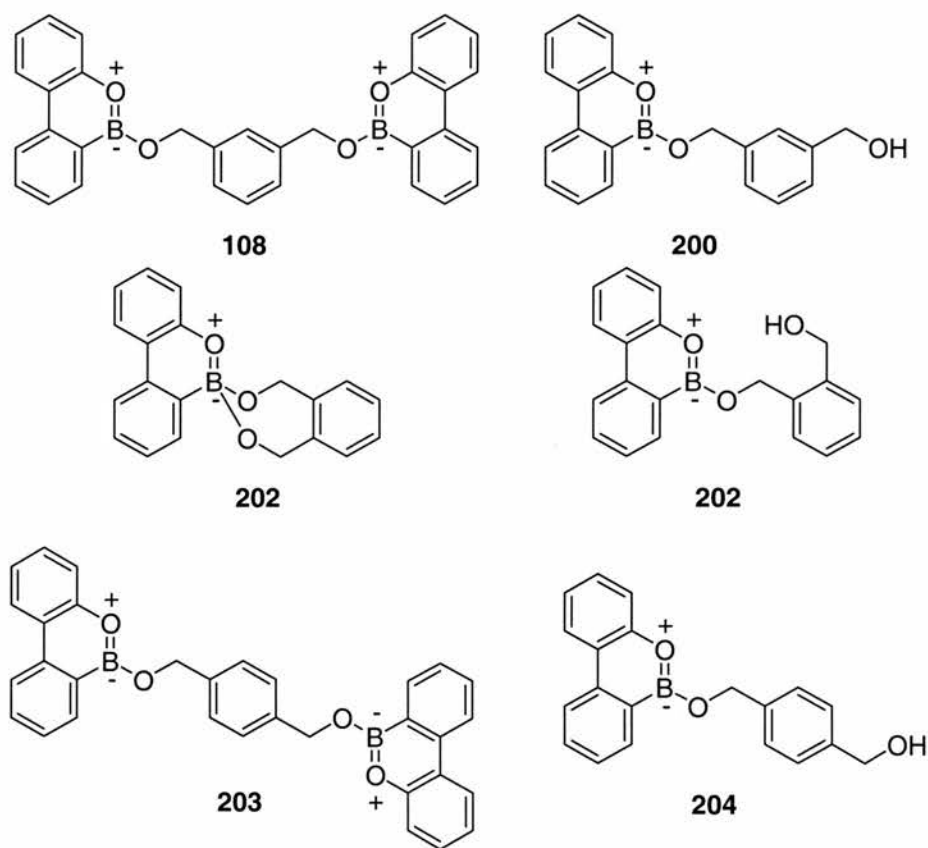
The reactions of **62** with different nucleophiles were analysed using  $^{11}\text{B}$  and  $^1\text{H}$  NMR spectroscopy, and also MALDI-TOF mass spectrometry.

## 4.2 Reaction of **62** with Benzenedimethanols

In **Section 2.6** an experiment was described in which a 1:1 solution of **62** with 1,3-benzenedimethanol **107** in  $\text{CHCl}_3$  was analysed using MALDI-TOF mass spectrometry, and was found to afford almost exclusively the 2:1 adduct **108**. This experiment was repeated and the reaction of **62** with the regioisomers 1,2-benzenedimethanol **199** and 1,4-benzenedimethanol **125** also investigated.



Benzenedimethanol isomers **107** and **125** may combine with two molecules of **62** to form 2:1 adducts (e.g. **108** and **203**, **Figure 86**), but, due to their rigid nature, both hydroxyl groups cannot react with the same boron atom. It is possible that one molecule of benzene dimethanol **199** could react twice with the same boron atom, resulting in a tetrahedral environment around the boron (**202**, **Figure 86**). It is also possible that all three isomers could react to form a simple 1:1 adduct, such as **200**, **202** and **204** (**Figure 86**).



**Figure 86** Possible products formed by reaction of **62** with **107**, **199** and **125**.

**Table 6** lists the chemical shift of the resonances observed in the  $^{11}\text{B}$  160.4 MHz NMR spectrum, recorded at 293 K, of 1:1 solutions of **62** with

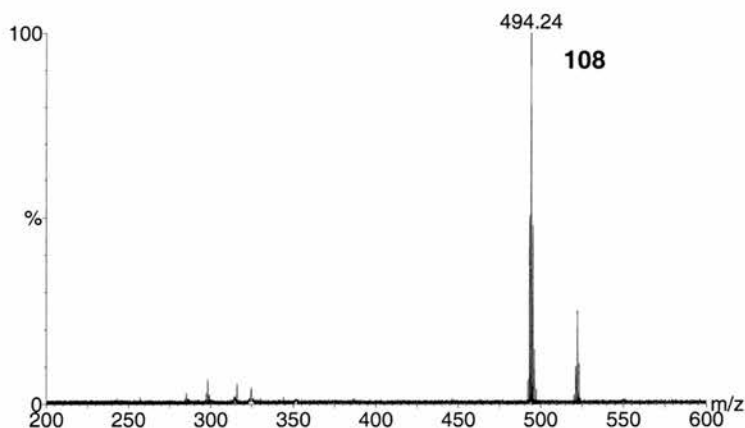
benzenedimethanols **107**, **125** and **199** in  $\text{CDCl}_3$ . Also provided are the  $m/z$  values of the major peaks in the MALDI-TOF mass spectra.

**Table 6**  $^{11}\text{B}$  NMR 160.4 MHz chemical shift data for 1:1 solutions of **62** in  $\text{CDCl}_3$  with different nucleophiles, recorded at 293 K,<sup>a</sup> and  $m/z$  values for the major peaks observed in the MALDI-TOF mass spectrum.

Nucleophile	$\delta$ / ppm	$m/z$	Relative Intensity <sup>b</sup>
<b>199</b>	9.51 <sup>c,d</sup>	494 (2:1)	60
		316 (1:1)	40
<b>107</b>	9.02 <sup>c</sup> , 0.53	494 (2:1)	100
<b>125</b>	9.55 <sup>c</sup>	494(2:1)	66
		316 (1:1)	33

<sup>a</sup> Chemical shifts in ppm downfield (positive) or upfield (negative) of external  $\text{B}(\text{OMe})_3$  in the same solvent ( $\delta = 0.0$ ). <sup>b</sup> Relative intensity of  $m/z$  494 vs.  $m/z$  316. <sup>c</sup> Indicates signal may be 2 peaks. <sup>d</sup> Possible small signal visible 0-1 ppm.

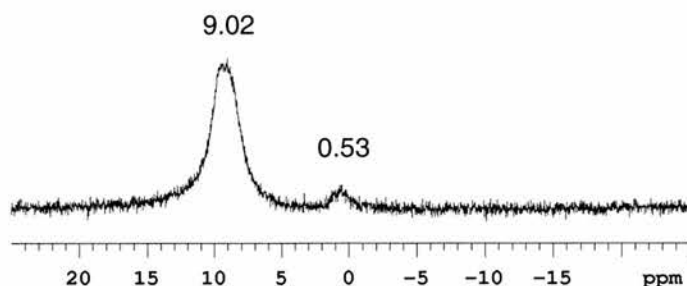
MALDI-TOF mass spectra (e.g. **Figure 87**) of the 1:1 solutions of **62** with each of the three benzenedimethanols show the major peak is due to the 2:1 adduct (e.g. **108**), at  $m/z$  494. The spectra of solutions of **62** with 1,2- and 1,4-benzenedimethanol also show a smaller peak at  $m/z$  316, the molecular ion of the 1:1 adduct.



**Figure 87** The MALDI-TOF mass spectrum of a 1:1 solution of **62** and **107** in  $\text{CHCl}_3$ , shows predominantly 2:1 adduct **108** ( $m/z$  494).

As expected, therefore, the major resonance in the three  $^{11}\text{B}$  spectra is that at around 9 ppm (**Figure 88**). In all three cases, this resonance may in fact to be two almost concurrent signals, possibly due to the 2:1 adduct and free **62**, although the resonances cannot be resolved. The spectra of 1:1 solutions of **62** and 1,2- and 1,3-benzenedimethanol also show a small peak at around 0 ppm, possibly due to

coordination by boron of an extra benzenedimethanol molecule, generating a tetrahedral environment, although there is no evidence of this species in the MALDI-TOF mass spectrum.



**Figure 88** The  $^{11}\text{B}$  160.4 MHz NMR spectrum of a 1:1 solution of **62** and **107** in  $\text{CDCl}_3$ , recorded at 293 K.

### 4.3 Reaction of **62** with Alkane diols

The more flexible alkane diols **126**, **205** and **206** have access to a range of possible adducts. They may form simple 1:1, 1:2 and 2:1 adducts, **207**, **208** and **209** respectively, as well as the “cyclised” 1:1 adducts, exhibiting an extra association with boron, such as **210** (**Figure 89**).

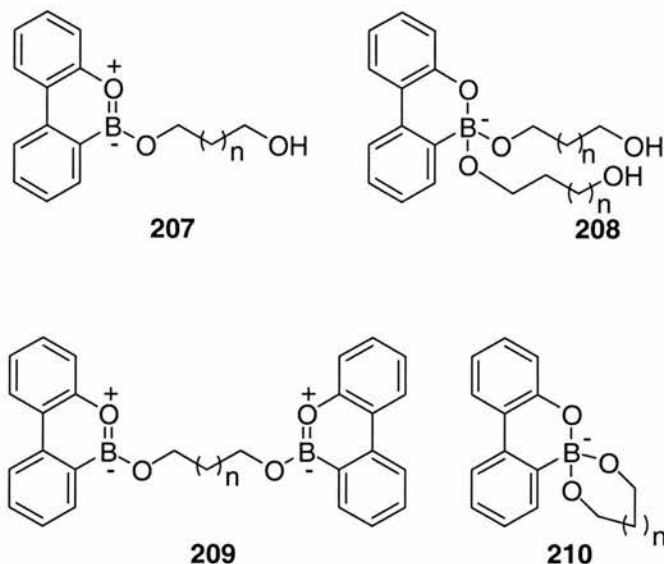


n=0, **205**

n=1, **126**

n=2, **206**

This last mode of association is expected to be more favoured in the case of 1,3-propanediol **126**, since it results in the formation of a six-membered ring, rather than a five- or seven-membered ring.



**Figure 89** Possible adducts formed by the reaction of **62** with alkanediols.

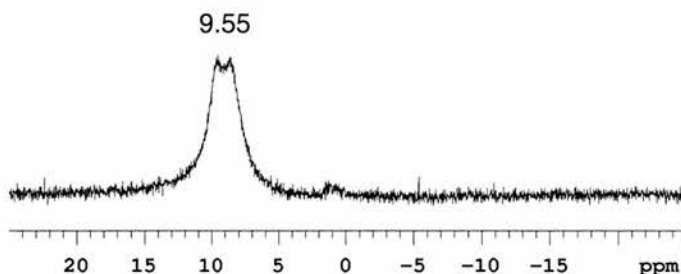
**Table 7** lists  $^{11}\text{B}$  160.4 MHz NMR data for 1:1 solutions of **62** and the three alkanediols in  $\text{CDCl}_3$ . Also listed are the  $m/z$  values for the major peaks observed in the MALDI-TOF mass spectrum. It should be noted that in all three cases, the only peak observed in the MALDI-TOF mass spectrum is that due to the 2:1 adduct, and none of the 1:1 adduct is seen at all.

**Table 7**  $^{11}\text{B}$  NMR 160.4 MHz chemical shift data for 1:1 solutions of **62** in  $\text{CDCl}_3$  with different nucleophiles, recorded at 293 K,<sup>a</sup> and  $m/z$  values for major peaks observed in the MALDI-TOF mass spectrum.

Nucleophile	$\delta$ / ppm	$m/z$
<b>206</b>	9.55 <sup>b,c</sup>	446 (2:1)
<b>126</b>	9.82 <sup>b</sup> , 0.00	432 (2:1)
<b>205</b>	9.76 <sup>b</sup> , 4.95	418 (2:1)

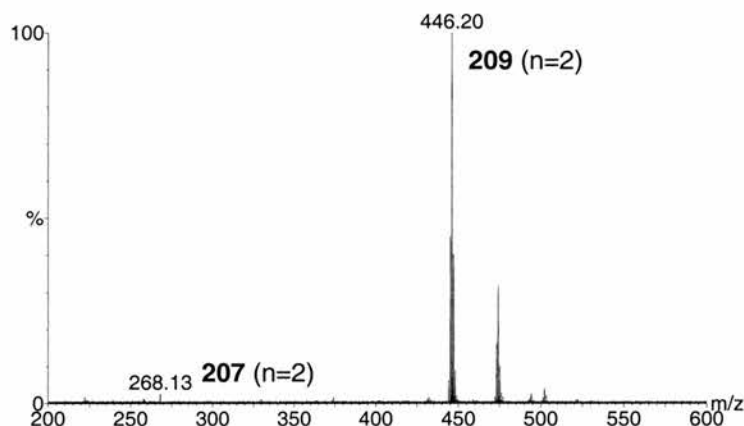
<sup>a</sup> Chemical shifts in ppm downfield (positive) or upfield (negative) of external  $\text{B}(\text{OMe})_3$  in the same solvent ( $\delta = 0.0$ ). <sup>b</sup> Indicates signal may be 2 peaks. <sup>c</sup> Possible small signal visible 1-2 ppm.





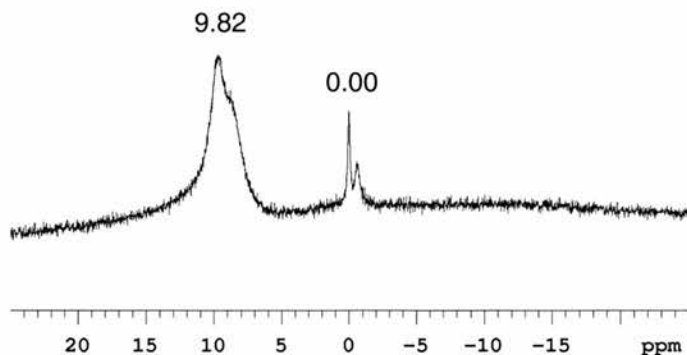
**Figure 90**  $^{11}\text{B}$  NMR 160.4 MHz spectrum of a 1:1 solution of **203** and **62** in  $\text{CDCl}_3$ , recorded at 293 K.

1,4-Butanediol **206** reacts to form a 2:1 complex **209** ( $n=2$ ) only, indicated by the peak at  $\delta$  9.6 in the  $^{11}\text{B}$  spectrum (**Figure 90**), and the  $m/z$  446 peak in the MALDI-TOF mass spectrum (**Figure 91**). Again, the peak at  $\delta$  9.6 appears to be two almost coincident peaks, probably indicating a mixture of the adduct and free **62**.



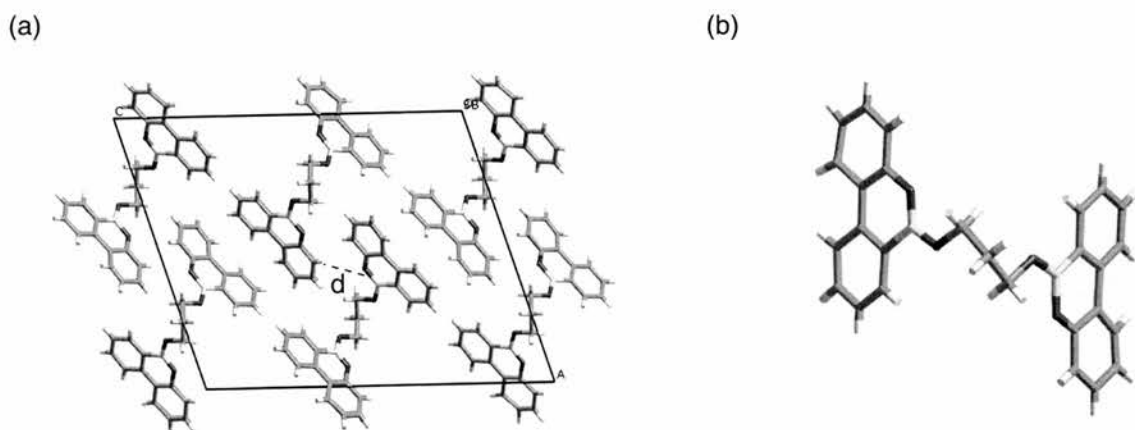
**Figure 91** The MALDI-TOF spectrum of a 1:1 solution of **62** and **206** shows mainly the 2:1 adduct **209** ( $n=2$ ) ( $m/z$  446).

The  $^{11}\text{B}$  spectrum of a 1:1 solution of **62** and **126** in  $\text{CDCl}_3$  (**Figure 92**) shows two signals, one at  $\delta$  9.8, indicative of the 2:1 adduct **209** ( $n=1$ ), and one of a similar intensity at  $\delta$  0.0. This is likely to be the cyclised 1:1 adduct **210** ( $n=1$ ), in which the boron adopts a tetrahedral ( $sp^3$  hybridised) conformation. The MALDI-TOF mass spectrum shows predominantly 2:1 adduct **209** ( $n=1$ ), although there is also a very small signal at  $m/z$  253, the expected molecular ion of the cyclised 1:1 adduct **210** ( $n=1$ ).



**Figure 92**  $^{11}\text{B}$  160.4 MHz NMR spectrum of a 1:1 solution of **126** and **62** in  $\text{CDCl}_3$  recorded at 293 K.

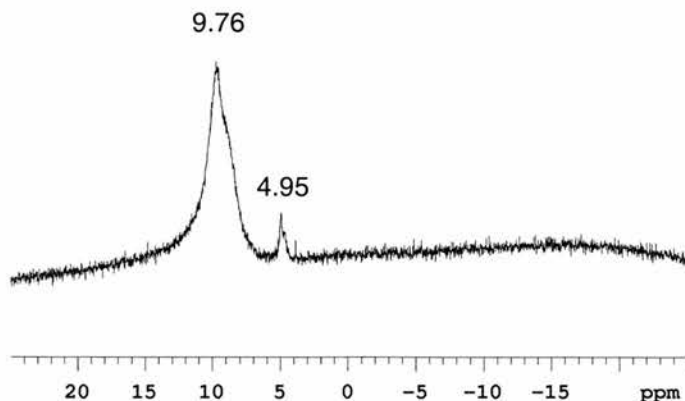
Crystals of the 2:1 adduct were grown by slow evaporation of solvent from a 1:1 mixture of **62** and **126** in acetonitrile. The crystal structure (**Figure 93**) shows the presence of the **209** ( $n=1$ ) only.



**Figure 93** (a) Stick representation of the unit cell of the crystal structure of the 2:1 adduct formed by reaction of **62** with **126**,  $d=3.44 \text{ \AA}$ . The solid lines represent the unit cell. (b) Stick representation of a single molecule of the 2:1 adduct **209** ( $n=1$ ).

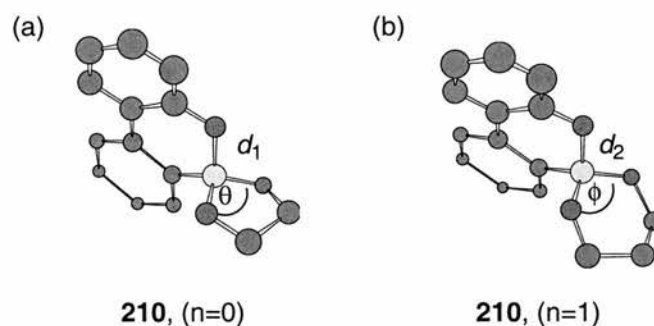
The two phenanthrene units are oriented at an angle of almost  $90^\circ$  to each other, and the structure shows stacks of these “L-shaped” molecules. There is also a short contact ( $3.44 \text{ \AA}$ ) between the endocyclic oxygen atom and an aromatic proton.

The  $^{11}\text{B}$  spectrum of a 1:1 solution of **62** and ethanediol **205** (**Figure 94**) also shows two resonances, but in this case, the resonance due to the tetrahedral boron is much less intense, and appears further downfield at  $\delta 5.0$ .



**Figure 94**  $^{11}\text{B}$  160.4 MHz NMR spectrum of a 1:1 solution of **205** and **62** in  $\text{CDCl}_3$  recorded at 293 K.

The strained 5-membered ring formed by reaction of **62** with **205** is less stable than the 6-membered ring formed by reaction of **62** with **126**. This is due to the compressed  $\text{O}_{\text{exo}}\text{-B-O}_{\text{exo}}$  angle ( $105^\circ$  vs.  $113^\circ$ ), which leads to a decreased opportunity for electron transfer from the oxygen lone pair to the empty boron  $p$ -orbital (**Figure 95**). (The calculated minimum natural atomic occupancies (N.A.O.) of the boron  $p_z$  orbitals are 0.38 (**210**,  $n=0$ ) and 0.39 (**210**,  $n=1$ .) Thus, the boron atom in **210** ( $n=0$ ) is less shielded than in **210** ( $n=1$ ). This explains the decreased upfield shift observed for the boron signal ( $\delta$  5.0 vs  $\delta$  0.0). The lower stability of the ethanediol adduct **210** ( $n=0$ ) may also explain why the resonance due to  $sp^3$  hybridised boron is not so prominent.

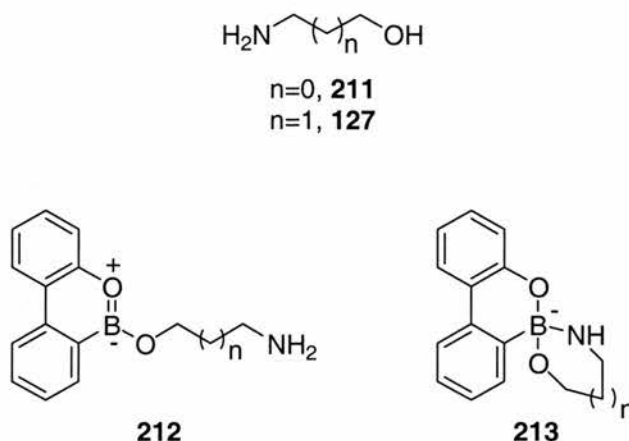


**Figure 95** (a) Calculated (HF/6-31G(d,p)) structure of **210** ( $n=0$ ), formed by reaction of **62** with **205**.  $d_1 = 1.50 \text{ \AA}$ ,  $\theta = 105^\circ$ . (b) Calculated (HF/6-31G(d,p)) structure of **210** ( $n=1$ ), formed by reaction of **62** with **126**.  $d_2 = 1.48 \text{ \AA}$ ,  $\phi = 113^\circ$ .

#### 4.4 Reaction of **62** with Amino alcohols

The amino alcohols **127** and **211** are clearly closely related to the alkane diols described above, and may form either the acyclic (**212**, **Figure 96**) or cyclised (**213**) 1:1 adducts, in addition to the 2:1 adducts. However, nitrogen is a stronger donor

than oxygen, and we might expect this to make a difference to the relative stability of the different adducts.



**Figure 96** Possible adducts formed by the reaction of **62** with amino alcohols **127** and **211**.

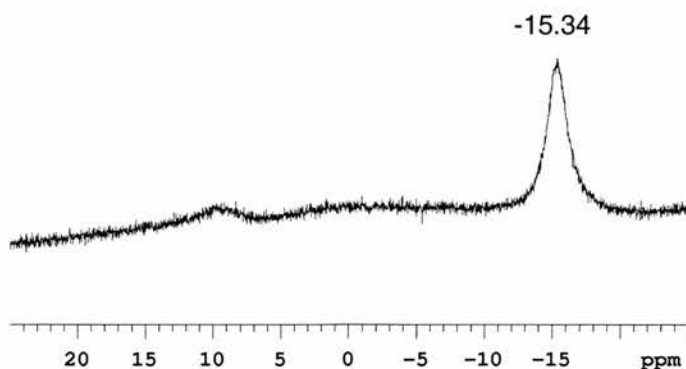
**Table 8** lists the resonances observed in the  $^{11}\text{B}$  160.4 MHz NMR spectra, recorded at 293 K, of 1:1 solutions of **62** with **127** and **211** in  $\text{CDCl}_3$ . Also provided are the  $m/z$  values of the major peaks in the MALDI-TOF mass spectrum.

**Table 8**  $^{11}\text{B}$  NMR 160.4 MHz chemical shift data for 1:1 solutions of **62** in  $\text{CDCl}_3$  with different nucleophiles, recorded at 293 K<sup>a</sup> and  $m/z$  values for the major peaks observed in the MALDI-TOF mass spectrum.

Nucleophile	$\delta$ / ppm	$m/z$
<b>127</b>	-15.34 <sup>b</sup>	253 (1:1)
<b>211</b>	9.70, -5.42	239 (1:1)

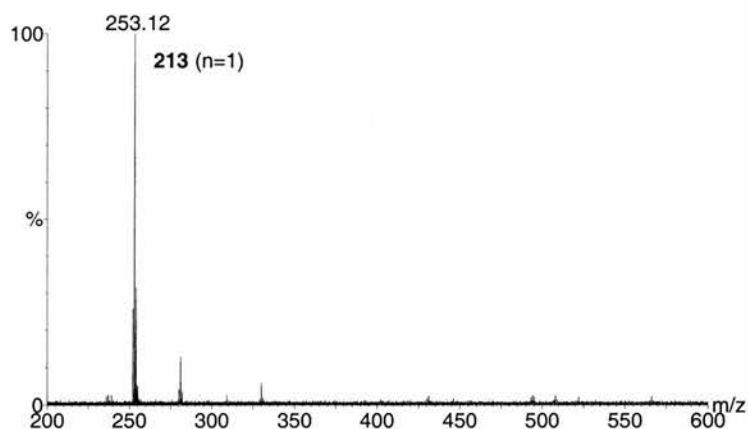
<sup>a</sup> Chemical shifts in ppm downfield (positive) or upfield (negative) of external  $\text{B}(\text{OMe})_3$  in the same solvent ( $\delta = 0.0$ ). <sup>b</sup> Possible small signal visible 9-10 ppm.

The  $^{11}\text{B}$  spectrum of a 1:1 solution of **62** and aminopropanol **127** (**Figure 97**) shows a very strong signal at  $\delta -15.3$ , and a small signal at around  $\delta 9.0$ . It appears likely that the major resonance is due to the coordination of nitrogen to boron in a cyclised 1:1 adduct **213** ( $n=1$ ).



**Figure 97**  $^{11}\text{B}$  160.4 MHz NMR spectrum of a 1:1 solution of **127** and **62** in  $\text{CDCl}_3$ , recorded at 293 K.

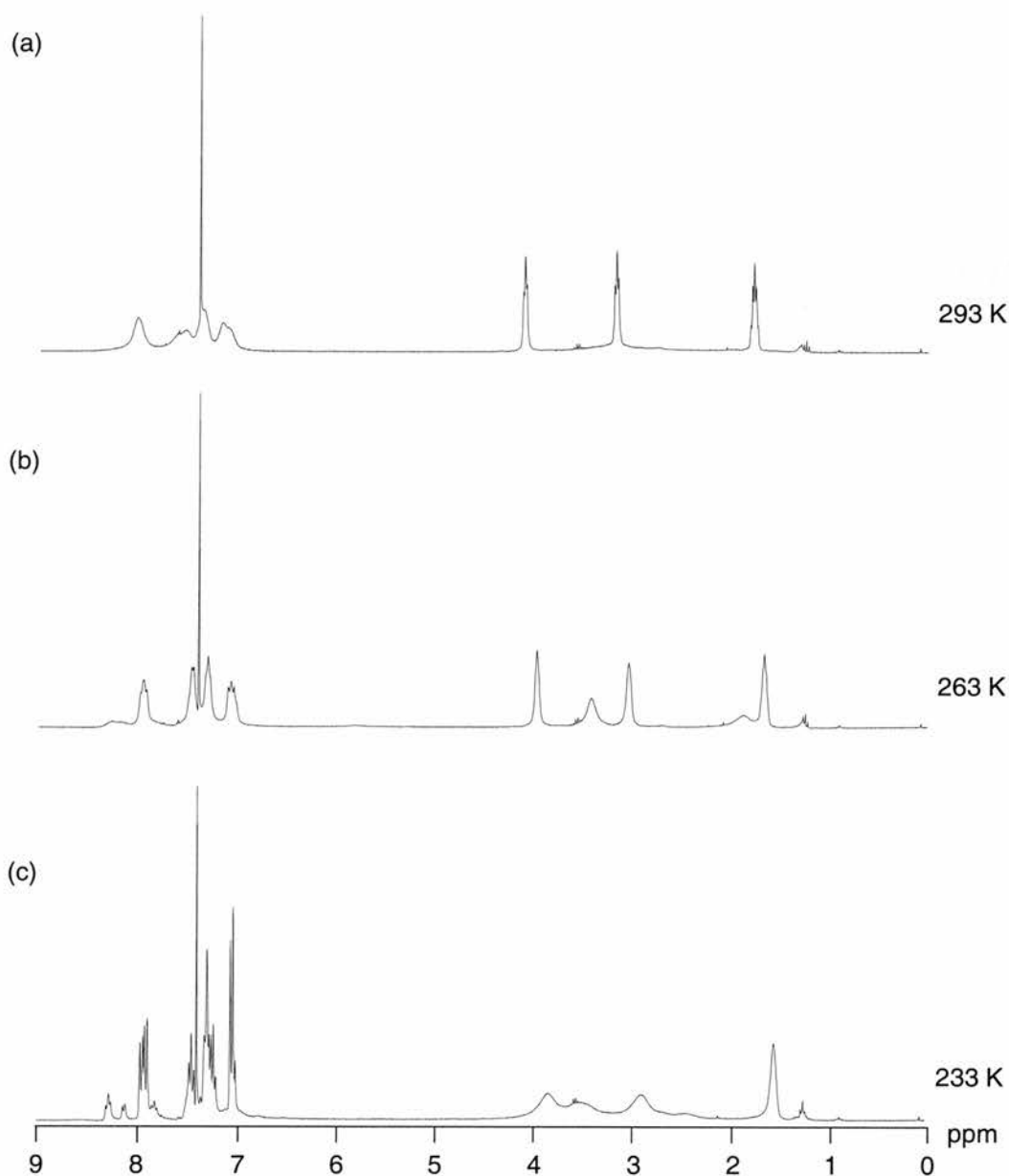
Nitrogen is a stronger donor than oxygen, which explains the increased downfield shift of this resonance, over the shift observed ( $\delta$  0.0) after reaction with propanediol **126**. If we assume that the B-N bond is labile, this explains the presence of the resonance at  $\delta$  9.0, which would be due to the uncyclised 1:1 adduct **212** ( $n=1$ ). The formation of the cyclic adduct **213** ( $n=1$ ) is supported by the MALDI-TOF mass spectrum (**Figure 98**), which shows almost exclusively the expected molecular ion at  $m/z$  253.



**Figure 98** The MALDI-TOF mass spectrum of a 1:1 solution of **62** and **127** shows a single peak at  $m/z$  253.

$^1\text{H}$  NMR spectroscopy provides further evidence for this theory. At room temperature (**Figure 99a**), the spectrum is not clearly resolved. The broad resonances are suggestive of the occurrence of several possible processes, including flipping of the 6-membered ring, and the reversible exchange of the labile B-N bond. In a separate experiment, the  $^1\text{H}$  NMR spectrum of a 1:1 solution of **127** and **62** was recorded at intervals of 10 K from 223 K to 293 K. Generally, at 293 K (**Figure 99a**), the peaks in

the aromatic region are poorly resolved, whilst those in the range  $\delta$  1-4 are relatively sharp. At 223 K, the reverse is true, and at intermediate temperatures (**Figure 99b-c**), both regions show little defined structure.

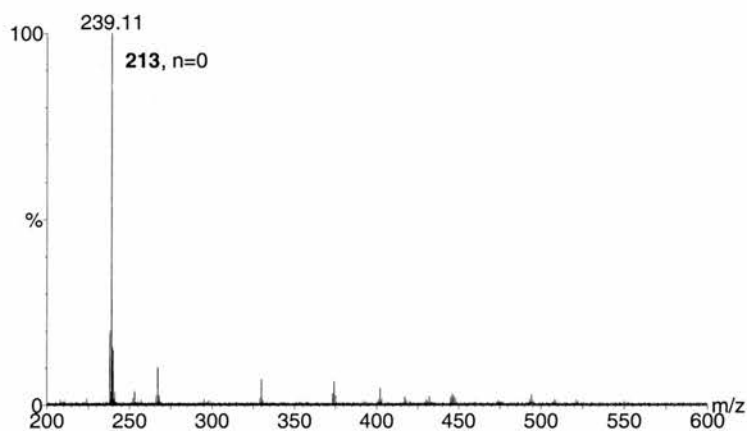


**Figure 99**  $^1\text{H}$  300 MHz NMR spectrum of a 1:1 mixture of **62** and **127** in  $\text{CDCl}_3$ , recorded at (a) 293 K, (b) 263 K and (c) 233 K.

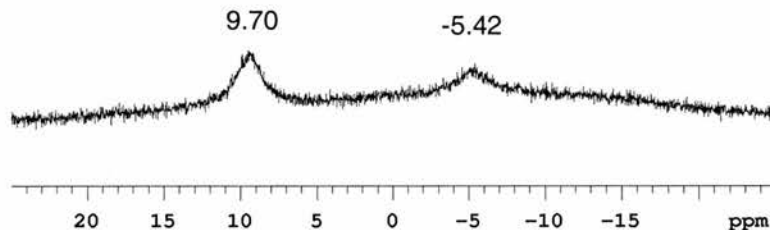
Reaction of **62** with 1-amino-2-ethanol **211** also results in the formation of a cyclic 1:1 adduct **213** ( $n=0$ ), and the predominant signal in the MALDI-TOF mass spectrum ( $m/z$  239) is due to this compound (**Figure 100a**). However, the  $^{11}\text{B}$  NMR spectrum displays two signals. In contrast to the spectrum of **62:127**, the resonance due to  $sp^3$  boron, at  $\delta$  -5.4, is considerably less intense and does not occur so far upfield. In fact,

this resonance is of a similar intensity to that of the  $sp^2$  hybridised boron. This confirms the hypothesis that the 6-membered ring, formed by aminopropanol **127** with **62**, is more stable than the 5-membered ring formed by aminoethanol **211** with **62**.

(a)



(b)



**Figure 100** (a) MALDI-TOF mass spectrum of a 1:1 solution of **62** and **211**, showing almost exclusively the 1:1 adduct **213** ( $n=0$ ) at  $m/z$  239. (b) The  $^{11}\text{B}$  160.4 MHz NMR spectrum of a 1:1 solution of **211** and **62** in  $\text{CDCl}_3$ , recorded at 293 K, shows resonances due to both the cyclised and acyclic 1:1 adduct.

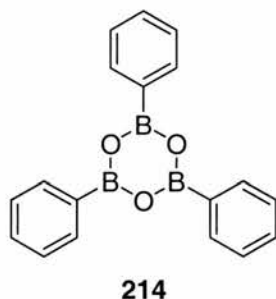
## 4.5 Reactivity of Phenylboronic Acid with Nucleophiles

10-Hydroxy-10,9-boroxophenanthrene **62** was compared earlier (**Section 2.3.1**) with phenylboronic acid **80**. Both behave as Lewis acids in the presence of hydroxide, although **62** is a rather stronger acid than **80**. We were interested to compare the solution phase reactivity of **80** with different bis-nucleophilic compounds, with that described above for **62**. This may provide more evidence as to whether **62** behaves as a cyclic boronic acid, or as an aromatic compound.



Boronic acids have long been known to form<sup>176</sup> cyclic esters with diols, and boronic esters are widely used<sup>177</sup> in stereoselective asymmetric synthesis. Other recent research on boronic esters has focussed on their use as linkers<sup>178</sup> in solid phase synthesis, and as agents<sup>179</sup> for boron neutron capture therapy (BNCT). Boronic acids form more stable complexes with rigid diols, such as saccharides, than with simple acyclic diols like ethylene glycol, and have indeed been used<sup>180</sup> as selective sensors for polysaccharides.

Phenylboronic acid **80** was mixed with three different nucleophiles, 1,3-benzenedimethanol **107**, 1,2-ethanediol **205** and 3-amino-1-propanol **127**, in CDCl<sub>3</sub> solution. Each 1:1 solution was examined by MALDI-TOF mass spectrometry and <sup>11</sup>B NMR spectroscopy. In all cases, the base peak in the MALDI-TOF mass spectrum was that at *m/z* 311, which is the molecular ion of the phenylboronic acid trimer **211**. This peak also appears in the spectrum of a CDCl<sub>3</sub> solution of **80** alone. **Table 9** gives <sup>11</sup>B 160.4 MHz NMR and MALDI-TOF mass spectrometry data for all three solutions, as well as providing data for **80** alone.

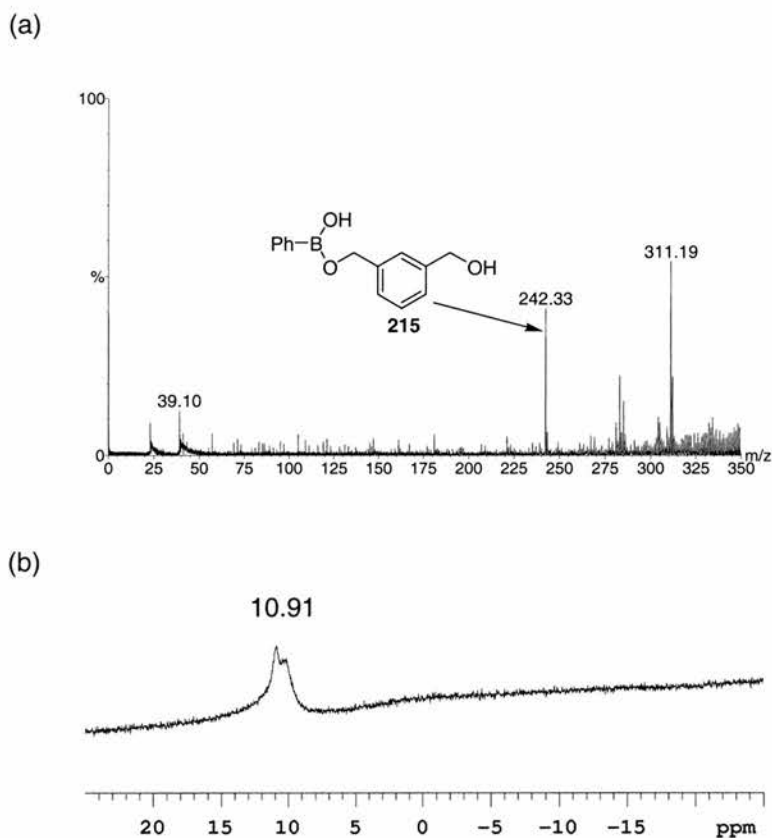


**Table 9** <sup>11</sup>B NMR 160.4 MHz chemical shift data for 1:1 solutions of **80** in CDCl<sub>3</sub> with different nucleophiles, recorded at 293 K<sup>a</sup>. Also provided are the *m/z* values for the major peaks observed in the MALDI-TOF mass spectrum.

Nucleophile	$\delta$ / ppm	<i>m/z</i>
<b>80</b>	10.9	311
<b>107</b>	10.9 <sup>b</sup>	242 (1:1)
<b>205</b>	13.1	212 (1:2)
<b>127</b>	10.4, -15.4	161 (1:1 <sup>c</sup> ) 179 (1:1 <sup>d</sup> )

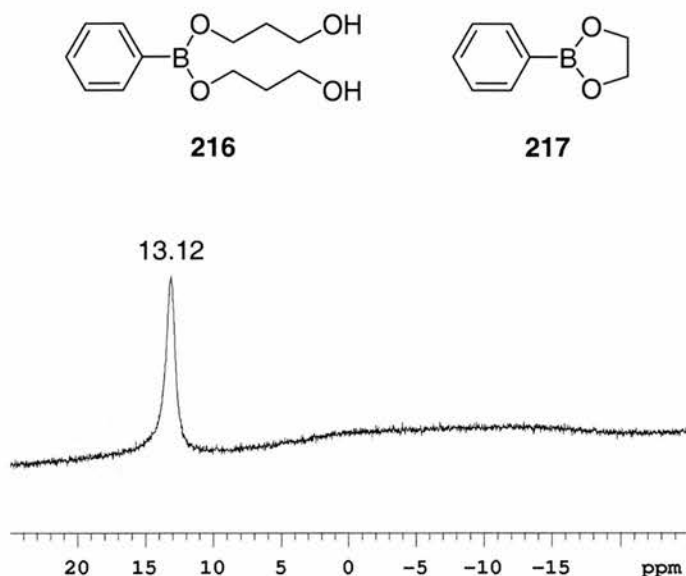
<sup>a</sup> Chemical shifts in ppm downfield (positive) or upfield (negative) of external B(OMe)<sub>3</sub> in the same solvent ( $\delta = 0.0$ ). <sup>b</sup> Indicates signal may be 2 peaks. <sup>c</sup> Cyclised 1:1 adduct **219** (Figure 104). <sup>d</sup> Linear 1:1 adduct **218** (Figure 104).

The MALDI-TOF mass spectrum (**Figure 101a**) of a 1:1 solution of **80** and **107** shows only the 1:1 adduct **215** at  $m/z$  242. This is consistent with the  $^{11}\text{B}$  NMR spectrum (**Figure 101b**), in which the main signal is at  $\delta$  10.9, and appears actually to be two almost concomitant signals, probably due to a mixture of free phenylboronic acid **80** and **215**.

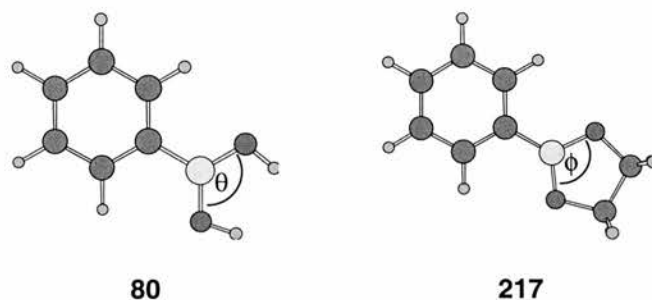


**Figure 101** (a) MALDI-TOF mass spectrum of a 1:1 solution of **80** and **107** in  $\text{CDCl}_3$ . (b)  $^{11}\text{B}$  160.4 MHz NMR spectrum of the same solution, recorded at 293 K.

The main signal in the MALDI-TOF mass spectrum of a 1:1 solution of **80** with **205** is that at  $m/z$  212, which is presumably due to the 1:2 complex **216**. However, the significant downfield shift of the  $^{11}\text{B}$  NMR signal (**Figure 102**) points to the formation of the expected cyclic ester **214**. The downfield shift, associated with decreased shielding of the boron atom, is explained by the fact that the formation of the ester forces a decrease in the O-B-O angle ( $111^\circ$  vs  $120^\circ$ , **Figure 103**), and, hence, a decrease in the O $\rightarrow$ B charge donation.

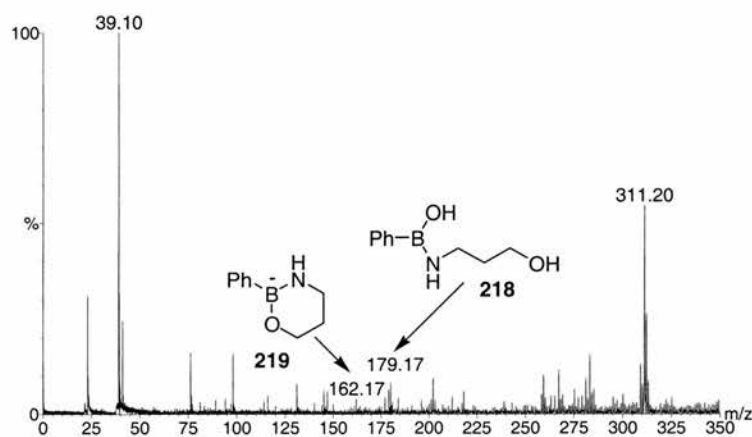


**Figure 102**  $^{11}\text{B}$  160.4 MHz NMR spectrum of a 1:1 solution of **80** and **205** in  $\text{CDCl}_3$ , recorded at 293 K.

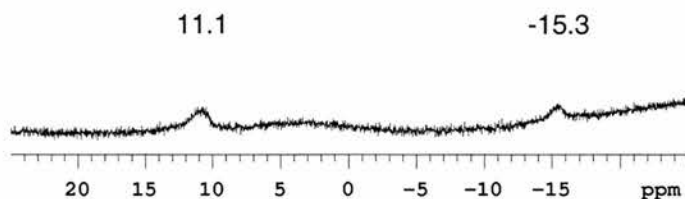


**Figure 103** The calculated (AM1) structures of **80** and **217** illustrate the decreased O-B-O angle in the cyclised structure:  $\theta = 120^\circ$ ,  $\phi = 111^\circ$ .

The MALDI-TOF mass spectrum (**Figure 104**) and  $^{11}\text{B}$  NMR spectrum (**Figure 105**) of a 1:1 solution of **80** and **127** are consistent with each other, both showing the acyclic **218** and cyclic **219** 1:1 adducts.

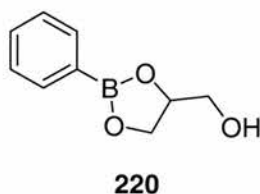


**Figure 104** MALDI-TOF mass spectrum of a 1:1 solution of **80** and **127** in  $\text{CDCl}_3$ .



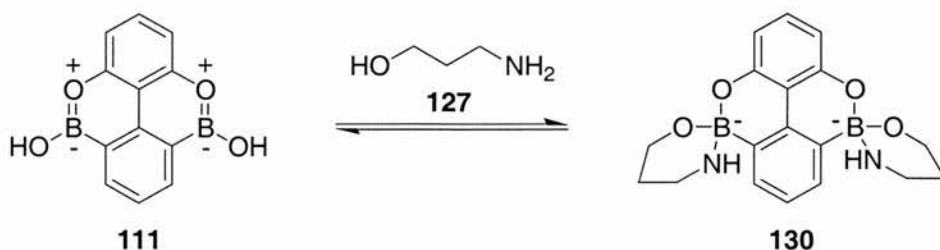
**Figure 105**  $^{11}\text{B}$  160.4 MHz NMR spectrum of a 1:1 solution of **80** and **127** in  $\text{CDCl}_3$ , recorded at 293 K. The resonance at  $\delta$  11.1 is due to **218** and that at  $\delta$  -15.3 is due to **219**.

Incidentally, reaction of **80** with glycerol **198** results in the formation of the cyclic ester **220**.



#### 4.6 Solution Phase Reactivity of 5,9-Dihydroxy-5,9-dibora-4,10-dioxopyrene Revisited

As discussed in **Section 3.1.4**, the analysis of the solution phase reactivity of **111** was hampered by the poor solubility of **111** in non-polar solvents. However, some reaction was observed with 3-aminopropanol **127**, giving a strong  $^{11}\text{B}$  NMR signal at  $\delta$  -16. A comparison with the results obtained above suggests **130** (**Figure 106**) as the most likely structure of the adduct, although clearly it is impossible to be sure without confirmation by MALDI-TOF mass spectrometry, or some other method of analysis.



**Figure 106** **111** reacts with **127** in a solution of acetone to form the adduct **130**.

The results described above also suggest that it should be possible to form linear oligomers in solution, by reaction of **111** with alkane diols or benzenedimethanols,

however, this obviously requires the synthesis of a more soluble pyrene-based bis-boroxoaromatic.

## 4.7 Conclusions

The experiments described above serve to illustrate further the rapid reaction of **62** with different nucleophiles. With benzenedimethanols, they typically form a 2:1 adduct, suggesting that a bifunctional boroxoaromatic may be capable of the solution phase formation of extended linear oligomers with bis-nucleophiles. With alkane diols, **62** also forms 2:1 adducts, as shown by the crystal structure solution obtained for the propanediol adduct. On reaction with amino alcohols, the increased nucleophilicity of the amino group leads to the formation of a cyclised adduct, in which the boron atom adopts a tetrahedral conformation. The solution phase reactivity of phenylboronic acid **80** is different to that shown by **62**. Phenylboronic acid **80** forms a 1:1 adduct with 1,3-benzenedimethanol **107**, a cyclic ester with 1,2-ethanediol **205**, and a mixture of the cyclised and acyclic 1:1 adduct with 3-aminopropanol **127**. It appears that, although **62** resembles a cyclic boronic acid in a structural sense, the presence of the additional O-C bond and the existence of aromatic stabilisation (**Section 2.7**) is enough to ensure significantly different reactivity.

## 5 General Conclusions

This thesis has described an extensive investigation into the potential of boron-containing heteroaromatic compounds as building blocks for covalent self-assembly. A complete characterisation of the structural and reactivity properties of our model building block, 10-hydroxy-10,9-boroxophenanthrene has been carried out. The polarisation pattern and self-assembly motif of the boron-oxygen functionality was found to be almost identical to that of a carboxylic acid, and this was proven by the crystal structure solution. The similarities of the solid state reactivity of hydroxyboroxophenanthrene, with that of the analogous boron-nitrogen compound have been explained, and, perhaps more interestingly, so have the differences in the solution phase reactivities. Hydroxyboroxophenanthrene reacts extremely rapidly with nucleophiles in solution, suggesting that this functionality may prove useful in the development of a dynamic combinatorial library. Building blocks incorporating this motif would possibly be capable of sampling a large number of compounds in a small space of time. The solid state reactivity of hydroxyboroxoaromatics also allows the formation of large oligomeric molecular solids *via* self-assembly, followed by a dehydration reaction that occurs at relatively low temperatures. However, hydroxyboroxophenanthrene has only one reactive centre, and this limits the complexity of assembly which can be constructed. The synthesis of one bifunctional building block, 5,9-dihydroxy-5,9-dibora-4,10-dioxopyrene, has been described, together with an analysis of its solid state properties. In particular, this compound was found to form oligomeric anhydrides on heating, although no evidence was found for the existence of these polyanhydrides in solution. Efforts towards the synthesis of several other bifunctional boron-containing heteroaromatics have been described, with the successful isolation and characterisation of the precursor compounds in each case. Evidence that the cyclisation of these compounds may eventually be achieved by the extension of the synthetic methods employed previously has also been revealed.

Finally, a thorough analysis of the structural properties of boroxo- and borazaaromatic compounds has been presented, in order to clarify the extent to which these compounds can be considered aromatic. Undoubtedly, both families of compounds have some aromatic character, although boroxoaromatics are less aromatic than boroozaaromatics, which, in turn, are less aromatic than their arene analogues. A further investigation, focussing on a comparison of hydroxyboroxophenanthrene with phenylboronic acid, found that the reactivity of the

---

boroxoaromatic compound with nucleophiles suggested that it was not closely related to a boronic acid.



## 6 Experimental Section

### 6.1 General Section

Diethyl ether (Et<sub>2</sub>O) and tetrahydrofuran (THF) were dried by refluxing with sodium-benzophenone under an N<sub>2</sub> atmosphere and collected by distillation. Toluene and xylene were distilled over sodium under N<sub>2</sub> and stored over 4 Å molecular sieves. Hexane and dichloromethane (CH<sub>2</sub>Cl<sub>2</sub>) were dried by heating under reflux over calcium hydride and distilled under N<sub>2</sub>. All alkyllithium reagents were titrated<sup>181</sup> against *N*-pivaloyl-*o*-toluidine. All other solvents and reagents were used as received. Thin-layer chromatography (TLC) was performed on aluminium plates coated with Merck Kieselgel 60 F<sub>254</sub>. Developed plates were scrutinised under a UV lamp, and, where necessary, stained with iodine or PMA dip (phosphomolybdic acid in ethanol) to aid identification. Column chromatography was performed using Kieselgel 60 (0.040-0.063 mm mesh, Merck 9385). Microanalyses (CHN) were carried out at the University of London, the University of Birmingham or the University of St. Andrews.

### 6.2 NMR Spectroscopy

<sup>1</sup>H Nuclear magnetic resonance (NMR) spectra were recorded on a Bruker AC300 (300 MHz), Bruker Avance 300 (300 MHz), Varian Gemini 2000 (300 MHz), or Bruker DRX500 (500 MHz) spectrometer using the deuterated solvent as the lock and the residual solvent as the internal reference in all cases. <sup>13</sup>C NMR spectra using the PENDANT sequence were recorded on either a Bruker AC300 (75.5 MHz) spectrometer or a Bruker Avance 300 (75.5 MHz) spectrometer. All other <sup>13</sup>C spectra were recorded on a Varian Gemini 2000 (75.5 MHz) spectrometer using broadband <sup>1</sup>H decoupling. <sup>11</sup>B NMR spectra were recorded on a Bruker DRX500 (160.4 MHz) or a Varian UNITYplus (160.4 MHz) spectrometer using the deuterated solvent as the lock and trimethyl borate as the external reference. All coupling constants are quoted to the nearest 0.1 Hz.

### 6.3 Mass Spectrometry

Electron impact mass spectrometry (EIMS) and high-resolution mass spectrometry (HRMS) were carried out on either a VG PROSPEC or a VG AUTOSPEC mass spectrometer. Electrospray mass spectrometry (ESMS) was recorded on a VG

PLATFORM mass spectrometer. Matrix assisted laser desorption ionisation time-of-flight (MALDI-TOF) spectra were recorded on either a Kratos Kompact Maldi III or a Micromass Tof Spec 2E spectrometer. A nitrogen laser (337 nm, 85 kW peak laser power, 4 ns pulse width) was used to desorb the sample ions. The instrument was operated in positive linear time-of-flight mode, and results from 50 laser shots were signal averaged to give one spectrum. The matrix used was a suspension of cobalt in a methanol/glycerol mixture and was applied to the plate surface in 1  $\mu$ L aliquots and allowed to dry before deposition of the analyte solution onto the matrix.

## 6.4 Thermal Studies

Melting points were determined on an Electrothermal 9200 melting point apparatus and are uncorrected. All melting points are quoted to the nearest 0.5 °C. Thermogravimetric analysis (TGA) experiments (typical sample mass *ca.* 10 mg) were performed on a Perkin Elmer TGA 6 Thermogravimetric Analyzer, using nitrogen as the sample purge gas or a RheoTherm TG1000M+, using argon as the purge gas. Differential scanning calorimetry (DSC) experiments (typical sample mass *ca.* 5 mg) were carried out using a Perkin Elmer Pyris 1 Differential Scanning Calorimeter under helium purge or a Perkin Elmer DSC 7 under nitrogen purge.

## 6.5 Infra-Red Spectroscopy

Infra-red spectra were recorded on a Perkin Elmer 1605 FTIR spectrometer, using samples prepared as KBr discs or as thin films.

## 6.6 X-Ray Diffraction Studies

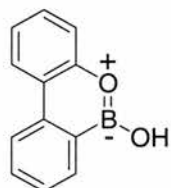
Ambient temperature powder X-ray diffractograms were recorded on a Siemens D5000 diffractometer operating in transmission mode using Ge monochromatised  $\text{CuK}_{\alpha 1}$  radiation. The data were recorded for  $2\theta$  in the range 4-40° in steps  $\Delta(2\theta) = 0.02^\circ$  and collection times varied. Variable temperature powder X-ray diffraction experiments were performed on a Siemens D5005 diffractometer equipped with an Auton Paar HTK 1200 heating stage.

## 6.7 Computational Studies

All semi-empirical (AM1) and Hartree-Fock *ab initio* electronic structure calculations were performed using either SPARTAN (version 5.0, Wavefunction, Inc., Irvine, CA, 1997) or Jaguar (version 4.1, release 53, Schrödinger, Inc., Portland, OR, 2001) on a Silicon Graphics O2 workstation.

## 6.8 Experimental Procedures

### 10-Hydroxy-10,9-boroxophenanthrene 62

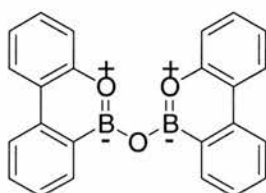


2-Phenylphenol (5.0 g, 29.4 mmol) was stirred at  $-78\text{ }^{\circ}\text{C}$  in dry diethyl ether ( $50\text{ cm}^3$ ) under a  $\text{N}_2$  atmosphere. A solution of boron trichloride (1M in hexane,  $35.3\text{ cm}^3$ , 35.3 mmol) was added dropwise whilst keeping the temperature below  $-70\text{ }^{\circ}\text{C}$ . Once the addition was complete, the mixture was allowed to warm to room temperature over 2 hours and all solvent was removed under a reduced pressure (1mm Hg). Dry hexane ( $60\text{ cm}^3$ ) and anhydrous aluminium chloride (0.6 g, 4.4 mmol) were added to the residues and the reaction mixture heated under reflux. After 3 hours the mixture was allowed to cool, filtered through Celite<sup>®</sup> 521 and the solid residue washed with diethyl ether ( $50\text{ cm}^3$ ). The filtrate was quenched with water ( $50\text{ cm}^3$ ) and the aqueous phase extracted with diethyl ether ( $3 \times 100\text{ cm}^3$ ). The combined organic extracts were dried ( $\text{MgSO}_4$ ) and concentrated under a reduced pressure. The solid was recrystallised ( $\text{Et}_2\text{O}/\text{hexane}$ ) to afford the product (3.1 g, 56%) as colourless crystals.

Found: C, 73.7; H, 4.8%. Calc. for  $\text{C}_{12}\text{H}_9\text{BO}_2$ : C, 73.5; H, 4.6%. m.p.:  $214\text{-}216\text{ }^{\circ}\text{C}$  (as anhydride) (lit.m.p.:<sup>125</sup>  $205\text{-}206\text{ }^{\circ}\text{C}$ ); IR  $\nu_{\text{max}}$  ( $\text{cm}^{-1}$ ) 3455br, (OH), 1395s, (BO);  $\delta_{\text{H}}$  (300 MHz;  $\text{CDCl}_3$ ) 7.99-8.10 (3H, m, Ar), 7.64 (1H, td,  $^3J=8.2\text{ Hz}$ ,  $^4J=1.5\text{ Hz}$ , Ar) 7.40 (1H, td,  $^3J=7.4\text{ Hz}$ ,  $^4J=0.9\text{ Hz}$ , Ar), 7.27-7.33 (1H, m, Ar), 7.13-7.22 (2H, m, Ar) and 4.71 (1H, br s, OH);  $\delta_{\text{C}}$  (75.5 MHz;  $\text{CDCl}_3$ ) 151.1 (Ar, quat), 140.3 (Ar, quat), 133.3 (Ar, CH), 132.6

(Ar, CH), 129.0 (Ar, CH), 127.2 (Ar, CH), 123.6 (Ar, CH), 122.8 (Ar, quat), 122.7 (Ar, CH), 121.6 (Ar, CH) and 119.6 (Ar, CH);  $\delta_B$  (160.4 MHz;  $CDCl_3$ ) 9.68;  $m/z$  (EI) 196 ( $M^+$ , 100%) and 152 (10); HRMS: Found: 196.0698; Calc. for  $C_{12}H_9BO_2$ : 196.0696.

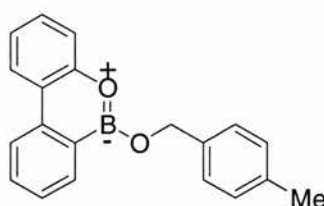
### Bis-boroxophenathryl ether 96



10-Hydroxy-10,9-boroxophenanthrene (1.00g, 5.1mmol) was heated to 100 °C under a reduced pressure for 2 hours to afford bis-boroxophenanthryl ether (1.60g, 4.3mmol, 84%). Some sample was lost due to sublimation, as is observed during the TGA experiments. Solution phase NMR spectra of this compound could not be obtained, as the anhydride is very unstable to hydrolysis. Mass spectra were obtained by dry application of the sample onto the probe tip.

m.p.: 214-215 °C (lit.m.p.:<sup>125</sup> 205-206 °C);  $m/z$  (EI) 374 ( $M^+$ , 73%) and 198 (100); HRMS: Found: 374.1267; Calc. for  $C_{24}H_{16}B_2O_3$ : 374.1286.

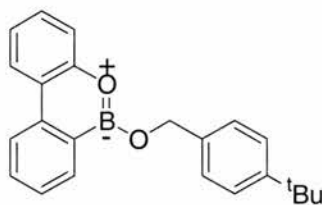
### 10-(4-Methylbenzyloxy)-10,9-boroxophenanthrene 104



10-Hydroxy-10,9-boroxophenanthrene (19.6mg, 0.1mmol) and 4-methylbenzyl alcohol (12.2mg, 0.1mmol) were rigorously dried under a reduced pressure before dissolving in  $CDCl_3$  (pre-dried over 4Å molecular sieves, 1cm<sup>3</sup>). The mixture was stirred over 4Å molecular sieves for a further 72 hours. The solvent was removed under a reduced pressure to afford 10-(4-methylbenzyloxy)-10,9-boroxophenanthrene as a colourless solid (30mg, 99%).

m.p.: 82-84 °C;  $\delta_{\text{H}}$  (300 MHz;  $\text{CDCl}_3$ ) 8.09-8.20 (3H, m, Ar), 7.65-7.72 (1H, m, Ar), 7.39-7.46 (2H, m, Ar), 7.18-7.25 (4H, m, Ar), 5.36 (2H, s,  $\text{CH}_2$ ) and 2.38 (3H, s,  $\text{CH}_3$ );  $\delta_{\text{C}}$  (75.5 MHz;  $\text{CDCl}_3$ ) 151.4 (Ar, quat), 140.2 (Ar, quat), 137.4 (Ar, quat), 136.8 (Ar, quat), 133.6 (Ar, CH), 132.4 (Ar, CH), 129.3 (Ar, CH), 129.0 (Ar, CH), 127.4 (Ar, CH), 127.3 (Ar, CH), 123.8 (Ar, CH), 123.3 (Ar, quat), 122.9 (Ar, CH), 121.6 (Ar, CH), 119.9 (Ar, CH), 65.3 ( $\text{CH}_2$ ) and 21.4 ( $\text{CH}_3$ );  $m/z$  (EI) 300 ( $\text{M}^+$ , 100%) and 285 (36); HRMS: Found: 300.1665; Calc. for  $\text{C}_{20}\text{H}_{17}\text{BO}_2$ : 300.1660.

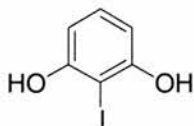
### 10-(4-*tert*-Butyl)benzyloxy-10,9-boroxophenanthrene 106



10-Hydroxy-10,9-boroxophenanthrene (58.8 mg, 0.3 mmol) and 4-*tert*-butylbenzyl alcohol (49.3 mg, 0.3 mmol) were dried thoroughly under reduced pressure before dissolving in  $\text{CDCl}_3$  (pre-dried over 4Å molecular sieves, 1  $\text{cm}^3$ ). The mixture was stirred over 4Å molecular sieves for a further 72 hours. The solvent was removed under a reduced pressure to afford 10-(4-*tert*-butyl)benzyloxy-10,9-boroxophenanthrene as a colourless solid (103 mg, 100%).

m.p.: 70-72°C;  $\delta_{\text{H}}$  (300 MHz;  $\text{CDCl}_3$ ) 8.15 (2H, AA'XX', Ar), 7.67-7.73 (1H, m, Ar), 7.30-7.54 (6H, m, Ar), 7.15-7.28 (3H, m, Ar), 5.38 (2H, s,  $\text{CH}_2$ ) and 1.35 (9H, s, *t*-Bu);  $\delta_{\text{C}}$  (75.5 MHz;  $\text{CDCl}_3$ ) 151.4 (Ar, quat), 150.5 (Ar, quat), 140.1 (Ar, quat), 136.6 (Ar, quat), 133.5 (Ar, CH), 132.2 (Ar, CH), 128.9 (Ar, CH), 127.2 (Ar, CH), 127.0 (Ar, CH), 125.4 (Ar, CH), 125.2 (Ar, CH), 123.6 (Ar, quat), 122.7 (Ar, CH), 121.4 (Ar, CH), 119.8 (Ar, CH), 65.0 ( $\text{CH}_2$ ), 34.5 (*t*-Bu, quat) and 31.3 (*t*-Bu,  $\text{CH}_3$ );  $m/z$  (EI) 342 ( $\text{M}^+$ , 100%) and 285 (36); HRMS: Found: 342.1798; Calc. for  $\text{C}_{23}\text{H}_{23}\text{BO}_2$ : 342.1791.

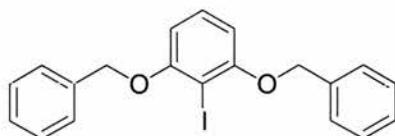
## 2-Iodoresorcinol 117



Iodine (6.7 g, 26 mmol) and  $\text{NaHCO}_3$  (2.3 g, 27 mmol) were added to resorcinol (2.75g, 25 mmol) in water (20  $\text{cm}^3$ ), and the mixture stirred at room temperature for 30 minutes, during which time a white precipitate was observed. The precipitate was collected by filtration, and the filtrate extracted with diethyl ether (3 x 50  $\text{cm}^3$ ). The combined organic extracts were dried ( $\text{MgSO}_4$ ) and concentrated *in vacuo* to afford the crude product. Recrystallisation ( $\text{CHCl}_3$ /hexane) afforded clean 2-iodoresorcinol (4.0 g, 67%) as a colourless solid.

m.p.: 107-108 °C (lit.m.p.:<sup>182</sup> 105-108 °C);  $\delta_{\text{H}}$  (300 MHz;  $\text{CDCl}_3$ ) 7.11 (1H, t,  $^3J=8.1$  Hz, Ar), 6.55 (2H, d,  $^3J=8.1$  Hz, Ar) and 5.33 (2H, s, OH);  $\delta_{\text{C}}$  (75.5 MHz;  $\text{CDCl}_3$ ) 156.1 (Ar, quat), 150.0 (Ar, quat), 130.8 (Ar, CH) and 107.7 (Ar, CH);  $m/z$  (EI) 236 ( $\text{M}^+$ , 100), 218 (26).

## 2,6-Benzyloxyiodobenzene 118



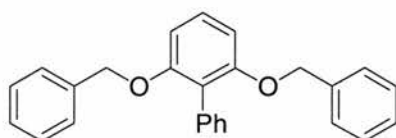
2-Iodoresorcinol (3.5 g, 14.8 mmol), benzyl bromide (3.5  $\text{cm}^3$ , 29.7 mmol), potassium carbonate (5.1 g, 37.1 mmol) and 18-crown-6 (0.2 g, 0.74 mmol) were stirred in dry acetone (120  $\text{cm}^3$ ), and the mixture heated under reflux for 15 hours. After cooling, the solvent was removed *in vacuo* to yield a brown solid. The residue was taken up in  $\text{CH}_2\text{Cl}_2$  (40  $\text{cm}^3$ ), water (30  $\text{cm}^3$ ) added, and the aqueous layer extracted with  $\text{CH}_2\text{Cl}_2$  (3 x 20  $\text{cm}^3$ ). The combined organic extracts were dried ( $\text{MgSO}_4$ ), and evaporated under a reduced pressure. The crude product was purified by column chromatography



(Et<sub>2</sub>O:hexane, v:v, 2:3) to afford 2,6-benzyloxyiodobenzene (5.5 g, 89%) as a yellow crystalline solid.

Found: C, 57.9; H, 3.9%. Calc. for C<sub>20</sub>H<sub>17</sub>O<sub>2</sub>I: C, 57.7; H, 4.1%; m.p.: 90-91 °C; δ<sub>H</sub> (300 MHz; CDCl<sub>3</sub>) 7.43 (4H, d, <sup>3</sup>J=7.4 Hz, Ar), 7.21-7.34 (6H, m, Ar), 7.07-7.17 (1H, m, Ar), 6.46 (2H, d, <sup>3</sup>J=8.3 Hz, Ar) and 5.09 (4H, s, CH<sub>2</sub>); δ<sub>C</sub> (75.5 MHz; CDCl<sub>3</sub>) 159.1 (Ar, quat), 137.1 (Ar, quat), 130.1 (Ar, CH), 128.9 (Ar, CH), 128.2 (Ar, CH), 127.4 (Ar, CH), 106.4 (Ar, CH), 80.2 (Ar, quat) and 71.4 (CH<sub>2</sub>); *m/z* (EI) 416 (M<sup>+</sup>, 12%), 91 (100); HRMS: Found: 416.0284; Calc. for C<sub>20</sub>H<sub>17</sub>O<sub>2</sub>I: 416.0273.

### 2,6-Benzyloxybiphenyl 119



#### Method A

To 2,6-benzyloxybiphenyl (0.2 g, 0.48 mmol) and Pd(PPh<sub>3</sub>)<sub>4</sub> (0.08 g, 0.072 mmol) in dry, degassed DME (20 cm<sup>3</sup>) was added a solution of phenyl boronic acid (0.09 g, 0.72 mmol) in EtOH (2 cm<sup>3</sup>), followed by Na<sub>2</sub>CO<sub>3</sub> (0.16 g, 1.54 mmol) in water (5 cm<sup>3</sup>). The mixture was heated under reflux for 3 hours, and then allowed to cool. CH<sub>2</sub>Cl<sub>2</sub> (20 cm<sup>3</sup>) was added, and the mixture filtered through a short pad of Celite<sup>®</sup> 521 filter agent. The filtrate was dried (MgSO<sub>4</sub>), filtered and concentrated under a reduced pressure to afford a brown oil. Column chromatography (Et<sub>2</sub>O:hexane, v:v, 2:3) affords the clean product (30 mg, 16%) as a colourless solid.

#### Method B

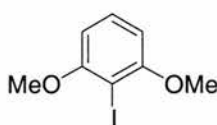
A solution of bromobenzene (1.5 g, 9.6 mmol) in dry diethyl ether (20 cm<sup>3</sup>) was added in small portions to magnesium turnings (0.23 g, 9.6 mmol), at such a rate as to maintain a gentle reflux. After the addition was complete, the reaction mixture was heated under reflux for a further hour to ensure a complete reaction. The solution of phenyl magnesium bromide was added slowly to a stirred suspension of 2,6-benzyloxybiphenyl (2.0 g, 4.8 mmol) and Ni(dppe)Cl<sub>2</sub> (0.1 g, 0.19 mmol) in dry diethyl ether (20 cm<sup>3</sup>). The mixture was heated under reflux for 5 hours, and after cooling, diethyl ether (20 cm<sup>3</sup>)



and water (20 cm<sup>3</sup>) were added. The aqueous layer was extracted with diethyl ether (3 x 20 cm<sup>3</sup>), the combined organic extracts dried (MgSO<sub>4</sub>), filtered and concentrated to afford a yellow oil, which was purified by column chromatography (CH<sub>2</sub>Cl<sub>2</sub>:hexane, v:v, 1:2) to afford 2,6-benzyloxybiphenyl (0.77 g, 44%) as a colourless solid.

Found: C, 85.5; H, 5.8%. Calc. for C<sub>26</sub>H<sub>22</sub>O<sub>2</sub>: C, 85.2; H, 6.05%; m.p.: 87-88 °C; δ<sub>H</sub> (300 MHz; CDCl<sub>3</sub>) 7.42-7.51 (4H, m, Ar), 7.22-7.38 (12H, m, Ar), 6.73 (2H, d, <sup>3</sup>J = 8.3 Hz, Ar) and 5.05 (4H, s, CH<sub>2</sub>); δ<sub>C</sub> (75.5 MHz; CDCl<sub>3</sub>) 157.2 (Ar, quat), 137.8 (Ar, quat), 135.1 (Ar, quat), 131.5 (Ar, CH), 129.0 (Ar, CH), 128.7 (Ar, CH), 127.9 (Ar, CH), 127.8 (Ar, CH), 127.2 (Ar, CH), 127.0 (Ar, CH), 123.0 (Ar, quat), 107.2 (Ar, CH) and 70.9 (CH<sub>2</sub>); *m/z* (EI) 366 (M<sup>+</sup>, 21%), 91 (100); HRMS: Found: 366.1629; Calc. for C<sub>26</sub>H<sub>22</sub>O<sub>2</sub>: 366.1620.

### 2,6-Dimethoxyiodobenzene 121

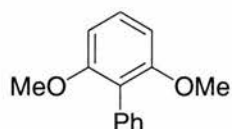


*n*-Butyllithium (10 cm<sup>3</sup>, 20 mmol, 1.2 mol. eq.) was added dropwise to a stirred solution of 1,3-dimethoxybenzene (2.5 g, 18 mmol) in THF (75 cm<sup>3</sup>) under N<sub>2</sub> at 0°C and the mixture was stirred at this temperature for a further 30 minutes. A solution of I<sub>2</sub> (4.6 g, 18 mmol) in THF (30 cm<sup>3</sup>) was added dropwise whilst maintaining the temperature of the mixture at 0°C. The mixture was then allowed to warm to room temperature. After 2 hours, ethyl acetate (20 cm<sup>3</sup>) was added and the mixture washed with sodium sulfite solution (2 x 40 cm<sup>3</sup>, saturated aqueous solution). The organic extract was washed with aqueous NaCl solution, dried (MgSO<sub>4</sub>), filtered and concentrated under a reduced pressure to afford a pale yellow solid. Recrystallisation (CHCl<sub>3</sub>/hexane) afforded 2,6-dimethoxyiodobenzene (3.0 g, 63%) as a colourless solid.

Found: C, 36.5; H, 3.3%. Calc. for C<sub>8</sub>H<sub>9</sub>IO<sub>2</sub>: C, 36.4; H, 3.4%; m.p.: 103-105 °C (lit.m.p.:<sup>183</sup> 99-100 °C); IR ν<sub>max</sub> (cm<sup>-1</sup>) 2840m, (OMe); δ<sub>H</sub> (300 MHz; CDCl<sub>3</sub>) 7.26 (1H, t, <sup>3</sup>J=8.1 Hz, Ar), 6.50 (2H, d, <sup>3</sup>J=8.1 Hz, Ar) and 3.88 (6H, s); δ<sub>C</sub> (75.5 MHz; CDCl<sub>3</sub>) 159.5 (Ar, quat), 129.8 (Ar, CH), 104.1 (Ar, CH), 77.6 (Ar, quat) and 56.5 (OMe, CH<sub>3</sub>); *m/z* (EI)

264 ( $M^+$ , 100 %), 249 (10), 234 (5), 221 (50) and 206 (15); HRMS: Found: 263.9652; Calc. for  $C_8H_9IO_2$ : 263.9647.

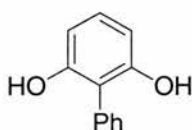
### 2,6-Dimethoxybiphenyl 122



Bromobenzene (1.6 g, 10.2 mmol) in dry diethyl ether (20 cm<sup>3</sup>) was added in small portions to magnesium turnings (0.3 g, 12.3 mmol) under N<sub>2</sub>, at such a rate as to maintain a gentle reflux. After addition was complete, the mixture was stirred under reflux for a further hour to ensure complete reaction. The ethereal solution of phenylmagnesium bromide was allowed to cool before it was added dropwise to a stirred solution of 2,6-dimethoxyiodobenzene (1.3 g, 4.92 mmol) and Ni(PPh<sub>3</sub>)<sub>2</sub>Cl<sub>2</sub> (64 mg, 2 mol%) in dry diethyl ether (20 cm<sup>3</sup>) under N<sub>2</sub>. The resulting black mixture was stirred under reflux for 24 hours. After cooling, water (50 cm<sup>3</sup>) was added, and the aqueous layer extracted with ether (2 x 20 cm<sup>3</sup>). Combined organic extracts were dried (MgSO<sub>4</sub>) and evaporated under a reduced pressure. Column chromatography (Et<sub>2</sub>O:hexane, v:v, 1:4) afforded 2,6-dimethoxybiphenyl (0.8 g, 76%) as a colourless solid.

Found: C, 78.3; H, 6.55%. Calc. for C<sub>14</sub>H<sub>14</sub>O<sub>2</sub>: C, 78.5; H, 6.6%; m.p.: 87-88 °C (lit.m.p.:<sup>184</sup> 83-85 °C); IR  $\nu_{\max}$  (cm<sup>-1</sup>) 2838m, (OMe);  $\delta_H$  (300 MHz; CDCl<sub>3</sub>) 7.48-7.29 (6H, m, Ar), 6.69 (2H, d, <sup>3</sup>J=8.5 Hz, Ar) and 3.76 (6H, s, Me);  $\delta_C$  (75.5 MHz; CDCl<sub>3</sub>) 157.9 (Ar, quat), 134.4 (Ar, quat), 131.1 (Ar, CH), 128.9 (Ar, CH), 127.9 (Ar, CH), 127.0 (Ar, CH), 119.7 (Ar, quat), 104.4 (Ar, CH) and 56.1 (OMe, CH<sub>3</sub>);  $m/z$  (EI) 214 ( $M^+$ , 100 %), 199 (16), 184 (24), and 128 (18).

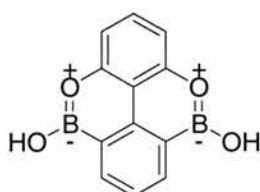
### 2,6-Dihydroxybiphenyl 114



A solution of 2,6-dimethoxybiphenyl (0.8 g, 3.7 mmol) was stirred in dry  $\text{CH}_2\text{Cl}_2$  (20  $\text{cm}^3$ ) at  $-78^\circ\text{C}$  under  $\text{N}_2$ . Boron tribromide (1M solution in  $\text{CH}_2\text{Cl}_2$ , 7.5  $\text{cm}^3$ , 7.5 mmol) was added dropwise *via* a syringe and the mixture allowed to warm slowly to room temperature. After re-cooling to  $0^\circ\text{C}$ , MeOH (10  $\text{cm}^3$ ) was added dropwise to quench any remaining  $\text{BBr}_3$ , and the solvents were removed on a water aspirator. Water (20  $\text{cm}^3$ ) and  $\text{CH}_2\text{Cl}_2$  (20  $\text{cm}^3$ ) were added to the residue and the aqueous layer was extracted with  $\text{CH}_2\text{Cl}_2$  (3 x 20  $\text{cm}^3$ ). Combined organic extracts were washed with water, dried ( $\text{MgSO}_4$ ), filtered and evaporated to dryness to afford a pale brown powder. Flash column chromatography ( $\text{CH}_2\text{Cl}_2$ ) gave the clean compound (0.62 g, 89%) as a colourless solid.

Found: C, 77.2; H, 5.3%. Calc. for  $\text{C}_{12}\text{H}_{10}\text{O}_2$ : C, 77.4; H, 5.4%; m.p.: 116-118  $^\circ\text{C}$  (lit.m.p.:<sup>185</sup> 118-119  $^\circ\text{C}$ ); IR  $\nu_{\text{max}}$  ( $\text{cm}^{-1}$ ) 3402br, (OH);  $\delta_{\text{H}}$  (300 MHz;  $\text{CDCl}_3$ ) 7.54-7.59 (2H, m, Ar), 7.40-7.49 (3H, m, Ar), 7.15 (1H, t,  $^3J=8.1$  Hz, Ar), 6.58 (2H, d,  $^3J=8.1$  Hz, Ar) and 4.91 (2H, br s, OH);  $\delta_{\text{C}}$  (75.5 MHz;  $\text{CDCl}_3$ ) 153.4 (Ar, quat), 131.0 (Ar, CH), 130.8 (Ar, quat), 130.2 (Ar, CH), 129.6 (Ar, CH), 129.2 (Ar, CH), 115.5 (Ar, quat) and 107.8 (Ar, CH);  $m/z$  (EI) 186 ( $\text{M}^+$ , 100 %), 168 (15) and 139 (12); HRMS: Found: 186.0688; Calc. for  $\text{C}_{12}\text{H}_{10}\text{O}_2$ : 186.0681.

### 5,9-Dihydroxy-5,9-dibora-4,10-dioxopyrene 111

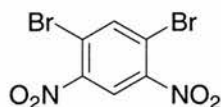


Dichloroborane-dimethylsulfide complex (0.5  $\text{cm}^3$ , 4 mmol) was added in small portions to a cooled, stirred solution of boron trichloride in hexane (1M, 4  $\text{cm}^3$ , 4 mmol). A white precipitate ( $\text{BCl}_3 \cdot \text{DMS}$ ) formed immediately upon addition. The mixture was stirred with cooling for a further 10 minutes, and then allowed to warm to room temperature and stirred for one hour. The resulting solution of  $\text{BHCl}_2$  in hexane was added dropwise to a stirred solution of 2,6-dihydroxybiphenyl (0.3 g, 1.6 mmol) in dry toluene (20  $\text{cm}^3$ ) at room temperature. After stirring at room temperature for 2 hours,  $\text{AlCl}_3$  (90 mg, 0.6

mmol) was added and the mixture heated under reflux overnight. After cooling, water (20 cm<sup>3</sup>) was added carefully, and the aqueous layer extracted with diethyl ether (3 x 20 cm<sup>3</sup>). Combined organic extracts were dried (MgSO<sub>4</sub>), filtered and concentrated under vacuum to afford a pale brown solid. Recrystallisation (CH<sub>2</sub>Cl<sub>2</sub> / hexane) afforded the pure product (330 mg, 87%) as an off-white solid.

Found: C, 60.3; H, 3.7%. Calc. for C<sub>12</sub>H<sub>8</sub>B<sub>2</sub>O<sub>4</sub>: C, 60.6; H, 3.4%; m.p.: 400 °C (decomp.); IR  $\nu_{\max}$  (cm<sup>-1</sup>) 3350br, (OH), 1370s, (OB);  $\delta_{\text{H}}$  (300 MHz; (CD<sub>3</sub>)<sub>2</sub>CO) 8.45 (2H, s, OH), 8.39 (2H, d, <sup>3</sup>J=7.4 Hz, Ar), 7.68 (1H, t, <sup>3</sup>J=7.4 Hz, Ar), 7.43 (1H, t, <sup>3</sup>J=8.2 Hz, Ar) and 7.04 (2H, d, <sup>3</sup>J=8.2 Hz, Ar);  $\delta_{\text{C}}$  (75.5 MHz; (CD<sub>3</sub>)<sub>2</sub>CO) 152.9 (Ar, quat), 145.3 (Ar, quat), 138.0 (Ar, CH), 130.1 (Ar, CH), 128.0 (Ar, CH) and 113.0 (Ar, CH); *m/z* (EI) 238 (M<sup>+</sup>, 100); HRMS: Found: 238.0516; Calc. for C<sub>12</sub>H<sub>8</sub>B<sub>2</sub>O<sub>4</sub>: 238.0838.

### 1,5-Dibromo-2,4-dinitrobenzene 140



1,3-Dibromobenzene (5.0 g, 21.2 mmol) was added dropwise over 10 minutes to a vigorously stirred mixture of sulfuric acid (31.5 cm<sup>3</sup>) and nitric acid (22.5 cm<sup>3</sup>) at 0 °C. The mixture was heated under reflux to 90 °C for 30 minutes, during which time it turned yellow. After cooling, the mixture was poured slowly onto stirred iced water (300 cm<sup>3</sup>). The resulting yellow precipitate was collected by vacuum filtration and washed with water (20 cm<sup>3</sup>) and saturated aqueous NaHCO<sub>3</sub> solution (50 cm<sup>3</sup>). The precipitate was dried to afford the product (6.7 g, 97%) as a yellow crystalline solid.

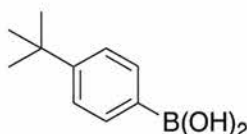
m.p.: 114-116 °C, (lit.m.p.:<sup>186</sup> 115 °C); UV  $\lambda_{\max}$  (EtOH)/nm 244 ( $\epsilon$ /dm<sup>3</sup>mol<sup>-1</sup>cm<sup>-1</sup> 310), 277 (291) and 329 (300);  $\delta_{\text{H}}$  (300 MHz; CDCl<sub>3</sub>) 8.46 (1H, s, Ar) and 8.23 (1H, s, Ar);  $\delta_{\text{C}}$  (75.5 MHz; CDCl<sub>3</sub>) 148.1 (Ar, quat), 141.4 (Ar, CH), 123.0 (Ar, CH) and 119.9 (Ar, quat); *m/z* (EI) 326 (M<sup>+</sup>, 86%), 296 (45), 234 (38), 155 (37), and 74 (100).

### General Procedure for the Synthesis of Aryl Boronic Acids

Magnesium turnings were washed with dry diethyl ether and dried at 140 °C. In addition, all glassware used was dried at 140 °C overnight. The magnesium turnings were

activated by gentle heating with a crystal of iodine. Small portions of a solution of the appropriate aryl bromide (1 equivalent) in dry diethyl ether were added to the magnesium turnings (1 equivalent) under  $N_2$ . The addition was carried out at such a rate as to maintain a gentle self-reflux until the addition was complete. The mixture was refluxed for a further hour to ensure complete reaction. The ethereal solution of the aryl magnesium bromide was allowed to cool before it was added dropwise to a stirred solution of trimethyl borate (1 equivalent) in dry diethyl ether at  $-78\text{ }^\circ\text{C}$ . The mixture was stirred under  $N_2$  and allowed to warm to room temperature overnight before water ( $10\text{ cm}^3$ ) was added to hydrolyse the boronic acid dimethyl ester. The aqueous layer was extracted with diethyl ether ( $2 \times 100\text{ cm}^3$ ), the combined organic extracts were dried ( $MgSO_4$ ), filtered, and the solvent removed under reduced pressure. The crude products were purified as outlined below.

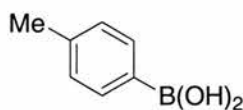
#### 4-*tert*-Butylphenylboronic acid 142



4-*tert*-Butylphenylboronic acid was prepared from 1-bromo-4-*tert*-butylbenzene (15 g, 70.4 mmol), and was purified by recrystallisation from water to afford the product (3.8 g, 30%) as colourless crystals.

m.p.:  $166\text{--}168\text{ }^\circ\text{C}$  (lit.m.p.:<sup>187</sup>  $168\text{--}170\text{ }^\circ\text{C}$ ); IR  $\nu_{\text{max}}$  ( $\text{cm}^{-1}$ ) 3333br (OH), 1609, 1406 and 1348br;  $\delta_{\text{H}}$  (300 MHz;  $\text{CDCl}_3$ ) 8.17 (2H, AA'XX', Ar), 7.54 (2H, AA'XX', Ar), 6.35 (2H, br s, OH), and 1.38 (9H, s, *t*-Bu);  $\delta_{\text{C}}$  (75.5 MHz;  $\text{CDCl}_3$ ) 155.8 (Ar, quat), 135.4 (Ar, CH), 124.8 (Ar, CH), 34.9 (*t*-Bu, quat) and 31.1 ( $\text{CH}_3$ );  $m/z$  (EI) 178 ( $M^+$ , 18%), 163 (96), 91 (47) and 45 (100).

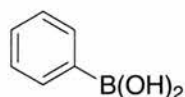
#### 4-Methylphenylboronic acid 143



4-Methylphenylboronic acid was prepared from 4-bromotoluene (11.3 g, 66 mmol), and purified by recrystallisation from water to afford the required product (5.4 g, 60%) as colourless crystals.

m.p.: 258-260 °C (lit.m.p.:<sup>188</sup> 259-260 °C); IR  $\nu_{\max}$  (cm<sup>-1</sup>) 3263br (OH), 1616, 1403 and 1364br;  $\delta_{\text{H}}$  (300 MHz; (CD<sub>3</sub>)<sub>2</sub>CO) 7.77 (2H, AA'XX', Ar), 7.17 (2H, AA'XX', Ar), 7.08 (2H, br s, OH) and 2.32 (3H, s, Me);  $\delta_{\text{C}}$  (75.5 MHz; (CD<sub>3</sub>)<sub>2</sub>CO) 206.4 (Ar, quat), 135.0 (Ar, CH), 129.0 (Ar, CH) and 21.5 (CH<sub>3</sub>); *m/z* (EI) 136 (M<sup>+</sup>, 67%), 117 (24), 91 (100) and 65 (66).

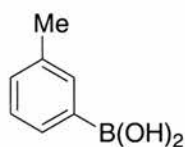
### Phenylboronic acid 144



Phenylboronic acid was prepared from bromobenzene (10 g, 63 mmol), and recrystallised from water to give the product (4.2 g, 55%) as colourless crystals.

m.p.: 101-103 °C (lit.m.p.:<sup>188</sup> 102-104 °C); IR  $\nu_{\max}$  (cm<sup>-1</sup>) 3284br (OH), 1604s, 1440 and 1348br;  $\delta_{\text{H}}$  (300 MHz; (CD<sub>3</sub>)<sub>2</sub>CO) 7.89-7.91 (2H, m, Ar), 7.33-7.42 (3H, m, Ar) and 7.22 (2H, s, OH);  $\delta_{\text{C}}$  (75.5 MHz; (CD<sub>3</sub>)<sub>2</sub>CO) 134.9 (Ar, CH), 131.1 (Ar, CH), and 128.3 (Ar, CH); *m/z* (EI) 312 (trimer, 10 %), 122 (M<sup>+</sup>, 92), 104 (18), 78 (100) and 51 (76).

### 3-Methylphenylboronic acid 162



3-Methylphenylboronic acid was prepared from 3-iodotoluene (10 g, 45.8 mmol), and was recrystallised from water to afford the product (1.25 g, 20%) as colourless crystals.

m.p.: 160-162 °C (lit.m.p.:<sup>188</sup> 162-163 °C); IR  $\nu_{\max}$  (cm<sup>-1</sup>) 3276br (OH), 1604 and 1344;  $\delta_{\text{H}}$  (300 MHz; (CD<sub>3</sub>)<sub>2</sub>CO) 7.65-7.69 (1H, m, Ar), 7.23 (2H, d, <sup>3</sup>J=5.5 Hz, Ar), 7.12 (1H, s, Ar) and 2.32 (3H, s, Me);  $\delta_{\text{C}}$  (75.5 MHz; (CD<sub>3</sub>)<sub>2</sub>CO) 137.2 (Ar, quat), 135.5 (Ar, CH),

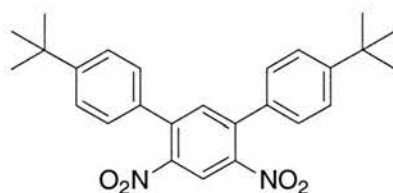


132.0 (Ar, CH), 131.6 (Ar, CH), 128.1 (Ar, CH) and 21.4 (CH<sub>3</sub>); *m/z* (EI) 136 (M<sup>+</sup>, 35%), 91 (100) and 65 (31).

### General Suzuki Coupling Procedure for Synthesis of Dinitroterphenyls

1,5-Dibromo-2,4-dinitrobenzene (2.5 g, 7.7 mmol) was added to a stirred suspension of Pd(PPh<sub>3</sub>)<sub>4</sub> (0.6 g) in DME (40 cm<sup>3</sup>) and the mixture degassed with N<sub>2</sub> for 10 minutes. The appropriate boronic acid (2.5 equivalents) dissolved in a minimum of ethanol (approx. 10 cm<sup>3</sup>) was added, followed by sodium carbonate (3.2 g) in water (10 cm<sup>3</sup>). The mixture was heated under reflux for 24 hours and after cooling, the mixture was poured onto CH<sub>2</sub>Cl<sub>2</sub> (200 cm<sup>3</sup>), stirred with decolourising charcoal, and filtered through a short pad of Celite<sup>®</sup> 521 filter agent. Concentration *in vacuo* afforded a series of brown solids, which were purified as outlined below.

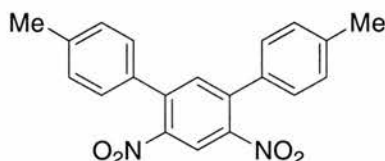
### 1,5-Dinitro-2,4-bis(4'-*tert*-butylphenyl)benzene 145



1,5-Dinitro-2,4-bis(4'-*tert*-butylphenyl)benzene was prepared from 4-(*tert*-butyl)phenyl boronic acid (3.5 g, 19.7 mmol) and purified by column chromatography (CH<sub>2</sub>Cl<sub>2</sub>:hexane, v:v, 1:4). Recrystallisation (CH<sub>2</sub>Cl<sub>2</sub> / hexane) afforded the product (2.22 g, 65%) as a yellow solid.

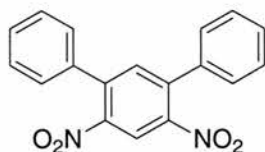
Found: C, 72.5; H, 6.8; N, 6.1%. Calc. for C<sub>26</sub>H<sub>28</sub>N<sub>2</sub>O<sub>4</sub>: C, 72.2; H, 6.5; N, 6.5%; m.p.: 199-201 °C; UV λ<sub>max</sub> (EtOH)/nm 243 (ε/dm<sup>3</sup>mol<sup>-1</sup>cm<sup>-1</sup> 3240), 280 (3100) and 330 (2900); δ<sub>H</sub> (300 MHz; CDCl<sub>3</sub>) 8.39 (1H, s, Ar), 7.56 (1H, s, Ar), 7.47 (4H, AA'XX', Ar), 7.28 (4H, AA'XX', Ar) and 1.35 (18H, s, *t*-Bu); δ<sub>C</sub> (75.5 MHz; CDCl<sub>3</sub>) 152.6 (Ar, quat), 147.1 (Ar, quat), 140.1 (Ar, quat), 135.9 (Ar, CH), 132.4 (Ar, quat), 127.5 (Ar, CH), 126.0 (Ar, CH), 120.7 (Ar, CH), 34.8 (*t*-Bu, quat) and 31.2 (*t*-Bu, CH<sub>3</sub>); *m/z* (EI) 432 (M<sup>+</sup>, 22%), 417 (100), 404 (5), 389 (8) and 201 (9).



**1,5-Dinitro-2,4-bis(4'-methylphenyl)benzene 146**

1,5-Dinitro-2,4-bis(4'-methylphenyl)benzene was synthesised using 4-methylphenyl boronic acid (2.6 g, 19.2 mmol) and purified by column chromatography (CH<sub>2</sub>Cl<sub>2</sub>:hexane, v:v, 1:1). Subsequent recrystallisation (CH<sub>2</sub>Cl<sub>2</sub> / hexane) afforded the product (2.28 g, 85%) as a yellow powder.

Found: C, 68.9; H, 4.5; N, 8.05%. Calc. for C<sub>20</sub>H<sub>16</sub>N<sub>2</sub>O<sub>4</sub>: C, 69.0; H, 4.6; N, 8.0%; m.p.: 183-185 °C; UV λ<sub>max</sub> (EtOH)/nm 245 (ε/dm<sup>3</sup>mol<sup>-1</sup>cm<sup>-1</sup> 3912), 271 (3750) and 334 (3750); δ<sub>H</sub> (300 MHz; (CD<sub>3</sub>)<sub>2</sub>CO) 8.56 (1H, s, Ar), 7.69 (1H, s, Ar), 7.41 (4H, AA'XX', Ar), 7.33 (4H, AA'XX', Ar) and 2.40 (6H, s, Me); δ<sub>C</sub> (75.5 MHz; CDCl<sub>3</sub>) 147.1 (Ar, quat), 140.2 (Ar, quat), 139.6 (Ar, quat), 135.7 (Ar, CH), 132.5 (Ar, quat), 129.8 (Ar, CH), 127.7 (Ar, CH), 120.8 (Ar, CH) and 21.4 (CH<sub>3</sub>); *m/z* (EI) 348 (M<sup>+</sup>, 100%), 239 (44).

**1,5-Dinitro-2,4-bis(phenyl)benzene 147**

1,5-Dinitro-2,4-bis(phenyl)benzene was prepared using phenyl boronic acid (2.3 g, 19.2 mmol) and purified by column chromatography on silica (CH<sub>2</sub>Cl<sub>2</sub>:hexane, v:v, 1:1). Subsequent recrystallisation (CH<sub>2</sub>Cl<sub>2</sub> / hexane) afforded the product (0.8 g, 50%) as a yellow powder.

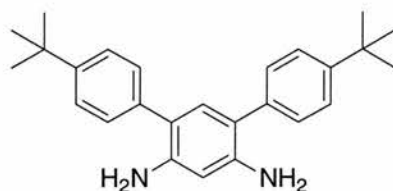
Found: C, 67.7; H, 3.6; N, 8.5%. Calc. for C<sub>18</sub>H<sub>12</sub>N<sub>2</sub>O<sub>4</sub>: C, 67.5; H, 3.8; N, 8.8%; m.p.: 160-162 °C (lit.m.p.:<sup>189</sup> 149 °C) ; UV λ<sub>max</sub> (EtOH)/nm 248 (ε/dm<sup>3</sup>mol<sup>-1</sup>cm<sup>-1</sup> 3940), 270

(3642) and 338 (3695);  $\delta_{\text{H}}$  (300 MHz;  $\text{CDCl}_3$ ) 8.46 (1H, s, Ar), 7.56 (1H, s, Ar), 7.47 (6H, m, Ar) and 7.36 (4H, m, Ar);  $\delta_{\text{C}}$  (75.5 MHz;  $\text{CDCl}_3$ ) 147.3 (Ar quat), 140.3 (Ar quat), 135.9 (Ar CH), 135.4 (Ar quat), 129.4 (Ar CH), 129.1 (Ar CH), 127.8 (Ar CH) and 120.8 (Ar CH);  $m/z$  (EI) 320 ( $\text{M}^+$ , 57%), 292 (90), 244 (58), 226 (100) and 215 (63).

### General Procedure for the Reduction of Dinitroterphenyl Compounds

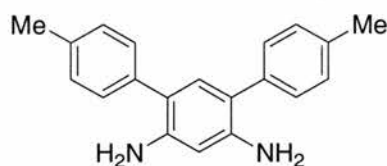
The appropriate 1,5-dinitro-terphenyl compound and palladium on carbon (10% w/w, 20 mol%) were stirred in ethyl acetate (100  $\text{cm}^3$ ), and the mixture degassed thoroughly with  $\text{N}_2$  for 30 minutes. The mixture was then held under a slight over-pressure of  $\text{H}_2$  for 8 hours before filtering through a short pad of Celite<sup>®</sup> 521 filter agent and washing thoroughly with ethyl acetate (300  $\text{cm}^3$ ). Concentration of the filtrate under a reduced pressure afforded an orange oil. The products were found to decompose readily and were used without further purification in the next step. Minimal characterisation was carried out as indicated below.

### 1,5-Diamino-2,4-bis(4'-*tert*-butylphenyl)benzene 148

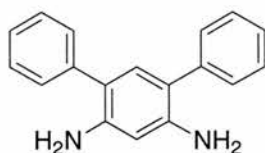


1,5-Diamino-2,4-bis(4'-*tert*-butylphenyl)benzene was prepared from 1,5-dinitro-2,4-bis(4'-*tert*-butylphenyl)benzene (2 g, 4.6 mmol). The product (1.7 g, 100%) was obtained as an orange oil. Minimal characterisation was carried out as the compound decomposed readily.

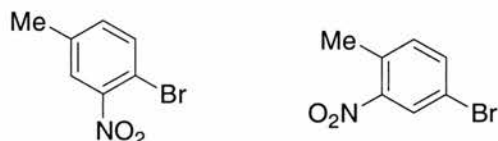
$\delta_{\text{H}}$  (300 MHz;  $\text{CDCl}_3$ ) 7.82 (1H, s, Ar), 7.32-7.46 (8H, m, Ar), 7.27 (1H, s, Ar), 1.95 (4H, br s,  $\text{NH}_2$ ) and 1.36 (18H, s, *t*-Bu);  $\delta_{\text{C}}$  (75.5 MHz;  $\text{CDCl}_3$ ) 149.3 (Ar, quat), 143.6 (Ar, quat), 136.4 (Ar, quat), 132.6 (CH, Ar), 128.8 (Ar, CH), 125.6 (Ar, CH), 119.2 (Ar, quat), 102.2 (Ar, CH), 34.5 (*t*-Bu, quat) and 31.4 (*t*-Bu,  $\text{CH}_3$ );  $m/z$  (EI) 372 ( $\text{M}^+$ , 100%) and 357 (39).

**1,5-Diamino-2,4-bis(4'-methylphenyl)benzene 149**

1,5-Diamino-2,4-bis(4'-methylphenyl)benzene was prepared from 1,5-dinitro-2,4-bis(4'-methylphenyl)benzene (1.0 g, 2.9 mmol) and was recovered as an orange oil (0.84 g, 100%). Minimal characterisation was carried out as the compound decomposed readily.  $\delta_{\text{H}}$  (300 MHz;  $\text{CDCl}_3$ ) 7.34 (4H, AA'XX', Ar), 7.22 (4H, AA'XX', Ar), 6.95 (1H, s), 6.23 (1H, s), 3.89 (4H, br s,  $\text{NH}_2$ ) and 2.37 (6H, s, Me);  $\delta_{\text{C}}$  (75.5 MHz;  $\text{CDCl}_3$ ) 143.6 (Ar, quat), 136.4 (Ar, quat), 136.2 (Ar, quat), 132.6 (Ar, CH), 129.5 (Ar, CH), 129.1 (Ar, CH), 119.4 (Ar, quat), 102.3 (Ar, CH) and 21.2 ( $\text{CH}_3$ );  $m/z$  (EI) 288 ( $\text{M}^+$ , 35%).

**1,5-Diamino-2,4-bis(phenyl)benzene 138**

1,5-Diamino-2,4-bis(phenyl)benzene was prepared by reduction of 1,5-dinitro-2,4-bis(phenyl)benzene (1.0 g, 3.1 mmol) and was isolated as a yellow oil (0.81 g, 90%). Minimal characterisation was carried out as the compound decomposed readily.  $\delta_{\text{H}}$  (300 MHz;  $\text{CDCl}_3$ ) 7.53 (8H, m, Ar), 7.36 (2H, t,  $^3J=7.2$  Hz, Ar), 7.08 (1H, s, Ar), 6.19 (1H, s, Ar) and 3.85 (4H, s,  $\text{NH}_2$ );  $m/z$  (EI) 260 ( $\text{M}^+$ , 100%).

**3-Nitro-4-bromotoluene and 2-nitro-4-bromotoluene 154**

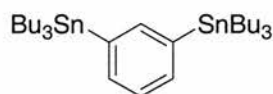
4-Bromotoluene (5.0 g, 29.2 mmol) was added to an ice-cooled mixture of sulfuric acid (5.0 cm<sup>3</sup>) and nitric acid (5.0 cm<sup>3</sup>) over a period of 30 minutes. The mixture was allowed to warm to room temperature, stirred for 2 hours and then poured onto iced water (100 cm<sup>3</sup>). The aqueous layer was extracted with diethyl ether (2 x 100 cm<sup>3</sup>) and the combined organic extracts were washed with water (100 cm<sup>3</sup>) and NaHCO<sub>3</sub> (saturated aqueous solution, 100 cm<sup>3</sup>) and dried over MgSO<sub>4</sub>. The solution was filtered and the solvent was removed under a reduced pressure to afford a yellow oil that crystallised on standing. The two regioisomers, 3-nitro-4-bromotoluene and 2-nitro-4-bromotoluene, were separated by column chromatography on silica (hexane:CH<sub>2</sub>Cl<sub>2</sub>, v:v, 4:1) and their identities determined by GOESY NMR experiments.

3-nitro-4-bromotoluene **154** was isolated (4.8 g, 38%) as a yellow crystalline solid.

Found: C, 38.8; H, 2.8; N, 6.4%. Calc. for C<sub>7</sub>H<sub>6</sub>NO<sub>2</sub>Br: C, 38.9; H, 2.8; N, 6.5%; m.p.: 30-32 °C (lit.m.p.:<sup>190</sup> 31-32 °C); UV λ<sub>max</sub> (EtOH)/nm 250 (ε/dm<sup>3</sup>mol<sup>-1</sup>cm<sup>-1</sup> 610), 293 (591) and 321 (608); δ<sub>H</sub> (300 MHz; CDCl<sub>3</sub>) 8.1 (1H, d, <sup>4</sup>J=2.0 Hz, Ar), 7.61 (1H, AA'XX', Ar), 7.22 (1H, d, <sup>3</sup>J=7.2 Hz, Ar) and 2.55 (3H, s, Me); δ<sub>C</sub> (75.5 MHz; CDCl<sub>3</sub>) 149.6 (Ar, quat), 136.0 (Ar, CH), 134.2 (Ar, CH), 132.6 (Ar, quat), 127.6 (Ar, CH), 119.7 (Ar, quat) and 20.1 (CH<sub>3</sub>); m/z (EI) 215 (M<sup>+</sup>, 12%), 198 (38), 119 (27), 90 (100), 78 (27) and 63 (55).

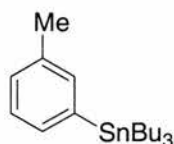
2-nitro-4-bromotoluene (3.8 g, 30%) was obtained as a yellow crystalline solid.

m.p.: 44-46 °C (lit.m.p.:<sup>191</sup> 45-46 °C); UV λ<sub>max</sub> (EtOH)/nm 245 (ε/dm<sup>3</sup>mol<sup>-1</sup>cm<sup>-1</sup> 606), 293 (580) and 325 (592); δ<sub>H</sub> (300 MHz; CDCl<sub>3</sub>) 8.83 (1H, d, <sup>4</sup>J=2.6 Hz, Ar), 8.36 (1H, AA'XX', Ar), 7.57 (1H, d, <sup>3</sup>J=7.2 Hz, Ar) and 2.73 (3H, s, Me); δ<sub>C</sub> (75.5 MHz; CDCl<sub>3</sub>) 148.8 (Ar, quat), 146.2 (Ar, quat), 140.7 (Ar, quat), 134.0 (Ar, CH), 126.9 (Ar, CH), 120.1 (Ar, CH) and 20.6 (CH<sub>3</sub>); m/z (EI) 215 (M<sup>+</sup>, 20%), 198 (36) and 119 (38).

**1,3-bis(Tributylstannyl)benzene 155**

A solution of 1,3-dibromobenzene (1.0 g, 4.2 mmol) in dry diethyl ether (20 cm<sup>3</sup>) was added dropwise to a solution of *tert*-butyllithium in diethyl ether (60 cm<sup>3</sup>) at -78 °C and the mixture was stirred under N<sub>2</sub> for 30 minutes. Tributyltin chloride (2.85 cm<sup>3</sup>, 10.5 mmol) was added carefully whilst maintaining the temperature of the mixture at -78 °C, and the mixture then allowed to warm to room temperature. After 2 hours the opaque white mixture was quenched with water (50 cm<sup>3</sup>) and the aqueous layer extracted with diethyl ether (3 x 100 cm<sup>3</sup>). The combined organic extracts were dried (MgSO<sub>4</sub>), filtered and concentrated *in vacuo* to give a transparent oil. After column chromatography (hexane) to remove tin residues, the product (1.95 g, 71%) was obtained as a transparent oil.

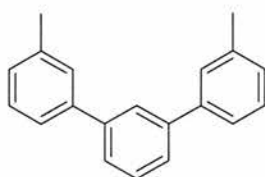
Found: C, 55.2; H, 9.1%. Calc. for C<sub>30</sub>H<sub>58</sub>Sn<sub>2</sub>: C, 54.9; H, 9.1%; IR  $\nu_{\max}$  (cm<sup>-1</sup>) 3050 and 3020 (Ar, CH), 2924br (Bu, CH) and 1463;  $\delta_{\text{H}}$  (300 MHz; CDCl<sub>3</sub>) 7.26-7.60 (4H, m, Ar), 1.52-1.61 (12H, m, CH<sub>2</sub>CH<sub>2</sub>CH<sub>2</sub>CH<sub>3</sub>), 1.28-1.40 (12H, m, CH<sub>2</sub>CH<sub>2</sub>CH<sub>2</sub>CH<sub>3</sub>), 1.04-1.12 (12H, m, CH<sub>2</sub>CH<sub>2</sub>CH<sub>2</sub>CH<sub>3</sub>) and 0.87-0.92 (18H, m, CH<sub>2</sub>CH<sub>2</sub>CH<sub>2</sub>CH<sub>3</sub>);  $\delta_{\text{C}}$  (75.5 MHz; CDCl<sub>3</sub>) 144.8 (Ar, CH), 141.3 (Ar, quat), 136.0 (Ar, CH), 127.7 (Ar, CH), 29.1 (n-Bu, CH<sub>2</sub>), 27.4 (n-Bu, CH<sub>2</sub>), 13.7 (n-Bu, CH<sub>3</sub>) and 9.5 (n-Bu, CH<sub>2</sub>); *m/z* (EI) 655 (M<sup>+</sup>, 6%), 599 (48), 373 (32), 314 (51), 235 (34), 177 (100).

**3-(Tributylstannyl)toluene 161**

*tert*-Butyllithium (1.56 M in pentanes, 6.5 cm<sup>3</sup>, 10.12 mmol) was added dropwise at -100 °C to a solution of 3-iodotoluene (1.0 g, 4.6 mmol) in dry diethyl ether (50 cm<sup>3</sup>) and the mixture stirred at this temperature for 1 hour. Tributyltin chloride (1.38 cm<sup>3</sup>, 5.1 mmol) was added dropwise at -100 °C before the mixture was allowed to warm to room temperature and stirred for 18 hours. Ammonium chloride (saturated aqueous solution, 5 cm<sup>3</sup>) was added, followed by water (10 cm<sup>3</sup>). The aqueous layer was extracted with diethyl ether (2 x 100 cm<sup>3</sup>) and the combined organic extracts dried (MgSO<sub>4</sub>), filtered and concentrated by rotary evaporation to afford a pale yellow oil. After column chromatography on silica (hexane:CH<sub>2</sub>Cl<sub>2</sub>, v:v, 4:1), the product (1.1 g, 59%) was obtained as a transparent oil.

Found: C, 59.6; H, 9.1%. Calc. for C<sub>17</sub>H<sub>34</sub>Sn: C, 59.9; H, 9.0%; IR  $\nu_{\max}$  (cm<sup>-1</sup>) 3074w (Ar CH), 2923br (Bu, CH) and 1586;  $\delta_{\text{H}}$  (300 MHz; CDCl<sub>3</sub>) 7.21-7.36 (4H, m), 2.35 (3H, s Me), 1.50-1.53 (6H, m, CH<sub>2</sub>CH<sub>2</sub>CH<sub>2</sub>CH<sub>3</sub>), 1.28-1.40 (6H, m, CH<sub>2</sub>CH<sub>2</sub>CH<sub>2</sub>CH<sub>3</sub>), 1.08-1.18 (6H, m, CH<sub>2</sub>CH<sub>2</sub>CH<sub>2</sub>CH<sub>3</sub>) and 0.75-0.85 (9H, m, CH<sub>2</sub>CH<sub>2</sub>CH<sub>2</sub>CH<sub>3</sub>);  $\delta_{\text{C}}$  (75.5 MHz; CDCl<sub>3</sub>) 141.6 (Ar, quat), 137.1 (Ar, quat), 137.1 (Ar, CH), 133.4 (Ar, CH), 128.7 (Ar, CH), 127.7 (Ar, CH), 29.1 (CH<sub>2</sub>), 27.4 (CH<sub>2</sub>), 21.5 (CH<sub>3</sub>), 13.6 (CH<sub>3</sub>) and 9.5 (CH<sub>2</sub>); *m/z* (EI) 381 (M<sup>+</sup>, 8%), 325 (100), 269 (80), 211 (95), 120 (35), 91 (85), 56 (52) and 41 (95).

### 1,3-Bis-(3'-methylphenyl)-benzene 159



#### Method A

3-(Tributylstannyl)-toluene (0.25 g, 0.65 mmol) was added to a stirred suspension of 1,3-dibromobenzene (0.05 g, 0.22 mmol) and Pd(PPh<sub>3</sub>)<sub>4</sub> (0.02 g, 0.02 mmol) in dry toluene (10 cm<sup>3</sup>). The mixture was heated under reflux for 3 days, before being allowed to cool. CH<sub>2</sub>Cl<sub>2</sub> (50 cm<sup>3</sup>) was added, and the mixture washed through a short pad of Celite<sup>®</sup> 521 filter agent to remove palladium solids. The solvent was removed under vacuum to afford a yellow oil. Column chromatography (CH<sub>2</sub>Cl<sub>2</sub>:hexane, v:v, 1:4) afforded the clean product (0.015 g, 25%) as a colourless crystalline solid.

**Method B**

1,3-Dibromobenzene (0.35g, 1.5 mmol) and Pd(PPh<sub>3</sub>)<sub>4</sub> (0.2 g, 0.17 mmol) were stirred in DME (10 cm<sup>3</sup>) at room temperature for 10 minutes. 3-Tolylboronic acid (0.5 g, 3.7 mmol) in EtOH (4 cm<sup>3</sup>) and Na<sub>2</sub>CO<sub>3</sub> (0.6 g, 5.7 mmol) in water (4 cm<sup>3</sup>) were added and the mixture was heated under reflux for 15 hours. The cooled mixture was poured onto CH<sub>2</sub>Cl<sub>2</sub> (100 cm<sup>3</sup>), the organic layer separated and filtered through Celite<sup>®</sup> 521 filter agent. Concentration under reduced pressure of the filtrate afforded a brown oil. Column chromatography (CH<sub>2</sub>Cl<sub>2</sub>:hexane, v:v, 1:1) afforded 1,3-bis-(3'-methylphenyl)-benzene (0.19 g, 50%) as a colourless solid.

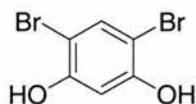
**Method C**

3-Iodotoluene (2.3 g, 10.7 mmol) in dry diethyl ether (10 cm<sup>3</sup>) was added dropwise to magnesium turnings (0.26 g, 10.7 mmol) activated by heating with a crystal of iodine. After addition was complete, the mixture was heated under reflux for a further hour to ensure complete reaction. The ethereal solution of 3-tolylmagnesium iodide was added dropwise to a solution of 1,3-dibromobenzene (0.5 g, 2.12 mmol) and Ni(dppe)Cl<sub>2</sub> (0.22 g, 0.42 mmol) in dry diethyl ether, and the mixture heated under reflux for 15 hours. After cooling, NH<sub>4</sub>Cl (saturated aqueous solution, 10 cm<sup>3</sup>) was added, and the aqueous phase separated and extracted with diethyl ether (3 x 50 cm<sup>3</sup>). Combined organic extracts were dried (MgSO<sub>4</sub>), filtered and concentrated under vacuum to afford a brown oil. Column chromatography (CH<sub>2</sub>Cl<sub>2</sub>:hexane, v:v, 1:3) afforded the clean product (0.14 g, 25%) as a colourless solid.

m.p.: 54-55 °C (lit.m.p.:<sup>192</sup> 54 °C) ; δ<sub>H</sub> (300 MHz; CDCl<sub>3</sub>) 7.81-7.84 (1H, m, Ar), 7.35-7.66 (9H, m, Ar), 7.22 (2H, d, <sup>3</sup>J=7.0 Hz, Ar) and 2.47 (6H, s, Me); δ<sub>C</sub> (75.5 MHz; CDCl<sub>3</sub>) 141.9 (Ar, quat), 141.3 (Ar, quat), 138.4 (Ar, quat), 129.1 (Ar, CH), 128.8 (Ar, CH), 128.1 (Ar, CH), 127.2 (Ar, CH), 126.2 (Ar, CH), 126.1 (Ar, CH), 124.4 (Ar, CH) and 21.6 (Me, CH<sub>3</sub>); *m/z* (EI) 258 (M<sup>+</sup>, 100%); HRMS: Found: 258.1402; Calc. for C<sub>20</sub>H<sub>18</sub>: 258.1409.

**4,6-Dibromoresorcinol 165**

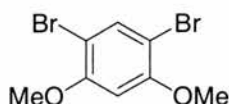




Resorcinol (1.1 g, 10 mmol) was stirred in  $\text{CHCl}_3$  ( $30 \text{ cm}^3$ ) and a solution of bromine (3.2g, 20 mmol) in  $\text{CHCl}_3$  ( $10 \text{ cm}^3$ ) was added dropwise over a period of 50 minutes. After the addition was complete, the mixture was stirred for a further hour at room temperature. All solvent was removed on a water aspirator, to afford a pale brown solid. Column chromatography ( $\text{CHCl}_3$ :MeOH, v:v, 97:3) afforded 4,6-dibromoresorcinol (2.4 g, 88%) as a colourless powder.

Found: C, 26.7; H, 1.3%. Calc. for  $\text{C}_6\text{H}_4\text{Br}_2\text{O}_2$ : C, 26.9; H, 1.5%; m.p.: 116-117 °C;  $\delta_{\text{H}}$  (300 MHz;  $\text{CDCl}_3$ ) 7.52 (1H, s, Ar), 6.73 (1H, s, Ar), 5.52 (2H, br s, OH);  $\delta_{\text{C}}$  (75.5 MHz;  $\text{CDCl}_3$ ) 134.4 (Ar, quat), 114.7 (Ar, CH), 84.9 (Ar, CH) and 82.7 (Ar, quat);  $m/z$  (EI) 268 ( $\text{M}^+$ , 100%); HRMS: Found: 265.8580; Calc. for  $\text{C}_6\text{H}_4\text{Br}_2\text{O}_2$ : 265.8578.

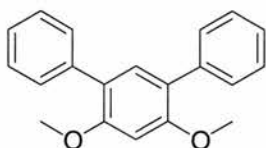
### 1,5-Dibromo-2,4-dimethoxybenzene 166



A solution of bromine (3.20 g, 20 mmol) in  $\text{CH}_2\text{Cl}_2$  ( $30 \text{ cm}^3$ ) was added dropwise to a stirred solution of 1,3-dimethoxybenzene (1.38 g, 10 mmol) in  $\text{CH}_2\text{Cl}_2$  ( $30 \text{ cm}^3$ ). The mixture was stirred at room temperature for 1 hour, and all solvent removed under a reduced pressure to afford the product as a pale brown solid (2.9 g, 100%).

Found: C, 32.7; H, 2.7%. Calc. for  $\text{C}_8\text{H}_8\text{Br}_2\text{O}_2$ : C, 32.5; H, 2.7%; m.p.: 137-138 °C (lit.m.p.:<sup>193</sup> 139-141 °C); IR  $\nu_{\text{max}}$  ( $\text{cm}^{-1}$ ) 2851m, (OMe), 718w, (CBr);  $\delta_{\text{H}}$  (300 MHz;  $\text{CDCl}_3$ ) 7.66 (1H, s, Ar), 6.49 (1H, s, Ar), 3.91 (6H, s, Me);  $\delta_{\text{C}}$  (75.5 MHz;  $\text{CDCl}_3$ ) 156.3 (Ar, quat), 136.0 (Ar, CH), 102.5 (Ar, quat), 97.5 (Ar, CH) and 56.5 (OMe  $\text{CH}_3$ );  $m/z$  (EI) 296 ( $\text{M}^+$ , 100%) and 253 (52); HRMS: Found: 295.8879; Calc. for  $\text{C}_8\text{H}_8\text{Br}_2\text{O}_2$ : 295.8871.

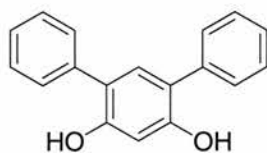
### 1,3-Dimethoxy-4,6-diphenylbenzene 168



1,3-Dimethoxy-4,6-dibromobenzene (1.0 g, 3.38 mmol) and Pd(PPh<sub>3</sub>)<sub>4</sub> (0.78 g, 0.68 mmol) were stirred at room temperature in DME (40 cm<sup>3</sup>) and degassed with N<sub>2</sub> for 30 minutes. To this mixture was added a solution of phenylboronic acid (1.03 g, 8.45 mmol) in EtOH (1 cm<sup>3</sup>) and Na<sub>2</sub>CO<sub>3</sub> (1.4 g, 13.5 mmol) in H<sub>2</sub>O (10 cm<sup>3</sup>). The stirred mixture was heated under reflux for 15 hours and then allowed to cool before pouring onto CH<sub>2</sub>Cl<sub>2</sub> (50 cm<sup>3</sup>). The reaction mixture was washed through a short pad of Celite<sup>®</sup> 521 filter agent with CH<sub>2</sub>Cl<sub>2</sub>, and the filtrate was dried (MgSO<sub>4</sub>), filtered and concentrated under a reduced pressure to afford a brown oil. Column chromatography (Et<sub>2</sub>O:hexane, v:v, 2:3) gave the desired product (0.76 g, 78%) as a colourless powder.

Found: C, 82.4; H, 6.1%. Calc. for C<sub>20</sub>H<sub>18</sub>O<sub>2</sub>: C, 82.7; H, 6.3%; m.p.: 95-96 °C (lit.m.p.:<sup>194</sup> 99 °C); IR  $\nu_{\max}$  (cm<sup>-1</sup>) 3000m, (OMe);  $\delta_{\text{H}}$  (300 MHz; CDCl<sub>3</sub>) 7.66-7.69 (4H, m, Ar), 7.50-7.55 (4H, m, Ar), 7.42-7.45 (3H, m, Ar), 6.79 (1H, s, Ar) and 4.01 (6H, s, CH<sub>3</sub>);  $\delta_{\text{C}}$  (75.5 MHz; CDCl<sub>3</sub>) 156.7 (Ar, quat), 138.1 (Ar, quat), 132.9 (Ar, CH), 129.4 (Ar, CH), 128.0 (Ar, CH), 126.5 (Ar, CH) 123.2 (Ar, quat), 96.3 (Ar, CH) and 55.9 (CH<sub>3</sub>); *m/z* (EI) 290 (M<sup>+</sup>, 40%), 260 (5), 163 (57) and 91 (100); HRMS: Found: 290.1298; Calc. for C<sub>20</sub>H<sub>18</sub>O<sub>2</sub>: 290.1307.

### 1,3-Dihydroxy-4,6-diphenylbenzene 169

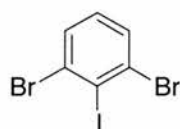


A solution of 1,3-dimethoxy-4,6-diphenylbenzene (0.5 g, 1.7 mmol) in dry CH<sub>2</sub>Cl<sub>2</sub> (40 cm<sup>3</sup>) was stirred under N<sub>2</sub> at -78 °C, and BBr<sub>3</sub> (1 M in CH<sub>2</sub>Cl<sub>2</sub>, 4.3 cm<sup>3</sup>, 4.3 mmol) was added dropwise. After addition was complete, the reaction mixture was allowed to warm to room temperature, and stirred for a further 24 hours. TLC analysis indicated the reaction was complete, and the mixture was re-cooled to 0 °C in an ice bath, and MeOH (10 cm<sup>3</sup>) added carefully to quench any remaining BBr<sub>3</sub>. All solvents were removed

using a water aspirator, and  $\text{CH}_2\text{Cl}_2$  ( $50 \text{ cm}^3$ ) added to the brown, oily residue. The solution was washed with water ( $3 \times 20 \text{ cm}^3$ ) and the organic layer dried ( $\text{MgSO}_4$ ), filtered and concentrated to afford a brown solid. Column chromatography ( $\text{Et}_2\text{O}$ :hexane, v:v, 1:1) gave the desired product (0.4 g, 89%) as a cream coloured solid.

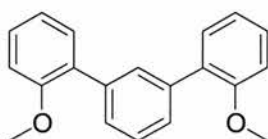
Found: C, 82.5; H, 5.4%. Calc. for  $\text{C}_{18}\text{H}_{14}\text{O}_2$ : C, 82.4; H, 5.4%; m.p.: 128-130 °C (lit.m.p.:<sup>195</sup> 125-126 °C); IR  $\nu_{\text{max}}$  ( $\text{cm}^{-1}$ ) 3478br, (OH);  $\delta_{\text{H}}$  (300 MHz;  $\text{CDCl}_3$ ) 7.48-7.50 (8H, m, Ar), 7.36-7.43 (2H, m, Ar), 7.16 (1H, s, Ar), 6.66 (1H, s, Ar) and 5.29 (2H, br s, OH);  $\delta_{\text{C}}$  (75.5 MHz;  $\text{CDCl}_3$ ) 153.1 (Ar, quat), 136.7 (Ar, quat), 131.6 (Ar, CH), 129.3 (Ar, CH), 129.1 (Ar, CH), 127.6 (Ar, CH), 121.3 (Ar, quat) and 103.1 (Ar, CH);  $m/z$  (EI) 262 ( $\text{M}^+$ , 100); HRMS: Found: 262.1002; Calc. for  $\text{C}_{18}\text{H}_{14}\text{O}_2$ : 262.0994.

### 2,6-Dibromiodobenzene 171



A solution of sodium nitrite (2.89 g, 42 mmol) in water ( $20 \text{ cm}^3$ ) was added dropwise to a stirred solution of 2,6-dibromoaniline (10 g, 39.9 mmol) in hydrochloric acid ( $30 \text{ cm}^3$ ) at 0°C. After 30 minutes, the solution was poured through a glass wool filter into a solution of potassium iodide (66 g, 400 mmol) in water ( $150 \text{ cm}^3$ ) and stirred vigorously for 1 hour.  $\text{CH}_2\text{Cl}_2$  ( $130 \text{ cm}^3$ ) and sodium sulfite solution (1M, aqueous solution,  $60 \text{ cm}^3$ ) were added, and the aqueous layer extracted with  $\text{CH}_2\text{Cl}_2$  ( $3 \times 100 \text{ cm}^3$ ). The combined organic extracts were dried ( $\text{MgSO}_4$ ), filtered and concentrated under a reduced pressure to afford the crude product as an orange solid. Recrystallisation (PhMe/EtOH) afforded 2,6-dibromiodobenzene (10.6 g, 74%) as a colourless crystalline solid.

Found: C, 19.9; H, 0.43%. Calc. for  $\text{C}_6\text{H}_3\text{Br}_2\text{I}$ : C, 19.9; H, 0.84%\*; m.p.: 97.5-98°C (lit.m.p.:<sup>196</sup> 98-99°C);  $\delta_{\text{H}}$  (300 MHz;  $\text{CDCl}_3$ ) 7.06 (1H, t,  $^3J=8.0 \text{ Hz}$ , Ar) and 7.55 (2H, d,  $^3J=8.0 \text{ Hz}$ , Ar);  $\delta_{\text{C}}$  (75.5 MHz;  $\text{CDCl}_3$ ) 131.2 (Ar, quat), 131.0 (Ar, CH), 130.3 (Ar, CH) and 109.3 (Ar, quat);  $m/z$  (EI) 362 ( $\text{M}^+$ , 100%), 235 (25) and 75 (35); HRMS: Found: 361.7620; Calc. for  $\text{C}_6\text{H}_3\text{Br}_2\text{I}$ : 361.7626. \* Due to the high proportion of halogen in this compound, elemental analysis could not accurately determine the % hydrogen.

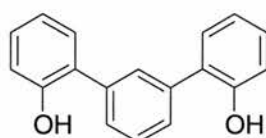
**1,3-Bis-(2'-methoxyphenyl)benzene 170**

2-Bromoanisole (2.71 g, 14.5 mmol) in THF (33 cm<sup>3</sup>) was added slowly to magnesium turnings (0.4 g, 16.6 mmol) in a round-bottomed flask. The addition was performed at such a rate as to maintain the mixture at reflux, and once the addition was complete, the mixture was heated under reflux for a further hour to ensure the reaction was finished. A solution of 2,6-dibromoiodobenzene (1.5 g, 4.15 mmol) in THF (16 cm<sup>3</sup>) was added dropwise to the Grignard reagent, and the mixture heated under reflux for 11 hours. After cooling, the reaction was quenched with dilute hydrochloric acid (0.1 M, aqueous solution, 30 cm<sup>3</sup>), and all THF removed under a reduced pressure. The aqueous residue was extracted with CH<sub>2</sub>Cl<sub>2</sub> (3 x 50 cm<sup>3</sup>) and the combined organic extracts washed with sodium sulfite solution (saturated aqueous solution, 2 x 50 cm<sup>3</sup>) and water (50 cm<sup>3</sup>). After drying (MgSO<sub>4</sub>) and filtering, concentration under vacuum afforded the crude product as a yellow oil. Column chromatography (CH<sub>2</sub>Cl<sub>2</sub>:hexane, v:v, 1:2) gave pure 1,3-bis-(2-methoxyphenyl)benzene (0.71 g, 59%) as a colourless solid.

Found: C, 82.6; H, 6.5%. Calc. for C<sub>20</sub>H<sub>18</sub>O<sub>2</sub>: C, 82.7; H, 6.25%; m.p.: 99-100°C (lit.m.p.:<sup>197</sup> 97-98°C); IR  $\nu_{\max}$  (cm<sup>-1</sup>) 2832m, (OMe);  $\delta_{\text{H}}$  (300 MHz; CDCl<sub>3</sub>) 7.72-7.73 (1H, m, Ar), 7.55-7.56 (1H, m, Ar), 7.53 (1H, d, <sup>4</sup>J=1.8 Hz, Ar), 7.44-7.49 (1H, m, Ar), 7.39-7.43 (2H, dd, <sup>3</sup>J=7.5 Hz, <sup>4</sup>J=1.8 Hz, Ar), 7.32-7.38 (2H, dd, <sup>3</sup>J=8.1 Hz, <sup>4</sup>J=1.8 Hz, Ar), 7.01-7.09 (4H, m, Ar) and 3.85 (6H, s, Me);  $\delta_{\text{C}}$  (75.5 MHz; CDCl<sub>3</sub>) 156.6 (Ar, quat), 138.2 (Ar, CH), 131.0 (Ar, CH), 130.8 (Ar, quat), 130.7 (Ar, quat), 128.5 (Ar, CH), 128.2 (Ar, CH), 127.5 (Ar, CH), 120.8 (Ar, CH), 111.2 (Ar, CH) and 55.5 (CH<sub>3</sub>); *m/z* (EI) 290 (M<sup>+</sup>,

17%), 166 (44), 146 (46) and 70 (100); HRMS: Found: 290.1300; Calc. for  $C_{20}H_{18}O_2$ : 290.1307.

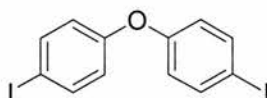
### 1,3-Bis-(2'-hydroxyphenyl)benzene 172



Boron tribromide (1M solution in  $CH_2Cl_2$ , 4.3  $cm^3$ , 4.3 mmol) was added dropwise under  $N_2$  to a stirred solution of 1,3-bis-(2'-methoxyphenyl)benzene (0.5 g, 1.72 mmol) in dry  $CH_2Cl_2$  (20 $cm^3$ ) at  $-78^\circ C$ . The reaction mixture was allowed to warm to room temperature and stirred for 18 hours. After re-cooling to  $0^\circ C$ , methanol (5  $cm^3$ ) was added slowly to quench any excess  $BBr_3$ , and all solvents removed on a water aspirator.  $CH_2Cl_2$  (50  $cm^3$ ) was added and the organic layer washed with water (2 x 50  $cm^3$ ), dried ( $MgSO_4$ ), filtered and concentrated under vacuum to afford a brown solid. Recrystallisation ( $CH_2Cl_2$ /hexane) afforded 1,3-bis-(2-hydroxyphenyl)benzene (0.3 g, 67%) as a colourless solid.

m.p.:  $125-126^\circ C$  (lit.m.p.:<sup>169</sup>  $119-121^\circ C$ ); IR  $\nu_{max}$  ( $cm^{-1}$ ) 3392br, (OH);  $\delta_H$  (300 MHz;  $CDCl_3$ ) 7.69-7.77 (4H, m, Ar), 7.64 (2H, d,  $^4J=1.5$  Hz, Ar), 7.61 (2H, m, Ar), 7.36-7.44 (4H, m, Ar) and 5.20 (2H, br s, OH);  $\delta_C$  (75.5 MHz;  $CDCl_3$ ) 152.3 (Ar, quat), 137.9 (Ar, quat), 130.3 (Ar, CH), 129.9 (Ar, CH), 129.7 (Ar, CH), 129.2 (Ar, CH), 128.2 (Ar, CH), 127.7 (Ar, quat), 121.0 (Ar, CH) and 116.0 (Ar, CH);  $m/z$  (EI) 262 ( $M^+$ , 100%), 247 (6) and 215 (21); HRMS: Found: 262.0999; Calc. for  $C_{18}H_{14}O_2$ : 262.0994.

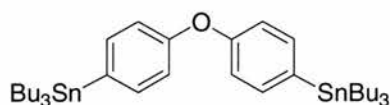
### 4,4'-Bis(iodo)diphenylether 175



A mixture of diphenylether (8.0 g, 47 mmol), iodine (11.36 g, 45 mmol), periodic acid (5.1 g, 22 mmol), sulfuric acid (3 cm<sup>3</sup>), acetic acid (120 cm<sup>3</sup>) and water (30 cm<sup>3</sup>) was heated to 95 °C in an oil bath for 6 hours. The mixture was allowed to cool and stand at room temperature overnight, after which time it was filtered under suction. The solid collected was washed with diethyl ether (150 cm<sup>3</sup>) and recrystallised (Et<sub>2</sub>O/hexane) to afford the product (14.27 g, 72%) as a colourless crystalline solid.

Found: C, 33.9; H, 1.7%. Calc. for C<sub>12</sub>H<sub>8</sub>OI<sub>2</sub>: C, 34.2; H, 1.9%; m.p.: 138-140 °C (lit.m.p.:<sup>198</sup> 139-141 °C); IR  $\nu_{\max}$  (cm<sup>-1</sup>) 1251s, (Ar-O-Ar);  $\delta_{\text{H}}$  (300 MHz; CDCl<sub>3</sub>) 7.62 (4H, AA'XX', Ar) and 6.76 (4H, AA'XX', Ar);  $\delta_{\text{C}}$  (75.5 MHz; CDCl<sub>3</sub>) 156.7 (Ar, quat), 138.9 (Ar, CH), 121.1 (Ar, CH) and 86.7 (Ar, quat);  $m/z$  (EI) 422 (M<sup>+</sup>, 100%) and 168 (20); HRMS: Found: 421.8661; Calc. for C<sub>12</sub>H<sub>8</sub>OI<sub>2</sub>: 421.8665.

#### 4,4'-Bis(tributylstannyl)diphenylether 176



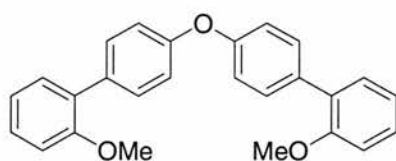
A suspension of 4,4'-bis(iodo)diphenylether (6.0 g, 14.2 mmol) in dry hexane (280 cm<sup>3</sup>) was cooled to -78 °C under N<sub>2</sub> and *tert*-butyllithium added dropwise over a period of 30 minutes. The mixture was stirred at this temperature for a further 20 minutes before careful addition of tributyl tin chloride (9.5 cm<sup>3</sup>, 35 mmol). The mixture was allowed to warm slowly to room temperature and stirred for 18 hours. After this time, water (150 cm<sup>3</sup>) was added, the layers separated, and the aqueous layer extracted with diethyl ether (2 x 100 cm<sup>3</sup>). The combined organic phases were dried (MgSO<sub>4</sub>), filtered and concentrated under a vacuum to give a colourless oil. All excess tributyl tin chloride was distilled at 124 °C (5 mm Hg), and the residual yellow oil purified by silica gel column chromatography (hexane). The required product was obtained (4.47 g, 42%) as a colourless oil.

IR  $\nu_{\max}$  (cm<sup>-1</sup>) 3070w (Ar CH), 2922br (Bu, CH) and 1573;  $\delta_{\text{H}}$  (300 MHz; CDCl<sub>3</sub>) 7.42 (4H, AA'XX', Ar), 7.01 (4H, AA'XX', Ar), 1.51-1.64 (6H, m, CH<sub>2</sub>CH<sub>2</sub>CH<sub>2</sub>CH<sub>3</sub>), 1.28-1.40 (6H, m, CH<sub>2</sub>CH<sub>2</sub>CH<sub>2</sub>CH<sub>3</sub>), 1.03-1.12 (6H, m, CH<sub>2</sub>CH<sub>2</sub>CH<sub>2</sub>CH<sub>3</sub>) and 0.87-0.93 (9H, m,



$\text{CH}_2\text{CH}_2\text{CH}_2\text{CH}_3$ );  $\delta_{\text{C}}$  (75.5 MHz;  $\text{CDCl}_3$ ) 157.2 (Ar, quat), 137.5 (Ar, CH), 135.4 (Ar, quat), 118.5 (Ar, CH), 29.0 (*n*-Bu,  $\text{CH}_2$ ), 27.3 (*n*-Bu,  $\text{CH}_2$ ), 13.6 (*n*-Bu,  $\text{CH}_3$ ) and 9.5 (*n*-Bu,  $\text{CH}_2$ );  $m/z$  (EI) 746 ( $\text{M}^+$ , 3%) and 690 (100).

#### 4,4'-Bis(2-methoxyphenyl)diphenyl ether 177



#### Method A

2-Bromoanisole (0.76 g, 4.1 mmol) was added dropwise to a stirred solution of 4,4'-bis(tributylstannyl)diphenylether (1.0 g, 1.3 mmol) and  $\text{Pd}(\text{PPh}_3)_4$  (150 mg, 0.13 mmol) in dry degassed toluene (20  $\text{cm}^3$ ). The mixture was heated under reflux for 18 hours and, after cooling, was filtered through Celite<sup>®</sup> 521 filter agent, and the solid residues washed thoroughly with  $\text{CH}_2\text{Cl}_2$ . The filtrate was collected and the solvent removed under a reduced pressure to afford a brown oil. Column chromatography ( $\text{CH}_2\text{Cl}_2$ :hexane, v:v, 1:1) gave the clean product (0.12 g, 24%) as a colourless solid.

#### Method B

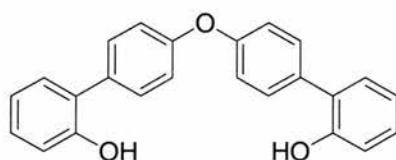
Magnesium turnings (1.4 g, 59.2 mmol) were activated by heating with a crystal of iodine. A solution of 2-bromoanisole (11.1 g, 59.2 mmol) in dry diethyl ether (60  $\text{cm}^3$ ) was added in small portions *via* a syringe so as to maintain a gentle reflux. After addition is complete the mixture was heated under reflux for a further hour to ensure the reaction is finished. The resulting 2-methoxyphenyl magnesium bromide was added slowly to a stirred suspension of 4,4'-bis(iodo)diphenyl ether (5.0 g, 11.85 mmol) and  $\text{Ni}(\text{PPh}_3)_2\text{Cl}_2$  (0.6 g, 0.94 mmol) in dry, degassed diethyl ether (200  $\text{cm}^3$ ). The mixture was heated under reflux for 18 hours. After cooling, water (100  $\text{cm}^3$ ) was added slowly to quench any remaining Grignard reagent. The organic layer was separated and the aqueous layer extracted with diethyl ether (2 x 50  $\text{cm}^3$ ). Combined organic extracts were dried



(MgSO<sub>4</sub>), filtered and concentrated under a reduced pressure to afford the crude product as a yellow solid. Column chromatography (Et<sub>2</sub>O:hexane, v:v, 1:4) afforded the clean product (2.90 g, 64%) as a colourless solid.

Found: C, 81.45; H, 5.7%. Calc. for C<sub>26</sub>H<sub>22</sub>O<sub>3</sub>: C, 81.65; H, 5.8%; m.p.: 102-104 °C; IR  $\nu_{\max}$  (cm<sup>-1</sup>) 2835m, (OMe), 1237s, (Ar-O-Ar);  $\delta_{\text{H}}$  (300 MHz; CDCl<sub>3</sub>) 7.54-7.51 (4H, m, Ar), 7.35-7.30 (4H, m, Ar), 7.13-6.98 (8H, m, Ar) and 3.84 (6H, s, Me);  $\delta_{\text{C}}$  (75.5 MHz; CDCl<sub>3</sub>) 156.4 (Ar, quat), 156.2 (Ar, quat), 133.5 (Ar, quat), 130.9 (Ar, CH), 130.8 (Ar, CH), 130.0 (Ar, quat), 128.5 (Ar, CH), 120.9 (Ar, CH), 118.5 (Ar, CH), 111.2 (Ar, CH) and 55.5 (CH<sub>3</sub>, OMe); *m/z* (EI) 382 (M<sup>+</sup>, 100) and 168 (42); HRMS: Found: 382.1576; Calc. for C<sub>26</sub>H<sub>22</sub>O<sub>3</sub>: 382.1569.

#### 4,4'-Bis(2-hydroxyphenyl)diphenyl ether 178

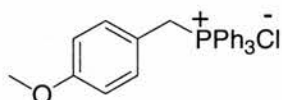


A solution of 4,4'-bis(2-methoxyphenyl)diphenyl ether (2.0 g, 5.2 mmol) in dry CH<sub>2</sub>Cl<sub>2</sub> (80 cm<sup>3</sup>) was cooled to -78°C under N<sub>2</sub> with stirring. Boron tribromide (1M solution in CH<sub>2</sub>Cl<sub>2</sub>, 13 cm<sup>3</sup>, 13 mmol) was added dropwise *via* a syringe and the mixture allowed to warm slowly to room temperature. The mixture was then re-cooled to 0°C and MeOH (15 cm<sup>3</sup>) added carefully to quench any excess boron tribromide. The solvents were removed on a water aspirator affording an oily brown residue. CH<sub>2</sub>Cl<sub>2</sub> (80 cm<sup>3</sup>) was added and the solution washed with water (80 cm<sup>3</sup>). The aqueous phase was extracted with CH<sub>2</sub>Cl<sub>2</sub> (2 x 40 cm<sup>3</sup>) and the combined organic extracts dried (MgSO<sub>4</sub>), filtered and concentrated to afford a brown solid. Flash column chromatography (100% CH<sub>2</sub>Cl<sub>2</sub>) afforded the clean product as a colourless solid.

Found: C, 81.2; H, 5.0%. Calc. for C<sub>24</sub>H<sub>18</sub>O<sub>3</sub>: C, 81.3; H, 5.1%; m.p.: 130-132 °C; IR  $\nu_{\max}$  (cm<sup>-1</sup>) 3370br, (OH), 1222s, (Ar-O-Ar);  $\delta_{\text{H}}$  (300 MHz; CDCl<sub>3</sub>) 7.50-7.47 (4H, dd, <sup>3</sup>J=6.0 Hz, <sup>4</sup>J=1.8 Hz, Ar), 7.30-7.25 (4H, m, Ar), 7.20-7.17 (4H, dd, <sup>3</sup>J=6.0 Hz, <sup>4</sup>J=1.8 Hz, Ar), 7.03-6.97 (4H, m, Ar) and 5.19 (2H, br s, OH);  $\delta_{\text{C}}$  (75.5 MHz; CDCl<sub>3</sub>) 156.8 (Ar, quat), 152.5 (Ar, quat), 132.4 (Ar, quat), 130.7 (Ar, CH), 130.4 (Ar, CH), 129.1 (Ar, CH), 127.5

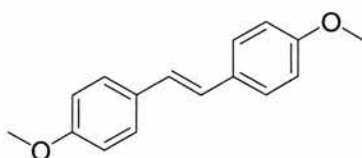
(Ar, quat), 121.0 (Ar, CH), 119.6 (Ar, CH) and 115.9 (Ar, CH);  $m/z$  (EI) 354 ( $M^+$ , 100%); HRMS: Found: 354.1249; Calc. for  $C_{24}H_{18}O_3$ : 354.1256.

#### 4-(Methoxybenzyl)-triphenylphosphonium chloride 183



A solution of 4-methoxybenzyl chloride (10 g, 64 mmol) and triphenylphosphine (18.4 g, 70 mmol) in toluene ( $70\text{ cm}^3$ ) was heated at reflux for 24 hours during which time a white precipitate formed. The precipitate was collected by suction filtration, washed with hexane and dried *in vacuo* until of constant mass to afford the desired product (21.7 g, 81%) as a colourless powder which was used without further purification or characterisation.

#### 1,2-Bis-(4-methoxyphenyl)-ethene 182

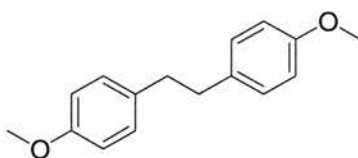


Potassium *tert*-butoxide (5.77 g, 51.4 mmol) was added to a stirred mixture of *p*-anisaldehyde (5.0 g, 36.7 mmol), 4-(methoxybenzyl)-triphenylphosphonium chloride (15.4 g, 36.7 mmol) and ethanol ( $50\text{ cm}^3$ ). After stirring under  $N_2$  for 1 hour, water ( $50\text{ cm}^3$ ) was added and the precipitate collected by suction filtration and dried to afford the product (5.4 g, 62%) as a colourless crystalline solid.

m.p.: 213-214 °C (lit.m.p.:<sup>199</sup> 214-215°C); IR  $\nu_{\text{max}}$  ( $\text{cm}^{-1}$ ) 3017w, (alkene C-H), 2838m, (OMe), 1608s, (alkene C-C);  $\delta_{\text{H}}$  (300 MHz; $\text{CDCl}_3$ ) 7.44 (4H, AA'XX', Ar), 6.93 (4H, AA'XX', Ar), 6.89 (2H, s, vinylic) and 3.84 (6H, s, Me);  $\delta_{\text{C}}$  (75.5 MHz;  $\text{CDCl}_3$ ) 159.2 (Ar, quat), 130.6 (Ar, quat), 127.5 (Ar, CH), 126.3 (vinylic, CH), 114.2 (Ar, CH) and 55.3

(OMe, CH<sub>3</sub>); *m/z* (EI) 240 (M<sup>+</sup>, 100 %) and 225 (38); HRMS: Found: 240.1145; Calc. for C<sub>16</sub>H<sub>16</sub>O<sub>2</sub>: 240.1150.

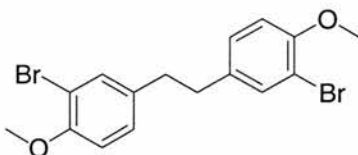
### 1,2-Bis-(4-methoxyphenyl)-ethane 186



Palladium on carbon (10% w/w, 3.5 g, 3.3 mmol) was added to a stirred solution of 1,2-bis-(4-methoxyphenyl)ethene (4.0 g, 16.7 mmol) in ethyl acetate (200 cm<sup>3</sup>). The suspension was degassed thoroughly and then subjected to a slight overpressure of H<sub>2</sub> for about 18 hours. The mixture was washed through a short pad of Celite<sup>®</sup> 521 filter agent with ethyl acetate, and the filtrate concentrated under vacuum to afford the product (3.1 g, 77%) as a white crystalline solid.

Found: C, 79.2; H, 7.6%. Calc. for C<sub>16</sub>H<sub>18</sub>O<sub>2</sub>: C, 79.3; H, 7.5%; m.p.: 125-126°C (lit.m.p.:<sup>200</sup> 128-129°C); IR  $\nu_{\max}$  (cm<sup>-1</sup>) 2915m, (C-H), 2852m, (OMe);  $\delta_{\text{H}}$  (300 MHz; CDCl<sub>3</sub>) 7.09-7.12 (4H, AA'XX', Ar), 6.83-6.86 (4H, AA'XX', Ar), 3.81 (6H, s, Me), 2.86 (4H, s);  $\delta_{\text{C}}$  (75.5 MHz; CDCl<sub>3</sub>) 158.0 (Ar, quat), 134.1 (Ar, quat), 129.5 (Ar, CH), 113.8 (Ar, CH), 55.2 (Me, CH<sub>3</sub>) and 37.3 (CH<sub>2</sub>); *m/z* (EI) 242 (M<sup>+</sup>, 18%) and 121 (100); HRMS: Found: 242.1301; Calc. for C<sub>16</sub>H<sub>18</sub>O<sub>2</sub>: 242.1307.

### 1,2-Bis-(3-bromo-4-methoxyphenyl)-ethane 187

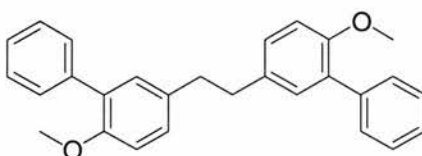


Bromine (0.5 cm<sup>3</sup>, 9.8 mmol) was added dropwise to a stirred solution of 1,2-bis-(4-methoxyphenyl)-ethane (1.5 g, 6.2 mmol) in CHCl<sub>3</sub> (30 cm<sup>3</sup>). Light was excluded from

the reaction. The mixture was stirred overnight and the solvent was then removed under a reduced pressure to afford the crude product. Recrystallisation (CH<sub>2</sub>Cl<sub>2</sub>/hexane) afforded 1,2-bis-(3-bromo-4-methoxyphenyl)-ethane (2.48 g, 87%) as an orange crystalline solid.

Found: C, 48.08; H, 3.74%. Calc. for C<sub>16</sub>H<sub>16</sub>O<sub>2</sub>Br<sub>2</sub>: C, 48.03; H, 4.03%; m.p.: 146-147°C (lit.m.p.:<sup>201</sup> 147°C); IR  $\nu_{\max}$  (cm<sup>-1</sup>) 2856m, (OMe);  $\delta_{\text{H}}$  (300 MHz; CDCl<sub>3</sub>) 7.36 (2H, d, <sup>4</sup>J=2.4 Hz, Ar), 7.01 (2H, AA'XX', Ar), 6.81 (2H, AA'XX', Ar), 3.88 (6H, s, Me), 2.80 (4H, s, CH<sub>2</sub>);  $\delta_{\text{C}}$  (75.5 MHz; CDCl<sub>3</sub>) 154.2 (Ar, quat), 135.0 (Ar, quat), 133.2 (Ar, CH), 128.4 (Ar, CH), 111.9 (Ar, CH), 111.4 (Ar, quat), 56.2 (CH<sub>3</sub>) and 36.6 (CH<sub>2</sub>); *m/z* (EI) 400 (M<sup>+</sup>, 30%) and 199 (100); HRMS: Found: 399.9506; Calc. for C<sub>16</sub>H<sub>16</sub>O<sub>2</sub>Br<sub>2</sub>: 399.9497.

### 1,2-Bis-(3-phenyl-4-methoxyphenyl)-ethane 188

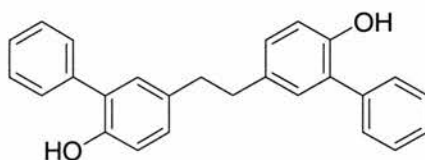


A mixture of 1,2-bis-(3-bromo-4-methoxyphenyl)-ethane (0.5 g, 1.25 mmol) and Pd(PPh<sub>3</sub>)<sub>4</sub> (0.29 g, 0.25 mmol) in DME (40 cm<sup>3</sup>) was stirred at room temperature and degassed thoroughly with N<sub>2</sub> for 30 minutes. Phenylboronic acid (0.38 g, 3.13 mmol) dissolved in the minimum of EtOH (1cm<sup>3</sup>) was added, followed by Na<sub>2</sub>CO<sub>3</sub> (0.53 g, 5 mmol) in H<sub>2</sub>O (5 cm<sup>3</sup>). The mixture was heated under reflux for 18 hours, after which time TLC analysis indicated that no starting material remained. After cooling, the reaction mixture was poured onto CH<sub>2</sub>Cl<sub>2</sub> (50 cm<sup>3</sup>) and filtered through Celite<sup>®</sup> 521 filter agent to remove palladium residues. The filtrate was dried (MgSO<sub>4</sub>), filtered and concentrated under a reduced pressure, affording the crude product as a black oil. Column chromatography (Et<sub>2</sub>O:hexane, v:v, 2:3) gave clean 1,2-bis-(3-phenyl-4-methoxyphenyl)-ethane (0.4 g, 82%) as a colourless crystalline solid.

Found: C, 85.2; H, 6.7%. Calc. for C<sub>28</sub>H<sub>26</sub>O<sub>2</sub>: C, 85.25; H, 6.6%; m.p.: 118-119 °C; IR  $\nu_{\max}$  (cm<sup>-1</sup>) 3015w, (C-H), 2834m, (OMe);  $\delta_{\text{H}}$  (300 MHz; CDCl<sub>3</sub>) 7.61-7.64 (4H, m, Ar), 7.43-7.55 (6H, m, Ar), 7.23-7.27 (4H, m, Ar), 7.02-7.05 (2H, m, Ar), 3.91 (6H, s, CH<sub>3</sub>) and 3.04 (4H, s, CH<sub>2</sub>);  $\delta_{\text{C}}$  (75.5 MHz; CDCl<sub>3</sub>) 154.7 (Ar, quat), 138.6 (Ar, quat), 134.0

(Ar, quat), 131.1 (Ar, CH), 130.4 (Ar, quat), 129.5 (Ar, CH), 128.3 (Ar, CH), 127.9 (Ar, CH), 126.8 (Ar, CH), 111.3 (Ar, CH), 55.7 (CH<sub>3</sub>) and 37.3 (CH<sub>2</sub>); *m/z* (EI) 394 (M<sup>+</sup>, 29%) and 197 (100); HRMS: Found: 394.1926; Calc. for C<sub>28</sub>H<sub>26</sub>O<sub>2</sub>: 394.1933.

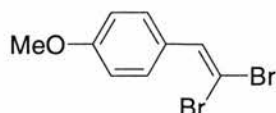
### 1,2-Bis-(3-phenyl-4-hydroxyphenyl)-ethane 181



1,2-Bis-(2-phenyl-3-methoxyphenyl)-ethane (0.22 g, 0.56 mmol) was stirred in dry CH<sub>2</sub>Cl<sub>2</sub> (20 cm<sup>3</sup>) at -78 °C under N<sub>2</sub>. Boron tribromide (1 M in CH<sub>2</sub>Cl<sub>2</sub>, 1.4 cm<sup>3</sup>, 1.4 mmol) was added dropwise, and the mixture allowed to warm to room temperature over a period of 2 hours. The mixture was cooled in an ice bath, and MeOH (10 cm<sup>3</sup>) was added slowly to quench any excess BBr<sub>3</sub>. All solvents were removed on a water aspirator, and CH<sub>2</sub>Cl<sub>2</sub> (20 cm<sup>3</sup>) added to the oily brown residue. The solution was washed with water (20 cm<sup>3</sup>) and the aqueous layer was extracted with CH<sub>2</sub>Cl<sub>2</sub> (3 x 20 cm<sup>3</sup>). The combined organic extracts were dried (MgSO<sub>4</sub>), filtered and concentrated under a reduced pressure to afford the crude product as a brown oil. Flash column chromatography (Et<sub>2</sub>O:hexane, v:v, 1:1) to remove baseline impurities gave 1,2-bis(2-phenyl-3-hydroxyphenyl)-ethane (0.18 g, 86%) as a brown oil.

$\delta_{\text{H}}$  (300 MHz; CDCl<sub>3</sub>) 7.25-7.39 (10H, m, Ar), 6.94-6.99 (4H, m, Ar), 6.80 (2H, d, <sup>3</sup>*J*=8.1 Hz, Ar), 5.06 (2H, br s, OH) and 2.79 (4H, s, CH<sub>2</sub>);  $\delta_{\text{C}}$  (75.5 MHz; CDCl<sub>3</sub>) 151.0 (Ar, quat), 137.7 (Ar, quat), 134.5 (Ar, quat), 130.7 (Ar, CH), 130.6 (Ar, CH) 129.6 (Ar, CH), 129.5 (Ar, CH), 128.3 (Ar, quat), 128.2 (Ar, CH), 116.2 (Ar, CH) and 37.8 (CH<sub>2</sub>); *m/z* (EI) 366 (M<sup>+</sup>, 48%) and 183 (100); HRMS: Found: 366.1629; Calc. for C<sub>26</sub>H<sub>22</sub>O<sub>2</sub>: 366.1620.

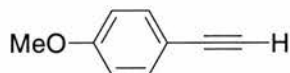
### 1-(2,2-Dibromo-vinyl)-4-methoxybenzene 192



Triphenylphosphine (52.5 g, 200 mmol) was stirred in  $\text{CH}_2\text{Cl}_2$  (250  $\text{cm}^3$ ) and the solution cooled in an ice-bath under  $\text{N}_2$  for 10 minutes. Zinc powder (13.1 g, 200 mmol) and carbon tetrabromide (66.3 g, 200 mmol) were added sequentially, with care taken to avoid a large exotherm. The reaction mixture was allowed to warm to room temperature and stirred for 18 hours, after which time the mixture was re-cooled to  $0^\circ\text{C}$  and 4-methoxybenzaldehyde (13.6 g, 100 mmol) added with stirring. Hexane (100  $\text{cm}^3$ ) was added, causing the precipitation of triphenylphosphine oxide, which was removed by washing the mixture through a short pad of silica gel ( $\text{CH}_2\text{Cl}_2$ :hexane, v:v, 1;1). The solvent was removed under a reduced pressure to afford a pale yellow crystalline solid (29.2 g, 100%).

Found: C, 36.8; H, 2.5%. Calc. for  $\text{C}_9\text{H}_8\text{OBr}_2$ : C, 37.0; H, 2.8%; m.p.:  $32\text{--}34^\circ\text{C}$  (lit.m.p.:<sup>202</sup>  $31\text{--}33^\circ\text{C}$ );  $\delta_{\text{H}}$  (300 MHz;  $\text{CDCl}_3$ ) 7.51–7.54 (2H, m, Ar), 7.42 (1H, s), 6.89–6.92 (2H, m, Ar), and 3.84 (3H, s, Me);  $\delta_{\text{C}}$  (75.5 MHz;  $\text{CDCl}_3$ ) 159.8 (Ar, quat), 136.4 (vinylic, CH), 129.9 (Ar, CH), 127.9 (Ar, quat), 113.8 (Ar, CH), 87.3 (vinylic, quat), and 55.2 ( $\text{CH}_3$ , OMe);  $m/z$  (EI) 292 ( $\text{M}^+$ , 100%), 277 (20) and 132 (45); HRMS: Found: 291.8913; Calc for  $\text{C}_9\text{H}_8\text{OBr}_2$ : 291.8921.

### 1-Ethynyl-4-methoxybenzene 193



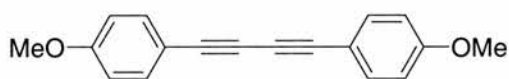
A stirred solution of 1-(2,2-dibromo-1-vinyl)-4-methoxybenzene (29.2 g, 100 mmol) in dry THF (200  $\text{cm}^3$ ) was cooled to  $-78^\circ\text{C}$  under  $\text{N}_2$ . *n*-Butyllithium (2.5 M in hexanes, 100  $\text{cm}^3$ , 250 mmol) was added slowly *via* a syringe and the mixture stirred at  $-78^\circ\text{C}$  for a further 15 minutes before cooling was removed and the mixture allowed to warm to room temperature. The resulting orange/brown solution was cooled to  $0^\circ\text{C}$  and saturated aqueous ammonium chloride solution (50  $\text{cm}^3$ ) was added. THF was evaporated under a reduced pressure and diethyl ether (75  $\text{cm}^3$ ) added. The aqueous layer was extracted



with diethyl ether (2 x 75 cm<sup>3</sup>) and the combined organic extracts were dried (MgSO<sub>4</sub>), filtered and concentrated under reduced pressure to afford the crude product. Flash column chromatography (Et<sub>2</sub>O:hexane, v:v, 2:3) gave the desired product (10.6 g, 80%) as a yellow oil.

Found: C, 81.5; H, 5.8%. Calc. for C<sub>9</sub>H<sub>8</sub>O: C, 81.8; H, 6.1%; m.p.: 28-29 °C (lit.m.p.:<sup>203</sup> 27-28 °C); IR  $\nu_{\max}$  (cm<sup>-1</sup>) 3290m, (alkyne CH), 2956m, (OMe), 2107w, (alkyne C-C);  $\delta_{\text{H}}$  (300 MHz; CDCl<sub>3</sub>) 7.43-7.46 (2H, AA'XX', Ar), 6.83-6.86 (2H, AA'XX', Ar), 3.80 (3H, s, Me), 3.02 (1H, s, acetylenic);  $\delta_{\text{C}}$  (75.5 MHz; CDCl<sub>3</sub>) 160.0 (Ar, quat), 133.6 (Ar, CH), 114.2 (Ar, quat), 113.9 (Ar, CH), 83.6 (acetylinic, quat), 75.7 (acetylinic, CH) and 55.1 (OMe, CH<sub>3</sub>); *m/z* (EI) 132 (M<sup>+</sup>, 100%), 117 (32) and 89 (58); HRMS: Found: 132.0581; Calc. for C<sub>9</sub>H<sub>8</sub>O: 132.0575.

### Bis-(4-methoxyphenyl)-butadiyne 191



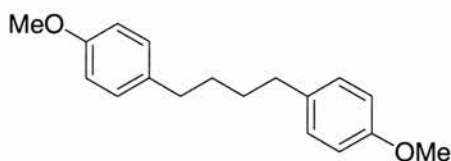
Anhydrous copper (II) acetate (6.18 g, 34.05 mmol) was added to a stirred solution of 1-ethynyl-4-methoxybenzene (4.5 g, 34.05 mmol) in pyridine (150 cm<sup>3</sup>). Air was bubbled through the mixture at room temperature for 3 hours, after which time TLC analysis indicated that no starting material remained. Any insoluble copper salt residues were removed by filtration under vacuum and washed with CH<sub>2</sub>Cl<sub>2</sub> (100 cm<sup>3</sup>). Organic solvents were removed under a reduced pressure and CHCl<sub>3</sub> (100 cm<sup>3</sup>) added. The organic layer was washed with aqueous HCl solution (0.1 M, 3 x 75 cm<sup>3</sup>) to extract any remaining pyridine, followed by saturated aqueous NaHCO<sub>3</sub> solution (3 x 75 cm<sup>3</sup>). The organic layer was dried (MgSO<sub>4</sub>), filtered and concentrated *in vacuo* to afford the crude product as a yellow solid. Recrystallisation (CHCl<sub>3</sub>/hexane) gave clean bis-(4-methoxyphenyl)-butadiyne as a pale yellow, crystalline solid (3.6 g, 80%).

Found: C, 82.7; H, 5.2%. Calc. for C<sub>18</sub>H<sub>14</sub>O<sub>2</sub>: C, 82.4; H, 5.4%; m.p.: 144-145°C (lit. m.p.:<sup>204</sup> 144°C); IR  $\nu_{\max}$  (cm<sup>-1</sup>) 2840m, (OMe), 2137w, (alkyne C-C);  $\delta_{\text{H}}$  (300 MHz; CDCl<sub>3</sub>) 7.56-7.59 (4H, AA'XX', Ar), 6.95-6.98 (4H, AA'XX', Ar) and 3.93 (6H, s, Me);  $\delta_{\text{C}}$  (75.5 MHz; CDCl<sub>3</sub>) 160.2 (Ar, quat), 134.0 (Ar, CH), 114.1 (Ar, CH), 113.9 (Ar, quat),



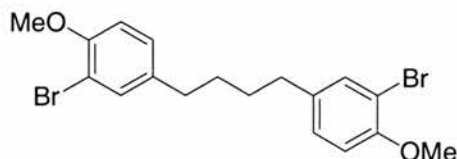
81.2 (acetylenic, quat), 72.9 (acetylenic, quat) and 55.3 (OMe, CH<sub>3</sub>); *m/z* (EI) 262 (M<sup>+</sup>, 100 %), 247 (43) and 219 (10); HRMS: Found: 262.0990; Calc. for C<sub>18</sub>H<sub>14</sub>O<sub>2</sub>: 262.0994.

### 1,4-Bis-(4-methoxyphenyl)-butane 194



A stirred, degassed suspension of 1,4-bis-(4-methoxyphenyl)-butadiyne (4.0 g, 15.25 mmol) and Pd/C (10% w/w, 3.2 g, 3 mmol) in ethyl acetate (200 cm<sup>3</sup>) was subjected to a slight overpressure of hydrogen gas. The mixture was stirred until TLC analysis indicated that the reaction was complete, and was then washed through a short pad of Celite<sup>®</sup> 521 filter agent with ethyl acetate. The solvent was removed under a reduced pressure to afford 1,4-bis-(4-methoxyphenyl)-butane (3.73 g, 92%) as a colourless solid. Found: C, 79.9; H, 8.4%. Calc. for C<sub>18</sub>H<sub>22</sub>O<sub>2</sub>: C, 80.0; H, 8.2%; m.p.: 73-74°C (lit.m.p.:<sup>205</sup> 73-74°C); IR  $\nu_{\max}$  (cm<sup>-1</sup>) 2930m, (CH), 2851m, (OMe);  $\delta_{\text{H}}$  (300 MHz; CDCl<sub>3</sub>) 7.08-7.11 (4H, AA'XX', Ar), 6.82-6.85 (4H, AA'XX', Ar), 3.80 (6H, s, Me), 2.57-2.61 (4H, t, <sup>3</sup>J=7.2 Hz) and 1.61-1.66 (4H, tt, <sup>3</sup>J=3.3 Hz);  $\delta_{\text{C}}$  (75.5 MHz; CDCl<sub>3</sub>) 157.6 (Ar, quat), 134.7 (Ar, quat), 129.2 (Ar, CH), 113.7 (Ar, CH), 55.2 (OMe, CH<sub>3</sub>), 34.9 (CH<sub>2</sub>) and 31.3 (CH<sub>2</sub>); *m/z* (EI) 270 (M<sup>+</sup>, 100%) and 121 (89); HRMS: Found: 270.1613; Calc. for C<sub>18</sub>H<sub>22</sub>O<sub>2</sub>: 270.1620.

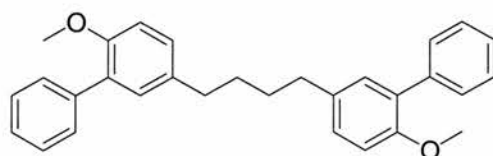
### 1,4-Bis-(3-bromo-4-methoxyphenyl)-butane 195



Bromine (0.8 cm<sup>3</sup>, 14.8 mmol) was added dropwise to a stirred solution of 1,4-bis-(4-methoxyphenyl)-butane (2.0 g, 7.4 mmol) in CHCl<sub>3</sub> (200 cm<sup>3</sup>) under N<sub>2</sub>. Light was excluded from the reaction and it was stirred at room temperature overnight. The solvent was removed under a reduced pressure to afford the crude product as a brown oil. Purification by column chromatography (Et<sub>2</sub>O:hexane, v:v, 1:2) afforded 1,4-bis-(3-bromo-4-methoxyphenyl)-butane (0.6 g, 19%) as a colourless solid.

Found: C, 51.0; H, 4.8%. Calc. for C<sub>18</sub>H<sub>20</sub>O<sub>2</sub>Br<sub>2</sub>: C, 50.5; H, 4.7%; m.p.: 115-116°C; IR  $\nu_{\max}$  (cm<sup>-1</sup>) 2934m, (C-H), 2854m, (OMe), 752w, (CBr);  $\delta_{\text{H}}$  (300 MHz; CDCl<sub>3</sub>) 7.35 (2H, AA'XX', Ar), 7.05 (2H, AA'XX', Ar), 6.82 (2H, d, <sup>3</sup>J=8.7 Hz, Ar), 3.88 (6H, s, Me), 2.55 (4H, m, CH<sub>2</sub>) and 1.61 (4H, m, CH<sub>2</sub>);  $\delta_{\text{C}}$  (75.5 MHz; CDCl<sub>3</sub>) 153.9 (Ar, quat), 136.1 (Ar, quat), 133.1 (Ar, CH), 128.2 (Ar, CH), 111.9 (Ar, CH), 111.4 (Ar, quat), 56.3 (Me, CH<sub>3</sub>), 34.5 (CH<sub>2</sub>) and 30.9 (CH<sub>2</sub>); *m/z* (EI) 428 (M<sup>+</sup>, 84%) and 201 (100); HRMS: Found: 427.9803; Calc. for C<sub>18</sub>H<sub>20</sub>O<sub>2</sub>Br<sub>2</sub>: 427.9810.

### 1,4-Bis-(3-phenyl-4-methoxyphenyl)-butane 196

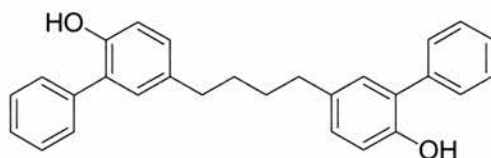


A mixture of 1,4-bis-(3-bromo-4-methoxyphenyl)-butane (0.3 g, 0.7 mmol) and Pd(PPh<sub>3</sub>)<sub>4</sub> (20 mg, 0.014 mmol) in DME (30 cm<sup>3</sup>) was stirred at room temperature and degassed with N<sub>2</sub> for 20 minutes. To this mixture was added a solution of phenylboronic acid (0.21 g, 1.75 mmol) in EtOH (0.5 cm<sup>3</sup>) and Na<sub>2</sub>CO<sub>3</sub> (0.30 g) in H<sub>2</sub>O (2 cm<sup>3</sup>). The reaction mixture was stirred under reflux for 18 hours, and then allowed to cool prior to being poured onto CH<sub>2</sub>Cl<sub>2</sub> (30 cm<sup>3</sup>). The mixture was filtered through Celite<sup>®</sup> 521 filter agent to remove palladium solids, and the filtrate dried (MgSO<sub>4</sub>), filtered before concentration under vacuum afforded the crude product as a black oil. Column

chromatography (Et<sub>2</sub>O:hexane, v:v, 2:3) gave clean 1,4-bis-(3-phenyl-4-methoxyphenyl)-butane (0.24 g, 80%) as a colourless solid.

Found: C, 85.0; H, 6.85%. Calc. for C<sub>30</sub>H<sub>30</sub>O<sub>2</sub>: C, 85.3; H, 7.2%; m.p.: 103-104 °C; IR  $\nu_{\text{max}}$  (cm<sup>-1</sup>) 2930m, (OMe);  $\delta_{\text{H}}$  (300 MHz; CDCl<sub>3</sub>) 7.54 (4H, AA'XX', Ar), 7.33-7.44 (6H, m, Ar), 7.12-7.15 (4H, m, Ar), 6.91 (2H, AA'XX', Ar), 3.80 (6H, s, CH<sub>3</sub>), 2.65 (4H, m, CH<sub>2</sub>) and 1.71 (4H, m, CH<sub>2</sub>);  $\delta_{\text{C}}$  (75.5 MHz; CDCl<sub>3</sub>) 154.5 (Ar, quat), 138.6 (Ar, quat), 134.8 (Ar, quat), 130.9 (Ar, CH), 130.4 (Ar, quat), 129.5 (Ar, CH), 128.2 (Ar, CH), 127.9 (Ar, CH), 126.8 (Ar, CH), 111.1 (Ar, CH), 55.7 (CH<sub>3</sub>), 34.9 (CH<sub>2</sub>) and 31.3 (CH<sub>2</sub>); *m/z* (EI) 422 (M<sup>+</sup>, 90), 197 (100); HRMS: Found: 422.2240; Calc. for C<sub>30</sub>H<sub>30</sub>O<sub>2</sub>: 422.2246.

### 1,4-Bis-(3-phenyl-4-hydroxyphenyl)-butane 189



1,4-Bis-(2-phenyl-3-methoxyphenyl)-butane (0.1 g, 0.24 mmol) was stirred in dry CH<sub>2</sub>Cl<sub>2</sub> (20 cm<sup>3</sup>) at -78 °C under N<sub>2</sub>. Boron tribromide (1 M in CH<sub>2</sub>Cl<sub>2</sub>, 0.6 cm<sup>3</sup>, 0.6 mmol) was added dropwise, and the mixture allowed to warm to room temperature over a period of 2 hours. The mixture was cooled in an ice bath, and MeOH (10 cm<sup>3</sup>) was added slowly to quench any excess BBr<sub>3</sub>. All solvents were removed on a water aspirator, and CH<sub>2</sub>Cl<sub>2</sub> (20 cm<sup>3</sup>) added to the oily brown residue. The solution was washed with water (20 cm<sup>3</sup>) and the aqueous layer was extracted with CH<sub>2</sub>Cl<sub>2</sub> (3 x 20 cm<sup>3</sup>). The combined organic extracts were dried (MgSO<sub>4</sub>), filtered and concentrated under a reduced pressure to afford the crude product as a brown oil. Flash column chromatography (Et<sub>2</sub>O:hexane, v:v, 1:1) to remove baseline impurities gave 1,4-bis-(2-phenyl-3-hydroxyphenyl)-butane (80 mg, 84%) as a brown oil.

$\delta_{\text{H}}$  (300 MHz;  $\text{CDCl}_3$ ) 7.26-7.39 (10H, m, Ar), 6.96-6.99 (4H, m, Ar), 6.79-6.83 (2H, m, Ar), 5.01 (2H, br s, OH), 2.46-2.54 (4H, m,  $\text{CH}_2$ ) and 1.54-1.61 (4H, m,  $\text{CH}_2$ );  $\delta_{\text{C}}$  (75.5 MHz;  $\text{CDCl}_3$ ) 150.3 (Ar, quat), 137.3 (Ar, quat), 134.9 (Ar, quat), 131.5 (Ar, CH), 130.0 (Ar, CH), 129.2 (Ar, CH), 128.9 (Ar, CH), 127.8 (Ar, quat), 127.7 (Ar, CH), 115.6 (Ar, CH), 34.9 ( $\text{CH}_2$ ) and 31.2 ( $\text{CH}_2$ );  $m/z$  (EI) 394 ( $\text{M}^+$ , 66%) and 183 (100); HRMS: Found: 394.1922; Calc. for  $\text{C}_{28}\text{H}_{26}\text{O}_2$ : 394.1933.

## 7 References and Footnotes

- (1) F. L. Carter, in *US Naval Research Laboratory Memorandum Report No. 3960*; L. B. Lockhardt (Ed), Washington DC, **1979**, p. 121; J. R. Barker, *Hybrid Circuits* **1987**, *14*(9), 19; D. Haarer, *Angew. Chem., Int. Ed. Engl. Adv. Mater.*, **1989**, *28*, 1544; R. C. Haddon, A. A. Lamola, *Proc. Natl. Acad. Sci.*, **1985**, *82*, 1874; J. S. Miller, *Adv. Mater.* **1990**, *2*, 378, 495, 601; H. Kuhn in *Molecular Electronics*, F. T. Hong (Ed), Plenum Publishing Corporation, New York, **1989**, p. 5.
- (2) J.-M. Lehn, *Chem. Eur. J.*, **2000**, *6*, 2097; M. Albrecht, *J. Inc. Phen. Macro. Chem.*, **2000**, *36*, 127; S. Leininger, B. Olenyuk, P. J. Stang, *Chem. Rev.*, **2000**, *100*, 853; P. J. Stang, *Chem. Eur. J.*, **1998**, *4*, 19; D. Philp, J. F. Stoddart, *Angew. Chem., Int. Ed. Engl.*, **1996**, *35*, 1154; J.-M. Lehn, J. L. Atwood, J. E. D. Davies, D. D. MacNicol, F. Vogtle, Eds, *Comprehensive Supramolecular Chemistry*, **1996**, Pergamon, Oxford; D. S. Lawrence, T. Jiang, M. Levett *Chem. Rev.*, **1995**, *95*, 2229; J. S. Lindsey, *New J. Chem.*, **1991**, *15*, 153; G. M. Whitesides, J. P. Mathias, C. T. Seto, *Science*, **1991**, *254*, 1312.
- (3) Y. Xia, G. M. Whitesides, *Angew. Chem., Int. Ed. Engl.*, **1998**, *37*, 550; B. Deal, J. Talbot, *Electrochem. Soc. Interface*, **1997**, *6*, 18.
- (4) R. W. Armstrong, J.-M. Beau, S. H. Cheon, W. J. Christ, H. Fujioka, W.-H. Ham, L. D. Hawkins, H. Jin, S. H. Kang, Y. Kishi, M. J. Martinelli, W. W. McWhorter, Jr., M. Mizuno, M. Nakata, A. E. Stutz, F. X. Talamas, M. Taniguchi, J. A. Tino, K. Ueda, J. Uenishi, J. B. White, M. Yonaga, *J. Am. Chem. Soc.*, **1989**, *111*, 7525.
- (5) A. E. Eschenmoser, C. E. Wintner, *Science*, **1977**, *196*, 1410; R. B. Woodward, *Pure Appl. Chem.*, **1973**, *33*, 145.
- (6) P. L. Felgner, *J. Gene Med.*, **1999**, *1*, 290; S. P. Vyas, V. Jaitely, P. Kanaujia, *Pharmazie*, **1997**, *52*, 259.
- (7) L. Stryer, *Biochemistry*, W. H. Freeman and Co., New York, 3<sup>rd</sup> Ed., **1988**, Ch. 2.
- (8) D. J. Brockwell, D. A. Smith, S. E. Radford, *Curr. Opin. Struct. Biol.*, **2000**, *10*, 16; S. W. Englander, *Annu. Rev. Bioph. Biom.*, **2000**, *29*, 213; O. B. Ptitsyn, A. V. Finkelstein, C. M. Dobson, *Molecular Biology*, **1999**, *33*, 893; S. E. Radford,

- C. M. Dobson, *Cell*, **1999**, *97*, 291; C. M. Dobson, A. Sâli, M. Karplus, *Angew. Chem., Int. Ed.*, **1998**, *37*, 868.
- (9) D. H. Cribbs, B. Y. Azizeh, C. W. Cotman, F. M. LaFerla, *Biochemistry*, **2000**, *39*, 5988; C. W. Cotman, *Ann. New York Acad. Sci.*, **1997**, *814*, 1.
- (10) V. Percec, *Pure Appl. Chem.*, **1996**, *10*, 1479.
- (11) A. Klug, *Angew. Chem., Int. Ed. Engl.*, **1983**, *22*, 565.
- (12) A. Klug, *Phil. Trans. R. Soc. Lond. B*, **1999**, *354*, 531; P. J. G. Butler, *ibid.*, **1999**, *354*, 537.
- (13) L. Stryer, in "Biochemistry", 3<sup>rd</sup> ed., **1988**, W. H. Freeman and Co., New York, p.855.
- (14) A. Vianelli, G. R. Wang, M. Gingery, R. L. Duda, F. A. Eiserling, E. B. Goldberg, *J. Bacteriology*, **2000**, *182*, 680; G. R. Wang, A. Vianelli, E. B. Goldberg, *ibid.*, **2000**, *182*, 672.
- (15) J.-M. Lehn, *Angew. Chem., Int. Ed. Engl.*, **1988**, *27*, 89.
- (16) D. J. Cram, *Angew. Chem., Int. Ed. Engl.*, **1988**, *27*, 1009.
- (17) M. Yamamoto, M. Takeuchi, S. Shinkai, *Tetrahedron. Lett.*, **2000**, *41*, 3137; S. Leininger, M. Schmitz, P. J. Stang, *Org. Lett.*, **1999**, *1*, 1921; R. Anwander, *Angew. Chem., Int. Ed.*, **1998**, *37*, 599.
- (18) M. Greenwald, D. Wessely, E. Katz, I. Willner, Y. Cohen, *J. Org. Chem.*, **2000**, *65*, 1050; M. Elhabiri, R. Scopelliti, J.-C. G. Bünzli, C. Piguet, *J. Am. Chem. Soc.*, **1999**, *121*, 10747; N. Martin, J.-C. G. Bünzli, V. McKee, C. Piguet, G. Hopfgartner, *Inorg. Chem.*, **1998**, *37*, 577; C. Provent, E. Rivara-Minten, S. Hewage, G. Brunner, A. F. Williams, *Chem. Eur. J.*, **1999**, *5*, 3487.
- (19) W. Yue, R. Bishop, M. L. Scudder, D. C. Craig, *Chem. Lett.*, **1998**, 803; O. Mamula, A. von Zelewsky, G. Bernardinalli, *Angew. Chem., Int. Ed.*, **1998**, *37*, 290; B. Hasenknopf, J.-M. Lehn, N. Boumediene, A. Dupont-Gervaise, A. van Dorsselaer, B. Kniessel, D. Fenske, *J. Am. Chem. Soc.*, **1997**, *119*, 10956; B. Hasenknopf, J.-M. Lehn, G. Baum, B. O. Kniessel, D. Fenske, *Angew. Chem., Int. Ed. Engl.*, **1996**, *35*, 1838.
- (20) M. Fujita, *Acc. Chem. Res.*, **1999**, *32*, 53; C. P. McArdle, M. J. Irwin, M. C. Jennings, R. J. Puddephat, *Angew. Chem., Int. Ed.*, **1999**, *38*, 3376; D. G. Hamilton, N. Feeder, L. Prodi, S. J. Teat, W. Clegg, J. K. M. Sanders, *J. Am. Chem. Soc.*, **1998**, *120*, 1096.
- (21) P. Lipkowski, A. Bielejewska, H. Kooijman, A. L. Spek, P. Timmerman, D. N. Reinhoudt, *Chem. Commun*, **1999**, 1311; L. R. MacGillivray, R. H.

- Groeneman, J. L. Atwood, *J. Am. Chem. Soc.*, **1998**, *120*, 2676; P. N. W. Baxter, J.-M. Lehn, J. Fischer, M.-T. Youinou, *Angew. Chem., Int. Ed. Engl.*, **1994**, *33*, 2284.
- (22) T. Kusakawa, M. Fujita, *J. Am. Chem. Soc.*, **1999**, *121*, 1397; P. Jacopozzi, E. Dalcanale, *Angew. Chem., Int. Ed. Engl.*, **1997**, *36*, 613.
- (23) P. N. Taylor, H. L. Anderson, *J. Am. Chem. Soc.*, **1999**, *121*, 11538; M. Fujita, O. Sasaki, K. Watanabe, K. Ogura, K. Yamaguchi, *New J. Chem.*, **1998**, *22*, 189.
- (24) V. V. Narayanan, E. C. Wiener, *Macromol.*, **2000**, *33*, 3944; T. Emrick, J. M. J. Fréchet, *Curr. Opin. Coll. Inter. Sci.*, **1999**, *4*, 15; M. Kawa, J. M. J. Fréchet, *Chem. Mater.*, **1998**, *10*, 286; F. Zeng, S. C. Zimmerman, *Chem. Rev.*, **1997**, *97*, 1681, and references therein.
- (25) R. W. Saalfrank, I. Bernt, *Curr. Opin. Solid State Mater. Sci.*, **1998**, *3*, 407.
- (26) P. N. W. Baxter, J.-M. Lehn, B. O. Kniessel, D. Fenske, *Angew. Chem., Int. Ed. Engl.*, **1997**, *36*, 1978.
- (27) D. P. Funeriu, J.-M. Lehn, G. Baum, D. Fenske, *Chem. Eur. J.*, **1997**, *3*, 99.
- (28) B. Hasenknopf, J.-M. Lehn, N. Boumediene, E. Leize, A. van Dorsselaer, *Angew. Chem., Int. Ed.*, **1998**, *37*, 3265.
- (29) B. Hasenknopf, J.-M. Lehn, B.O. Kneisel, G. Baum, D. Fenske, *Angew. Chem., Int. Ed. Engl.*, **1996**, *35*, 1838.
- (30) B. Hasenknopf, J.-M. Lehn, N. Boumediene, A. Dupont-Gervais, A. van Dorsselaer, B.O. Kneisel, D. Fenske, *J. Am. Chem. Soc.*, **1997**, *119*, 10956. See also V. Berl, M.J. Krische, I. Huc, J.-M. Lehn, M. Schmutz, *Chem. Eur. J.*, **2000**, *6*, 1938.
- (31) M. Fujita, *Chem. Soc. Rev.*, **1998**, *27*, 417; B. Linton, A. D. Hamilton, *Chem. Rev.*, **1997**, *97*, 1669.
- (32) X. Chi, A. J. Guerin, R. A. Haycock, C. A. Hunter, L. D. Sarson, *J. Chem. Soc., Chem. Commun.*, **1995**, 2563.
- (33) M. Fujita, O. Sasaki, T. Mitsuhashi, T. Fujita, J. Yazaki, K. Yamaguchi, K. Ogura, *Chem. Commun.*, **1996**, 1535.
- (34) S. B. Lee, S. Hwang, D. S. Chung, H. Yun, J.-I. Hong, *Tetrahedron Lett.*, **1998**, *39*, 873.
- (35) F. Ibukuro, T. Kusakawa, M. Fujita, *J. Am. Chem. Soc.*, **1998**, *120*, 8561.



- (36) S. Hiraoka, Y. Kubota, M. Fujita, *Chem. Commun.*, **2000**, 1509; K. Umemoto, K. Yamaguchi, M. Fujita, *J. Am. Chem. Soc.*, **2000**, *122*, 7150; S. Hiraoka, M. Fujita, *J. Am. Chem. Soc.*, **1999**, *121*, 10239.
- (37) R. P. Sijbesma, E. W. Meijer, *Curr. Opin. Colloid. Inter. Sci.*, **1999**, *4*, 24; M. M. Conn, J. Rebek, Jr., *Chem Rev.*, **1997**, *97*, 1647.
- (38) S. C. Zimmerman, F. Zeng, D. E. C. Reichert, S. V. Kolotuchin, *Science*, **1996**, *271*, 1095.
- (39) S. V. Kolotuchin, S. C. Zimmerman, *J. Am. Chem. Soc.*, **1998**, *120*, 9092.
- (40) R. H. Vreekamp, J. P. M. van Duynhoven, M. Hubert, W. Verboom, D. N. Reinhoudt, *Angew. Chem., Int. Ed. Engl.*, **1996**, *35*, 1215; P. Timmerman, R. H. Vreekamp, R. Hulst, W. Verboon, D. N. Reinhoudt, K. Rissanen, K. A. Udachin, J. Ripmeester, *Chem. Eur. J.*, **1997**, *3*, 1823; K. A. Joliffe, M. C. Calama, R. Fokkens, N. M. M. Nibbering, P. Timmerman, D. N. Reinhoudt, *Angew. Chem., Int. Ed.*, **1998**, *37*, 1247.
- (41) G. M. Whitesides, E. E. Simanek, J. P. Mathias, C. T. Seto, D. N. Chin, M. Mammen, D. M. Gordon, *Acc. Chem. Res.*, **1995**, *28*, 37.
- (42) F. Cardullo, M. C. Calama, R. H. M. Snellink-Ruël, J.-L. Weidmann, A. Bielejewska, R. Fokkens, N. M. M. Nibbering, P. Timmerman, D. N. Reinhoudt, *Chem. Commun.*, **2000**, 367.
- (43) H.-A. Klok, K. A. Joliffe, C. L. Schauer, L. J. Prins, J. P. Spatz, M. Möller, P. Timmerman, D. N. Reinhoudt, *J. Am. Chem. Soc.*, **1999**, *121*, 7154.
- (44) J. M. Rivera, T. Martín, J. Rebek, Jr., *Science*, **1998**, *279*, 1021; R. S. Meissner, X. Garcias, S. Mecozzi, J. Rebek, Jr., *J. Am. Chem. Soc.*, **1997**, *119*, 77.
- (45) Y. Tokunaga, D. M. Rudkevich, J. Rebek, Jr., *Angew. Chem., Int. Ed. Engl.*, **1997**, *36*, 2656.
- (46) J. Kang, J. Rebek, Jr., *Nature*, **1996**, *382*, 239.
- (47) J. Kang, J. Santamaría, G. Hilmersson, J. Rebek, Jr., *J. Am. Chem. Soc.*, **1998**, *120*, 3650; J. Kang, J. Rebek, Jr., *Nature*, **1997**, *385*, 50.
- (48) J. Kang, J. Santamaría, G. Hilmersson, J. Rebek, Jr., *J. Am. Chem. Soc.*, **1998**, *120*, 7389.
- (49) M. Yoshizawa, T. Kusukawa, M. Fujita, K. Yamaguchi, *J. Am. Chem. Soc.*, **2000**, *122*, 6311.
- (50) R. H. Baney, M. Itoh, A. Sakakibara, T. Suzuki, *Chem. Rev.*, **1995**, *95*, 1409.

- (51) T. Kusukawa, M. Fujita, *Angew. Chem., Int. Ed.*, **1998**, *37*, 3142; F. Ibukuro, T. Kusukawa, M. Fujita, *J. Am. Chem. Soc.*, **1998**, *120*, 8561; M. Fujita, D. Oguro, M. Miyazawa, H. Oka, K. Yamaguchi, K. Ogura, *Nature*, **1995**, *378*, 469.
- (52) Fujita has also described the “ship-in-a-bottle” formation of stable hydrophobic dimers of azobenzenes in a similar coordination cage. See T. Kusukawa, M. Fujita, *J. Am. Chem. Soc.*, **1999**, *121*, 1397.
- (53) H. Ito, T. Kusukawa, M. Fujita, *Chem. Lett.*, **2000**, *6*, 598.
- (54) M. O. Vysotsky, I. Thondorf, V. Böhmer, *Angew. Chem., Int. Ed.*, **2000**, *39*, 1264; L. Frish, S. E. Matthews, V. Böhmer, Y. Cohen, *J. Chem. Soc., Perkin Trans. 2*, **1999**, 669; O. Mogck, M. Pons, V. Böhmer, W. Vogt, *J. Am. Chem. Soc.*, **1997**, *119*, 5706; O. Mogck, E. F. Paulus, V. Böhmer, I. Thondorf, W. Vogt, *Chem. Commun.*, **1996**, 2533 O. Mogck, V. Böhmer, W. Vogt, *Tetrahedron*, **1996**, *52*, 8489. See also A. Shivanyuk, E. F. Paulus, V. Böhmer, *Angew. Chem., Int. Ed.*, **1999**, *38*, 2906.
- (55) J. J. González, R. Ferdani, E. Albertini, J. M. Blasco, A. Arduini, A. Pochini, P. Prados, J. de Mendoza, *Chem. Eur. J.*, **2000**, *6*, 73; J. J. González, P. Prados, J. de Mendoza, *Angew. Chem., Int. Ed.*, **1999**, *38*, 525; J. de Mendoza, *Chem. Eur. J.*, **1998**, *4*, 1373.
- (56) D. Pörschke, M. J. Eigen, *J. Mol. Biol.*, **1971**, *62*, 361; M. E. Craig, D. M. Crothers, P. Doty, *ibid.*, **1971**, *62*, 383.
- (57) S. J. Rowan, J. K. M. Sanders, *J. Org. Chem.*, **1998**, *63*, 1536; S. J. Rowan, P. A. Brady, J. K. M. Sanders, *Angew. Chem., Int. Ed. Engl.*, **1996**, *35*, 2143.
- (58) G. Ercolani, *J. Phys. Chem. B*, **1998**, *102*, 5699.
- (59) S. J. Rowan, P. A. Brady, J. K. M. Sanders, *Tetrahedron Lett.*, **1996**, *37*, 6013.
- (60) E. C. Constable, *Comprehensive Supramolecular Chemistry*, Vol. 9, J. L. Atwood, J. E. D. Davies, D. D. MacNicol, F. Vögtle, Eds., Elsevier, New York, **1996**, p.218.
- (61) T. W. Bell, H. Jousselin, *Nature*, **1994**, *367*, 441.
- (62) J. K. Judice, S. J. Keipert, D. J. Cram, *J. Chem. Soc., Chem. Commun.*, **1993**, 1323.
- (63) D. Philp, A. Robertson, *Chem. Commun*, **1998**, 879; D. Philp, C. A. Booth, *Tetrahedron Lett.*, **1998**, *39*, 6987; A. Robertson, D. Philp, N. Spencer, *Tetrahedron*, **1999**, *55*, 11365.

- (64) R. Bennes, D. Philp, N. Spencer, B. M. Kariuki, K. D. M. Harris, *Org. Lett.*, **1999**, *1*, 1087.
- (65) T. C. Bruice, F. C. Lightstone, *Acc. Chem. Res.*, **1999**, *32*, 127; A. J. Kirby, *Philos. Trans. R. Soc. London A*, **1993**, *345*, 67; F. M. Menger, *Acc. Chem. Res.*, **1993**, *26*, 206; M. I. Page, W. P. Jencks, *Proc. Natl. Acad. Sci. USA*, **1971**, *68*, 1678.
- (66) S. J. Rowan, D. G. Hamilton, P. A. Brady, J. K. M. Sanders, *J. Am. Chem. Soc.*, **1997**, *119*, 2578.
- (67) R. Krämer, J.-M. Lehn, A. Marquis-Rigault, *Proc. Natl. Acad. Sci. USA*, **1993**, *90*, 5394.
- (68) S. J. Rowan, D. J. Reynolds, J. K. M. Sanders, *J. Org. Chem.*, **1999**, *64*, 5804.
- (69) P. A. Brady, R. P. Bonar-Law, S. J. Rowan, C. J. Suckling, J. K. M. Sanders, *Chem. Commun.*, **1996**, 319.
- (70) P. A. Brady, J. K. M. Sanders, *J. Chem. Soc., Perkin Trans. 1*, **1997**, 3237.
- (71) J. Ipaktschi, R. Hosseinzadeh, P. Schlaf, T. Eckert *Helv. Chim. Acta*, **2000**, *83*, 1224; J. Ipaktschi, R. Hosseinzadeh, P. Schlaf, *Angew. Chem., Int. Ed.*, **1999**, *38*, 1658; J. Ipaktschi, R. Hosseinzadeh, P. Schlaf, E. Dreiseidler, R. Goddard, *Helv. Chim. Acta*, **1998**, *81*, 1821.
- (72) S.-W. T. Chang, J. S. Stewouwer, J. Hao, *J. Org. Chem.*, **1999**, *64*, 334.
- (73) Recent reviews include; D. R. Liu, P. G. Schultz, *Angew. Chem., Int. Ed.*, **1999**, *38*, 36; B. Jandeleit, D. J. Schaefer, T. S. Powers, H. W. Turner, W. H. Weinberg, *Angew. Chem., Int. Ed.*, **1999**, *38*, 2495; R. C. D. Brown, *J. Chem. Soc., Perkin Trans. 1*, **1998**, 3293; J. W. Szostak, (ed.), *Chem. Rev.*, **1997**, *97*, 1; F. Balkenhohl, C. von dem Bussche-Hünnefeld, A. Lansky, C. Zechel, *Angew. Chem., Int. Ed. Engl.*, **1996**, *35*, 2288; A. W. Czarnik, J. A. Ellman, eds., *Acc. Chem. Res., Special Issue*, **1996**, *29*, 112.
- (74) M. Albrecht, *J. Inc. Phen. Macro. Chem.*, **2000**, *36*, 127; G. R. L. Cousins, S.-A. Poulsen, J. K. M. Sanders, *Curr. Opin. Chem. Biol.*, **2000**, *4*, 270; B. Klekota, B. L. Miller, *Trends Biotechnol.*, **1999**, *17*, 205; A. Ganesan, *Angew. Chem., Int. Ed.*, **1998**, *37*, 2828.
- (75) For a review of selection techniques see: P. A. Brady, J. K. M. Sanders, *Chem. Soc. Rev.*, **1997**, *26*, 327.
- (76) This process can be considered as similar to induced fit selection of substrates by enzymes. The enzyme may only have a structure complementary to the

- substrate transition site after binding. See A. Fersht, *Structure and Mechanism in Protein Science*, **1999**, 2<sup>nd</sup> ed., W. H. Freeman and Co., New York, p. 369.
- (77) J.-M. Lehn, *Chem. Eur. J.*, **1999**, *5*, 2455. For reviews see Ref. 74.
- (78) A. V. Eliseev, M. I. Nelen, *J. Am. Chem. Soc.*, **1997**, *119*, 1147.
- (79) A. V. Eliseev, M. I. Nelen, *Chem. Eur. J.*, **1998**, *4*, 825.
- (80) H. Hioki, W. C. Still, *J. Org. Chem.*, **1998**, *63*, 904; M. T. Burger, P. A. Bartlett, *J. Am. Chem. Soc.*, **1997**, *119*, 12697; P. N. W. Baxter, J.-M. Lehn, K. Rissanen, *Chem. Commun*, **1997**, 1323.
- (81) H. Hioki, W. C. Still, *J. Org. Chem.*, **1998**, *63*, 904; M. T. Reetz, *Angew. Chem., Int. Ed.*, **2001**, *40*, 285.
- (82) I. Huc, J.-M. Lehn, *Proc. Natl. Acad. Sci. USA*, **1997**, *94*, 2106. See also O. Ramström, *ChemBioChem*, **2000**, *1*, 41.
- (83) T. Mann, D. Keilin, *Nature*, **1940**, *146*, 164; S. J. Dogson, R. E. Tahian, G. Gros, N. D. Cartor, Eds., *The Carbonic Anhydrases: Cellular Physiology and Molecular Genetics*, **1991**, Plenum Publishing, New York.
- (84) R. L. E. Furlan, G. R. L. Cousins, J. K. M. Sanders, *Chem. Commun.*, **2000**, 1761; G. R. L. Cousins, S.-A. Poulsen, J. K. M. Sanders, *Chem. Commun.*, **1999**, 1575.
- (85) G. R. L. Cousins, R. L. E. Furlan, Y.-F. Ng, J. E. Redman, J. K. M. Sanders, *Angew. Chem., Int. Ed.*, **2001**, *40*, 423.
- (86) G. Kaiser, J. K. M. Sanders, *Chem. Commun.*, **2000**, 1763. See also S. Otto, R. L. E. Furlan, J. K. M. Sanders, *J. Am. Chem. Soc.*, **2000**, *122*, 12063.
- (87) M. C. Calama, P. Timmerman, D. N. Reinhoudt, *Angew. Chem. Int. Ed.*, **2000**, *39*, 755; F. Cardullo, M. C. Calama, B. H. M. Snellink-Ruël, J.-L. Weidman, A. Bielejewska, R. Fokkens, N. M. M. Nibbering, P. Timmerman, D. N. Reinhoudt, *Chem. Commun.*, **2000**, 367; M. C. Calama, R. Hulst, R. Fokkens, N. M. M. Nibbering, P. Timmerman, D. N. Reinhoudt, *Chem. Commun.*, **1998**, 1021.
- (88) M. Albrecht, O. Blau, R. Fröhlich, *Chem. Eur. J.*, **1999**, *5*, 48.
- (89) B. Klekota, B. L. Miller, *Tetrahedron*, **1999**, *55*, 11687; B. Klekota, M. H. Hammond, B. L. Miller, *Tetrahedron Lett.*, **1997**, *38*, 8639.
- (90) J. S. Moore, N. W. Zimmerman, *Org. Lett.*, **2000**, *2*, 915.
- (91) P. Kazmaier, N. Chopra, *MRS Bulletin*, **2000**, 30; D. L. Feldheim, C. D. Keating, *Chem. Soc. Rev.*, **1998**, *27*, 1 and references therein.

- (92) J. F. Stoddart, Ed., *Acc. Chem. Res.*, **2001**, *34*, "Molecular Machines" special issue, 409-522; V. Balzani, M. Gómez-López, J. F. Stoddart, *Acc. Chem. Res.*, **1998**, *31*, 405.
- (93) R. Henderson, *Ciba Found. Symp.*, **1998**, *213*, 36.
- (94) W. Wang, *Annu. Rev. Physiol.*, **1997**, *59*, 413.
- (95) H. Rapaport, H. S. Kim, K. Kjaer, P. B. Howes, S. Cohen, J. Als-Nielsen, M. R. Ghadiri, L. Leiserowitz, M. Lahav, *J. Am. Chem. Soc.*, **1999**, *121*, 1186; J. D. Hartgerink, T. D. Clark, M. R. Ghadiri, *Chem. Eur. J.*, **1998**, *4*, 1367.
- (96) J. D. Hartgerink, J. R. Granja, R. A. Milligan, M. R. Ghadiri, *J. Am. Chem. Soc.*, **1996**, *118*, 43.
- (97) T. D. Clark, L. K. Buehler, M. R. Ghadiri, *J. Am. Chem. Soc.*, **1998**, *120*, 651.
- (98) H. S. Kim, J. D. Hartgerink, M. R. Ghadiri, *J. Am. Chem. Soc.*, **1998**, *120*, 4417.
- (99) R. M. Metzger, *J. Mater. Chem.*, **2000**, *10*, 55; J. Chen, M. A. Reed, A. M. Rawlett, J. M. Tour, *Science*, **1999**, *286*, 1550.
- (100) *Molecular Catenanes, Rotaxanes and Knots – A Journey through the World of Molecular Topology*, J.-P. Sauvage, C. O. Dietrich-Buchecker (Eds.), VCH, Weinheim, **1999**; D. B. Amabilino, J. F. Stoddart, *Chem. Rev.*, **1995**, *95*, 2725; R. Jäger, F. Vögtle, *Angew. Chem., Int. Ed. Engl.*, **1997**, *36*, 930; G. J. Clarkson, D. A. Leigh, D. A. Smith, *Curr. Opin. Solid State Mater. Sci.*, **1998**, *3*, 579; D. A. Leigh, A. Murphy, *Chem. Ind. (London)*, **1999**, 178; G. A. Breault, C. A. Hunter, P. C. Mayers, *Tetrahedron*, **1999**, *55*, 5265.
- (101) For a review see; V. Balzani, A. Credi, F. M. Raymo, J. F. Stoddart, *Angew. Chem., Int. Ed.*, **2000**, *39*, 3348.
- (102) N. Armaroli, V. Balzani, J.-P. Collin, P. Gavina, J.-P. Sauvage, B. Ventura, *J. Am. Chem. Soc.*, **1999**, *121*, 4397; P. Gavina, J.-P. Sauvage, *Tetrahedron Lett.*, **1997**, *38*, 3521; A. Livoreil, J.-P. Sauvage, N. Armaroli, V. Balzani, L. Flamigni, B. Ventura, *J. Am. Chem. Soc.*, **1997**, *119*, 12114; D. J. Cárdenas, A. Livoreil, J.-P. Sauvage, *J. Am. Chem. Soc.*, **1996**, *118*, 11980.
- (103) V. Bermudez, N. Capron, T. Gase, F. G. Gatti, F. Kajzar, D. A. Leigh, F. Zerbetto, S. W. Zhang, *Nature*, **2000**, *406*, 608; D. A. Leigh, A. Troisi, F. Zerbetto, *Angew. Chem., Int. Ed.*, **2000**, *39*, 350; P. Ceroni, D. A. Leigh, L. Mottier, F. Paolucci, S. Roffia, D. Tetard, F. Zerbetto, *J. Phys. Chem. B*, **1999**, *103*, 10171.



- (104) H. Murakami, A. Kawabuchi, K. Kotoo, M. Kunitake, N. Nakashima, *J. Am. Chem. Soc.*, **1997**, *119*, 7605; M. J. Gunther, M. R. Johnston, *J. Chem. Soc., Chem. Commun.*, **1994**, 829. See also B. L. Feringa, W. F. Jager, B. de Lange, A. W. Meijer, *J. Am. Chem. Soc.*, **1991**, *113*, 5468; N. Koumura, R. W. J. Zijlstra, R. A. van Delden, N. Harada, B. L. Feringa, *Nature*, **1999**, *401*, 152.
- (105) S. J. Cantrill, A. R. Pease, J. F. Stoddart, *J. Chem. Soc., Dalton Trans.*, **2000**, 3715; F. M. Raymo, J. F. Stoddart, *Chem. Rev.*, **1999**, *99*, 1643; V. Balzani, M. Gómez-López, J. F. Stoddart, *Acc. Chem. Res.*, **1998**, *31*, 405.
- (106) V. Balzani, A. Credi, G. Mattersteig, O. A. Matthews, F. M. Raymo, J. F. Stoddart, M. Venturi, A. J. P. White, D. J. Williams, *J. Org. Chem.*, **2000**, *65*, 1924; M. Asakawa, P. R. Ashton, V. Balzani, S. E. Boyd, A. Credi, G. Mattersteig, S. Menzer, M. Montalti, F. M. Raymo, C. Ruffilli, J. F. Stoddart, M. Venturi, D. J. Williams, *Eur. J. Org. Chem.*, **1999**, 985.
- (107) C. P. Collier, G. Mattersteig, E. W. Wong, Y. Luo, K. Beverly, J. Sampaio, F. M. Raymo, J. F. Stoddart, J. R. Heath, *Science*, **2000**, *289*, 1172. See also C. P. Collier, E. W. Wong, M. Belohradsky, F. M. Raymo, J. F. Stoddart, P. J. Kuekes, R. S. Williams, J. R. Heath, *Science*, **1999**, *285*, 391.
- (108) W. Shenton, S. A. Davies, S. Mann, *Adv. Mater.*, **1999**, *11*, 449.
- (109) M. J. Dabrowski, W. M. Atkins, *Adv. Mater.*, **1995**, *7*, 1015.
- (110) I. S. Choi, M. Weck, B. Xu, N. L. Jeon, G. M. Whitesides, *Langmuir*, **2000**, *16*, 2997. W. T. S. Huck, J. Tien, G. M. Whitesides, *J. Am. Chem. Soc.*, **1998**, *120*, 8267. N. Bowden, A. Terfort, J. Carbeck, G. M. Whitesides, *Science*, **1997**, *276*, 233.
- (111) A. Terfort, N. Bowden, G. M. Whitesides, *Nature*, **1997**, *386*, 162.
- (112) N. Bowden, I. S. Choi, B. A. Grzybowski, G. M. Whitesides, *J. Am. Chem. Soc.*, **1999**, *121*, 5373.
- (113) I. S. Choi, N. Bowden, G. M. Whitesides, *Angew. Chem., Int. Ed.*, **1999**, *38*, 3078. See also I. S. Choi, M. Weck, N. L. Jeon, G. M. Whitesides *J. Am. Chem. Soc.* **2000**, *122*, 11997.
- (114) I. S. Choi, N. Bowden, G. M. Whitesides, *J. Am. Chem. Soc.*, **1999**, *121*, 1754.
- (115) P. M. Maitlis, *Chem. Rev.*, **1962**, *62*, 245; M. J. S. Dewar, *Prog. Boron Chem.*, **1964**, *1*, 235.
- (116) M. J. S. Dewar, V. P. Kubba, R. Pettit, *J. Chem. Soc.*, **1958**, 3073.
- (117) M. J. S. Dewar, V. P. Kubba, *Tetrahedron*, **1959**, *7*, 213.
- (118) M. J. S. Dewar, R. Dietz, *J. Chem. Soc.*, **1959**, 2728.

- (119) S. S. Chissick, M. J. S. Dewar, P. M. Maitlis, *Tetrahedron Lett.*, **1960**, 8.
- (120) S. S. Chissick, M. J. S. Dewar, P. M. Maitlis, *J. Am. Chem. Soc.*, **1959**, *81*, 6329; S. S. Chissick, M. J. S. Dewar, P. M. Maitlis, *J. Am. Chem. Soc.*, **1961**, *83*, 2708.
- (121) M. J. S. Dewar, C. Kaneko, M. K. Bhattacharjee, *J. Am. Chem. Soc.*, **1962**, *84*, 4884.
- (122) M. J. S. Dewar, G. J. Gleicher, B. P. Robinson, *J. Am. Chem. Soc.*, **1964**, *86*, 5698.
- (123) G. C. Culling, M. J. S. Dewar, P. A. Marr, *J. Am. Chem. Soc.*, **1964**, *86*, 1125.
- (124) E. Nyilas, A. H. Soloway, *J. Am. Chem. Soc.*, **1959**, *81*, 2681; M. J. S. Dewar, J. Hashmall, V. P. Kubba, *J. Org. Chem.*, **1964**, *29*, 1755.
- (125) M. J. S. Dewar, R. Dietz, *Tetrahedron Lett.*, **1959**, 21.
- (126) M. J. S. Dewar, R. Dietz, V. P. Kubba, A. R. Lepley, *J. Am. Chem. Soc.*, **1961**, *83*, 1754.
- (127) M. J. S. Dewar, V. P. Kubba, R. Pettit, *J. Chem. Soc.*, **1958**, 3076.
- (128) M. J. S. Dewar, W. H. Poesche, *J. Am. Chem. Soc.*, **1963**, *85*, 2253.
- (129) M. J. S. Dewar, R. C. Dougherty, *J. Am. Chem. Soc.*, **1964**, *86*, 433.
- (130) H. R. Snyder, A. J. Reedy, W. J. Lennarz, *J. Am. Chem. Soc.*, **1958**, *80*, 835.
- (131) W. J. Lennarz, H. R. Snyder, *J. Am. Chem. Soc.*, **1960**, *82*, 2172.
- (132) M. J. S. Dewar, R. Dietz, *Tetrahedron*, **1961**, *15*, 26.
- (133) R. Carbó, M. Segre de Giambiagi, M. Giambiagi, *Bull. Soc. Chim. Fr.*, **1971**, 2515.
- (134) P. C. Lauterbur, in "Determination of Organic Structures by Physical Methods", Vol. II, F. C. Nachod, W. D. Phillips, Eds., **1962**, Academic Press Inc., New York, p.475.
- (135) F. A. Davies, M. J. S. Dewar, R. Jones, *J. Am. Chem. Soc.*, **1968**, *90*, 706; M. J. S. Dewar, R. Jones, *J. Am. Chem. Soc.*, **1967**, *89*, 2408.
- (136) F. A. Davies, M. J. S. Dewar, *J. Org. Chem.*, **1968**, *33*, 3324.
- (137) B. M. Mikhailov, M. E. Kuimova, *J. Organomet. Chem.*, **1976**, *116*, 123.
- (138) M. P. Groziak, A. D. Ganguly, P. D. Robinson, *J. Am. Chem. Soc.*, **1994**, *116*, 7597.
- (139) M. P. Hughes, B. D. Smith, *J. Org. Chem.*, **1997**, *62*, 4492; M. P. Hughes, M. Shang, B. D. Smith, *J. Org. Chem.*, **1996**, *61*, 4510.
- (140) K. D. M. Harris, B. M. Kariuki, C. Lambropoulos, D. Philp, J. M. A. Robinson, *Tetrahedron*, **1997**, *53*, 8599.



- (141) P. R. Ashton, K. D. M. Harris, B. M. Kariuki, D. Philp, J. M. A. Robinson, *J. Chem. Soc., Perkin Trans. 2*, In Press.
- (142) P. J. Comina, D. Philp, B. M. Kariuki, K. D. M. Harris, *Chem. Commun.*, **1999**, 2279.
- (143) T. C. Bruice, F. C. Lightstone, *Acc. Chem. Res.*, **1999**, 32, 127.
- (144) G. Ercolani, *J. Phys. Chem. B*, **1998**, 102, 5699; A. J. Kirby, *Adv. Phys. Org. Chem.*, **1980**, 17, 183.
- (145) M. J. S. Dewar, R. Dietz, *J. Chem. Soc.*, **1960**, 1344.
- (146) J. P. Lorand, J. O. Edwards, *J. Org. Chem.*, **1959**, 24, 769.
- (147) P.-Q. Löwdin, *Adv. Quantum Chem.*, **1970**, 5, 185.
- (148) L. Pauling, in *The Nature of the Chemical Bond*, 3rd ed., Cornell University Press, Ithaca, New York, **1960**, p.93.
- (149) Single crystal X-ray diffraction data were recorded with  $\lambda = 0.68850 \text{ \AA}$  at the Synchrotron Radiation Source (Daresbury Laboratory) on Station 9.8 which is equipped with a Siemens SMART CCD diffractometer. The structure was solved using the program SHELXS [G. M. Sheldrick, SHELXS86, Program for the Solution of Crystal Structures, University of Göttingen, Germany, **1986**] and refined using the program SHELXL [G. M. Sheldrick, SHELXL92, Program for the refinement of Crystal Structures, University of Göttingen, Germany, **1993**]. The positions of all non-hydrogen atoms were refined with anisotropic displacement parameters, and all hydrogen atoms (except the hydroxyl hydrogen atom) were placed in calculated positions. Final refined  $R_1 = 4.71\%$ ,  $R_w = 13.05\%$ . *Crystal Data* for **62** at 150 K:  $[\text{C}_{12}\text{H}_9\text{BO}_2]$ ,  $M = 196.00 \text{ g mol}^{-1}$ , orthorhombic, space group  $Pna2_1$ ,  $a = 14.683(2) \text{ \AA}$ ,  $b = 5.1589(7) \text{ \AA}$ ,  $c = 24.502(3) \text{ \AA}$ ,  $V = 1856.0(4) \text{ \AA}^3$ ,  $Z = 8$ ,  $D_c = 1.403 \text{ g cm}^{-3}$ ,  $F(000) = 816$ .
- (150) M. C. Etter, *Acc. Chem. Res.*, **1990**, 23, 120.
- (151) W. Maringgele, A. Meller, M. Noltemeyer, G. M. Sheldrick, *Z. Anorg. Allg. Chem.*, **1986**, 536, 24.
- (152) The powder X-ray diffraction pattern of the anhydride **96** was recorded at 22 °C on Station 2.3 at the Synchrotron Radiation Source, Daresbury Laboratory using a wavelength of 1.4000 Å. A capillary sample holder was used with the data recorded over the  $2\theta$  range 5° to 60° in steps of 0.01°. The powder X-ray diffraction pattern was indexed by the program ITO [J. W. Visser, *J. Appl. Crystallogr.*, **1969**, 2, 89], giving the monoclinic unit cell:  $a = 9.357 \text{ \AA}$ ,  $b = 15.248 \text{ \AA}$ ,  $c = 6.407 \text{ \AA}$ ,  $\beta = 99.16^\circ$ . On the basis of systematic absences, the

space group was assigned as  $P2_1/c$ , and density considerations suggest that there are two molecules of the anhydride in the unit cell. In space group  $P2_1/c$  (which has four general positions), this situation implies that there is disorder of the molecules of **96** in the crystal structure. To simplify the structural analysis, structure solution was carried out initially in space group  $P2_1$  (with one molecule of anhydride in the asymmetric unit), with a view to exploring subsequently whether the description in the higher symmetry space group  $P2_1/c$  would be more appropriate.

Structure solution was carried out directly from the powder diffraction data using the Genetic Algorithm (GA) method [B. M. Kariuki, H. Serrano-González, R. L. Johnston, K. D. M. Harris, *Chem. Phys. Lett.*, **1997**, *280*, 189; K. D. M. Harris, R. L. Johnston, B. M. Kariuki, *Acta Crystallogr.*, **1998**, *A54*, 632], which is based on the direct-space strategy for structure solution [K. D. M. Harris, M. Tremayne, P. Lightfoot, P. G. Bruce, *J. Am. Chem. Soc.*, **1994**, *116*, 3543; K. D. M. Harris, M. Tremayne, *Chem. Mater.*, **1996**, *8*, 2554]. In this strategy, trial crystal structures are sampled in direct space, with the “quality” of each trial structure assessed by directly comparing the powder diffraction pattern calculated for the trial structure and the experimental diffraction pattern. In the present work, this comparison is made using the powder profile R-factor  $R_{wp}$ . In the GA method, a population of trial structures is allowed to evolve subject to the normal rules and operations (mating, mutation and natural selection) that govern evolutionary systems.

In the GA structure solution calculation, the structural fragment comprised all non-hydrogen atoms of the molecule, which was constructed using standard bond lengths and bond angles. The two boroxophenanthrene ring systems were maintained as rigid units, with the molecular conformation defined by the two O-B-O-B torsion angles. (variables  $\tau_1$  and  $\tau_2$ ) at the centre of the molecule. Thus, the structure is defined by 8 variables  $\{x, y, z, \theta, \phi, \psi, \tau_1, \tau_2\}$ , where  $\{x, y, z\}$  refers to the position of the central oxygen atom. The GA calculation involved the evolution of 200 generations of a population of 100 structures. In each generation, 100 offspring, (obtained from 50 pairs of parents) and 10 mutations were generated. In the evolution of the population, the value of  $R_{wp}$  for the best structure in the population dropped from *ca.* 38% in the first generation to *ca.* 21% in the final generation.

The best structure solution (lowest  $R_{wp}$  in the final generation) was taken as the starting model for Rietveld refinement using the GSAS program [A. C. Larson, R. B. Von Dreele, Los Alamos Lab. Report No. LA-UR-86-748, **1987**]. The positions of all non-hydrogen atoms were refined, with standard geometric restraints applied to bond lengths and bond angles, and a common isotropic displacement parameter was used for all atoms. In the final stages a preferred orientation parameter was refined. The final Rietveld refinement gave  $R_{wp} \approx 8\%$  and  $R_p \approx 11\%$ .

Following successful Rietveld refinement in space group  $P2_1$ , the possibility to describe the structure in the higher symmetry space group  $P2_1/c$  was explored, recalling that this space group implies the introduction of disorder within the crystal structure. In particular, addition of an inversion centre to the structure refined in space group  $P2_1$  corresponds to a model involving disorder only in the position of the central oxygen atom of the anhydride, with this atom disordered between two sites of half occupancy. These two positions of the central oxygen atom correspond to two different molecular orientations (related by a  $180^\circ$  flip) such that the positions of all atoms except the central oxygen atom are identical in the two molecular orientations. Rietveld refinement of this structural model in space group  $P2_1/c$  was successful, and gave rise to an equally good fit to the powder diffraction data as the refinement discussed above in space group  $P2_1$ .

- (153) W. E. Brown, D. Dollimore, A. K. Galwey, in *Comprehensive Chemical Kinetics*, (Eds.: C. H. Bamford, C. F. H. Tipper), Elsevier Scientific Publishing, Oxford, **1980**, p.57.
- (154) P. W. Atkins, in *Physical Chemistry*, 4<sup>th</sup> Ed., Oxford University Press, Oxford, **1990**, p.792.
- (155) N. B. Singh, R. J. Singh, N. P. Singh, *Tetrahedron*, **1994**, *50*, 6441; F. Toda, *Synlett*, **1992**, 303.
- (156) G. Desiraju, *Solid State Ionics*, **1997**, *101*, 839.
- (157) S. P. Stanforth, *Tetrahedron*, **1998**, *54*, 263.
- (158) I. Thomsen, K. B. G. Torssell, *Acta Chem. Scand.*, **1991**, *45*, 539.
- (159) N. A. Bumagin, E. V. Luzikova, *J. Organomet. Chem.*, **1997**, *532*, 271. Also: K. V. Gothelf, K. B. G. Torssell, *Acta Chem. Scand.*, **1994**, *48*, 61.

- (160) M. Kumada, *Pure Appl. Chem.*, **1980**, *52*, 669; K. Tamo, K. Sumitani, M. Kumada, *J. Am. Chem. Soc.*, **1972**, *94*, 4374; R. J. P. Corriu, J. P. Mase, *J. Chem. Soc., Chem. Commun.*, **1972**, 144.
- (161) A. Suzuki, *J. Organomet. Chem.*, **1999**, *576*, 147; N. Miyaura, A. Suzuki, *Chem. Rev.*, **1995**, *95*, 2457.
- (162) C. Banzatti, N. Carfagna, R. Commisso, F. Heidempergher, L. Pegrassi, P. Melloni, *J. Med. Chem.*, **1988**, *31*, 1466.
- (163) J. K. Stille, *J. Org. Chem.*, **1987**, *52*, 422; J. K. Stille, A. M. Echavarren, R. M. Williams, J. A. Hendrix, *Org. Synth.*, **1992**, *71*, 97.
- (164) A related bis-boroxoaromatic compound, 5,12-dihydroxy-5,12-dibora-6,13-dioxodibenz[a,h]anthracene, has been reported as showing similar behaviour. Unfortunately, no structural details were provided: R. D. Offenbauer, P. G. Rodewald, *J. Polym. Sci., Part B*, **1968**, *6*, 573.
- (165) R. N. Icke, C. E. Redemann, B. B. Wisegarver, G. A. Alles, *Org. Synth. Coll.*, **1955**, *3*, 644.
- (166) W. Seaman, J. R. Johnson, *J. Am. Chem. Soc.*, **1931**, *53*, 711.
- (167) J. M. A. Robinson, PhD Thesis, University of Birmingham, 2000.
- (168) J. K. Stille, *Angew. Chem., Int. Ed. Engl.*, **1986**, *25*, 508.
- (169) R. P. Sijbesma, A. P. M. Kentgens, E. T. G. Lutz, J. H. van der Maas, R. J. M. Nolte, *J. Am. Chem. Soc.*, **1993**, *115*, 8999.
- (170) R. Bolton, J. P. B. Sandall, *J. Chem. Soc., Perkin Trans. 2*, **1977**, 278.
- (171) A. Saednya, H. Hart, *Synthesis*, **1996**, 1455; C.-J. F. Du, H. Hart, K.-K. D. Ng, *J. Org. Chem.*, **1986**, *51*, 3162.
- (172) E. M. Hyde, B. L. Shaw, I. Shepherd, *J. Chem. Soc., Dalton Trans.*, **1978**, 1696.
- (173) P. Warner, R. Sutherland, *J. Org. Chem.*, **1992**, *57*, 6294.
- (174) E. J. Corey, P. L. Fuchs, *Tetrahedron Lett.*, **1972**, *36*, 3769; N. Miyaura, H. Suginome, A. Suzuki, *Bull. Chem. Soc. Jpn.*, **1982**, *55*, 2221.
- (175) L. J. Todd, A. R. Siedle, *Prog. Nucl. Magn. Reson. Spectros.*, **1979**, *13*, 87.
- (176) H. G. Kuivila, A. H. Keough, E. J. Soboczinski, *J. Org. Chem.*, **1954**, *19*, 780.
- (177) D. S. Matteson, *J. Organomet. Chem.*, **1999**, *581*, 51.
- (178) B. Carboni, C. Pourbaix, F. Carreaux, H. Deleuze, B. Maillard, *Tetrahedron Lett.*, **1999**, *40*, 7979.

- (179) A. H. Soloway, J.-C. Zhuo, F.-G. Rong, A. J. Lunato, D. H. Ives, R. F. Barth, A. K. M. Anisuzzamann, C. D. Barth, B. A. Barnum, *J. Organomet. Chem.*, **1999**, *581*, 150.
- (180) J. H. Hartley, C. J. Ward, T. D. James, *J. Chem. Soc., Perkin Trans. 1*, **2000**, *19*, 3155; T. D. James, K. R. A. S. Sandanayake, S. Shinkai, *Angew. Chem., Int. Ed. Engl.*, **1996**, *35*, 1910.
- (181) J. Suffert, *J. Org. Chem.*, **1989**, *54*, 509.
- (182) F. L. Weitzl, *J. Org. Chem.*, **1976**, *41*, 2044.
- (183) J. C. Anderson, D. J. Pearson, *J. Chem. Soc., Perkin Trans. 1*, **1998**, 2023.
- (184) J. M. Saa, G. Martorell, A. Garcia-Raso, *J. Org. Chem.*, **1992**, *57*, 678.
- (185) H.-I. Joschek, S. I. Miller, *J. Am. Chem. Soc.*, **1966**, *88*, 3269.
- (186) P. Buck, G. Köbrich, *Chem. Ber.*, **1970**, *103*, 1420.
- (187) K. S. Chang, X. Zhou, M. T. Au, C. Y. Tam, *Tetrahedron*, **1995**, *51*, 3129.
- (188) D. L. Yabroff, G. E. K. Branch, B. Bettman, *J. Am. Chem. Soc.*, **1934**, *56*, 1850.
- (189) A. Kistenmacher, K. Mullen, *J. Heterocycl. Chem.*, **1992**, *29*, 1237.
- (190) J. F. Corbett, P. F. Holt, *J. Chem. Soc.*, **1963**, 2385.
- (191) L. M. Stock, T. L. Wright, *J. Org. Chem.*, **1977**, *42*, 2875.
- (192) H. Hart, P. Rajakumar, *Tetrahedron*, **1995**, *51*, 1313.
- (193) E. Kiehlmann, R. W. Lauener, *Can. J. Chem.*, **1989**, *67*, 335.
- (194) G. R. Ames, W. Davey, *J. Chem. Soc.*, **1958**, 1794.
- (195) H. Guesten, *Tetrahedron*, **1968**, *24*, 4393.
- (196) R. Bolton, J. P. B. Sandall, *J. Chem. Soc., Perkin Trans. 2*, **1977**, 278.
- (197) C.-J. F. Du, H. Hart, K.-K. D. Ng, *J. Org. Chem.*, **1986**, *51*, 3162.
- (198) R. Q. Brewster, F. Strain, *J. Am. Chem. Soc.*, **1934**, *56*, 117.
- (199) W. H. Laarhoven, R. J. F. Nivard, E. Havinga, *Recl. Trav. Chim., Pays-Bas*, **1961**, *80*, 775.
- (200) C. Imrie, T. A. Modro, E. R. Rohwer, C. C. P. Wagener, *J. Org. Chem.*, **1993**, *58*, 5643.
- (201) W. Manchot, C. Zahn, *Justus Liebigs Ann. Chem.*, **1906**, *345*, 330.
- (202) H. J. Bestmann, H. Frey, *Liebigs Ann. Chem.*, **1980**, *12*, 2061.
- (203) G. Modena, F. Rivetti, G. Scorrano, U. Tonellato, *J. Am. Chem. Soc.*, **1977**, *99*, 3392.
- (204) M. Cariou, *Tetrahedron*, **1991**, *47*, 799.
- (205) M. Kadkhodayan, T. Singleton, F. J. Heldrich, *Synth. Commun.*, **1984**, *14*, 707.